1,1-Dithiolate Complexes of Ruthenium and Osmium

by

A. Ewan D. M^{c}Queen

Thesis presented for the Degree of Doctor of Philosophy

University of Edinburgh

1988

For mum and dad,

and in memory of TAS.

Declaration

Except where specific reference is made to other sources, the work presented in this thesis is the original work of the author under the guidance of his supervisors. It has not been submitted, in whole or in part, for any other degree. Certain of the results have been submitted for publication.

Acknowledgements

Enthusiasm, and the capacity to encourage others, are highly desirable qualities. Those people who were fortunate enough to work with Tony Stephenson will agree that he had those qualities in abundance. As a consequence of his death, the work in this thesis may not have developed in the direction his guidance may have taken it. I would like to think that, at least in spirit, it has.

I would express my thanks to Drs. G. A. Heath and M. Schroder who were given the (arduous) task of my supervision after Tony's death. In particular, I would like to thank Dr. Lesley Yellowlees for making chemistry fun again, and for her unstinting efforts to make me understand the discipline of electrochemistry.

Amongst the many members of the staff of Edinburgh University who have assisted me, I would like to thank Dr. A. J. Blake for his help in solving the crystal structures and Dr. R. J. Nelmes of the Physics Department for the use of the Cad-4 diffractometer. For their technical help, I thank J. Broom, H. Grant, J. A. Millar, J. Grunbaum, E. McDougall and S. Mains. I am indebted to Ruth, Ken, Scott and Mandy for their patience and advice.

Finally, I am grateful to S.E.R.C. for financial assistance, the University of Edinburgh for the use of laboratory facilities and Johnson-Matthey P.L.C. for loans of precious metals.

Abstract

Chapter 1: The chemistry of 1,1-dithiolate complexes of Fe, Ru and Os is reviewed.

Chapter 2: A high yield synthetic route to the complexes, $[Ru(S-S)_3]$ ($S-S$ = $^-S_2P\{OEt\}_2$, $^-S_2CNR_2$, $R = Me$, Et, Pr^i) is reported. The crystal structure of $[Ru(S_2P\{OEt\}_2)_3]$ is presented. Electrochemical and spectroelectrochemical studies on $[Ru(S_2PR_2)_3]$ ($R = Ph$, OEt) show that these complexes undergo reversible one-electron reduction and oxidation steps affording the Ru^{II} and Ru^{IV} species, respectively. The aerobic reaction of $[Ru(S-S)_3]$ ($S-S = {}^-S_2PR_2$, $R = Ph$, OEt; $^-S_2CNEt_2$) with excess PR_3 ($PR_3 = PMe_2Ph, dppm$) affords *cis*-$[Ru(S-S)_2L_2]$ ($L_2 = PMe_2Ph$, $dppm$). The complexes, $[M(S_2P\{OEt\}_2)_2L_2]$ ($M = Ru$, $L = PPh_3$, $PEtPh_2$; PMe_2Ph; $M = Os$, $L = PPh_3$), are prepared from $[MCl_xL_3]$ ($M = Ru$, $x = 2$, $L = PPh_3$, $PEtPh_2$, $x = 3$, $L = PMe_2Ph$; $M = Os$, $x = 2$, $L = PPh_3$) and $K[S_2P\{OEt\}_2]$, and studied by $^{31}P-\{^1H\}$ and ^{1}H n.m.r. spectroscopy. Carbonylation of $[Ru(S_2P\{OEt\}_2)_2(PPh_3)_2]$ affords *cis*-$[Ru(S_2P\{OEt\}_2)_2(PPh_3)(CO)]$. The crystal structure of *cis*-$[Ru(S_2PPh_2)_2(PPh_3)(CO)]$ is presented. Electrochemical studies on $[M(S-S)_2L_2]$ ($M = Ru$, Os, $S-S = {}^-S_2PR_2$, $R = Me$, Ph, OEt, $L = PPh_3$; $M = Ru$, $S-S = {}^-S_2PR_2$, $R = Ph$, OEt, $S-S = {}^-S_2CNEt_2$, $L = dppm$, PMe_2Ph) reveal that the redox potential and reversibility of the $M^{II/III}$ couple is dependent on M, L and $S-S$.

Chapter 3: Transition metal complexes of tetracyanoethylene (*tcne*) are reviewed by metal-tcne bond type. Reaction of $[M(S_2PR_2)_2(PPh_3)_2]$ ($M = Ru$, Os; $R = Me$, Ph, OEt) with excess tcne affords $[M(S_2PR_2)_2(PPh_3)(tcne)]$. Spectroscopic studies assign a *cis*-configuration to the ligands, and N-co-ordination to tcne. X-ray diffraction studies of $[Os(S_2PR_2)_2(PPh_3)(tcne)]$ confirm the structure of these adducts in the solid state. For $R = Me$, an intermolecular interaction between ligated tcne moieties is observed. For $R = Ph$, an intramolecular interaction between the tcne ligand and a phenyl ring is reported. A binuclear adduct, $[\{Ru(S_2PR_2)_2(PPh_3)\}_2tcne]$ ($R = Me$, Ph, OEt), can be generated using equimolar amounts of tcne and $[Ru(S_2PR_2)_2(PPh_3)_2]$.

Chapter 4: Electrochemical and spectroelectrochemical studies reveal that the complexes, $[M(S_2PR_2)_2(PPh_3)(tcne)]$ ($M = Ru$, Os; $R = Me$, Ph, OEt), undergo two *tcne*-based reductions and two oxidations. Although the electronic nature of the Ru and Os adducts is slightly different, both can be considered as formally $M^{II}-tcne^0$ species. However, preliminary studies on the adducts, $[\{Ru(S_2PR_2)_2(PPh_3)\}_2tcne]$ *(R=Me, Ph, OEt)*, suggest that these complexes contain formally, co-ordinated $tcne^-$ and a Ru^{III} centre.

Chapter 5: Reaction of $[Ru(S_2PR_2)_2(PPh_3)_2]$ *(R = Me, Ph, OEt)*, with fumaronitrile *(fmn)* affords $[Ru(S_2PR_2)_2(PPh_3)(fmn)]$ and $[\{Ru(S_2PR_2)_2(PPh_3)\}_2(fmn)]$. These adducts are characterised by $^{31}P-\{^1H\}$ n.m.r spectroscopy and by infrared analysis. These complexes have a *cis*-configuration, and are analogous to the *tcne* complexes of Chapter 3.

CONTENTS. PAGE.

Chapter 1

Chapter 2

List of Tables. Page.

List of Figures

The following abbreviations are used in this thesis:

a.c.	alternating current
acn	acrylonitrile
bipy	2,2 bipyridyl
br	broad
cod	cyclo-ocata-1,5-diene
cot	cyclo-octatetraene
Cp	π-C_5H_5
CT	charge-transfer
c.v.	cyclic voltammogram
d	doublet
δ	chemical shift in p.p.m.
DMF	N,N-dimethylformamide
dppe	bis(diphenylphosphino)ethane
dppm	bis(diphenylphosphino)methane
ϵ	molar absoptivity ($cm^{-1}\,mole^{-1}\,dm^3$)
E_p	peak potential (V vs Ag/AgCl unless otherwise stated)
$E_{p_{f,r}}$	peak forward (f) and reverse (r) potentials
ΔE_p	$E_{pf} - E_{pr}$
e.s.r	electron spin resonance
fmn	fumaronitrile
Hz	Hertz
$i_{p_{f,r}}$	peak forward (f) and reverse (r) current
K	Kelvin
LMCT	Ligand to metal charge-transfer
m	multiplet
Me	methyl
MLCT	metal to ligand charge-transfer

mmol	millimole
M.O.	molecular orbital
nbd	bicyclo[2.2.1]hepta-2,5-diene
n.m.r.	nuclear magnetic resonance
O.T.E.	optically transparent electrode
O.T.T.L.E.	optically transparent thin-layer electrode
Ph	phenyl
ppm	parts per million
Pr	iso-propyl
py	pyridine
R	alkyl or aryl
SCE	saturated calomel electrode
t	triplet
$TBA^+BF_4^-$	tetra-n-butylammonium fluoroborate
tcne	tetracyanoethylene
tcnq	tetracyanoquinodimethan
THF	tetrahydrofuran
v	scan rate (mVs^{-1})
V	Volt

Chapter 1

Introduction

Some complexes of iron, ruthenium and osmium with 1,1-dithiolate ligands.

1.1 Transition-metal complexes of 1,1-dithiolates.

1,1-dithiolates are derivatives of oxy-acids in which two of the functional oxygen atoms of the acid are replaced by sulphur atoms. The more common dithiolate ligands are listed in Table 1.1. Metal complexes of 1,1-ditholates have been reviewed by Coucovanis,[1] McAuliffe[2] and Wasson,[3] while Eisenberg has presented a structural review of the dithiolate chelates.[4] In this chapter the complexes of the dithiocarbamate ($^{-}S_2CNR_2$), dithiophosphinate ($^{-}S_2PR_2$), and dithiophosphate ($^{-}S_2P\{OR\}_2$) ligands with iron, ruthenium and osmium will be reviewed.

1,1-dithiolates can co-ordinate to a metal centre (i) as a unidentate ligand through one sulphur atom (Figure 1.1a), (ii) as bidentate chelating ligands through both sulphurs (Figure 1.1b), or (iii) as a bridging ligand between two (or more) metal centres (Figures 1.1c and 1.1d).

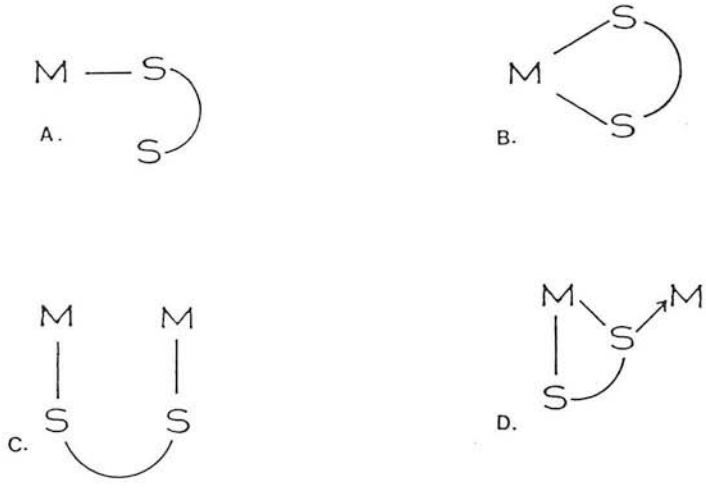

Figure 1.1: Co-ordination modes of dithiolate ligands.

Table 1.1: The more common 1,1-dithiolate ligands.

Ligand	Name	Abbreviation
$^{-}S_2CNR_2$	dithiocarbamate	$^{-}R_2dtc$
$^{-}S_2COR$	xanthate	$^{-}$Rxan
$^{-}S_2CSR$	thioxanthate	$^{-}$RSxan
$^{-}S_2CR$	dithiocarboxylate	-
$^{2-}S_2C{=}CR_2$	1,1-ethenedithiolate	-
$^{-}S_2PR_2$	dithiophosphinate	$^{-}$dtp
$^{-}S_2P\{OR\}_2$	dithiophosphate	$^{-}$Odtp
$^{-}S_2AsR_2$	dithioarsinate	-
$^{-}S_2As\{OR\}_2$	dithioarsenate	-

R = alkyl or aryl.

Infrared and n.m.r. spectroscopy have been used to distinguish between these different co-ordination modes, and complexes in which the dithiolate acts as a counter ion.[5-7]

The 1,1-dithiolates are versatile ligands forming complexes with many metal ions in a wide range of oxidation states.[1,2] The sulphur atoms are capable of σ-donation and weak π-donation (from the filled $3p$ orbitals of sulphur)[8] and thus, can stabilise metals in high oxidation states such as Cu^{III},[9] Ni^{IV},[10] Pt^{IV},[11] and Pd^{IV}.[12] The empty $3d$ orbitals of sulphur however, can accept electron density and so help stabilise metal ions in low oxidation states.[13]

The acceptor, or donor capacity of the sulphur atoms is influenced by the structure of the dithiolate. Experimental results have shown[14-16] that dithiocarbamate and xanthate ($^{-}S_2COR$) ligands can stabilise higher oxidation states of a metal more readily than dithiophosphinate ligands. Thus, the preparation of binary complexes of M^{II} ions (M=Fe, Mn, Co) is difficult for the dithiocarbamate and xanthates as they readily undergo oxidation to the corresponding M^{III} species.[14] The analogous M^{II} dithiophosphinate complexes however, are easily prepared and are unstable in the M^{III} oxidation state.[15,16] The ability of the dithiocarbamates and xanthates to stabilise higher oxidation states has been related by Chatt *et. al.* to the resonance forms available to

the 1,1-dithiolates[17] (see Figure 1.2). In addition to resonance forms (a) and (b) in which one sulphur atom carries a negative charge, a third structure, (c) can be drawn for the dithiocarbamates and xanthates in which both sulphur atoms are negatively charged. Structure (c) is constructed by donation of a lone pair of electrons from nitrogen ($^{-}S_2CNR_2$), or oxygen ($^{-}S_2COR$) to the carbon atom; such a resonance form can not be drawn for the dithiophosphinate ligand.

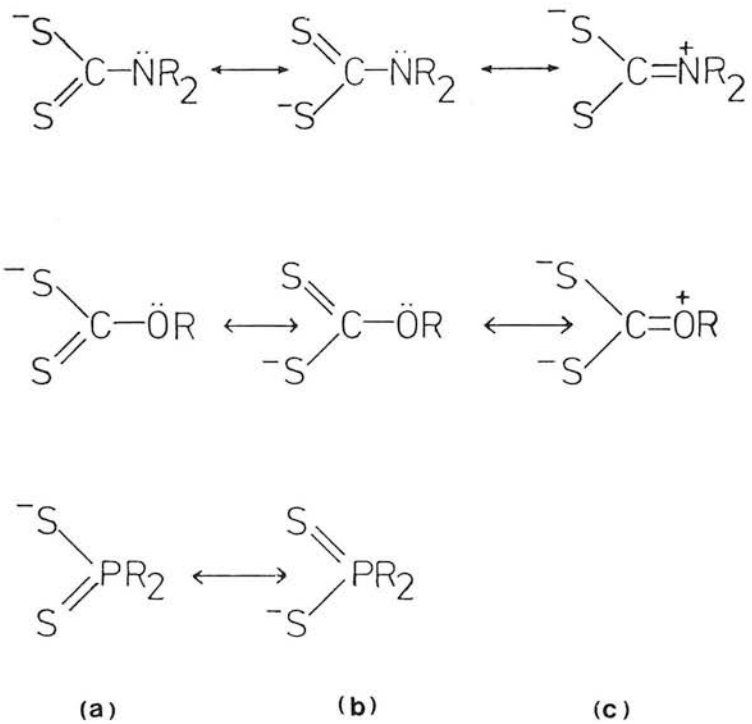

Figure 1.2: Resonance forms for 1,1-dithiolate ligands.

Chatt and Venanzi have proposed that the electronegativity of the oxygen will reduce the importance of structure (c) for the xanthates.[17]

The order of increasing electron density on the sulphur atom, and hence the ability to stabilise higher oxidation states would be[17]:

$$^{-}S_2PR_2 < {}^{-}S_2COR < {}^{-}S_2CNR_2$$

1.2 Binary complexes of iron, ruthenium, and osmium.

1.2.1 Dithiocarbamate complexes.

Few dithiocarbamate complexes of Fe^{II} have been prepared as they are difficult to isolate and are highly sensitive to aerial oxidation.[18] The high-spin complexes, $[Fe^{II}(S_2CNR_2)_2]$, (R=Me, Et, Pr^n, Bu^n) have been synthesised and the single-crystal X-ray diffraction study of $[Fe^{II}(S_2CNEt_2)_2]$ has been reported.[19]

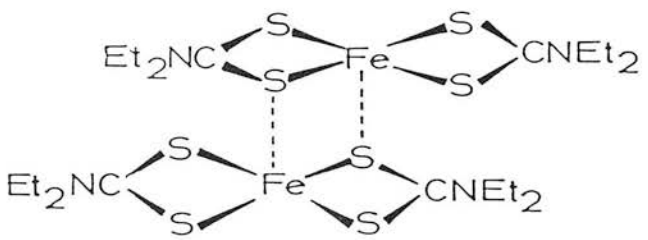

[1.1]

The complex is dimeric and the geometry around individual iron atoms is distorted trigonal bipyramidal[19]. Each iron centre is co-ordinated to four sulphurs, from two dithiocarbamates, and a fifth sulphur atom from an adjacent $[Fe^{II}(S_2CNEt_2)_2]$ molecule.

The tris-dithiocarbamate iron complexes, $[Fe^{III}(dtc)_3]$, have been studied in detail on account of their interesting electronic properties.[20] The dithiocarbamate ligands generate values of Ligand Field and Racah

parameters (Δ and B) which place $[Fe^{III}(S_2CNR_2)_3]$ complexes at the $^6A_1$-$^2T_2$ electronic crossover.[21] The energies of the high-spin and low-spin states in this region are almost equal and so the magnetic properties of the complex are very susceptible to variation in temperature and pressure.[22] Subtle changes in the organic substituents on the ligand can alter the position of the spin-state equilibrium through differences in inductive, mesomeric and steric effects.[23]

Several complexes of the type, $[Fe^{III}(S_2CNR_2)_3]$ (NR_2=NBu_2,[24] NMePh,[25] pyrolidine,[26] NEt_2[27]), have been characterised by X-ray crystallography. The complex, $[Fe^{III}(S_2CNEt_2)_3]$, has been structurally characterised in both high-spin (at 297K) and low-spin (at 79K) states.[27] The Fe-S bond length contracts (from 2.36Å) by 0.05Å on cooling, and the S-Fe-S "bite" angle of the dithiocarbamate increases by 1.6° (from 74.3°).

The low-spin complexes, $[Fe^{IV}(S_2CNR_2)_3]^+$ (R_2=Me_2, Et_2, Pr^i_2, pyrolidine, Cy_2), have been synthesised chemically by Pasek and Straub [1.2 and 1.3].[28]

$$[Fe^{III}(S_2CNR_2)_3] \xrightarrow{BF_3\,,\,O_2\,,\,\text{benzene}} [Fe^{IV}(S_2CNR_2)_3]BF_4 \qquad [1.2]$$

$$[Fe^{III}(S_2CNR_2)_3] \xrightarrow{PF_6^-\,,\,H^+,\,\text{acetone}} [Fe^{IV}(S_2CNR_2)_3]PF_6 \qquad [1.3]$$

The crystal structure of $[Fe^{IV}(S_2CN(CH_2)_4)_3]^+$ has been reported[29]; the $[FeS_6]$ core in $[Fe^{IV}(S_2CN(CH_2)_4)_3]^+$ is intermediate between octahedral and trigonal prismatic

geometry. The average Fe-S bond length of 2.300Å is 0.11Å shorter than the average Fe-S bond length in high-spin $[Fe^{III}(S_2CN(CH_2)_4)_3]$.[26] However, the Fe-S bond length in $[Fe^{IV}(S_2CN(CH_2)_4)_3]^+$ is similar to that found for $[Fe^{III}(S_2CNEt_2)_3]$ (2.306Å).[27] This suggests that the increased oxidation state of the metal has less effect on the Fe-S bond length than that of altering the electronic nature of the complex from high-spin to low-spin.

The Fe^{II} and Fe^{IV} tris-dithiocarbamate complexes can be synthesised electrochemically (in 90% yield and free from by-products)[30]; $[Fe^{III}(S_2CNR_2)_3]$ exhibits reversible, one-electron oxidation and reduction processes.

$$[Fe^{II}(dtc)_3]^- \underset{+e}{\overset{-e}{\rightleftharpoons}} [Fe^{III}(dtc)_3] \underset{+e}{\overset{-e}{\rightleftharpoons}} [Fe^{IV}(dtc)_3]^+ \quad [1.4]$$

The redox potentials are sensitive to the nature of the organic substituents; electron withdrawing substituents make reduction of $[Fe^{III}(S_2CNR_2)_3]$ easier (and oxidation harder).[31,32] Thus, the reduction potentials of $[Fe^{III}(S_2CNR_2)_3]$ decrease in the order[30]:-

$$NPh_2, NPhMe > NMe_2, NEt_2 > N(Pr^i)_2$$

The reduction and oxidation potentials correlate linearly reflecting the relative abilities of the organic substituents to stabilise Fe^{II}, or Fe^{IV} with respect to Fe^{III}.[30]

Few binary complexes of the 1,1-dithiolates and ruthenium are known.[2] Malatesta prepared $[Ru^{III}(S_2CNEt_2)_3]$ from $RuCl_3$ and the dithio-acid.[33] These complexes (as expected for a second row transition-metal species) are low-spin. The dithiolate ligands in $[Ru^{III}(S_2CNEt_2)_3]$ exhibit fluctionality in solution and Pignolet *et. al.* used variable-temperature ^1H n.m.r. spectroscopy to propose that the intramolecular rearrangment proceeds by a metal-centred trigonal twist mechanism.[34]

The subsequent diffraction study of $[Ru^{III}(S_2CNEt_2)_3]$ showed[35] that the $[RuS_6]$ core is twisted towards trigonal prismatic geometry with an average Ru-S distance of 2.376Å and an average S-Ru-S "bite" angle of 73.0°. The short S_2C-N and long C-S bond lengths (1.30 and 1.72Å respectively) suggest that the resonance structure in Figure 1.2c plays an important role in $[Ru^{III}(S_2CNEt_2)_3]$.[35] Other workers determined the structure of $[Ru^{III}(S_2CN(CH_2)_4O)_3]$ and the complex has similar bond lengths and geometry to the ethyl derivative.[36]

The electrochemical behaviour of $[Ru^{III}(S_2CNEt_2)_3]$ was first reported by Patterson and Holm who observed that the complex exhibits one reduction (-0.714V vs SCE) and one oxidation (+0.382V vs SCE) in DMF solution.[37] The similarity between the oxidation potentials of $[Ru^{III}(S_2CNEt_2)_3]$ and $[Fe^{III}(S_2CNEt_2)_3]$ (+0.432V vs SCE) prompted the authors to suggest that $[Ru^{IV}(S_2CNEt_2)_3]^+$ should be synthetically accessible.[37] However, the

chemical oxidation of $[Ru^{III}(S_2CNR_2)_3]$ (R=Me, Et, benzyl, $(CH_2)_4$) with BF_3 gas in air does not yield the expected Ru^{IV} species, rather the diamagnetic, binuclear complexes, $[Ru_2(S_2CNR_2)_5]^+[BF_4]^-$, which have been characterised in α and β forms [1.5 and 1.6].[38] Single crystal X-ray diffraction studies have been reported for both β-$[Ru_2(S_2CNEt_2)_5]^+$ and α-$[Ru_2(S_2CNPr^i_2)_5]^+$.[38,39]

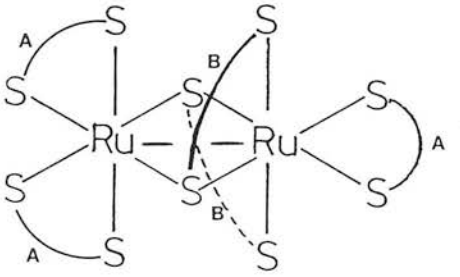

[1.5]

S-S = $S_2CNPr^i_2$

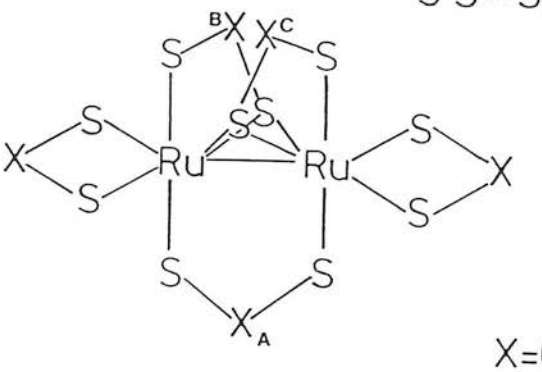

[1.6]

X=$CNEt_2$

The Ru-Ru distance in β-$[Ru_2(S_2CNEt_2)_5]^+$ is 2.743Å and, together with the observed diamagnetism of the complex, is evidence for the existence of a Ru-Ru bond.[38] Two forms of bridging dithiocarbamate ligand are apparent in β-$[Ru_2(S_2CNEt_2)_5]^+$ [1.6]. The first type (ligand A) is similar to that found for simple carboxylate anions of transition metal complexes and also for bridging thioxanthates.[40,41] In this bridging mode each sulphur atom

of the dithiocarbamate is bound exclusively to different metal centres. Ligands (B) and (C) in [1.6] however, have one sulphur atom co-ordinated to one metal centre, and the second sulphur atom is found to be equidistant from the two ruthenium atoms.

The complex, α-$[Ru_2(S_2CNPr^i_2)_5]^+$ [1.5], also exhibits an appreciable metal-metal interaction with a Ru-Ru distance of 2.789Å.[39] However, the arrangement of the dithiolate ligands, differs from $[Ru_2(S_2CNEt_2)_5]^+$. The structure of $[Ru_2(S_2CNPr^i_2)_5]^+$ is, with respect to the bridging ligands, similar to $[Co_2(S_2CNEt_2)_5]^+$,[42] and $[Rh_2(S_2CNMe_2)_5]^+$,[43] in which only one type of bridging dithio-ligand is present. In these structures the dithiocarbamates which function as bridging ligands, *via* the $p\pi$-electrons, are chelated to the same metal centre.

The redox properties of $[Ru(S_2CNR_2)_3]$ and $[Ru_2(S_2CNR_2)_5]^+$ have been studied in detail.[44,45] Martin *et. al.* found[44] that the one-electron reduction of $[Ru^{III}(S_2CNR_2)_3]$ (R,R'=Me_2, Et_2, Pr^i_2, Bu^i_2, Ph_2, pyrr, benzyl$_2$) to $[Ru^{II}(S_2CNR_2)_3]^-$ is reversible for all derivatives, and that the reduction potential is dependent on the nature of the organic substituent on the ligand. Exhaustive reductive electrolysis of $[Ru^{III}(S_2CNR_2)_3]$ affords solutions of $[Ru^{II}(S_2CNR_2)_3]^-$ which revert rapidly to $[Ru^{III}(S_2CNR_2)_3]$ on exposure to air. The redox potential and the degree of reversibility of the one-electron oxidation of $[Ru^{III}(S_2CNR_2)_3]$ are also

dependent on the organic groups on the dithio-ligand.[44,45] The oxidation products of all $[Ru^{III}(S_2CNR_2)_3]$ are not stable, although the primary electrode processes in acetone solution are believed to be[44]:-

$$[Ru^{II}(dtc)_3]^- \underset{+e}{\overset{-e}{\rightleftharpoons}} [Ru^{III}(dtc)_3] \underset{+e}{\overset{-e}{\rightleftharpoons}} [Ru^{IV}(dtc)_3]^+ \qquad [1.7]$$

However, exhaustive oxidative electrolysis affords (after chromatography) only $[Ru^{III}(S_2CNR_2)_3]$ and $[Ru_2(S_2CNR_2)_5]^+$.[44]

Pignolet and co-workers however, isolated the seven co-ordinate diamagnetic species, $[Ru^{IV}(S_2CNEt_2)_3(CH_3CN)]^+$, after electrochemical oxidation of $[Ru^{III}(S_2CNEt_2)_3]$ in acetonitrile.[45] The lifetime of the cationic Ru^{IV} complex, $[Ru^{IV}(S_2CNEt_2)_3]^+$, is estimated at less than 10^{-3}s by cyclic voltammetric measurements.[45]

The adducts, $[Os(S_2CNEt_2)_4]$ and $[Os(S_2CNR_2)_3]$ ($R_2=(CH_2)_5$,[46] Me_2, Et_2[47,41]), have been synthesised by Van der Linden and co-workers:-

$$NH_4[OsCl_6] + Na[S_2CNEt_2] \xrightarrow[MeOH,H_2O]{\Delta} [Os(S_2CNEt_2)_4]$$

$$[Os(S_2CNEt_2)_4] \xrightarrow[THF]{\Delta} [Os^{III}(S_2CNEt_2)_3] \qquad [1.8]$$

Redox studies on $[Os^{III}(S_2CNR_2)_3]$ (R=Me, Et) reveal[47,48] that the complex undergoes a single one-electron reduction, and two one-electron oxidations:-

$$[Os^{II}(S_2CNR_2)_3]^- \underset{+e}{\overset{-e}{\rightleftharpoons}} [Os^{III}(S_2CNR_2)_3] \underset{+e}{\overset{-e}{\rightleftharpoons}}$$

$$[Os^{IV}(S_2CNR_2)_3]^+ \underset{+e}{\overset{-e}{\rightleftharpoons}} [Os^{V}(S_2CNR_2)_3]^{2+} \qquad [1.9]$$

In contrast to $[Ru^{III}(S_2CNR_2)_3]$, all the redox processes of the complexes, $[Os^{III}(S_2CNR_2)_3]$, are electrochemically reversible.[46,48] $[Os^{IV}(S_2CNEt_2)_3]^+$ has been prepared electrochemically[47] and chemically (using BF_3 gas in air).[48] The paramagnetic $[Os^{IV}(S_2CNEt_2)_3]^+$ species reacts readily with donor ligands such as CH_3CN, I_2, and PPh_3 to yield the diamagnetic, seven co-ordinate complexes, $[Os(S_2CNR_2)_3L]^+$.[47] Seven co-ordinate complexes of this type have been prepared for Ru^{IV}, but not Fe^{IV}.

The complexes, $[Os^{III}(S_2CNR_2)_3]$, (R=Me, Et) exhibit[48] a novel monomer-dimer equilibrium:-

$$2[Os^{III}(S_2CNR_2)_3] \rightleftharpoons [Os_2(S_2CNR_2)_6] \qquad [1.10]$$

The structure of $[Os_2(S_2CNR_2)_6]$ has been reported.[48] The Os-Os distance is 3.68Å with the geometry about each osmium atom being distorted, pentagonal bipyramid in which the axial atom is a shared sulphur atom. Thus, only two dithiocarbamate ligands are involved in bridging.

The binuclear complexes, $[Os_2(S_2CNR_2)_5]^+$ (R=Me, Et,) are prepared by prolonged refluxing of $NH_4[S_2CNR_2]$ and $K_2[OsCl_6]$ in aqueous methanol.[48] The conformation of these complexes (α or β) has not been determined.

1.2.2 Dithiophosphate complexes.

The first $[Fe^{III}(S_2P\{OR\}_2)_3]$ complexes were prepared by Malatesta and Pizzotti from anhydrous $FeCl_3$ and $NH_4[S_2P\{OR\}_2]$.[49] Stability constants for the formation of these complexes have been reported by Russian researchers.[50] Until recently these complexes were believed to be inherently unstable.[51] $[Fe^{III}(S_2P\{OEt\}_2)_3]$ decomposes within several hours, while alcoholic solutions of the complex are reduced to Fe^{II} rapidly[52]; e.s.r. spectroscopy has been used to monitor this decomposition.[53] However, Colclough *et. al.* prepared and structurally characterised the stable high-spin complex, $[Fe^{III}(S_2P\{OPr^i\}_2)_3]$, from Fe_2O_3 (or iron dust) and the dithio-acid.[54] If prepared from $FeCl_3$ and $H[S_2P\{OPr^i\}_2]$, the isolated $[Fe^{III}(S_2P\{OPr^i\}_2)_3]$ decomposes but can be stabilised by the addition of amines; residual acid is believed to be responsible for the instability of these $[Fe(S_2P\{OR\}_2)_3]$ complexes.[54]

The $[FeS_6]$ core in $[Fe^{III}(S_2P\{OPr^i\}_2)_3]$ is distorted from octahedral.[54] The complex crystallises in the space group $C\,2/c$; the molecules have imposed C_2 symmetry and the metal centre and one phosphorus atom lie on the two fold axis. Three unique Fe-S bond lengths are observed (2.461, 2.492, and 2.473Å) and these are significantly longer than the Fe-S bonds in $[Fe^{III}(S_2CNEt_2)_3]$ (2.36Å). The authors suggest[54] that this is representative of the poorer donor ability of the dithiophosphates where the

electron density on the sulphur atoms is reduced by back-donation to the phosphorus and consequently that resonance structure [1.11] is of importance in the bonding of the dithiophosphates.

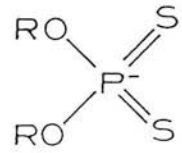

[1.11]

Polarographic studies of $[Fe(S_2P\{OEt\}_2)_3]$ in DMF show two waves, the first process is a reversible one-electron reduction and the second wave results from an irreversible two-electron reduction.[55]

Jorgensen prepared $[Ru^{III}(S_2P\{OEt\}_2)_3]$ (in low yield) from $K_2[RuCl_5(H_2O)]$ and $H[S_2P\{OEt\}_2]$.[56] The complex decomposes in solution, but co-crystallised samples of $[Ru^{III}(S_2P\{OEt\}_2)_3]$ and $[In^{III}(S_2P\{OPr^i\}_2)_3]$ were found to be stable.

Apart from research by Russian workers on the extraction of osmium ions from solution using dithiophosphate ligands,[57,58] no binary complexes of osmium with these dithiolate ligands have been reported.

1.2.3 Dithiophosphinate complexes.

Metal complexes of the dithiophosphinates have been reviewed by Kuchen and Hertel.[59] Cavell and co-workers prepared[60] a series of $[M(S_2PR_2)_n]$ complexes (n=3, M=Fe, Co; n=2, M=Mn, Fe, Co, Zn, Cd, Hg with R=CH_3, CF_3, C_2H_5) by the metathetical reaction:-

$$MCl_n + n\,Na[S_2PR_2] \longrightarrow [M(S_2PR_2)_n] + n\,NaCl \qquad [1.12]$$

The Fe^{II} adducts have a tetrahedral $[FeS_4]$ core, and powder diffraction studies show that they are polymeric in nature with bridging dithiolate ligands. The complexes are highly susceptible to attack by molecular oxygen, affording the corresponding $[Fe^{III}(S_2PR_2)_3]$ complex as one of the products. The high-spin Fe^{III} complexes are themselves unstable and decompose even under vacuum.[60] However, $[Fe^{III}(S_2PR_2)_3]$ (R=Ph, Cy) reacts with pyridine as shown.[61]

$$2[Fe^{III}(S_2PR_2)_3] + 4py \longrightarrow 2[Fe(S_2PR_2)_2(py)_2] + R_2P(S)PSS(S)PR_2 \qquad [1.13]$$

The tris-dithiolate species, $[Ru(S_2PR_2)_3]$ (R=Et,[59] Ph,[62,63] *p*-ethylphenyl, 3,4-dimethylphenyl,[64]), have been prepared and characterised by electronic and e.s.r. spectroscopy, and by magnetic measurements.

No binary complexes of dithiophosphinate ligands with osmium have been reported.

1.3 Complexes with group Vb ligands.

The versatility of the dithiolate ligands is reflected in the diversity of transition-metal complexes that they form with other ligands.

Pignolet and co-workers prepared the seven co-ordinate complex, $[Ru(PPh_3)(S_2CNR_2)_3]Cl$ (R=Me, Et) from $[Ru(S_2CNR_2)_3Cl]$ and triphenylphosphine.[65]

Wilkinson *et. al.* prepared $[Ru(S_2CNR_2)_2(PPh_3)_2]$ from $[RuCl_2(PPh_3)_3]$ and $Na[S_2CNR_2]$.[66] Stephenson and co-workers then synthesised a range of complexes of general formula *cis*-$[Ru(S\text{-}S)_2L_2]$ (S-S=$^-S_2PR_2$, $^-S_2CNR_2$; L=tertiary phosphine) by reaction of various Ru^{II} and Ru^{III} tertiary phosphine complexes with salts of the appropriate dithiolato ligand (see Figure 1.3).[67-74] Variable temperature ^1H n.m.r. spectroscopy confirms the *cis*-configuration of the $[Ru(S\text{-}S)_2L_2]$ complexes and the temperature dependent behaviour of the dithiophosphinate complexes was shown to result from facile interconversion of optical enantiomers; the spectral changes observed for the dithiocarbamate complexes arise from restricted rotation about the C-N bond.[71]

Cole-Hamilton and Stephenson determined rate constants and the associated activation parameters for the optical isomerism of $[Ru(S_2PMe_2)_2L_2]$ (L=PPh_3, $PMePh_2$, PMe_2Ph, $P\{OMe\}_3$, $P\{OPh\}_3$) by line-shape analysis of the temperature dependent ^1H n.m.r. spectra.[75] The authors

$[RuCl_2(PPh_3)_3]$ + $^-S\text{-}S$	$\longrightarrow$	$[Ru(S\text{-}S)_2(PPh_3)_2]$	$^-S\text{-}S=^-S_2CNR_2$, R=Me, Et, Ph.[66] $^-S_2PR_2$, R=Me, Ph.[71]
$[OsCl_2(PPh_3)_3]$ + $^-S\text{-}S$	$\longrightarrow$	$[Os(S\text{-}S)_2(PPh_3)_2]$	$^-S\text{-}S=^-S_2CNR_2$, R=Me, Et.[78] $^-S_2PR_2$, R=Me, Ph.[80]
$[RuCl_3(PR_3)_3]$ + $^-S\text{-}S$	$\longrightarrow$	$[Ru(S\text{-}S)_2(PR_3)_2]$	PR_3=$PMePh_2$, $^-S\text{-}S=^-S_2PR_2$, R=Me, Ph.[71] PR_3=PMe_2Ph, $^-S\text{-}S=^-S_2PR_2$, R=Me, Et, Ph.[71]
$[OsCl_3(PMe_2Ph)_3]$ + $^-S\text{-}S$	$\longrightarrow$	$[Os(S\text{-}S)_2(PMe_2Ph)_2]$	$^-S\text{-}S=^-S_2CNMe_2$, $^-S_2PR_2$, R=Me, Ph.[79]
$[RuCl_2(P\{OR\}_3)_4]$ + $^-S\text{-}S$	$\longrightarrow$	$[Ru(S\text{-}S)_2(P\{OR\}_3)_2]$	R=Me, Ph; $^-S\text{-}S=^-S_2PMe_2$.[71]
$[RuCl_3(PPh_3)_2(MeNO_2)]$ + $^-S\text{-}S$	$\longrightarrow$	$[Ru(S\text{-}S)_2(PPh_3)_2]$	$^-S\text{-}S=^-S_2PMe_2$.[71]
$[Ru_2Cl_3(PMePh_2)_6]^+$ + $^-S\text{-}S$	$\longrightarrow$	$[Ru(S\text{-}S)_2(PMePh_2)_2]$	$^-S\text{-}S=^-S_2PMe_2$.[71]
$[Ru(diene)(S\text{-}S)_2]$ + P-P	$\longrightarrow$	$[Ru(S\text{-}S)_2(P\text{-}P)]$	diene=cod, nbd; P-P=dppm, dppe $^-S\text{-}S=^-S_2PMe_2$,[76] $^-S_2CNMe_2$.[77]

Figure 1.3 Preparative routes to bis(dithiolate)bis(phosphine)M(II) complexes.

proposed that the mechanism of optical isomerism proceeds by solvent assisted cleavage of a Ru-S bond *trans* to L (see Figure 1.4).

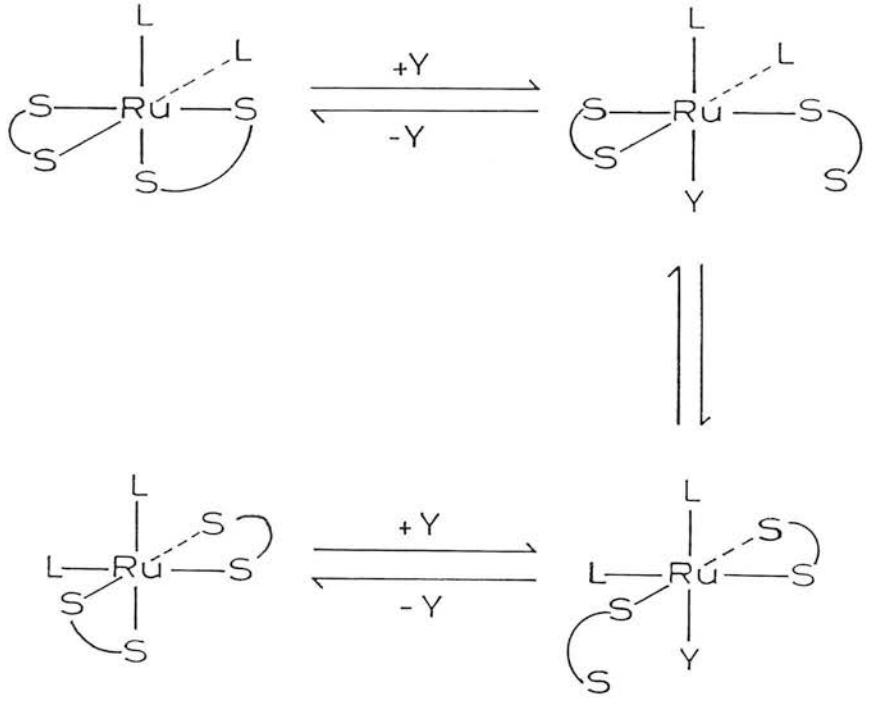

Figure 1.4: Optical isomerisation of $[Ru(S_2PMe_2)_2L_2]$.

In most cases *cis*-$[Ru(S\text{-}S)_2L_2]$ is the only product formed. However, in the reaction of *cis*-$[RuCl_2(PMe_2Ph)_4]$ and $[RuCl_2(P\{OR\}Ph_2)_3]$ with dithio-acids, the product isolated depends on the reaction conditions [1.14-1.18].[73,74]

$$[RuCl_2(PMe_2Ph)_4] + Na[S_2PMe_2] \xrightarrow[EtOH]{reflux} [Ru(S_2PMe_2)_2(PMe_2Ph)_2] \quad [1.14]$$

$$[RuCl_2(PMe_2Ph)_4] + Na[S_2PMe_2] \xrightarrow[C_6H_6]{shake} [RuCl(S_2PMe_2)(PMe_2Ph)_3] \quad [1.15]$$

$$[RuCl_2(PMe_2Ph)_4] + Na[S_2CNMe_2] \xrightarrow[EtOH]{reflux} [Ru(S_2CNMe_2)_2(PMe_2Ph)_2] \quad [1.16]$$

$$[RuCl_2(PMe_2Ph)_4] + Na[S_2CNMe_2] \xrightarrow[BPh_4^-,EtOH]{shake} [Ru(S_2CNMe_2)(PMe_2Ph)_4]BPh_4 \quad [1.17]$$

$$[RuCl_2(PMe_2Ph)_4] + Na[S_2CNMe_2] \xrightarrow[shake]{C_6H_6} [Ru(S_2CNMe_2)_2(PMe_2Ph)_3] \quad [1.18]$$

The isolation of these intermediates allowed Sime and Stephenson to formulate a mechanism for the reaction of $[RuCl_2(PR_3)_3]$ and $[RuCl_2(PR_3)_4]$ with dithiolate ligands (see Figure 1.5).[74]

The $[Ru(S\text{-}S)_2L_2]$ complexes readily undergo exchange reactions with phosphines of greater basicity (L') to yield $[Ru(S\text{-}S)_2LL']$ and/or $[Ru(S\text{-}S)_2L'_2]$.[71] The analogous diphosphine complexes, $[Ru(S\text{-}S)_2(P\text{-}P)]$ ($S\text{-}S=^-S_2PR_2$, R=Me, Ph,[76] $^-S_2CNEt_2$[77]; P-P=dppm, dppe), were prepared by displacing the diene from the complexes $[Ru(S\text{-}S)_2(diene)]$ (diene=cod, nbd).

Carbonylation of $[Ru(S_2PR_2)_2L_2]$ (R=Me, Ph; L=PPh_3, $PMePh_2$, PMe_2Ph) yields only *cis*-$[Ru(S_2PR_2)_2L(CO)]$ for most combinations of phosphine and dithiolate.[70,71] However, for $[Ru(S_2PR_2)_2(PMe_2Ph)_2]$ (R=Me, Ph), in addition to $[Ru(S_2PR_2)_2(PMe_2Ph)(CO)]$, two isomers of formula $[Ru(S_2PR_2)_2(PMe_2Ph_2)_2CO]$ have been characterised and a

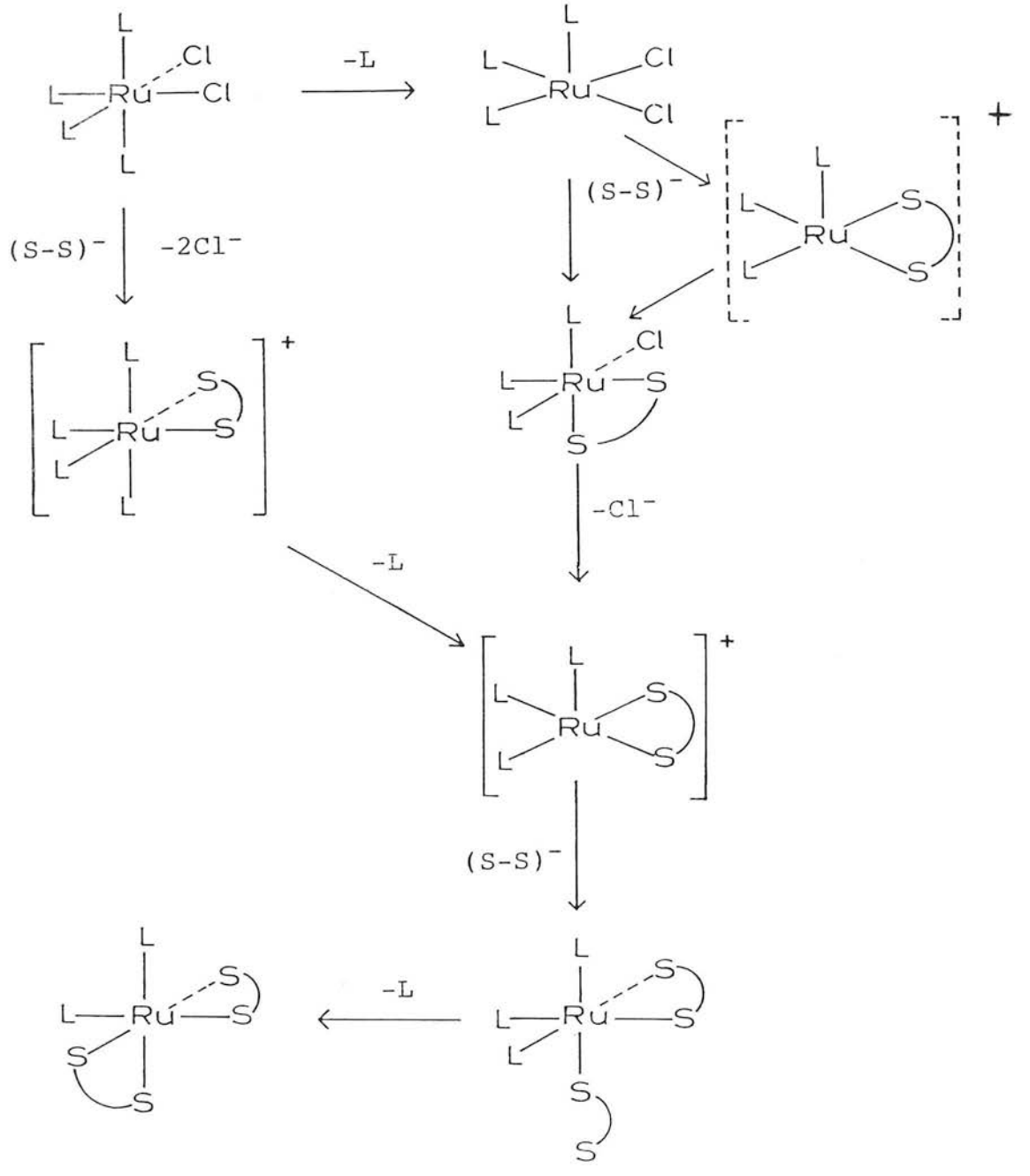

Figure 1.5: Mechanism for the reaction of $[RuCl_2L_{3,4}]$ (L=tertiary phosphine) with 1,1-dithiolate ligands.[74]

mechanism of carbonylation for $[Ru(S_2PR_2)_2(PMe_2Ph)_2]$ proposed :-

$$[Ru(S_2PR_2)_2(PMe_2Ph)_2] + CO \xrightarrow{\text{fast}} [Ru(S_2PR_2)_2(PMe_2Ph)_2(CO)]$$

$$[Ru(S_2PR_2)_2(PMe_2Ph)(CO)] + PMe_2Ph \underset{\text{slow}}{\overset{\text{slow}}{\rightleftharpoons}} [Ru(S_2PR_2)_2(PMe_2Ph)_2(CO)] \quad [1.19]$$

The complexes, $[Ru(S_2CNR_2)_2L_2]$, are resistant to carbonylation[71]; however, $[Ru(S_2CNR_2)_2(PPh_3)(CO)]$ (R=Me, Et) has been prepared from $[RuCl(OCOMe)(CO)(PPh_3)_2]$ and $Na[S_2CNR_2]$.[78]

$[Os(S_2CNR_2)_2(PPh_3)_2]$ has been prepared by Critchlow and Robinson from $[OsH(OCOMe)(PPh_3)_3]$ and $Na[S_2CNR_2]$ (R=Me, Et).[78] Cole-Hamilton and Stephenson examined[79] the reaction of *mer*-$[OsCl_3(PMe_2Ph)_3]$ with 1,1-dithiolates and found that the reaction is sensitive to the conditions employed:-

$$[OsCl_3(PMe_2Ph)_3] + Na[S_2CNEt_2] \xrightarrow[MeOH]{\text{reflux}} [Os(S_2CNEt_2)_2(PMe_2Ph)_2] \quad [1.20]$$

$$[OsCl_3(PMe_2Ph)_3] + Na[S_2CNEt_2] \xrightarrow[MeOH]{\text{shake}} [Os(S_2CNEt_2)Cl(PMe_2Ph)_3] \quad [1.21]$$

As observed for $[RuCl_3(PMe_2Ph)_3]$, carbonylation of $[Os(S_2PMe_2)_2(PMe_2Ph)_2]$ in refluxing ethanol afforded both $[Os(S_2PR_2)_2(PMe_2Ph)(CO)]$ and $[Os(S_2PR_2)_2(PMe_2Ph)(CO)]$. Duncan later prepared $[Os(S_2PR_2)_2(PPh_3)_2]$ (R=Me, Ph) from $[OsCl_2(PPh_3)_3]$ and $Na[S_2PR_2]$.[80]

1.4 Complexes with nitrosyl and carbonyl ligands.

The formally Fe(I) complexes, $[Fe(NO)(S_2CNR_2)_2]$ (R=Me, Et, Pr^i), have been prepared.[81-83] Crystallographic studies of $[Fe(NO)(S_2CNR_2)_2]$ (R=Me,[84,85] Et,[86] Pr^i [87]) show that the ligands display square pyramidal co-ordination around the metal centre. At 193K the methyl derivative exhibits an Fe-N-O bond angle of 170° and an average Fe-S bond length of 2.30Å.[85] The deviation from linearity is attributed to an interaction between a lone pair of the oxygen atom and a nitrogen of the dithiocarbamate ligand. Infrared and e.s.r. studies show that co-ordination of solvent occurs in solutions of $[Fe(NO)(S_2CNR_2)_2]$.[88,89] These complexes react with one-electron donors to afford the adduct, $[Fe(NO)X(S_2CNR_2)_2]$ (X=I, Br, NO_2).[90]

The ruthenium complexes, $[Ru(NO)(S_2CNR_2)_3]$, are prepared by reaction of $[Ru(S_2CNR_2)_3]$ with nitric oxide or from $Na[S_2CNR_2]$ and $K_2[RuNO(CN)_5]$.[91] The subsequent crystal structure of $[Ru(NO)(S_2CNEt_2)_3]$ revealed that this complex contains a monodentate dithiocarbamate ligand.[92]

The species, $[Fe(CO)_2(S_2CNR_2)_2]$ and $[Fe(CO)_3I(S_2CNR_2)]$, are prepared from reaction of $Na[S_2CNR_2]$ with $[Fe(CO)_4Br_2]$ and $[Fe(CO)_3I_2]$ respectively.[93,94]

Kingston and Wilkinson prepared[95] $[Ru(S_2CNR_2)_2(CO)_2]$ and $[Ru(S_2CNR_2)_2(CO)]$ (R=Me, Et) by reaction of $Na[S_2CNR_2]$ with the red carbonylated "ruthenium trichloride" solution.[96] The latter complex was later shown (by

crystallography) to be the dimeric species, $[Ru(S_2CNEt_2)_2(CO)]_2$ [1.22].[97] The ruthenium atoms are six co-ordinate, but distorted from octahedral with two bridging sulphur atoms. The Ru-Ru distance is 3.65Å (compared with 2.79Å in $[Ru_2(S_2CNPr^i_2)_5]^+$)[39] suggesting no metal-metal interaction; Ru-C=1.80Å; average Ru-S distance=2.40Å.

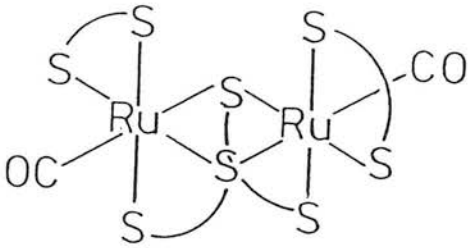

[1.22]

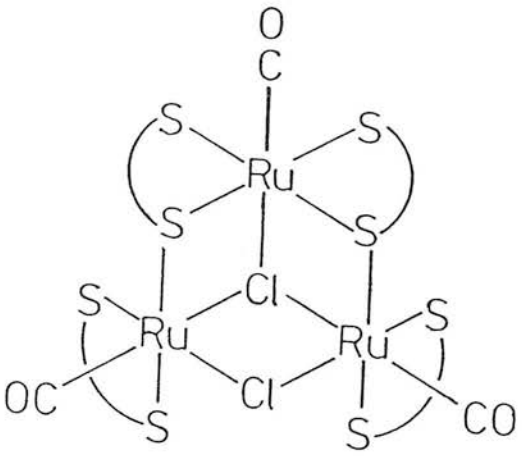

[1.23]

Prolonged treatment of the carbonylated ruthenium solution with $Na[S_2CNMe_2]$ affords very small quantities of the trinuclear species, $[Ru_3(S_2CNEt_2)_4(CO)_3Cl_2]$ [1.23], which was characterised by an X-ray diffraction study.[98]

The cluster compounds, $[Os_3H(S_2CNEt_2)(CO)_x]$ (x=10, 9), have been reported.[99] For x=10, the dithiocarbamate ligand is co-ordinated in a uni-dentate manner to one metal atom; thermal decarbonylation of this species affords the latter (x=9) complex in which the dithiolate bridges the three osmium centres.

1.5 Complexes with halogen ligands.

The Fe^{III} complexes of general formula, $[Fe(S_2CNR_2)_2X]$, have been prepared[100]; several of these complexes have been studied by X-ray crystallography (R=Et, X=Cl,[101] Br,[102] I,[103] SCN,[104]; R=Pr^i, X=Cl[105]). In all examples reported, the co-ordination is distorted from square pyramidal with an axial halogen ligand. The iron centre lies about 0.6Å above the plane of the sulphur atoms towards the halogen atom.

The binary complexes, $[Fe(S_2CNR_2)_3]$, react with iodine to afford products of formula $[Fe(S_2CNR_2)_xI_y]$ (x=2, y=2,3[106]; x=3, y=3,5[107]) and the crystal structure of $[Fe^{IV}(S_2CNR_2)_3][I_5]$ has been reported.[108]

A seven co-ordinate complex, $[Ru(S_2CNR_2)_3Cl]^-$ (R=Me, Et), is prepared from $[Ru^{III}(S_2CNR_2)_3]$ by photolysis in chlorinated solvents, or reaction with HCl in benzene.[109] The subsequent X-ray diffraction study of $[Ru(S_2CNEt_2)_3Cl]^-$ revealed that the geometry of the complex is distorted pentagonal bipyramidal with S-Ru-S angles in the pentagonal base ranging from 79.0 to 69.3°.

The Ru-S bond lengths are comparable to other dithiocarbamate complexes of ruthenium. The ^1H n.m.r. of $[Ru(S_2CNEt_2)_3Cl]^-$ shows one ethyl resonance (even at 183K) implying that the molecule exhibits fluctionality[109] Similarly, the complexes, $[M(S_2CNEt_2)_3I_3]$ (M=Fe, Ru), are are prepared from $[M^{III}(S_2CNR_2)_3]$ and iodine.[65]

1.6 Complexes with other ligands.

Pignolet and co-workers have prepared and structurally characterised (by crystallography) the novel sulphur (and selenium) rich binuclear complexes, $[Os_2(S_3CNR_2)_2(S_2CNR_2)_3]^+$, $[Os_2(SeS_2CNR_2)_2(S_2CNR_2)_3]^+$, $[Os_2(S_5)(S_3CNR_2)(S_2CNR_2)_3]^+$ and the nitrido-bridged species, $[Os_2(\mu\text{-}N)(S_2CNR_2)_5]^+$ (see Figure 1.6).[110-113] The first three adducts have Os-Os bond lengths of 2.78-2.84Å, consistent with a metal metal bond.[111]

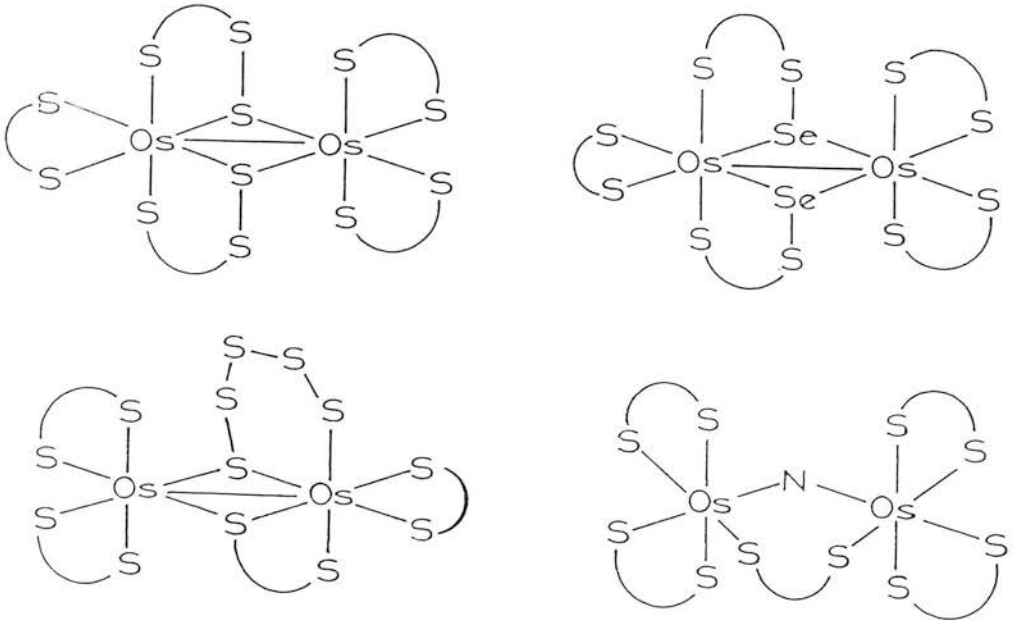

Figure 1.6: Binuclear adducts of dithiocarbamate ligands.

References

1. D. Coucouvanis, *Prog. Inorg. Chem.*, 1970, **11**, 233 and 1979, **26**, 301.

2. R. P. Burns, A. P. McCullough and C. A. McAuliffe, *Adv. Inorg. Chem. Radiochem.*, 1979, **22**, 303.

3. J. R. Wasson, G. M. Woltermann and H. J. Stoklosa, *Fortsch. Chem. Forschung*, 1973, **35**, 65.

4. R. Eisenberg, Prog. *Inorg. Chem.*, 1970, **12**, 295.

5. J. M. Allison, T. A. Stephenson and R. O. Gould, *J. Chem. Soc., A*, 1971, 3690.

6. G. St. Nikolov, *Inorg. Nucl. Chem. Lett.*, 1971, **7**, 1213.

7. D. C. Braddley and M. H. Gitlitz, *J. Chem. Soc., A*, 1969, 1152.

8. G. Contreras and R. Schmidt, *J. Inorg. Nucl. Chem.*, 1970, **32**, 127.

9. J. C. Winjhoven, Th. E. M. Van Den Hark and P. T. Beurskens, *J. Cryst. Molec. Structure*, 1972, **2**, 189.

10. J. P. Fackler, A. Avdeef and R. G. Fischer, *J. Am. Chem. Soc.*, 1973, **95**, 774.

11. J. Willemse and J. A. Cras, *Recl. Trav. Chim. Pays-Bas.*, 1971, **90**, 377.

12. T. R. Reddy and R. Srinivasan, *J. Chem. Phys.*, 1965, **43**, 1404.

13. J. P. Fackler and D. G. Holah, *J. Inorg. Nucl. Chem. Lett.*, 1966, **2**, 251.

14. R. G. Cavell, E. D. Day and W. Byers, *Inorg. Chem.*, 1972, **11**, 1759.

15. W. Kuchen and A. Judat, *Chem. Ber.*, 1967, **100**, 991.

16. J. Chatt, L. A. Duncanson and L. M. Venanzi, *Nature*, 1956, **177**, 1042.

17. J. Chatt, L. A. Duncanson and L. M. Venanzi, *Suomen Kimistilehte*, 1956, **298**, 75. From *Chem. Abstracts*, 1957, **51**, 5559d.

18. L. F. Larkworthy, B. W. Fitzsimmons and R. R. Patel, *J. Chem. Soc., Chem. Commun.*, 1973, 902.

19. O. A. Ileperuma and R.D Feltham, *Inorg. Chem.*, 1975, **14**, 3042.

20. R. L. Martin and A. H. White, *Transit. Met. Chem.*, 1968, **4**, 113.

21. A. H. Eward, R. L. Martin, I. G. Ross and A. H. White, *Proc. Roy. Soc., London, Ser. A*, 1964, **280**, 235.

22. A. H. White, R. L. Martin, E. K. Sinn and A. H. White, *Inorg. Chem.*, 1969, **8**, 1837.

23. A. H. White, E. Kokut, R. Kuper, H. Waterman and R. L. Martin, *Aust. J. Chem.*, 1964, **17**, 294.

24. B. F. Hoskins and B. P. Kelly, *J. Chem. Soc., Chem. Commun.*,1968, 1517.

25. P. C. Healy and A. H. White, *J. Chem. Soc., Dalton Trans.*, 1972, 1163.

26. P. C. Healy and A. H. White, *J. Chem. Soc., Chem. Commun.*, 1971, 1446.

27. J. G. Leipoldt and P. Coppens, *Inorg. Chem.*, 1973, **12**, 2269.

28. E. A. Pasek and D. K. Straub, *Inorg. Chem.*, 1972, **11**, 259.

29. R. L. Martin, N. M. Rhode, G. B. Robertson and D. Taylor, *J. Am. Chem. Soc.*, 1974, **91**, 3647.

30. R. Chant, A. R. Hendrickson, R. L. Martin and N. M. Rhode, *Inorg. Chem.*, 1975, **14**, 1894.

31. A. R. Hendrickson, R. L. Martin and N. M. Rhode, *Inorg. Chem.*, 1974, **13**, 1933.

32. R. Chant, A. R. Hendrickson, R. L. Martin and N. M. Rhode, *Aust. J. Chem.*, 1973, **26**, 2533.

33. L. Malatesta, *Gazz. Chim. Ital.*, 1938, **68**, 195. From *Chem. Abstracts*, 1938, **32**, 7364.

34. D. J. Duffy and L. H. Pignolet, *Inorg. Chem.*, 1974, **13**, 2045.

35. L. H. Pignolet, *Inorg. Chem.*, 1974, **13**, 2051.

36. C. L. Raston and A. H. White, *J. Chem. Soc., Dalton Trans.*, 1975, 2405.

37. G. S. Patterson and R. H. Holm, *Inorg. Chem.*, 1974, **11**, 2285.

38. B. M. Mattson, J. R. Heiman and L. H. Pignolet, *Inorg. Chem.*, 1976, **15**, 564.

39. C. L. Raston and A. H. White, *J. Chem. Soc., Dalton Trans.*, 1975, 2410.

40. C. Oldham, *Prog. Inorg. Chem.*, 1968, **10**, 223.

41. D. Coucouvanis, S. J. Lippard and J. A. Zubieta, *Inorg. Chem.* 1970, **9**, 2775.

42. A. R. Hendrickson, R. L. Martin and D. Taylor, *J. Chem. Soc., Dalton Trans.*, 1975, 2182.

43. A. R. Hendrickson and R. L. Martin, *J. Chem. Soc., Chem. Commun.*, 1974, 873.

44. A. R. Hendrickson, J. M. Hope and R. L. Martin, *J. Chem. Soc., Dalton Trans.*, 1976, 2032.

45. G. H. Wheeler, B. M. Mattson, C. L. Miessler and L. H. Pignolet, *Inorg. Chem.*, 1978, **17**, 340.

46. A. H. Dix, J. W. Diesweld and J. G. M. Van der Linden, *Inorg. Chim. Acta*, 1977, **24**, L51. R. A. Bozis, *Diss. Abstr. Int. B*, 1972, **32**, 6268. from *Chem. Absracts*, 1972, **77**, 108887y.

47. K. W. Given, S. H. Wheeler, B. S. Jick, L. J. Maheu and L. H. Pignolet, *Inorg. Chem.*, 1979, **18**, 1261.

48. S. H. Wheeler and L. H. Pignolet, *Inorg. Chem.*, 1980, **19**, 972.

49. L. Malatesta and R. Pizzotti, *Chemica e industria*, 1945, **27**, 6.

50. M. G. Gabdullin, A. R. Garifzyanov and V. F. Toropova, *Zh. Neorg. Khim.*, 1984, **29**, 29. From *Chem, Abstracts*, 1982, **101**, 199024t.

51. J. D. Lebedda and R. A. Palmer, *Spectrochim. Acta, Part A*, 1973, **29**, 1371.

52. C. K. Jorgensen, *J. Inorg. Nucl. Chem.*, 1962, **24**, 1571.

53. S. A. Cotton and J. F. Cotton, *J. Chem. Soc., A*, 1971, 803.

54. M. G. B. Drew, W. A. Hopkins, P. C. H. Mitchell and T. Colclough, *J. Chem. Soc., Dalton Trans.*, 1986, 351.

55. N. K. Shakirova, N. A. Ulakhovic, G. K. Budnikov, G.A Kutyrev and R. A. Cherkasov, *Zh. Obsch. Khim.*, 1979, **49**, 302. From *Chem. Abstracts*, 1979, **91**, 65214w.

56. C. K. Jorgensen, *Acta Chem. Scand.*, 1962, **16**, 1048.

57. L. K. Kabanova, P. M. Solozhenkin and S. V. Usova, *Izv. Akad. Nauk, Tadzh. SSR, Otd. Fiz-Mat. Geol.-Khim Nauk*, 1974, 53. From *Chem. Abstacts* 1976, **83**, 107706a.

58. L. K. Kabanova and S. V. Usova, *Zh. Anal. Khim*, 1974, **29**, 2248. From *Chem. Abstracts*, 1975, **82**, 92592s.

59. W. Kuchen and H. Hertel, *Angew. Chem., Int. Ed. (Engl.)*, 1969, **8**, 89.

60. R. G. Cavell, E. D. Day, W. Byers and P. M. Watkins, *Inorg. Chem.*, 1972, **11**, 1599.

61. R. Y. Saleh and D. K. Straub, *Inorg. Chem.*, 1974, **13**, 1559.

62. R. E. De Simone, *J. Am. Chem. Soc.*, 1973, **95**, 6238.

63. L. Ruiz-Ramirez, T. A. Stephenson and E. S. Switkes, *J. Chem. Soc., Dalton Trans.*, 1973, 1770.

64. R. N. Mukherjee and P. K. Gogoi, *Ind. J. Chem.*, 1980, **19A**, 6238.

65. K. W. Given, B. M. Mattson and L. H. Pignolet, *Inorg. Chem.*, 1976, **15**, 3152.

66. G. O'Connor, J. D. Gilbert and G. Wilkinson, *J. Chem. Soc., A*, 1969, 84.

67. T. A. Stephenson and G. Wilkinson, *J. Inorg. Nucl. Chem.*, 1966, **28**, 945.

68. T. A. Stephenson, *J. Chem. Soc., A*, 1970, 889.

69. P. W. Armit and T. A. Stephenson, *J. Organomet. Chem.*, 1973, **57**, C80.

70. D. J. Cole-Hamilton, P. W. Armit and T. A. Stephenson, *Inorg. Nucl. Chem. Lett.*, 1972, **8**, 917.

71. D. J. Cole-Hamilton and T. A. Stephenson, *J. Chem. Soc., Dalton Trans.*, 1974, 739.

72. D. J. Cole-Hamilton, T. A Stephenson and D. R. Robertson, *J. Chem. Soc., Dalton Trans.*, 1975, 1260.

73. W. J. Sime and T. A. Stephenson, *Inorg. Nucl. Chem. Lett.*, 1977, **13**, 311.

74. W. J. Sime and T. A. Stephenson, *J. Chem. Soc., Dalton Trans.*, 1978, 1647.

75. D. J. Cole-Hamilton and T. A. Stephenson, *J. Chem. Soc.*, [Dalton Trans.], 1974, 754.

76. D. J. Cole-Hamiton, T. A. Stephenson and D. R. Robertson, *J. Chem. Soc., Dalton Trans.*, 1975, 1260.

77. P. Powell, *J. Organomet. Chem.*, 1974, **65**, 89.

78. P.B. Critchlow and S. D. Robinson, *J. Chem. Soc., Dalton Trans.*, 1975, 1367.

79. D. J. Cole-Hamilton and T. A. Stephenson, *J. Chem. Soc., Dalton Trans.*, 1976, 2396.

80. J. A. S. Duncan, PhD Thesis, University of Edinburgh, 1983.

81. N. S. Garif'yanov and S. A. Luchkina, *Str. Mol. Kvantovaya Khim.*, 1971, **74**, 62. From *Chem. Abstracts*, 1971, **74** 150585m.

82. J. F. Gibson, *Nature*, 1962, **196**, 64.

83. G. A. Brewer, R. J. Butcher, B. Letafat and E. K. K. Sinn, *Inorg. Chem.*, 1983, **22**, 371.

84. G. R. Davies, R. H. B. Mais and P. G. Owston, *J. Chem. Soc., Chem. Commun.*, 1968, 81.

85. G. R. Davies, J. A. J. Jarvis, B. T. Kilbourn, R. H. B. Mais and P. G. Owston, *J. Chem. Soc., A*, 1970, 1275.

86. M. Colapietro, A. Domenicano, L. Scaramuzza, A. Vaciago and L. Zambonelli], *J. Chem. Soc., Chem. Commun.*, 1967, 583.

87. R. J. Butcher and E. K. K. Sinn, *Inorg. Chem.*, 1980, **19**, 3622.

88. D. M. Adams, *J. Chem. Soc., A*, 1969, 87.

89. C. M. Guzy, J. B. Raynor and M. R. C. Symons, *J. Chem. Soc., A*, 1969, 2987.

90. H. Buettner and R. D. Feltham, *Inorg. Chem.*, 1972, **11**, 971.

91. L. Cambi and L. Malatesta, *Rend. 1st. Lombardo Sci.*, 1938, **71**, 118. From *Chem. Abstracts*, 1940, **34**, 3200.

92. A. Domeniciano, A. Vaciago, L. Zambonelli, P. L. Loader and L. M. Venanzi, *J. Chem. Soc., Chem. Commun.*, 1966, 476.

93. F. A. Cotton and J. A. M^{c}Cleverty, *Inorg. Chem.*, 1964, **3**, 1398.

94. E. W. Abel and M. O. Dunster, *J. Chem. Soc., Dalton Trans.*, 1973, 98.

95. J. V. Kingston and G. Wilkinson, *J. Inorg. Nuclear Chem.*, 1966, **28**, 2709.

96. J. Chatt and B. L. Shaw, *J. Chem. Soc.*, 1964, 3466.

97. C. L. Raston and A. H. White, *J. Chem. Soc., Dalton Trans.*, 1975, 2418.

98. C. L. Raston and A. H. White, *J. Chem. Soc., Dalton Trans.*, 1975, 2422.

99. A. J. Arce, A. J. Deeming, S. Donovan-Mtunzi and S. E. Kabir, *J. Chem. Soc., Dalton Trans.*, 1985, 2479.

100. H. H. Wickman and A. M. Trazzolo, *Inorg. Chem.*, 1968, **7**, 63.

101. B. F. Hoskins and A. H. White, *J. Chem. Soc., A*, 1970, 1668.

102. G. E. Chapps, S. W. M^{c}Cann, H. H. Wickman and R. C. Sherwood, *J. Chem. Phys.*, 1974, **60**, 990.

103. P. C. Healy, A. H. White and B. F. Hoskins, *J. Chem. Soc., Dalton Trans.*, 1972, 1369.

104. C. L. Raston, W. G. Sly and A. H. White, *Aust. J. Chem.*, 1980, **33**, 221.

105. P. C. Christidis, P. J. Rentzeperis, F. Vakoulis and C. A. Tsipis, *Inorg. Chim. Acta*, 1984, **83**, 87.

106. E. A. Pasek and D. K. Straub, *Inorg. Chim. Acta*, 1977, **21**, 23.

107. D. Petridis, A Kostikas, A Simopoulos and D. Niarchos, *Inorg. Chem.*, 1982, **21**, 766.

108. G. L. Raston, A. H. White, D. Petridis and D. Taylor, *J. Chem. Soc., Dalton Trans.*, 1980, 1928.

109. B. M. Mattson and L. H. Pignolet, *Inorg. Chem.*, 1977, **16**, 487.

110. L. J. Maheu and L. H. Pignolet, *Inorg. Chem.*, 1979, **18**, 3626.

111. L. J. Maheu, G. L. Miesler, J. Berry, M. Burow and L. H. Pignolet, *Inorg. Chem.*, 1983, **22**, 405.

112. L. J. Maheu and L. H. Pignolet, *J. Am. Chem. Soc.*, 1980, **102**, 6346.

113. K. W. Given and L. H. Pignolet, *Inorg. Chem.*, 1977, **16**, 2983.

Chapter 2

Preparation and characterisation of diethyldithiophosphate complexes of ruthenium and osmium.

2.1 Introduction.

Many dithiolate complexes of the iron triad have been prepared (see Chapter 1). The majority of these are concerned with dithiocarbamate ($^-S_2CNR_2$), xanthate (^-S_2COR) or dithiophosphinate ($^-S_2PR_2$) ligands. Only a few dithiophosphate ($^-S_2P\{OR\}_2$) species have been prepared with these metals, and the purpose of the work described in this Chapter was to extend the chemistry of ruthenium and osmium with this ligand.

2.2 Preparation of $[Ru(S-S)_3]$ complexes.

Complexes of general formula, $[M(S-S)_3]$ (M=Fe, Ru, Os; S-S=$^-S_2CNR_2$, $^-S_2PR_2$), have previously been synthesised by the reaction of metal halides with the dithio-acid or alkali metal salt of the dithiolate.[1,2] By this method Jorgensen prepared $[Ru(S_2P\{OEt\}_2)_3]$ in low yield using a multi-stage synthetic route.[3] The complex prepared in this way decomposes rapidly, but can be stabilised by co-crystallisation with $[In(S_2P\{OEt\}_2)_3]$. The recently reported preparation of $[Fe(S_2P\{OEt\}_2)_3]$ has suggested that the instability of such tris-dithiophosphate complexes may be due to the presence of residual acid.[4] With this in mind, we have used an alternative route to prepare $[Ru(S_2P\{OEt\}_2)_3]$ and other $[Ru(S-S)_3]$ species.

Stephenson and co-workers reported the reaction between $[RuCl_3(AsPh_3)_2L]$ ($L = CH_3OH$, $NCCH_2Ph$) or $[RuBr_4(AsPh_3)_2]^-.2$acetone and $Na[S_2PPh_2]$ in which all of the

ligands of the starting complex are displaced to afford $[Ru(S_2PPh_2)_3]$.[5] We have now used this reaction to synthesise other $[Ru(S\text{-}S)_3]$ ($S\text{-}S = {}^{-}S_2P\{OEt\}_2$; ${}^{-}S_2CNR_2$, R=Me, Et, Pr^{i}) complexes.

When $[RuCl_3(AsPh_3)_2(CH_3OH)]$ is added to a four-fold excess of $K[S_2P\{OEt\}_2]$ in acetone a characteristic raspberry-red colouration appears. After several hours stirring (to ensure complete reaction) removal of solvent and recrystallisation from n-hexane affords purple-black crystals of $[Ru(S_2P\{OEt\}_2)_3]$ in high yield (*ca.* 90%). The complex is highly soluble in non-polar solvents (e.g. n-hexane, pet-ether). The solution electronic absorption spectrum of $[Ru(S_2P\{OEt\}_2)_3]$ prepared by this method is the same as that published.[3] In contrast with Jorgensen's earlier report, we have found that solutions of $[Ru(S_2P\{OEt\}_2)_3]$ (monitored by electronic spectroscopy) are stable indefinitely, even when exposed to air.

The preparation of $[Ru(S_2P\{OEt\}_2)_3]$ in good yield has allowed us to characterise this complex by X-ray crystallography and to study its electrochemistry and spectroelectrochemistry.

2.2.1 Crystal Structure of $[Ru^{III}(S_2P\{OEt\}_2)_3]$.

Slow evaporation of solvent from n-hexane solutions of $[Ru(S_2P\{OEt\}_2)_3]$ affords purple-black crystals of the complex which are suitable for single-crystal X-ray diffraction studies. The complex crystallises in the space group $C2/c$ with four molecules per unit cell. The molecular structure of $[Ru^{III}(S_2P\{OEt\}_2)_3]$ is shown in Figure 2.1, and Table 2.1 lists selected bond lengths and angles.

The complex has imposed C_2 symmetry with the ruthenium atom and one phosphorus atom (P1 in Figure 2.1) lying on the two-fold axis. The molecule is distorted from octahedral. The unique *trans* (S-Ru-S) angles are 168.92(9) and 169.03(9)° and the ligand "bite angles" are 82.26(8) and 81.43(8)°. The distortion from octahedral co-ordination in the complexes, [M(bidentate)$_3$], can be expressed[6,7] using the "twist angle" (θ)†. This angle is 22.8° for $[Ru^{III}(S_2P\{OEt\}_2)_3]$. Twist angles of 30 and 0° are required for octahedral and trigonal prismatic geometries respectively.

The diffraction study of $[Ru^{III}(S_2P\{OEt\}_2)_3]$ is the first reported crystal structure of a *tris*-dithiophosphate

---

†The twist angle, θ, relates the upper and lower triangles of the co-ordination polyhedron (see Figure 2.2). Additionally, the compression ratio (s/h) has been used to express distortion in [M(bidentate)$_3$] complexes.[8] If s/h>1.22, then the structure is termed "compressed" and is "elongated" if s/h<1.22. Complexes which have trigonal prismatic geometry have s/h=1.0. The complex, $[Ru(S_2P\{OEt\}_2)_3]$, has a compression ratio of 1.26.

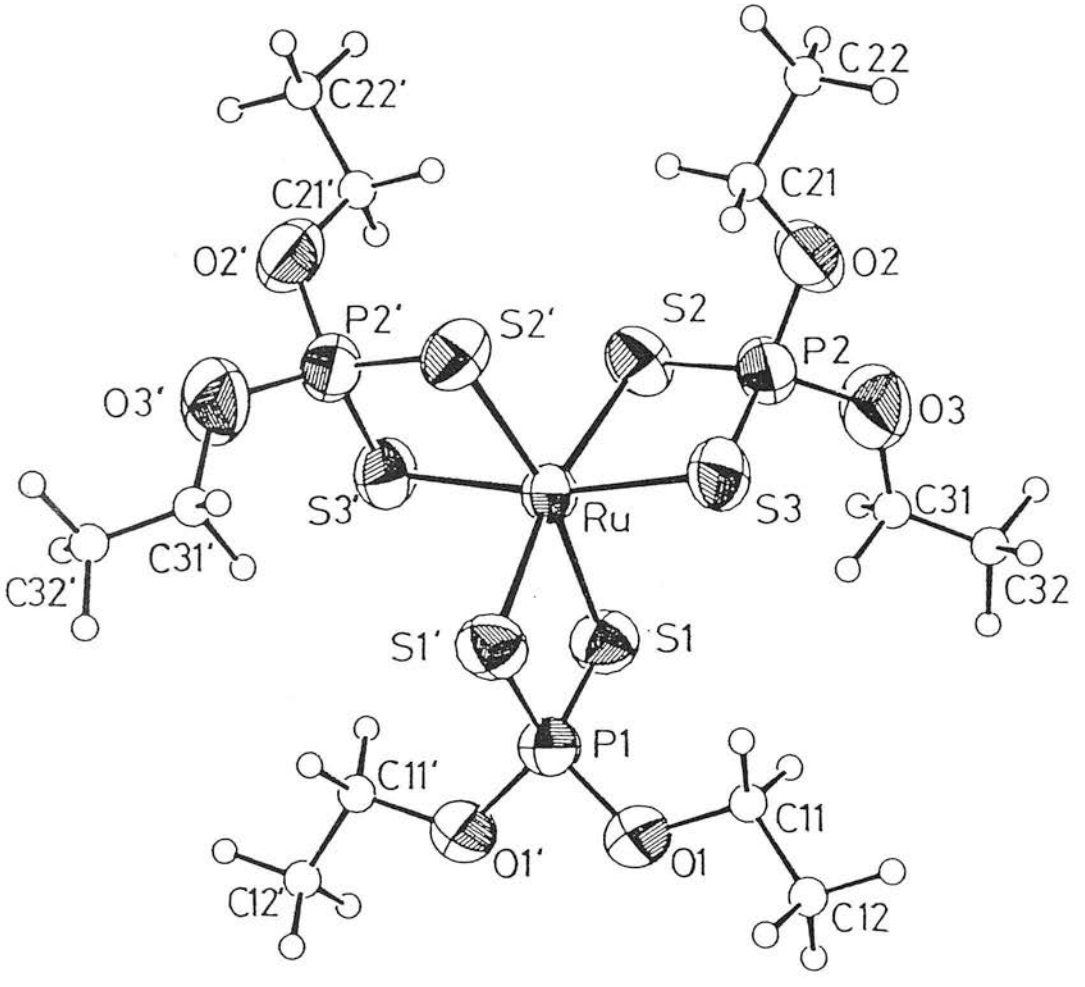

Figure 2.1: The molecular structure of $[Ru(S_2P\{OEt\}_2)_3]$.

Table 2.2: Selected bond lengths (Å) and angles (°) for $[Ru(S_2P\{OEt\}_2)_3]$.

Bond lengths (Å).

Ru	- S(1)	2.4035(25)	P(2)	- O(2)	1.564(7)
Ru	- S(2)	2.429 (3)	O(1)	- C(11)	1.457(14)
Ru	- S(3)	2.4026(25)	C(11)	- C(12)	1.390(18)
S(1)	- P(1)	2.003 (3)	O(2)	- C(21)	1.409(13)
S(2)	- P(2)	1.995 (4)	C(21)	- C(22)	1.425(15)
S(3)	- P(2)	1.995 (4)	O(3)	- C(31)	1.390(17)
P(1)	- O(1)	1.577 (7)	C(31)	- C(32)	1.292(22)
P(2)	- O(3)	1.577 (8)	S(1)	....S(1')	3.162(3)
			S(2)	....S(3)	3.152(4)

Bond Angles (°)

S(1)	- Ru	- S(1')	82.26(8)	S(1)	- P(1)	- O(1)	113.8(3)
S(2)	- Ru	- S(3)	81.43(8)	S(1)	- P(1)	- O(1')	114.7(3)
S(1)	- Ru	- S(2')	168.92(9)	S(2)	- P(2)	- O(2)	114.3(3)
S(3)	- Ru	- S(3')	169.03(9)	S(2)	- P(2)	- O(3)	114.7(3)
S(1)	- Ru	- S(2)	91.56(8)	S(3)	- P(2)	- O(2)	114.2(3)
S(1)	- Ru	- S(3)	97.99(8)	S(3)	- P(2)	- O(3)	113.8(3)
S(1)	- Ru	- S(3')	90.29(8)	O(1)	- P(1)	- O(1')	96.1(3)
S(2)	- Ru	- S(2')	95.94(9)	O(2)	- P(2)	- O(3)	95.9(4)
S(2)	- Ru	- S(3')	91.20(8)	P(1)	- O(1)	- C(11)	120.4(6)
S(1)	- P(1)	- S(1')	104.24(13)	P(2)	- O(2)	- C(21)	123.1(7)
S(2)	- P(1)	- S(3)	104.34(15)	P(2)	- O(3)	- C(31)	124.4(8)
Ru	- S(1)	- P(1)	86.76(10)	O(1)	- C(11)	- C(12)	109.8(10)
Ru	- S(2)	- P(2)	86.71(12)	O(2)	- C(21)	- C(22)	110.9(9)
Ru	- S(3)	- P(2)	87.44(12)	O(3)	- C(31)	- C(32)	118.9(13)

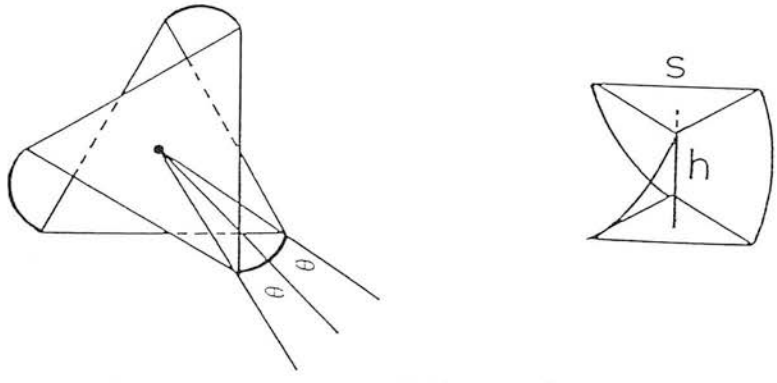

Figure 2.2: θ , s and h for [M(bidentate)$_3$] complexes.

complex with a second-row transition element. The *C2/c* space group and other features of $[Ru(S_2P\{OEt\}_2)_3]$ are common to other $[M^{III}(S_2P\{OR\}_2)_3]$ (M=Cr,[9] V,[10] R=Et; M=Co, R=Me[11]; M=Fe, R=Pr^i[4]) complexes which have been structurally characterised and Table 2.2 lists some structural parameters for these adducts.

In all the structures of $[M(S_2P\{OR\}_2)_3]$ listed in Table 2.2, one long M-S bond (Ru-S2 in Figure 2.1) and two shorter bonds are observed. This is believed to result from the imposed symmetry of the molecule.[11]

The Fe-S bond lengths in high-spin $[Fe^{III}(S_2P\{OPr^i\}_2)_3]$ (2.461[2], 2.492[2], and 2.473[2]Å)[4] are significantly longer than the Ru-S bonds in low-spin $[Ru(S_2P\{OEt\}_2)_3]$ (2.4035[25], 2.429[3], and 2.4026[25]Å). This can be readily explained by the different spin-states of the two complexes. In the complex, $[Fe^{III}(S_2CNEt_2)_3]$, the Fe-S bond has been observed to contract by 0.05Å as the spin-state of the complex changes from predominantly high to predominantly low spin, on cooling to 79K.[12] A similar effect might therefore be expected for $[Fe^{III}(S_2P\{OPr^i\}_2)_3]$.

The Ru-S bond is, however, shorter than the V-S bonds in $[V(S_2P\{OEt\}_2)_3]$ and is comparable to the Cr-S bonds in $[Cr(S_2P\{OEt\}_2)_3]$. These results are especially significant when the ionic radius of the metal ion is considered (see Table 2.2). The relatively short Ru-S distance suggests that the M-S bond is stronger for M=Ru.

Table 2.2: Selected structural parameters for $[M(S_2P\{OR\}_2)_3]$.

M	R	r/A [a]	d^n [b]	M-S/Å	P-S/Å	S...S/Å [c]	M...P/Å [d]	α/° [e]	β/° [f]	γ/° [g]	Ref.
V	Et	0.64	2	2.435(6) 2.473(6) 2.446(5)	1.986(9) 1.971(9) 1.989(9)	3.206(11) 3.203(9)	3.004(7) 3.037(7)	82.4(3) 81.1(2)	107.7(4) 108.1(4)	165.3(3) 164.5(3)	10
Cr	Et	0.62	3	2.421(3) 2.430(3) 2.423(3)	1.995(4) 2.000(5) 1.980(4)	3.187(4) 3.199(4)	3.022(3) 3.008(3)	82.4(1) 82.5(1)	106.2(2) 107.0(2)	169.04(12) 169.50(12)	9
Fe	Pr	0.64	5	2.461(2) 2.492(2) 2.473(2)	1.998(2) 2.007(3) 1.985(2)	3.185(4) 3.239(4)	3.082(3) 3.046(3)	80.64(7) 81.50(7)	105.70(13) 108.54(11)	165.80(7) 161.12(8)	4
Ru	Et	0.69	5	2.4035(25) 2.429(3) 2.4026(25)	2.003(3) 1.995(4) 1.995(4)	3.162(3) 3.152(4)	3.040(2) 3.054(3)	82.26(8) 81.43(8)	104.24(13) 104.34(15)	168.92(9) 169.03(9)	this work
Co	Me	0.55	6	2.312(3) 2.340(3) 2.315(2)	1.986(3) 1.981(4) 1.983(4)	3.089(4) -	2.963(3) 2.952(3)	84.1(2) 84.0(1)	102.3(2) 103.5(1)	172.03(11) -	11

(a) ionic radius for M^{3+} ion; (b) d^n configuration for M^{3+}; (c) non-bonded intra-chelate S-S distance;

(d) non-bonded M-P distance; (e) the ligand bite angle; (f) the intra-chelate S-P-S angle;

(h) the unique *trans* S-M-S angles.

The average Ru-S bond is longer for $[Ru(S_2P\{OEt\}_2)_3]$ (2.41Å) than for $[Ru(S_2CNEt_2)_3]$ (2.38Å).[13] Colclough *et. al.* have reported[4] that for the complexes, $[M(S-S)_3]$ (S-S= $^-S_2P\{OR\}_2$, $^-S_2CNR_2$), a linear relationship exists between θ and (i) the M-S bond length and (ii) the "normalised bite angle".[§] However, the *tris*-dithiophosphinate and *tris*-dithiocarbamate complexes do not lie on the same line, but on parallel lines. This has been interpreted[4] as an expression of the poorer donor capacity of $^-S_2P\{OR\}_2$ compared to $^-S_2CNR_2$; the parameters calculated for $[Ru(S_2P\{OEt\}_2)_3]$ place this complex on the line computed for other $[M(S_2P\{OR\}_2)_3]$ species.

2.2.2 ^1H n.m.r. spectrum.

The ^1H n.m.r. spectrum of $[Ru(S_2P\{OEt\}_2)_3]$ exhibits contact shifted resonances at δ0.36, -0.96 and -3.11ppm (see Figure 2.3). The resonance at positive chemical shift is assigned (by intensity measurements) to the methyl protons and the other signals (of equal intensity) to the methylene protons. Pignolet *et. al.* have examined[14] the variable-temperature ^1H n.m.r. spectrum of $[Ru(S_2CNEt_2)_3]$ and shown that, in the absence of isomerisation processes, two resonances are observed for the methylene protons of the ethyl groups which are in diastereotopic environments.[15]

[§] The normalised bite angle is defined as the ratio of the S-S distance (of the chelate), to the metal-sulphur bond length.[7]

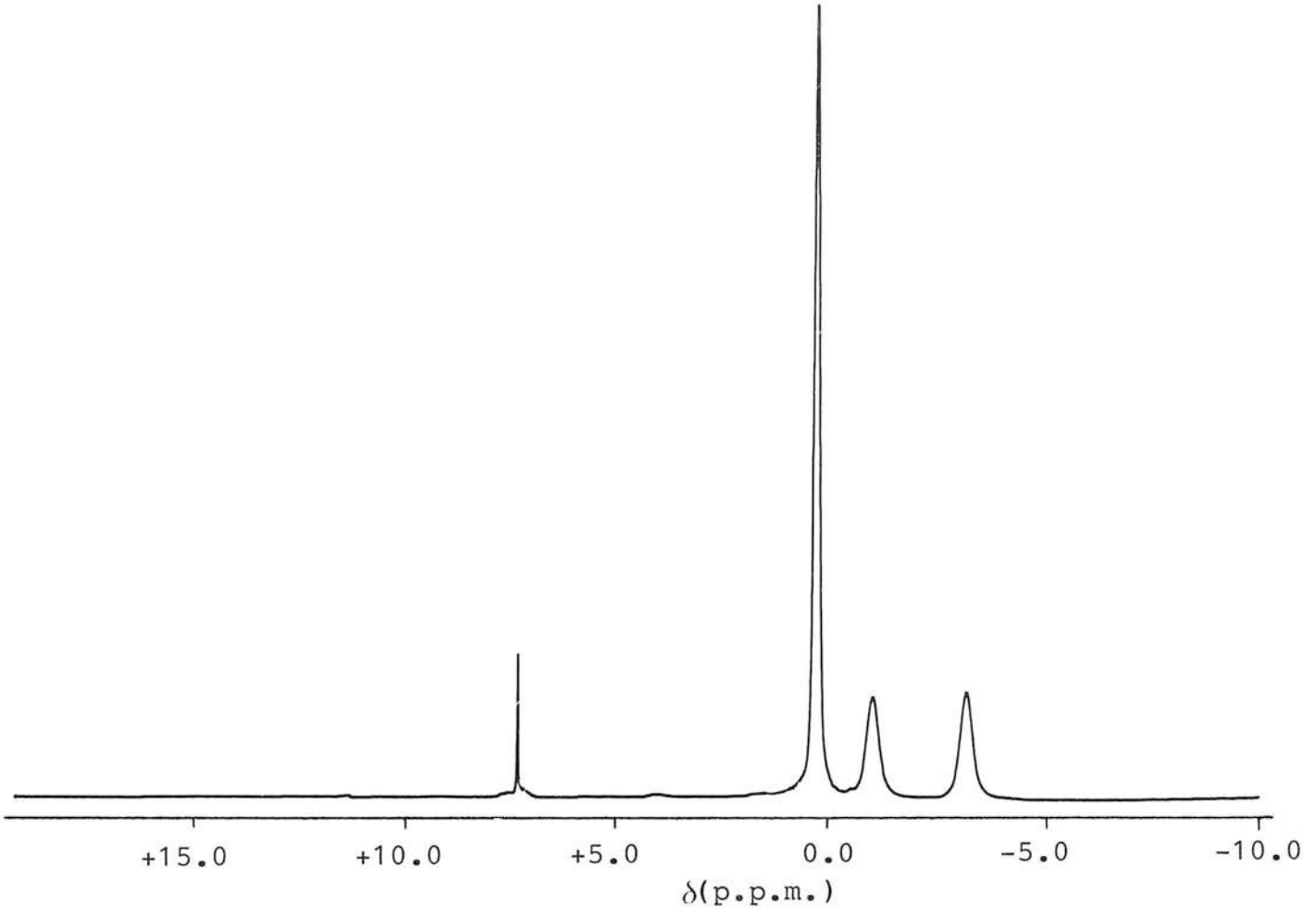

Figure 2.3: The ^{1}H n.m.r. spectrum of $[Ru(S_2P\{OEt\}_2)_3]$ ($CDCl_3$ solution, 293K).

2.2.3 Mass-Spectrum.

The FAB mass-spectrum of $[Ru(S_2P\{OEt\}_2)_3]$ exhibits parent ion peaks at 657 and 472 a.m.u. assigned to $[^{102}Ru(S_2P\{OEt\}_2)_3]^+$ and $[^{102}Ru(S_2P\{OEt\}_2)_2]^+$ respectively. Similarly, the FAB mass-spectrum of $[Ru(S_2PPh_2)_3]$ shows peaks at 849 and 600 a.m.u. resulting from the fragments, $[^{102}Ru(S_2PPh_2)_3]^+$ and $[^{102}Ru(S_2PPh_2)_2]^+$, respectively. All of these peaks show the correct isotope distribution.

2.2.4 Electrochemical studies.

The ability of the dithiocarbamate ligand to stabilize unusually high oxidation states of transition metals (see Chapter 1.1) has resulted in a detailed electrochemical study of $[Ru(S_2CNR_2)_3]$ in an attempt to prepare a stable complex of Ru^{IV}.[16,17] However, Martin *et. al.* found that electrochemical oxidation of $[Ru(S_2CNR_2)_3]$ in acetone affords (after chromatographic purification) only $[Ru(S_2CNR_2)_3]$ and α-$[Ru_2(S_2CNR_2)_5]^+$, but reported that the binuclear adduct is <u>not</u> the first oxidation product.[16] Subsequently, Pignolet and co-workers prepared the stable complex $[Ru(S_2CNR_2)_3(NCCH_3)]^+$ by electrochemical oxidation of $[Ru(S_2CNR_2)_3]$ in acetonitrile.[17] By also examining the redox behaviour of $[Ru(S_2CNR_2)_3]$ in a "weakly co-ordinating" solvent (propylene carbonate) and a "non-coordinating" solvent (methylene chloride), Pignolet proposed that a solvent- or "anion"-stabilised Ru^{IV} species is the first oxidation product of $[Ru(S_2CNR_2)_3]$.[17]

Thus, although electrochemical oxidation of $[M^{III}(S_2CNR_2)_3]$ (M=Fe, Os) does yield[18,19] the desired $[M^{IV}(S_2CNR_2)_3]^+$ complex, the analogous ruthenium species has proved elusive.[16,17] Pignolet has suggested that the isolation of the binuclear species, $[Ru_2(S_2CNR_2)_5]^+$, in preference to $[Ru^{IV}(S_2CNR_2)_3]^+$ is a result of the increased tendency towards metal-metal bonding for ruthenium.[20]

Electrochemical studies of $[Ru(S\text{-}S)_3]$ ($S\text{-}S=^-S_2PR_2$, $^-S_2P\{OR\}_2$) have not been reported in the literature. From the arguments outlined in Chapter 1.1, the $^-S_2PR_2$ and $^-S_2P\{OR\}_2$ ligands would be less likely to stabilise Ru^{IV} complexes. In order to confirm this experimentally, the redox properties of $[Ru(S_2P\{OEt\}_2)_3]$ and $[Ru(S_2PPh_2)_3]$ were examined in methylene chloride solution.

2.2.4.1 Reductive behaviour.

The cyclic voltammograms of $[Ru(S_2P\{OEt\}_2)_3]$ and $[Ru(S_2PPh_2)_3]$ recorded at 288K in methylene chloride are shown in Figure 2.4. At room temperature, the complexes, $[Ru(S_2PR_2)_3]$ (R=Ph, OEt), undergo a single reversible reduction ($E_{pf}-E_{pr}=60mV$; $i_{pf}/i_{pr}=1.0$ for $v=10\text{-}200mVs^{-1}$). Coulometric studies have shown this to be a one-electron process affording the light-brown species $[Ru(S_2PR_2)_3]^-$ which is stable under an argon atmosphere; on exposure to air the reduced species is rapidly oxidised back to $[Ru^{III}(S_2PR_2)_3]$. The one-electron reduction of $[Ru(S_2CNR_2)_3]$ has been assigned as metal-based.[16]

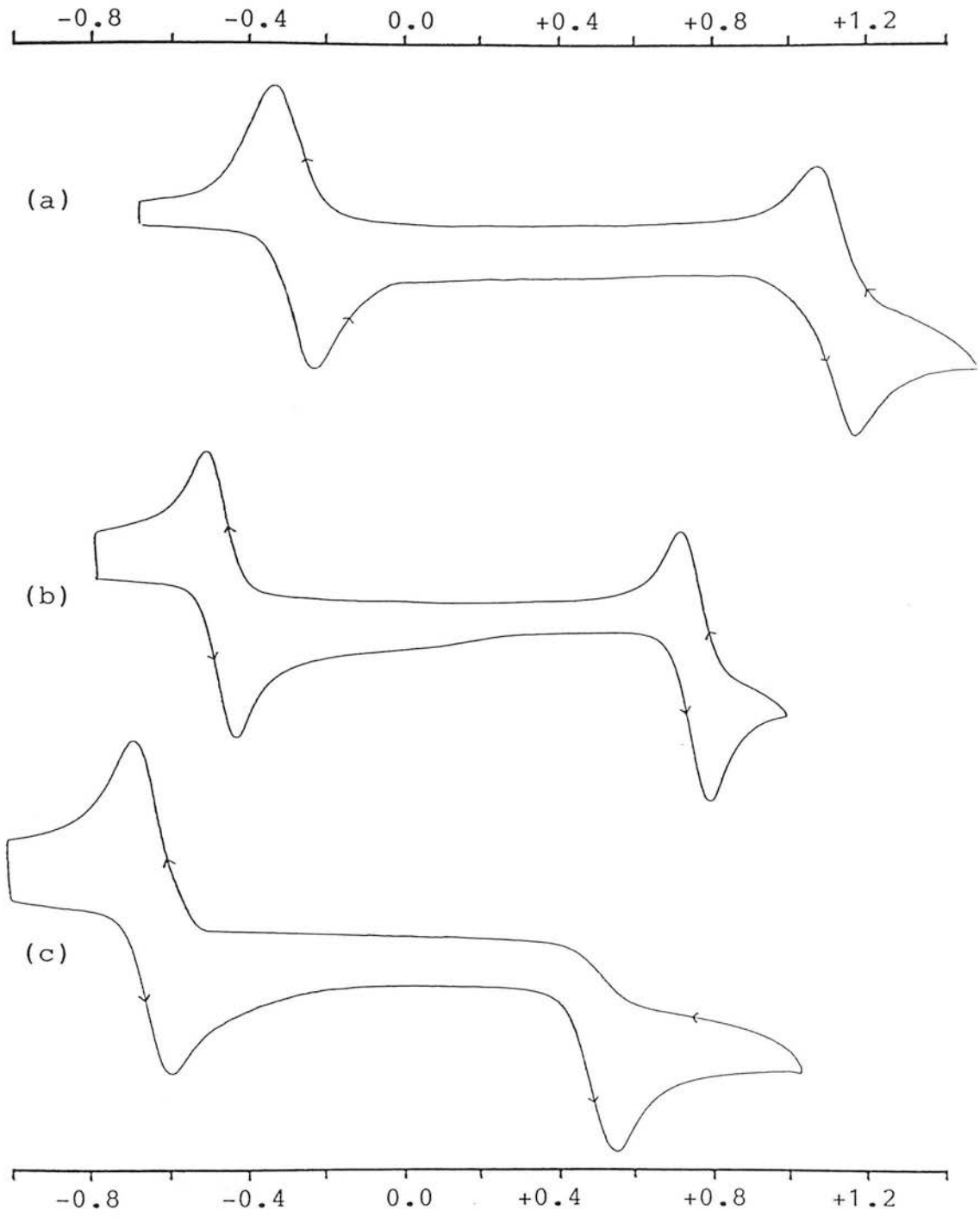

Figure 2.4: The cyclic voltamograms of (a) $[Ru(S_2P\{OEt\}_2)_3]$, (b) $[Ru(S_2PPh_2)_3]$ and (c) $[Ru(S_2CNEt_2)_3]$ measured in CH_2Cl_2 at 288K (0.5M TBA^+BF4^-).

2.2.4.2 Oxidative behaviour.

The oxidation of $[Ru^{III}(S_2PR_2)_3]$ (R=Ph, OEt) is electrochemically reversible ($E_{pf}-E_{pr}=60mV$; $i_{pf}/i_{pr}=1.0$ for $v=10-200mVs^{-1}$) in methylene chloride solution at 288K. Low temperature (T<248K) coulometry shows this process to be a one-electron oxidation of $[Ru^{III}(S_2PR_2)_3]$ to afford the violet $[Ru(S_2PR_2)_3]^+$ species.

The redox processes of $[Ru(S_2CNR_2)_3]$ are believed to be metal-based.[16,17] The ligands, $^-S_2PPh_2$ and $^-S_2P\{OEt\}_2$, are not redox-active within the potential range -1.5 to +1.5V. For these reasons we assign both redox steps of $[Ru(S_2PR_2)_3]$ (R=Ph, OEt) as metal-based.

The reversibility of the $Ru^{III/IV}$ couple is particularly interesting when compared with the analogous $[Ru(S_2CNR_2)_3]$ which exhibit[16,17] irreversible oxidations (even at low temperatures); Figure 2.4c shows the cyclic voltammogram of $[Ru(S_2CNEt_2)_3]$ in methylene chloride at 223K. The ability to stabilise higher oxidation states is expected to be (see Chapter 1.1):-

$$^-S_2CNR_2 > ^-S_2PR_2 > ^-S_2P\{OR\}_2$$

The observed reduction potentials agree with this correlation in that the $Ru^{II/III}$ couple is most negative for the dithiocarbamate complex. However, the $Ru^{III/IV}$ couple is reversible for $[Ru(S_2PR_2)_3]$ (R=Ph, OEt), and $[Ru(S_2PR_2)_3]^+$ can be reversibly electrogenerated in bulk at 250K.

The anomolous oxidative behaviour of $[Ru(S_2CNR_2)_3]$ is further highlighted by these studies which show that it is possible to generate a Ru^{IV} species for $[Ru(S-S)_3]$ (S-S=1,1-dithiolate). Further redox studies on other $[Ru(S_2PR_2)_3]$ complexes would be useful to determine if (as observed for the dithiocarbamate species)[21] the redox potentials exhibit significant dependence on the nature of the organic substituent.

2.2.5 Spectroelectrochemical studies.

The electronic absorption spectrum of $[Ru(S_2PR_2)_3]$ (R=Ph, OEt) exhibits bands of moderate intensity ($\varepsilon \simeq 10^3 cm^{-1}mole^{-1}dm^3$) between 18,000 and 24,000cm^{-1}. These bands have been assigned as resulting from charge-transfer between the metal centre and the dithiolate ligands.[3] To characterise these electronic transitions further we have examined the spectroelectrochemistry of $[Ru(S_2PR_2)_3]$ (R=Me, OEt) in methylene chloride.

Figures 2.5 and 2.6 show the electronic absorption spectra of $[Ru(S_2PR_2)_3]^{0/+1}$ (R=Ph, OEt) respectively. On oxidation, bands of greater intensity are observed at lower energy for $[Ru(S_2PR_2)_3]^+$ than for the neutral species. The general features of the absorption spectrum are very similar for both the Ru^{III} and Ru^{IV} complexes.

If the transitions observed at 18,000-24,000cm^{-1} for the neutral complex are from metal to ligand, then oxidising the metal centre would be expected to decrease

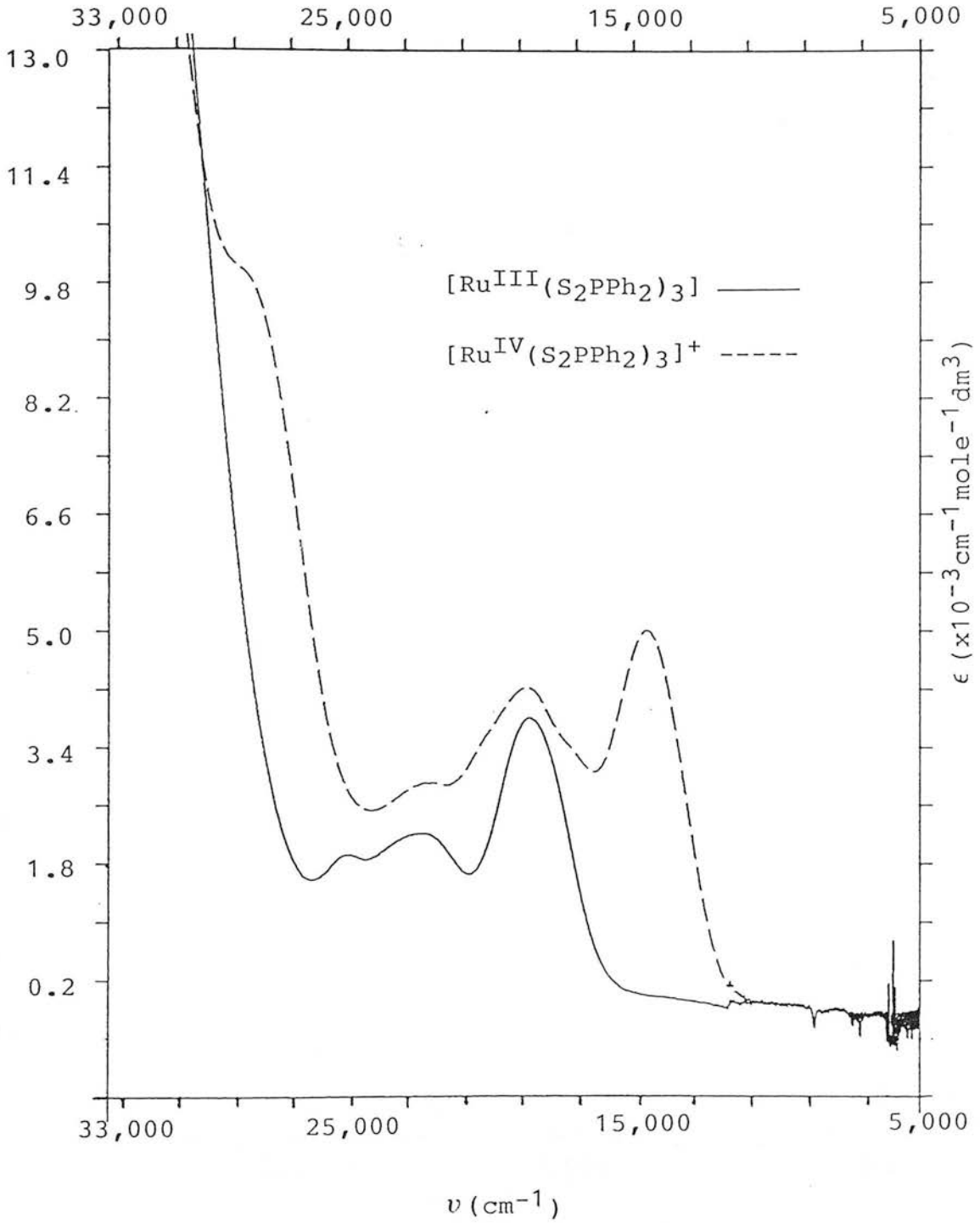

Figure 2.5: The electronic absorption spectrum of $[Ru(S_2PPh_2)_3]^{0/+1}$ in CH_2Cl_2 solution at 235K.

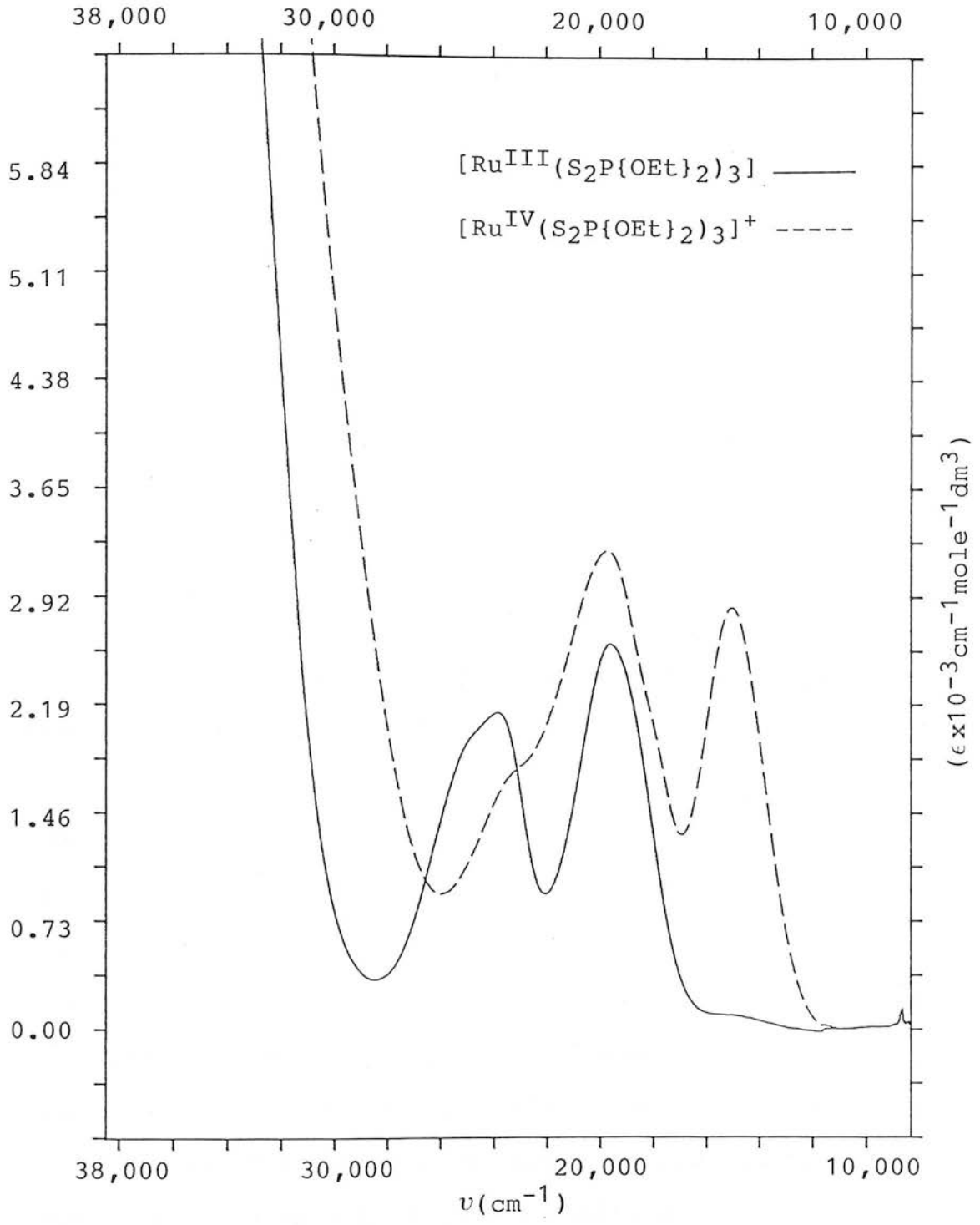

Figure 2.6: The electronic absorption spectrum of $[Ru(S_2P\{OEt\}_2)_3]^{0/+1}$ in CH_2Cl_2 solution at 235K.

the intensity of these absorptions as the available electron density on the metal is reduced. The energy of the absorptions may also be affected depending on the bonding character of the metal orbitals. However, if these absorptions represent transfer of electron density from the dithiolate ligand to the ruthenium centre, then they would be expected to increase in intensity as an electron is removed from the valence orbital of the metal. It is likely, therefore, that the transitions observed are from the dithiolate ligands to the ruthenium *d*-orbitals for both neutral and oxidised complexes.

Figures 2.7 and 2.8 show the electronic spectra of $[Ru(S_2PR_2)_3]^{0/-1}$ (R=Ph, OEt) respectively. For both adducts the absorption bands of the neutral complex collapse as the complex is reduced. For R=OEt (Figure 2.8) absorptions are observed at 18,250 and 21,900cm^{-1}. These bands are quite weak ($\varepsilon \simeq 10^2 cm^{-1}mole^{-1}dm^3$) and are, therefore, assigned as *d-d* bands of the ruthenium centre. For R=Ph (Figure 2.7) a band of moderate intensity is observed at higher energy (24,500cm^{-1}). A weak band observed at the low energy side of this absorption is again assigned to a metal *d-d* transition.

Reduction of the complexes, $[Ru(S_2PR_2)_3]$, generates the d^6 Ru^{II} complex and the additional electron enters (and fills) the metal-based LUMO. The LMCT band in the reduced complex would therefore be expected to occur at higher energies, as is observed.

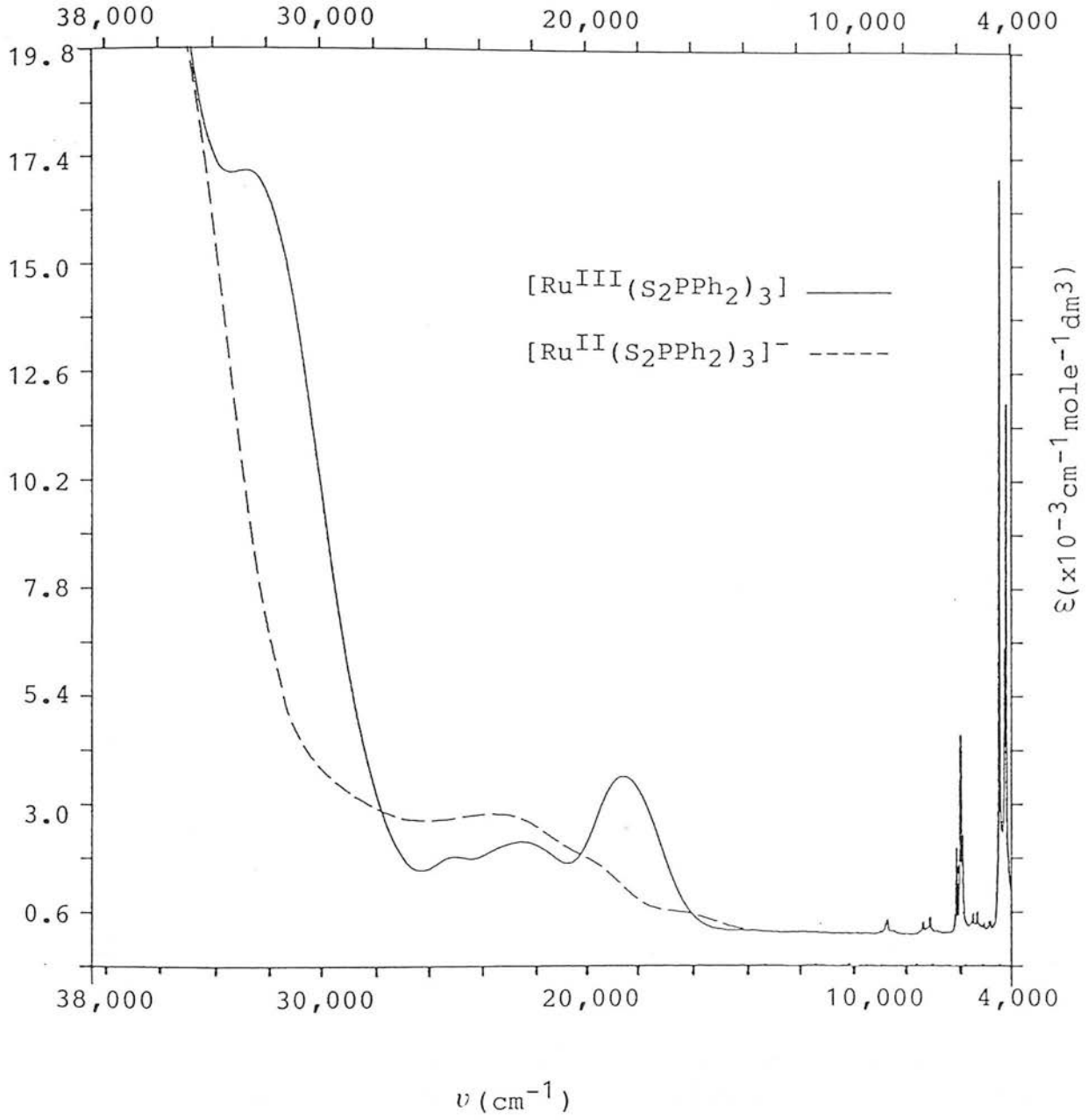

Figure 2.7: The electronic absorption spectrum of $[Ru(S_2PPh_2)_3]^{0/-1}$ in CH_2Cl_2 solution at 235K.

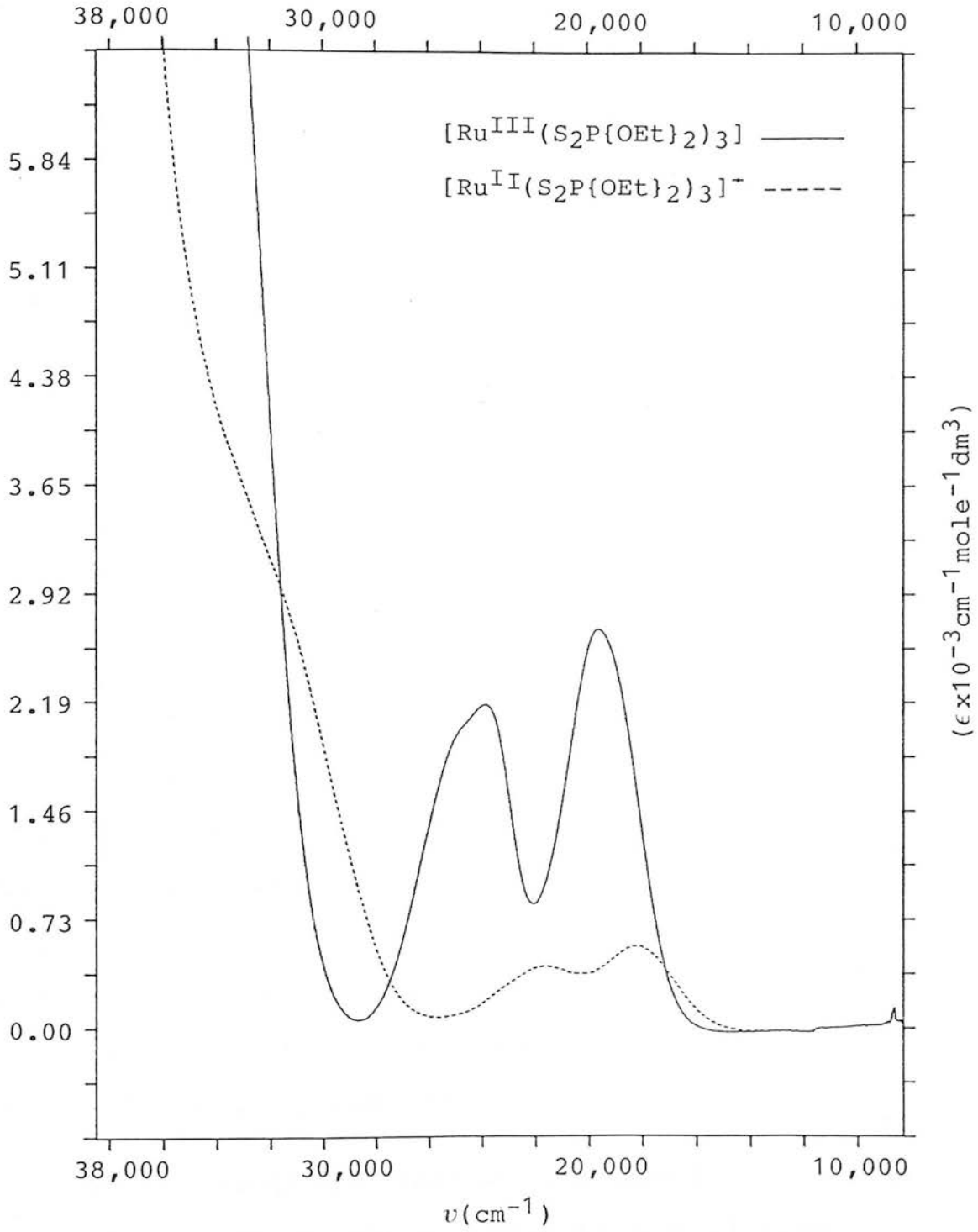

Figure 2.8: The electronic absorption spectrum of $[Ru(S_2P\{OEt\}_2)_3]^{0/-1}$ in CH_2Cl_2 solution at 235K.

2.2.6 Reaction of $[M(S\text{-}S)_3]$ with tertiary phosphines.

Stephenson and Cole-Hamilton reported that the complexes, $[M(S\text{-}S)_3]$ ($S\text{-}S = {}^{-}S_2CNR_2$, ${}^{-}S_2PR_2$) did not react with tertiary phosphines when ethanol solutions of the complex and the phosphine ligand were refluxed under an inert atmosphere. However, we have now found that if the reactants are allowed to react aerobically in methylene chloride, then the adducts, $[Ru(S\text{-}S)_2L_2]$ ($S\text{-}S = {}^{-}S_2CNEt_2$, ${}^{-}S_2PR_2$, R = Ph, OEt; L = dppm, PMe_2Ph), are obtained.

The orange adduct, $[Ru(S\text{-}S)_2L_2]$, is not the first product of the reaction. On addition of phosphine to solutions of $[M(S\text{-}S)_3]$ a green colouration forms initially. The reaction can be followed by electronic absorption spectroscopy. Thus, if an excess of PMe_2Ph is added to solutions of $[Ru(S_2PPh_2)_3]$, a green solution is afforded which reaches maximum intensity after *ca.* one hour. After several hours stirring, the solution turns orange in colour and the electronic spectrum of the solution is almost identical with that of an authentic sample of $[Ru(S_2PPh_2)_2(PMe_2Ph)_2]$.

The identity of the green adducts formed is uncertain as pure samples of these complexes are difficult to obtain. Elemental analysis suggests that these complexes are of general formula $[Ru(S\text{-}S)_3L]$. FAB mass-spectral studies on some samples show that in addition to $[Ru(S\text{-}S)_3L]^+$, fragments with higher values of m/z

(corresponding to binuclear adducts) are observed.

Although the exact nature of the green adduct is not known, it is possible to exclude charged species as solutions of the isolated green adducts do not conduct. Additionally, the formulation, $[Ru(S\text{-}S)_2L_2]^+$, is rejected as electrogenerated samples of this complex (see Chapter 2.17) are brown in colour.

Further work is obviously required to elucidate the reaction mechanism and the nature of the green adducts. The ability to follow the reaction by electronic spectroscopy may be useful in determining kinetic parameters for this process. Additionally, the nature of the reducing agent may be of interest. The dithiocarbamate ligand has been shown[20] to act as a reducing reagent in the formation of $[Ru_2(S_2CNR_2)_5]^+$ and it is likely that the dithiolate ligands act in a similar way in this reaction. However, complexes of general formula, $[Ru(S\text{-}S)_2L_2]$ (L=tertiary phosphine), have been prepared by other methods,[23] and these reactions are extended to the dithiophospate ligand in the next section.

2.3 Preparation of $[M(S_2P\{OEt\}_2)_2(PR_3)_2]$ complexes.

Stephenson and co-workers did prepare complexes of formula, $[M(S\text{-}S)_2L_2]$ (M=Ru, Os, S-S=$^-S_2PR_2$, $^-S_2CNR_2$; L=PR_3), by reaction of various tertiary phosphine complexes with alkali metal salts of the dithiolate (see Chapter 1.3).

This reaction has now been extended to the dithiophosphate ligand.

The complexes, $[MCl_x(PR_3)_3]$ (M=Ru, Os, x=2, PR_3=PPh_3; M=Ru, x=2, PR_3=$PEtPh_2$; M=Ru, x=3, PR_3=PMe_2Ph), react with excess $K[S_2P\{OR\}_2]$ under a variety of conditions (see experimental section) to generate $[M(S_2P\{OEt\}_2)_2(PR_3)_2]$. These complexes have been characterised by the spectroscopic techniques discussed below.

2.3.1 $^{31}P-\{^1H\}$ n.m.r. spectroscopy.

The $^{31}P-\{^1H\}$ n.m.r. spectra of the complexes, $[M(S_2P\{OEt\}_2)_2(PR_3)_2]$, exhibit two triplets and Figure 2.9 shows the spectrum of $[Ru(S_2P\{OEt\}_2)_2(PPh_3)_2]$. This spectral pattern is also observed for the complexes, $[M(S_2PR_2)_2(PR_3)_2]$ (R=Me, Ph), and is consistent with either a *cis*- or *trans*-arrangement of ligands.

There is a marked difference in intensity between the dithiophosphate and phosphine resonance. Robertson *et. al.* examined the $^{31}P-\{^1H\}$ n.m.r. spectra of the complexes, $[Ru(S_2PMe_2)_2(PR_3)_2]$ (PR_3=PPh_3, PPh_2Cl, $PPhCl_2$, PCl_3, PPh_2H, PPh_2OEt, $PPh_2\{OPr\}$), and they reported that (i) the dithiophosphinate resonance was of greatest intensity for all PR_3 and (ii) the relative intensity of the phosphine signal varies with PR_3 being largest for PPh_3 and smallest for PCl_3.[22] These differences were shown to be the result of varying Nuclear Overhauser Enhancements (N.O.E.) and

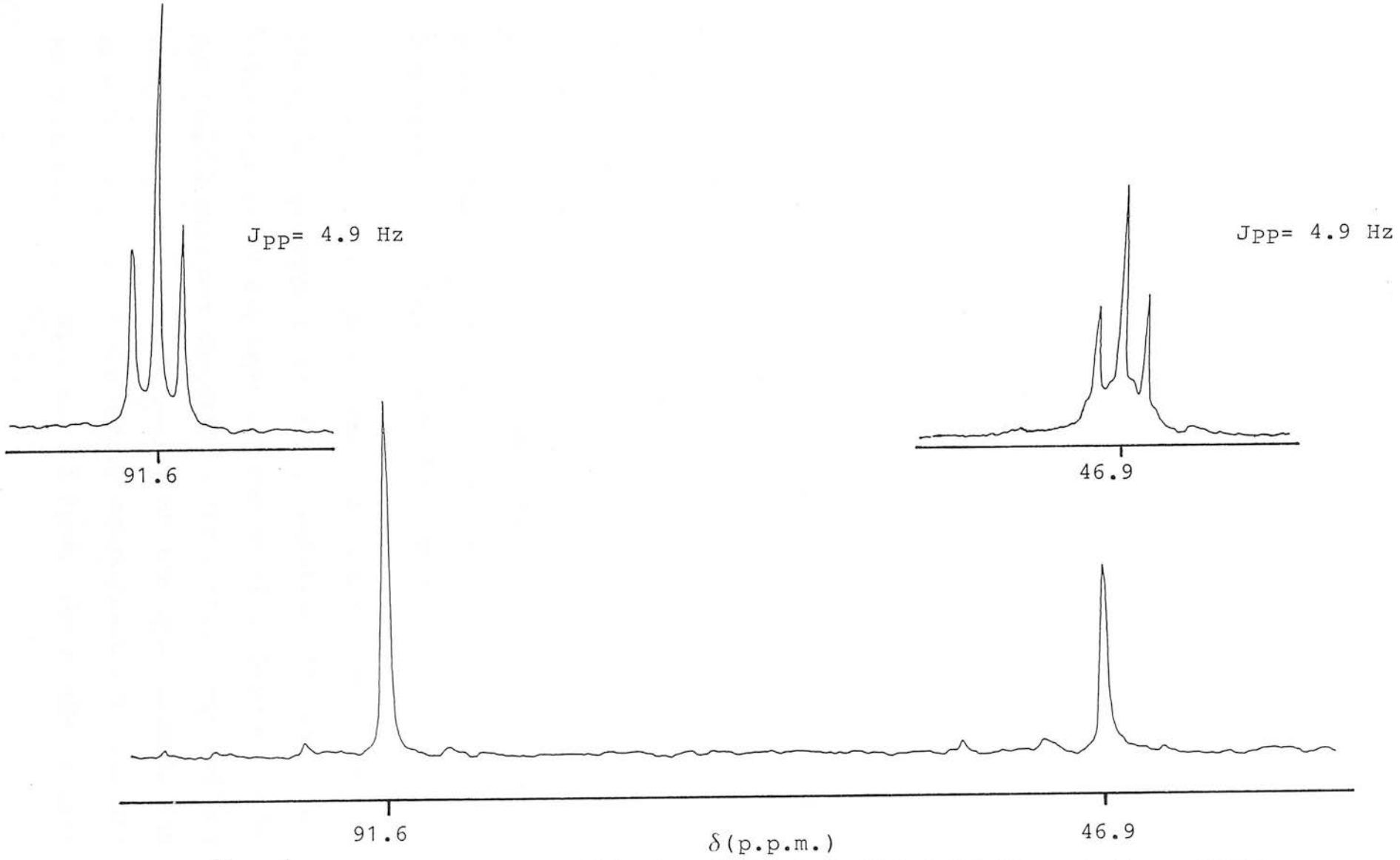

Figure 2.9: The $^{31}P-\{^{1}H\}$ n.m.r. spectrum of[$[Ru(S_2P\{OEt\}_2)_2(PPh_3)_2]$ ($CDCl_3$ solution, 293K).

not due to differences in the relaxation time T_1 (which was found to be similar for these complexes). It is likely that a similar effect is prevalent for the analogous $[M(S_2P\{OEt\}_2)_2(PPh_3)_2]$ complexes.

2.3.2 ^1H n.m.r. spectroscopy.

Stephenson and Cole-Hamilton have examined the variable temperature ^1H n.m.r. spectra of complexes of type, $[M(S-S)_2L_2]$ (M=Ru, Os; S-S = $^-S_2CNR_2$, $^-S_2PR_2$; L=tertiary phosphine) and have found that these complexes have a *cis*-arrangement of ligands.[23] This configuration results in two different chemical environments, one *syn*, and one *anti* to the phosphine ligands. Consequently, two distinct resonances are recorded for the protons of the organic substituent on the dithiolate ligand. By varying the phosphine ligand in the adduct, $[Ru(S_2PMe_2)_2(PR_3)_2]$, these workers suggested that the doublet observed at lower δ-value belonged to the methyl protons *syn* to the phosphine (as the chemical shift of this resonance was more sensitive to the nature of the phosphine ligand).

Figure 2.10 shows the ^1H n.m.r. spectrum of $[Ru(S_2P\{OEt\}_2)_2(dppm)]$ in $CDCl_3$ solution at 298K. The multiplets at δ7.0-8.0ppm and the small triplet at δ4.91 ppm (J_{PH}=10.5Hz) are assigned to the phenyl rings and the methylene protons respectively, of the dppm ligand. The methylene protons of the ethoxy substituent are recorded as multiplets at δ2.8 and 4.2ppm, while the methyl

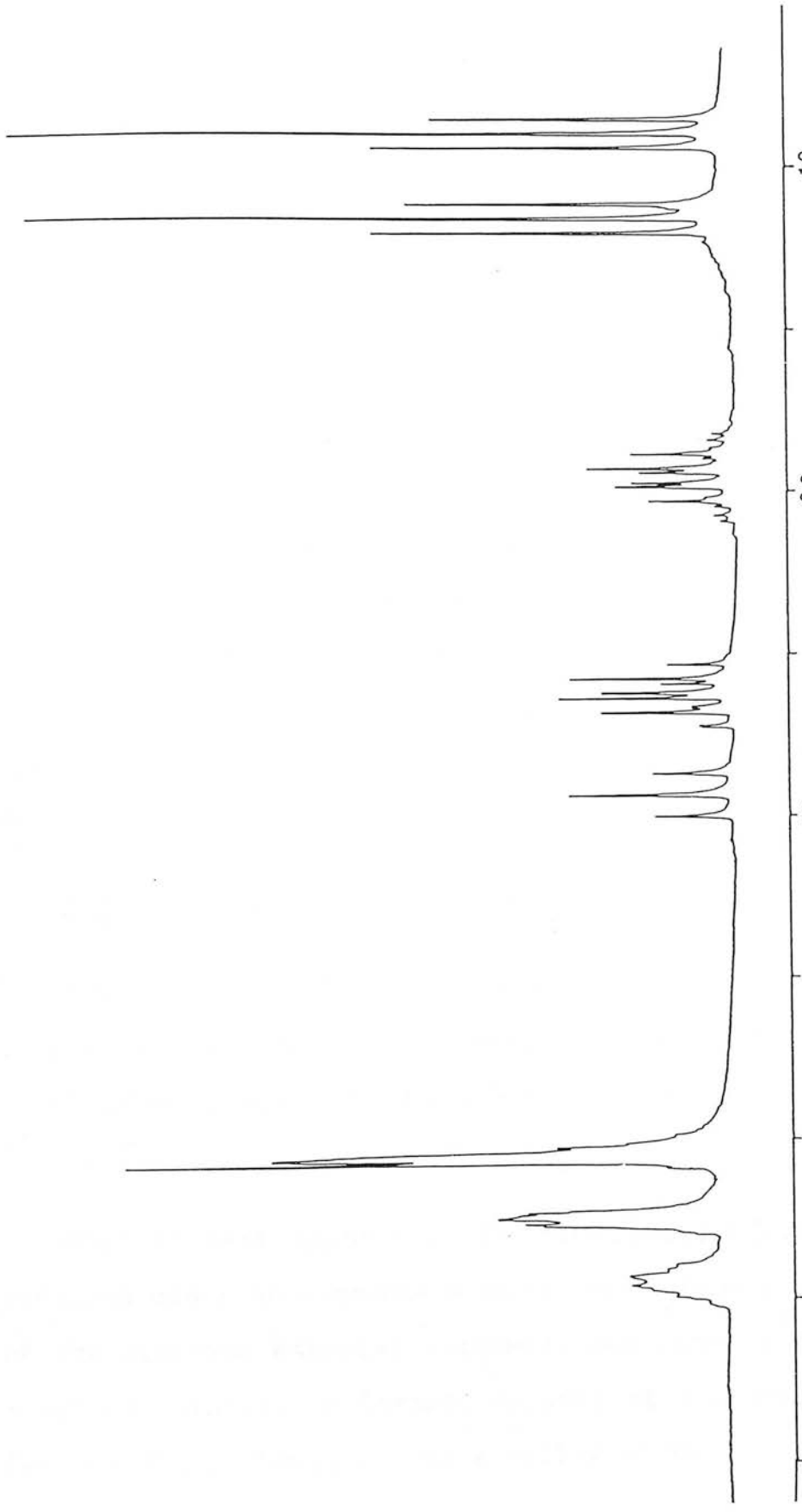

Figure 2.10: The ^{1}H n.m.r. spectrum of [Ru($S_2P\{OEt\}_2)_2$(dppm)] ($CDCl_3$ solution, 288k).

protons are observed as two triplets at δ0.8 and 1.2ppm. This suggests that the ligands are in a *cis*-configuration, which would be an expected result of the steric constraints imposed by the dppm ligand.

At room temperature, other $[M(S_2P\{OEt\}_2)_2(PR_3)_2]$ complexes do not give such simple spectra. The ^1H n.m.r. spectrum of $[Ru(S_2P\{OEt\}_2)_2(PPh_3)_2]$ for example, shows only one broad multiplet for the methylene protons, while other such complexes of the dithiophosphate ligand show broadened resonances at room temperature. Thus, although nearly all other complexes of the general type, $[M(S\text{-}S)_2L_2]$, exhibit *cis*-configurations, it will be neccesary to carry out ^1H n.m.r. studies at low temperatures to confirm the stereochemistry of the other dithiophosphate analogues.

2.3.3 Reaction with carbon monoxide.

Stephenson and co-workers reported that the complexes, $[M(S_2PR_2)_2(L)_2]$ (M=Ru, L =PPh_3, PMe_2Ph; M=Os, L =PMe_2Ph), afford $[M(S_2PR_2)_2(PPh_3)(CO)]$ on reaction with CO gas.[23]

When ethanol solutions of $[Ru(S_2P\{OEt\}_2)_2(PPh_3)_2]$ are refluxed under an atmosphere of CO the orange colouration of the starting material lightens, and after a few hours a yellow solution is formed. Removal of ethanol, affords $[Ru(S_2P\{OEt\}_2)_2(PPh_3)(CO)]$ as a yellow solid.

2.3.4 $^{31}P-\{^{1}H\}$ n.m.r. spectroscopy.

The $^{31}P-\{^{1}H\}$ n.m.r. parameters for the complexes, $[M(S_2PR_2)_2(PPh_3)(CO)]$ (R=Me, Ph), have not been reported, and we examined these to further characterise complexes of the type, *cis*-$[M(S\text{-}S)_2(PR_3)L]$. Figure 2.11 shows the $^{31}P-\{^{1}H\}$ n.m.r. spectrum of $[Ru(S_2P\{OEt\}_2)_2(PPh_3)(CO)]$ in $CDCl_3$ solution which is typical of other $[Ru(S_2PR_2)_2(PPh_3)(CO)]$ complexes. The spectrum consists of a doublet (J_{PP}=2.5Hz) and a singlet at high chemical shifts (δ85-110ppm) assigned to the phosphorus atom of the dithiolate ligands, and a second doublet (J_{PP}=2.5Hz) at lower δ values due to the phosphine ligand. The assignment of ligand type is based on analogy with the starting complexes.

This pattern is consistent with the *cis*-arrangement of ligands assigned to these species (a *trans*-configuration would lead to equivalent environments for the phosphorus atoms of the dithiolate ligand).

Differences in the magnitude of phosphorus-phosphorus coupling constants between the phosphine and the two dithiolate ligands has also been observed for the complexes, *cis*-$[M(S_2PR_2)_2(PPh_3)(tcne)]$ (M=Ru, Os, R=Me, Ph, OEt) (see Chapter 3). It is not immediately apparent if the variation in coupling constant is a result of the physical separation of the phosphorus nuclei, or due to the configuration ("cis" or "trans") of the ligands.

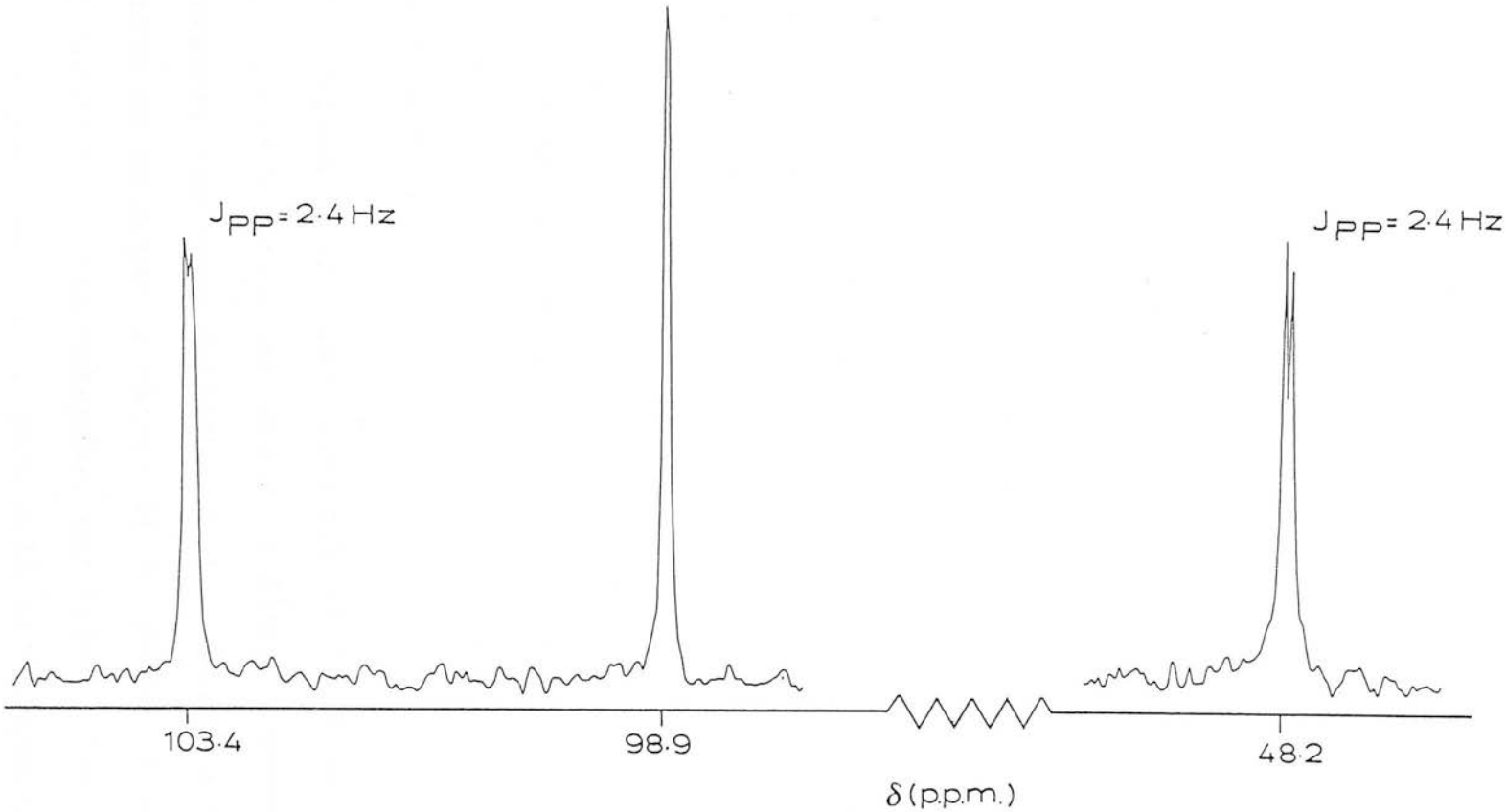

Figure 2.11: The ^{31}P n.m.r. spectrum of $[Ru(S_2P\{OEt\}_2)_2(PPh_3)(CO)]$ ($CDCl_3$ solution, 293K).

2.3.5 ^{1}H n.m.r. spectroscopy.

Figure 2.12 shows the ^{1}H n.m.r. spectrum of $[Ru(S_2P\{OEt\}_2)_2(PPh_3)(CO)]$ in $CDCl_3$ solution. The spectrum consists of (i) multiplets centred at δ7.40ppm assigned to the phenyl protons of triphenylphosphine, (ii) multiplets centred at δ4.2 and 3.1ppm (which have relative intensities of 3:1) that are assigned to the methylene protons of the ethoxy substituent and (iii) four triplets at δ1.40, 1.33, 1.28 and 0.92ppm for the methyl protons of the dithiolate ligand.

The ^{1}H n.m.r. spectrum of $[Ru(S_2PMe_2)_2(PPh_3)(CO)]$ exhibits a similar pattern, where the methyl protons of the dithiophosphinate ligand are observed as three doublets of similar chemical shift and a fourth doublet which is shifted to lower δ values.[23] The observation of four different environments is consistent with a *cis*-configuration of ligands about the metal centre (only two environments would be expected for a *trans*-arrangement).

The resonance at lower chemical shift is assigned to the CH_3 protons *syn* to the phosphine ligand. These protons are nearest the ring currents of the phenyl rings, and are shifted to lower δ values as a result of increased shielding.[23] Thus, the multiplet and triplet (at δ3.0 and 0.9ppm respectively) in Figure 2.12 are assigned to the ethoxy substituent *syn* to the phosphine.

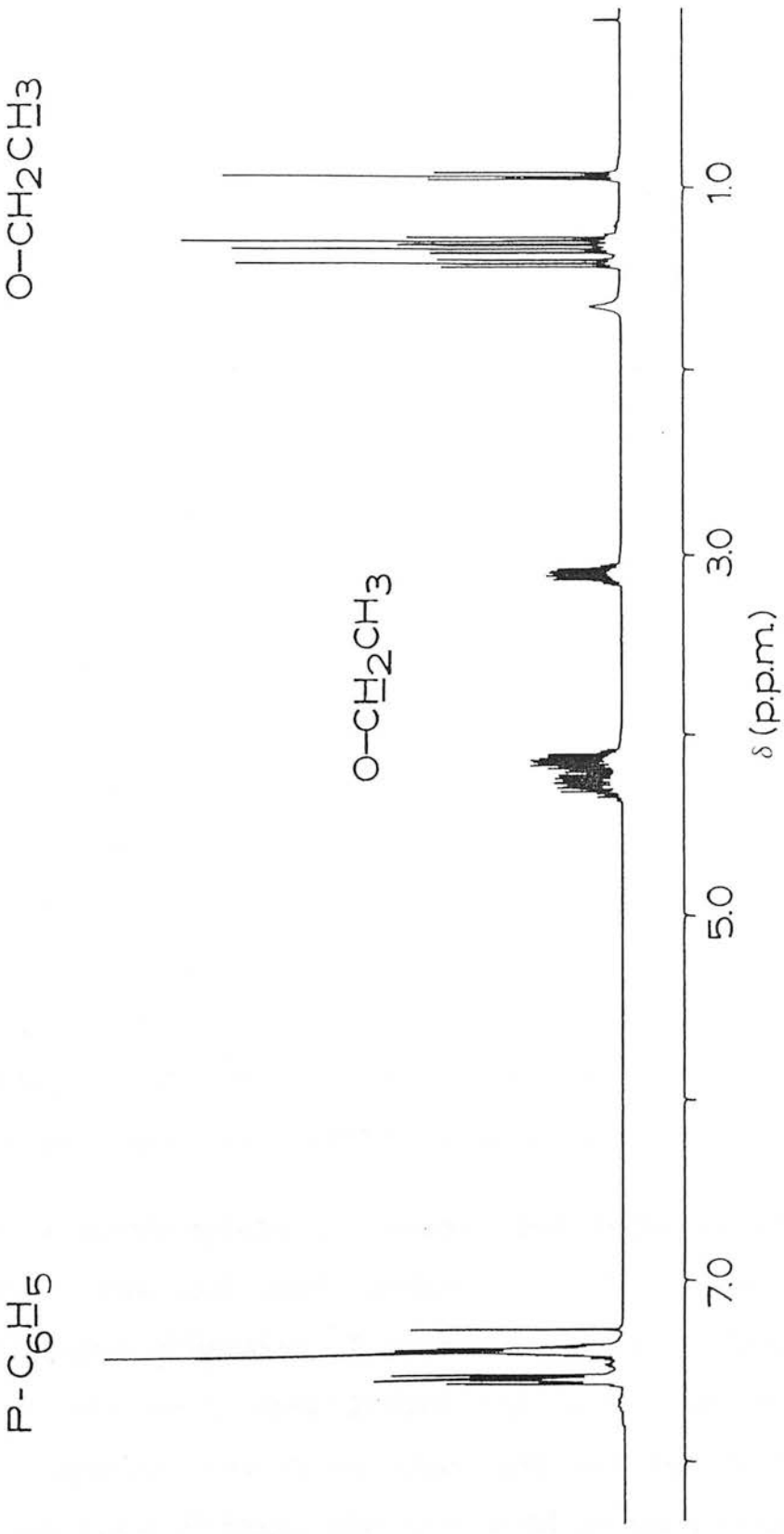

Figure 2.12: The ^{1}H n.m.r spectrum of $[Ru(S_2P\{OEt\}_2)_2(PPh_3)(CO)]$ ($CDCl_3$ solution, 288K).

2.3.6 Crystal structure of $[Ru(S_2PPh_2)_2(PPh_3)(CO)]$.

As part of our attempts to structurally characterise dithiolate complexes of ruthenium and osmium, we have studied $[Ru(S_2PPh_2)_2(PPh_3)(CO)]$ crystallographically.

Recrystallisation of $[Ru(S_2PPh_2)_2(PPh_3)(CO)]$ from $CHCl_3$-60/80° pet-ether mixtures affords small orange crystals suitable for X-ray diffraction study. The complex crystallises in the space group $P\bar{1}$ with two molecules per unit cell. The co-ordination sphere around the ruthenium centre is shown in Figure 2.13, and Table 2.3 lists selected bond lengths and angles.

The ruthenium atom is co-ordinated to two bidentate dithiolate ligands, one triphenylphosphine and one carbonyl ligand in a *cis*-configuration. The complex is distorted from an octahedral configuration as a result of the steric constraints imposed by the chelating ligands. The *trans*-angles range from 165.10(4)° (for the mutually *trans* sulphur ligands) to 173.78(4)° (for the S atom *trans* to carbonyl) and the *cis*-angles from 79.27(3)° (for the ligand bite angle) to 98.46(3)° (for P1-Ru-S1).

The carbonyl moiety is linear; the angle Ru-C1-O1 is 178.2(4)°. The C-O bond length (1.141Å) is similar to other carbonyl complexes of ruthenium.[25] Raston and White tabulated the Ru-C bond length for a number of Ru(0) carbonyl species and found that the average Ru-C bond length was 1.88Å.[25] Thus, the Ru-C bond is much shorter in

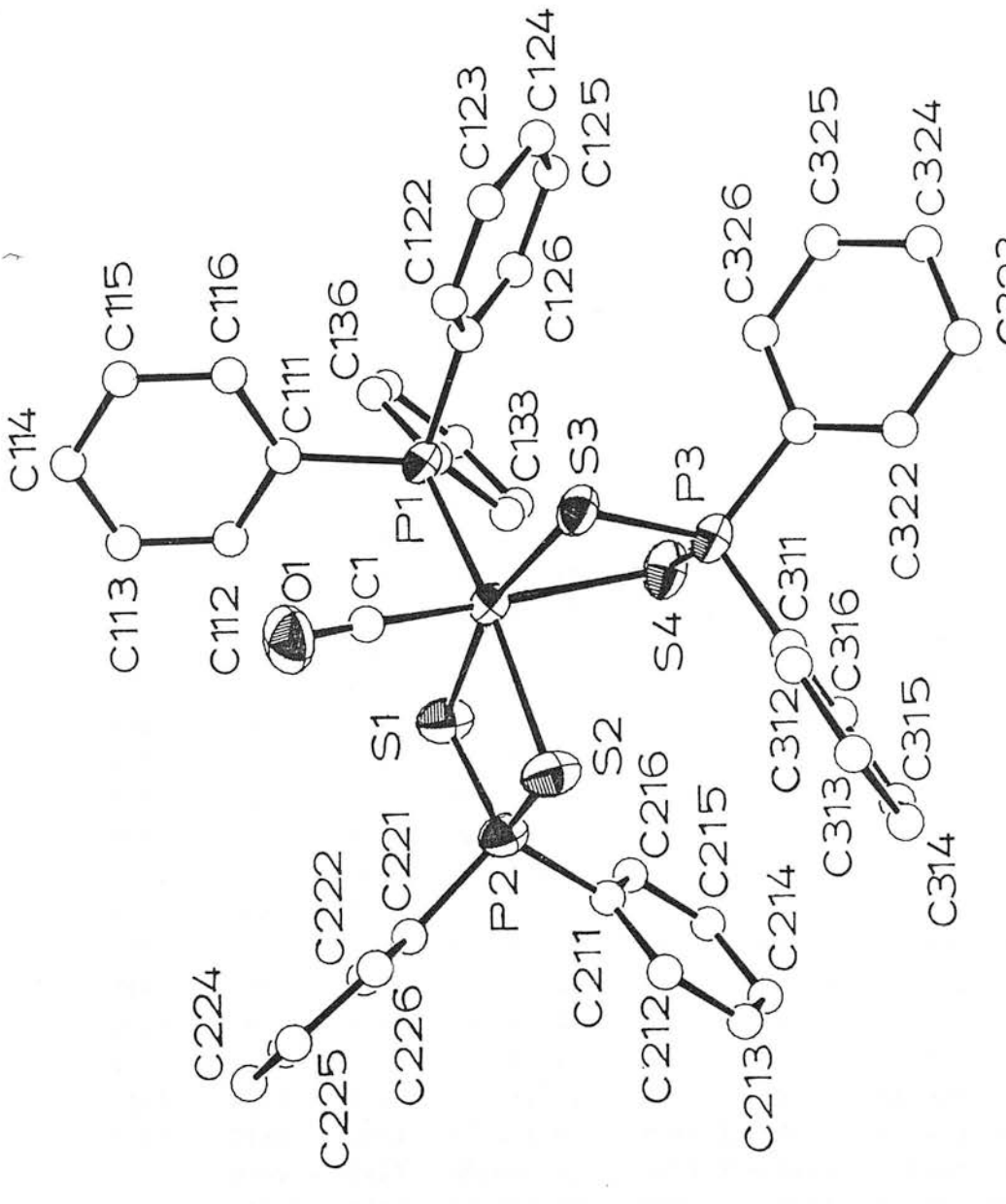

Figure 2.13: The molecular structure of $[Ru(S_2PPh_2)_2(PPh_3)(CO)]$. All H atoms are omitted clarity.

Table 2.3 :Selected bond lengths and angles for $[Ru(S_2PPh_2)_2(PPh_3)(CO)]$.

Bond lengths (Å)

Ru	-	S(1)	2.4286(11)			S(4)	-	P(3)	1.9952(14)		
Ru	-	S(2)	2.5220(11)			P(2)	-	C(211)	1.798(4)		
Ru	-	S(3)	2.4365(10)			P(2)	-	C(221)	1.793(4)		
Ru	-	S(4)	2.5399(10)			P(3)	-	C(311)	1.797(3)		
Ru	-	P(1)	2.3075(10)			P(3)	-	C(321)	1.798(3)		
Ru	-	C(1)	1.826(4)			P(1)	-	C(111)	1.824(3)		
S(1)	-	P(2)	2.0167(15)			P(1)	-	C(121)	1.820(3)		
S(2)	-	P(2)	1.9895(15)			P(1)	-	C(131)	1.830(3)		
S(3)	-	P(3)	2.0065(14)			C(1)	-	O(1)	1.141(5)		

Bond angles (°)

S(1)	-	Ru	-	S(2)	81.16(4)		S(3)	-	P(3)	-	C(321)	110.29(11)
S(3)	-	Ru	-	S(4)	79.27(3)		S(4)	-	P(3)	-	C(311)	110.86(10)
S(1)	-	Ru	-	S(3)	165.10(4)		S(4)	-	P(3)	-	C(321)	112.87(11)
S(2)	-	Ru	-	P(1)	173.78(4)		C(211)	-	P(2)	-	C(221)	103.89(16)
S(4)	-	Ru	-	C(1)	173.95(13)		C(311)	-	P(3)	-	C(321)	105.85(14)
P(1)	-	Ru	-	S(1)	93.52(4)		P(2)	-	C(211)	-	C(212)	118.5(3)
P(1)	-	Ru	-	S(3)	98.46(3)		P(2)	-	C(211)	-	C(216)	121.5(3)
P(1)	-	Ru	-	S(4)	91.01(3)		P(2)	-	C(221)	-	C(222)	119.42(22)
P(1)	-	Ru	-	C(1)	90.72(13)		P(2)	-	C(221)	-	C(226)	120.40(22)
C(1)	-	Ru	-	S(1)	93.91(13)		P(3)	-	C(311)	-	C(312)	119.85(20)
C(1)	-	Ru	-	S(2)	86.46(13)		P(3)	-	C(311)	-	C(316)	120.14(20)
C(1)	-	Ru	-	S(3)	94.74(13)		P(3)	-	C(321)	-	C(322)	122.51(23)
S(1)	-	Ru	-	S(4)	91.76(4)		P(3)	-	C(321)	-	C(326)	117.47(23)
S(2)	-	Ru	-	S(3)	87.30(3)		Ru	-	P(1)	-	C(111)	111.84(10)
S(2)	-	Ru	-	S(4)	92.36(3)		Ru	-	P(1)	-	C(121)	116.84(10)
S(1)	-	P(2)	-	S(2)	107.03(6)		Ru	-	P(1)	-	C(131)	118.70(9)
S(3)	-	P(3)	-	S(4)	105.03(6)		C(111)	-	P(1)	-	C(121)	104.31(13)
Ru	-	S(1)	-	P(2)	86.86(5)		C(111)	-	P(1)	-	C(131)	99.75(12)
Ru	-	S(2)	-	P(2)	84.91(5)		C(121)	-	P(1)	-	C(131)	103.16(12)
Ru	-	S(3)	-	P(3)	86.63(5)		P(1)	-	C(111)	-	C(112)	123.74(20)
Ru	-	S(4)	-	P(3)	84.09(5)		P(1)	-	C(111)	-	C(116)	116.18(20)
S(1)	-	P(2)	-	C(211)	112.76(14)		P(1)	-	C(121)	-	C(122)	117.98(20)
S(1)	-	P(2)	-	C(221)	109.83(11)		P(1)	-	C(121)	-	C(126)	121.99(20)
S(2)	-	P(2)	-	C(211)	110.88(14)		P(1)	-	C(131)	-	C(132)	121.31(18)
S(2)	-	P(2)	-	C(221)	112.55(11)		P(1)	-	C(131)	-	C(136)	118.61(18)
S(3)	-	P(3)	-	C(311)	112.08(10)		Ru	-	C(1)	-	O(1)	178.2(4)

$[Ru(S_2PPh_2)_2(PPh_3)(CO)]$ (1.826[4]Å), but is similar to that found in $[Ru(S_2CNEt_2)_4(CO)_2]$ (1.80Å).[25]

The relative *trans*-influence of the ligands can be inferred by examination of the M-S bond lengths. The longest M-S bond is that *trans* to the carbonyl ligand (2.5399[10]Å), the next largest *trans* to triphenylphosphine (2.5220[11]Å) and the shortest M-S bonds are those of the mutually *trans* sulphur atoms (2.4286[11] and 2.4365[10]Å). The lengthening of the M-S bond *trans* to carbonyl (or triphenylphosphine) is also reflected in the asymmetry of the chelate. Each dithiophosphinate ligand has a short P-S bond (for the sulphur *trans* to PPh_3 or CO) and a longer P-S bond (for the sulphur atom *trans* to sulphur). The Ru-S-P angles are also significantly different within the chelate being larger (by an average of 2.2°) for the sulphur *trans* to sulphur.

This type of asymmetry is also recorded for the dithiocarbamate ligands *trans* to the carbonyl ligand in $[Ru(S_2CNEt_2)_4(CO)_2]$.[25] The dithiocarbamate ligands in this complex are also involved in bridging, but no asymmetry is observed for the bridging ligands in the complexes $[Ru_2(S_2CNR_2)_5]^+$ and $[Ru_3Cl_2(S_2CNR_2)_4(CO)_3]$ in which the sulphur atoms are *trans* to sulphur and chloride respectively.[26,27] Thus, the asymmetry observed for the dithiolate ligands in $[Ru(S_2PPh_2)_2(PPh_3)(CO)]$ probably results from the *trans*-influence of the carbonyl and phosphine ligands.

2.3.7 Infra-red spectroscopy.

The complexes, $[M(S_2P\{OEt\}_2)_2L_2]$ (M=Ru, Os; L=tertiary phosphine) all show strong absorptions between 900-1000 and 700-800cm^{-1} in the infrared spectrum which are not observed for the analogous dithiophosphinate species. Bands at these energies in transition metal complexes of the dithiophosphate ligand to vibrational modes associated with the P-O-C linkage.[24]

Table 2.4 lists the carbonyl stretching frequencies for some complexes of ruthenium and osmium. The frequency of the ν_{CO} is observed to be dependent on both the metal type and the nature of the dithiolate ligand.

Complex	υ_{CO}/cm^{-1}
$[Ru(S_2PMe_2)_2(PPh_3)(CO)]$	1935
$[Ru(S_2P\{OEt\}_2)_2(PPh_3)(CO)]$	1958
$[Ru(S_2CNEt_2)_2(PPh_3)(CO)]$	1920
$[Os(S_2CNMe_2)_2(PPh_3)(CO)]$	1910
$[Os(S_2PMe_2)_2(PMe_2Ph)(CO)]$	1908

Table 2.4: ν_{CO} for some dithiolate complexes.

2.3.8 Mass-spectroscopy.

FAB mass-spectral studies of the complexes, $[M(S_2P\{OEt\}_2)_2(PPh_3)_2]$ ($M=^{102}Ru$, ^{194}Os), exhibit parent ion peaks due to $[M(S_2P\{OEt\}_2)_2(PPh_3)_2]^+$. Prominent fragments

observed at lower m/z values are $[M(S_2P\{OEt\}_2)_2(PPh_3)]$ and $[M(S_2P\{OEt\}_2)_2]^+$ formed by loss of one and two phosphine ligands respectively. For $[Ru(S_2P\{OEt\}_2)_2(PPh_3)_2]$ some fragmentation of the dithiophosphate ligand is apparent.

The complex, $[Ru(S_2P\{OEt\}_2)_2(PPh_3)(CO)]$, exhibits a parent ion peak at m/z=761, but the spectrum is dominated by the fragment $[^{102}Ru(S_2P\{OEt\})_2(PPh_3)]^+$ (m/z=734) formed by loss of CO. Other fragments observed include $[^{102}Ru(S_2P\{OEt\}_2)(PPh_3)(CO)]^+$ and $[^{102}Ru(S_2P\{OEt\}_2)_2]^+$.

2.3.9 Electrochemical Studies.

Preliminary redox studies on the dithiophosphinate complexes, $[M(S_2PR_2)_2(PPh_3)_2]$, (M=Ru, Os; R=Me, Ph) have been completed in this laboratory.[28,29] These studies have now been repeated in more detail and extended to the dithiophosphate complexes prepared above.

Table 2.5 lists redox potentials for various dithiolate complexes of ruthenium and osmium determined at 288K in methylene chloride solution. Coulometric studies on the reversible oxidations show that these are one-electron processes. The oxidised species (for those which can be reversibly generated in bulk) are dark-brown in colour. The redox steps are all believed to be metal-based and so for the complexes, $[M(S\text{-}S)_2L_2]$ (M=Ru, Os; S-S=$^-S_2PR_2$, R=Me, Ph, OEt; L=PR_3), the first oxidation process is assigned to the $M^{II/III}$ couple, and a second irreversible oxidation (which has not previously been

Table 2.5: Redox potentials for some dithiolate complexes.[a]

complex	$M^{II/III}/V$ [b]	$M^{III/IV}/V$ [c]
$[Ru(S_2PPh_2)_3]$	-0.43	+0.84[d]
$[Ru(S_2P\{OEt\}_2)_3]$	-0.23	+1.20[d]
$[Ru(S_2CNEt_2)_3]$	-0.59	+0.50
$[Ru(S_2PMe_2)_2(PPh_3)_2]$	+0.47[f]	+1.42
$[Ru(S_2PPh_2)_2(PPh_3)_2]$	+0.49[f]	+1.50
$[Ru(S_2P\{OEt\}_2)_2(PPh_3)_2]$	+0.63[f]	+1.60
$[Ru(S_2CNEt_2)_2(PPh_3)_2]$	+0.41[e]	-
$[Ru(S_2PPh_2)_2(PEtPh_2)_2]$	+0.45	+1.48
$[Ru(S_2P\{OEt\}_2)_2(PEtPh_2)_2]$	+0.59	+1.55
$[Ru(S_2PMe_2)_2(PMe_2Ph)_2]$	+0.41	+1.45
$[Ru(S_2PPh_2)_2(PMe_2Ph)_2]$	+0.45	+1.48
$[Ru(S_2P\{OEt\}_2)_2(PMe_2Ph)_2]$	+0.58	+1.54
$[Ru(S_2PPh_2)_2(dppm)]$	+0.40	+1.13
$[Ru(S_2P\{OEt\}_2)_2(dppm)]$	+0.52	+1.20
$[Os(S_2PMe_2)_2(PPh_3)_2]$	+0.27	+1.30
$[Os(S_2PPh_2)_2(PPh_3)_2]$	+0.30	+1.34
$[Os(S_2P\{OEt\}_2)_2(PPh_3)_2]$	+0.42	+1.54
$[Ru(S_2PMe_2)_2(PPh_3)(CO)]$	+0.84[e]	-
$[Ru(S_2P\{OEt\}_2)_2(PPh_3)(CO)]$	+1.16[e]	-

(a) measured in CH_2Cl_2 solution, 0.5 M in $[TBA]^+[BF_4]^-$ at 288K; (b) reversible, unless otherwise stated; (c) irreversible, unless otherwise stated; (d) reversible; (e) irreversible; (f) quasireversible at 288K, but reversible at T < 273K.

reported) is assigned to the $M^{III/IV}$ couple. Examination of these results allows some insight into the effect of (i) the dithiolate ligand, (ii) the metal centre and (iii) the phosphine ligand on both the electrochemical potential and reversibility of the redox processes in the $[M(S\text{-}S)_2(PR_3)_2]$ complexes.

The nature of the dithiolate ligand has great effect on both the degree of reversibility and the redox potential of the $M^{II/III}$ couple. Thus (for M=Ru), oxidation of the dithiocarbamate complexes is irreversible even at 223K while the dithiophosphate and dithiophosphinate complexes exhibit reversible oxidations at this temperature. Similarly, the oxidation of $[Ru(S\text{-}S)_3]$ is irreversible for $S\text{-}S=^{-}S_2CNR_2$, but is reversible for $S\text{-}S=^{-}S_2PR_2$ (R=Ph, OEt; see Chapter 2.6).

For any given dithiolate, the nature of the organic substituent affects the oxidation potential of the complex. However, for the $^{-}S_2PR_2$ ligand the effect on oxidation potential of changing from methyl to phenyl substituents is small (*ca.* 20mV) compared to that of the ethoxy group (R=OEt is *ca.* 150mV harder to oxidise than R=Me, Ph for a given metal and phosphine).

The osmium complexes are easier to oxidise than the analogous ruthenium species (by 150-200mV). In addition, as witnessed by reversibility studies and coulometry, the oxidised osmium complexes are more stable in that they

are less likely to form daughter products. This trend has been reported for osmium and ruthenium complexes.[30]

Altering the phosphine ligand has a small effect on the $M^{II/III}$ couple. Thus, the oxidation potential becomes more negative as the number of aryl groups on the phosphine is reduced. More markedly, the reversibility of the oxidation process increases as the phosphine becomes more basic. The complexes, $[Ru(S_2PR_2)_2(PPh_3)_2]$ (R=Me, Ph), were earlier reported as undergoing a reversible $Ru^{II/III}$ oxidation.[28,29] This study has revealed that the oxidation of $[Ru(S_2PR_2)_2(PPh_3)_2]$ (R=Me, Ph, OEt) is actually quasi-reversible at room temperature (with the clear formation of a daughter product). However, coulometric studies at 243K have shown that these complexes can be reversibly oxidised at this temperature. If the phosphine is changed to PMe_2Ph, then $[Ru^{III}(S_2PPh_2)_2(PMe_2Ph)_2]^+$ can be reversibly generated in bulk at room temperature and does not decompose if maintained under an inert atmosphere.

Altering the nature of the chelating ligands has a large effect on the redox potential of the $Ru^{II/III}$ couple. Thus, the effect of replacing one negatively-charged sulphur chelate in $[Ru(S\text{-}S)_3]$ ($S\text{-}S=^{-}S_2PR_2$, R=Ph, OEt) by a neutral, π-accepting phosphorus chelate in the complex, $[Ru(S\text{-}S)_2(dppm)]$ (R=Ph, OEt), is to make oxidation of the metal centre *ca.* 0.8V harder.

The first oxidation of the mono-carbonyl species

$[Ru(S_2PR_2)_2(PPh_3)(CO)]$ (R=Me, Ph, OEt) is irreversible and shifted to more positive potential (*ca.* 400mV) than the analogous $[Ru(S_2PR_2)_2(PPh_3)_2]$ (see Table 2.5).

The M-CO bond is stabilised by back donation into the π^*- orbital of the CO bond. Oxidation will effectively reduce the degree of back donation from the metal and consequently will reduce the stability of this bond.

2.4 Experimental Methods.

Microanalyses were performed in the Chemistry Departments of the Universities of Edinburgh and St. Andrews and by Butterworths analytical services. Infrared spectra were recorded on a Perkin-Elmer 557 grating spectrometer as Nujol mulls on CsI plates, as KBr pellets, and as solutions in methylene chloride or chloroform (CsI windows). ^1H and $^{31}P-\{^1H\}$ n.m.r. spectra were run on JEOL FX60Q and BRUKER WP80 and WP200 SY pulsed Fourier-transform spectrometers (^1H n.m.r. chemical shifts are reported in ppm to high frequency of $SiMe_4$, $^{31}P-\{^1H\}$ n.m.r. chemical shifts are reported in ppm to high frequency of 85% H_3PO_4). All reactions were carried out under an inert atmosphere and solvents used were of A.R. grade and/or were freshly stilled before use. Standard Schlenk line techniques were used when necessary. Electrochemical methods were as for Chapter 4.

2.5 Single-Crystal Structure Determinations.

The following programs were used in the solution and refinement of crystal structures; SHELX76[31], CALC[32], DIRDIF[33], DIFABS[35]. The scattering factors used were obtained from ref 36. The graphics programs ORTEP[37] and PLUTO[38] were used to obtain plots of molecules.

2.6 Materials.

Ruthenium and osmium metals were generously provided by Johnson-Matthey in the form of halides. [$RuCl_3.nH_2O$] was pretreated by boiling to dryness a solution of the chloride in distilled water. $Na_2[(OsCl_6)]$ was used as provided. The phosphine and dithiolate ligands were prepared by standard literature methods. Kieselgel (Silica gel) $60F_{254}$ T.L.C plates (Merck) were used for preparative thin-layer chromatography.

Preparation of $[Ru(S_2P\{OEt\}_2)_3]$.

$[RuCl_3(AsPh_3)_2(CH_3OH)]$ (0.10g, 0.12mmole) and $K[S_2P\{OEt\}_2]$ (0.11g, 0.49mmole) were added to degassed acetone (10ml). A strong raspberry-red colouration is observed to develop rapidly. After stirring at room temperature for several hours to ensure complete reaction, the solvent was removed on a schlenk line. Recrystallisation of the red solid from n-hexane affords large purple-red crystals of the desired complex. Preparative T.L.C. (silica plate, $CHCl_3$ eluent) was used

to obtain analytically pure samples of $[Ru(S_2P\{OEt\}_2)_3]$. Found C 21.9, H 4.6; Calculated for $C_{12}H_{30}O_6P_3RuS_6$: C 22.0, H 4.6.

Crystal Data for $[Ru^{III}(S_2P\{OEt\}_2)_3]$.

$C_{12}H_{30}O_6P_3RuS_6$, M=656.7. Monoclinic, a=14.3065(25), b=13.5766(25), c=14.2848(13)Å, β=90.338(13)° (from θ values of 38 reflections measured at ±ω with θ=13.5-14.5°, λ=0.71073Å), U=2774.5Å^3, space group $C2/c$, Z=4, i[D_x] =1.572gcm^{-3}. Purple-black plates, crystal dimensions 0.11x0.34x0.34mm, μ(Mo-Kα)=11.82cm^{-1}, F(000)=1340.

Data Collection.

The crystal was mounted on a Stoe-Siemens AED-2 four-circle diffractometer and data were collected in the ω-2θ mode with an ω scan width of (1.6 + 0.347tanθ)° using graphite-monochromated Mo-Kα radiation. Of 2073 unique reflections measured ($2.5 < \theta < 22.5°$, h -15 to 15, k 0 to 14, l 0 to 14), 1165 with $F > 6\sigma(F)$ were used in all calculations. Initial absorption corrections using 96 ψ scans (maximum and minimum transmission factors are 0.425 and 0.325 respectively). No crystal decay was apparent.

Structure analysis.

The Patterson function was used to locate the ruthenium atom which lies on a special position on

two-fold axis. All other non-hydrogen atoms were located by iterative cycles of least-squares refinement and difference Fourier synthesis and all atoms, except hydrogen, were refined anisotropically. At isotropic convergence, final absorption correction was made using DIFABS.[35] The hydrogen atoms of the ethyl groups were refined in fixed, calculated positions (AFIX)[31]. Partial disorder of the alkyl groups was apparent from the high thermal parameters of some carbon atoms. However, attempts to model this disorder did not significantly improve the structure. At final convergence, $(\Delta/\sigma)_{max}$ was 0.007 and the final difference Fourier synthesis showed no important features giving final values of R and R_w of 0.042 and 0.054 respectively, using a weighting scheme of $w^{-1}=\sigma^2(F)+0.00065F^2$. Calculations were carried out using SHELX76[31].

Preparation of $[Ru(S_2CNR_2)_3]$.

The complexes $[Ru(S_2CNR_2)_3]$ (R=Et, Me, Pr^i) were prepared in a similar manner to $[Ru(S_2P\{OEt\}_2)_3]$. On addition of a four fold excess of $Na[S_2CNR_2]$ to $[RuCl_3(AsPh_3)_2(CH_3OH)]$ in acetone, the solution darkens and turns red-brown. After stirring for 3 hours, reducing the volume of solvent affords a brown precipitate on addition of n-hexane. Extraction, using a water-chloroform mixtures removes excess dithiocarbamate ligand. The chloroform fra is dried over anhydrous $MgSO_4$. Careful addition of ethanol gives black crystals

of the desired $[Ru(S_2CNR_2)_3]$. The complexes prepared this way exhibit the same spectroscopic characteristics as samples reported previously.

Preparation of $[Ru(S_2P\{OEt\}_2)_2(PPh_3)_2]$.

$[RuCl_2(PPh_3)_3]$ (0.25g, 0.26mmole) and $K[S_2P\{OEt\}_2]$ (0.24g, 1.07mmole) were stirred overnight in degassed acetone. Filtration affords $[Ru(S_2P\{OEt\}_2)_2(PPh_3)_2]$ (in 80% yield) as an orange solid which was washed with water, diethyl ether and n-hexane and dried *in vacuo*. The complex is soluble in acetone, CH_2Cl_2 and $CHCl_3$, but solutions of the complex decompose slowly when exposed to air. Found: C, 52.9; H, 5.0. Calculated for $C_{44}H_{50}O_4P_4RuS_4$: C, 53.1; H, 5.0. Similarly, $[Ru(S_2P\{OEt\}_2)_2(PEtPh_2)_2]$ was prepared from $[RuCl_2(PEtPh_2)_3]$ and $K[S_2P\{OEt\}_2]$ in degassed acetone. Found: C, 47.9; H, 5.6. Calculated for $C_{36}H_{50}O_4P_4RuS_4$: C, 48.0; H, 5.6.

Preparation of $[Ru(S_2P\{OEt\}_2)_2(PMe_2Ph)_2]$.

(a) $[Ru(S_2P\{OEt\}_2)_3]$ (0.10g, 0.15mmole) and PMe_2Ph (0.20g, 1.45mmole) were added to CH_2Cl_2 (20ml) in a conical flask which was open to the atmosphere. After several hours stirring, the green solution which first forms is replaced by an orange solution from which $[Ru(S_2P\{OEt\}_2)_2(PMe_2Ph)_2]$ was separated using preparative T.L.C. as for (b).

(b) $[RuCl_3(PMe_2Ph)_3]$ (0.10g, 0.16mmole) and

$K[S_2P\{OEt\}_2]$ (0.15g, 0.67mmole) were refluxed in degassed ethanol for 4 hours. The ethanol solution turns orange as the reaction takes place. Removal of the solvent on a Schlenk line affords an orange oil. Attempts to precipitate out the complex by addition of organic solvents failed as a result of the high solubility of the complex. The complex was chromatographed (twice) on a silica T.L.C. plate using chloroform as an eluent. After the final chromatographic run the complex was dissolved in 60-80° pet-ether and when the solvent was allowed to evaporate a "wet" solid was afforded. Elemental analysis gave values which were high in both carbon and hydrogen, and this is consistent with the presence of a small amount of unreacted PMe_2Ph.

Preparation of $[Ru(S\text{-}S)_2(dppm)]$.

$[Ru(S\text{-}S)_3]$ (0.15mmole; S-S=$^-S_2CNEt_2$, $^-S_2PR_2$, R=Ph, OEt) was added to dppm (1.50mmole) in CH_2Cl_2 (25ml). The solution was stirred for two days. Preparative T.L.C., using a silica plate and chloroform eluent affords an orange (or yellow) band (R_f=0.75-0.6) which was extracted using CH_2Cl_2. Recrystallisation of this band from CH_2Cl_2/n-hexane mixtures affords $[Ru(S\text{-}S)_2(dppm)]$ as a microcrystalline solid. For $[Ru(S_2P\{OEt\}_2)_2(dppm)]$. Found: C, 46.3; H, 5.0. Calculated for $C_{33}H_{42}O_4P_4RuS_4$: C, 46.3; H, 4.9. For $[Ru(S_2PPh_2)_2(dppm)]$. Found: C, 59.7; H, 4.3. Calculated for $C_{49}H_{42}P_4RuS_4$: C, 59.8; H, 4.3. For $[Ru(S_2CNEt_2)_2(dppm)]$. Found: C, 54.0; H, 5.5; N, 3.7.

Calculated for $C_{35}H_{42}N_2P_2RuS_4$: C, 53.8; H, 5.4; N, 3.6.

Preparation of $[Os(S_2P\{OEt\}_2)_2(PPh_3)_2]$.

$[OsCl_2(PPh_3)_3]$ (0.15g, 0.14mmole) and $K[S_2P\{OEt\}_2]$ (0.13g, 0.58mmole) were stirred in degassed acetone (15ml) for 4 hours. Concentration of the filtrate and careful addition of n-hexane affords orange crystals of $[Os(S_2P\{OEt\}_2)_2(PPh_3)_2]$ in *ca.* 60 % yield. Found: C, 48.7; H, 4.5. Calculated for $C_{44}H_{50}O_4P_4OsS_4$: C, 48.7; H, 4.6.

Preparation of $[Ru(S_2P\{OEt\}_2)_2(PPh_3)(CO)]$.

$[Ru(S_2P\{OEt\}_2)_2(PPh_3)_2]$ (0.15g, 0.15mmole) was added to ethanol (25ml) which had been deareated by refluxing under an atmosphere of CO gas. On refluxing, the orange solution fades until a pale yellow colouration is observed. After 2-3 hours the solvent was removed on a Schlenk line and the yellow solid was purified by preparative T.L.C. (silica absorbent, chloroform eluent). The complex was isolated from a small volume of $CHCl_3$ by addition of 60-80°pet-ether as a pale yellow powder. Found: C, 42.6; H, 4.6; Calculated for $C_{27}H_{35}O_5P_3RuS_4$: C, 42.7; H, 4.6.

Preparation of $[Ru(S_2PPh_2)_2(PPh_3)(CO)]$.

The complex was prepared as outlined in reference 23. Recrystalisation from $CHCl_3$/n-hexane mixtures affords orange-brown crystals of suitable quality for X-ray diffraction study.

Crystal data for $[Ru(S_2PPh_2)_2(PPh_3)(CO)]$

$C_{43}H_{35}OP_3RuS_4$, M=890.0, triclinic, a=11.072(3), b=13.873(5), c=14.310(4)Å, α=92.38(3), β=98.583(24), γ=95.95(3)°, U=2158.9Å^3, (from θ values of 25 reflections measured at $\pm\omega$ with θ=14.5-15.0°, λ=0.71073Å), space group $P\bar{1}$, Z=2, D_x=1.369cm^{-3}. Dark-orange tablet with crystal dimensions 0.21x0.55x0.66mm, μ(Mo-Kα)=7.05cm^{-1}, $F(000)$=956.

Data collection and processing

The crystal was mounted on a CAD-4 diffractometer and data were collected in the ω-2θ mode using graphite-monochromated Mo-Kα radiation. Of 5605 reflections measured ($2.5 < \theta < 22.5°$, h -11 to 11, k -14 to 14, l 0 to 15), 4920 with $F > 6\sigma(F)$ were used in all calculations. No crystal decay was apparent.

Structure analysis

The Patterson function was used to locate the ruthenium centre. All other non-hydrogen atoms were located by iterative cycles of least-squares refinement and difference Fourier synthesis and were refined anisotropically. At isotropic convergence, final absorption correction was made using DIFABS.[35] All hydrogen atoms and the carbon atoms of the phenyl rings were refined in fixed, calculated positions (AFIX)[31]. A weighting scheme of $w^{-1}=\sigma^2(F)+0.001626F^2$ gave satisfactory

agreement analyses. At convergence, $(\Delta/\sigma)_{max}$ was 0.312 and the final values of R and R_w were 0.0372 and 0.0621 respectively for 398 parameters. The final Fourier synthesis showed no important features and the maximum and minimum residues were 0.64 and $-0.44 e\text{Å}^3$ respectively. Structure solution and refinement were carried out using SHELX76[31].

Table 2.6: Atomic co-ordinates with esds for $[Ru(S_2P\{OEt\}_2)_3]$.

	x	y	z	U_{iso}
Ru	0.0000	0.31836(7)	0.2500	0.0525(6)
S(1)	0.09024(17)	0.18501(18)	0.18666(17)	0.0722(15)
S(2)	0.11630(17)	0.43817(19)	0.20177(18)	0.0755(17)
S(3)	0.08202(17)	0.33528(19)	0.39637(16)	0.0733(16)
P(1)	0.0000	0.09442(24)	0.2500	0.0712(23)
P(2)	0.16802(17)	0.42829(18)	0.33145(20)	0.0730(17)
O(1)	0.0482(5)	0.0168(4)	0.3167(5)	0.089(5)
O(2)	0.1806(4)	0.5295(5)	0.3822(5)	0.092(5)
O(3)	0.2741(4)	0.3972(6)	0.3371(6)	0.110(6)
C(11)	0.1148(9)	0.0485(8)	0.3881(8)	0.114(10)
C(12)	0.1391(10)	-0.0308(10)	0.4447(9)	0.135(11)
C(21)	0.1052(7)	0.5918(8)	0.4045(9)	0.101(8)
C(22)	0.1376(7)	0.6819(7)	0.4442(7)	0.090(7)
C(31)	0.3082(9)	0.3056(11)	0.3104(12)	0.153(13)
C(32)	0.3841(11)	0.2732(12)	0.3490(11)	0.183(15)

Table 2.7: Atomic co-ordinates for H atoms in $[Ru(S_2P\{OEt\}_2)_3]$.

	x	y	z	U_{iso}
H(11A)	0.0835	0.1054	0.4304	0.0800
H(11B)	0.1767	0.0771	0.3547	0.0800
H(12A)	0.1884	-0.0069	0.4975	0.0800
H(12B)	0.1704	-0.0878	0.4025	0.0800
H(12C)	0.0772	-0.0595	0.4782	0.0800
H(21A)	0.0658	0.6077	0.3416	0.0800
H(21B)	0.0606	0.5550	0.4543	0.0800
H(22A)	0.0785	50.7282	70.4606	0.0800
H(22B)	0.1820	0.7192	30.3946	0.0800
H(22C)	0.1767	60.6666	10.5073	0.0800
H(31A)	0.3202	80.3087	80.2359	0.0800
H(31B)	0.2540	30.2524	30.3248	0.0800
H(32A)	0.4007	0.2016	0.3206	0.0800
H(32B)	0.3744	10.2672	50.4236	0.0800
H(32C)	0.4406	60.3236	0.3347	0.0800

Table 2.8: Anisotropic thermal parameters in $Å^2$.

	U_{11}	U_{22}	U_{33}	U_{23}	U_{13}	U_{12}
Ru	0.0546(6)	0.0537(6)	0.0492(6)	0.0000	-0.0022(4)	0.0000
S(1)	0.0778(15)	0.0660(15)	0.0729(16)	-0.0095(13)	0.0038(12)	0.0094(13)
S(2)	0.0749(16)	0.0791(16)	0.0725(17)	0.0008(13)	0.0026(13)	0.0180(13)
S(3)	0.0806(16)	0.0826(18)	0.0567(15)	-0.0003(13)	-0.0141(12)	0.0020(13)
P(1)	0.0856(24)	0.0542(20)	0.0738(25)	0.0000	-0.0243(20)	0.0000
P(2)	0.0596(14)	0.0729(17)	0.0864(19)	0.0159(14)	-0.0098(13)	-0.0027(12)
O(1)	0.103(5)	0.060(4)	0.105(5)	0.013(4)	-0.039(4)	-0.002(3)
O(2)	0.070(4)	0.084(5)	0.123(6)	0.033(4)	-0.012(4)	0.007(4)
O(3)	0.062(4)	0.117(6)	0.151(7)	0.033(5)	-0.008(4)	-0.015(4)
C(11)	0.136(10)	0.089(8)	0.118(10)	0.009(8)	-0.065(9)	-0.006(7)
C(12)	0.149(12)	0.128(11)	0.128(12)	0.009(10)	-0.048(10)	0.019(9)
C(21)	0.075(7)	0.093(8)	0.136(10)	0.037(8)	-0.005(7)	-0.008(6)
C(22)	0.103(7)	0.074(7)	0.093(8)	0.013(6)	0.011(6)	0.008(6)
C(31)	0.083(8)	0.167(14)	0.209(17)	0.070(13)	-0.018(10)	-0.036(9)
C(32)	0.174(15)	0.186(16)	0.187(16)	0.038(13)	-0.089(13)	-0.086(13)

Table 2.9: Atomic co-ordinates with esd's for $[Ru(S_2PPh_2)_2(PPh_3)(CO)]$.

	x	y	z	Ueq
Ru	0.18347(2)	0.23252(2)	0.21012(2)	0.0320(2)
P(1)	0.30086(9)	0.14084(7)	0.12900(7)	0.0345(6)
S(1)	0.27706(10)	0.18685(8)	0.36405(7)	0.0506(6)
S(4)	0.34070(9)	0.38046(7)	0.21596(7)	0.0451(6)
S(3)	0.08970(9)	0.31860(7)	0.07802(6)	0.0383(5)
P(3)	0.20734(9)	0.43441(7)	0.13123(7)	0.0372(6)
P(2)	0.16128(9)	0.26768(8)	0.41985(7)	0.0423(6)
S(2)	0.05667(10)	0.31914(8)	0.31211(7)	0.0515(7)
O(1)	-0.0181(3)	0.07097(23)	0.19001(24)	0.0662(21)
C(1)	0.0601(4)	0.1325(3)	0.1966(3)	0.0431(23)
C(111)	0.2419(3)	0.01246(18)	0.11857(15)	0.0426(23)
C(112)	0.1940(3)	-0.03839(18)	0.03266(15)	0.057(3)
C(113)	0.1449(3)	-0.13525(18)	0.03150(15)	0.073(3)
C(114)	0.1436(3)	-0.18125(18)	0.11625(15)	0.076(4)
C(115)	0.1915(3)	-0.13040(18)	0.20216(15)	0.085(4)
C(116)	0.2407(3)	-0.03354(18)	0.20332(15)	0.069(3)
C(121)	0.31308(21)	0.17133(20)	0.00801(19)	0.0446(23)
C(122)	0.20482(21)	0.16787(20)	-0.05653(19)	0.053(3)
C(123)	0.20939(21)	0.19350(20)	-0.14928(19)	0.074(4)
C(124)	0.32223(21)	0.22259(20)	-0.17748(19)	0.088(4)
C(125)	0.43049(21)	0.22605(20)	-0.11294(19)	0.087(4)
C(126)	0.42591(21)	0.20042(20)	-0.02019(19)	0.061(3)
C(131)	0.46039(21)	0.13218(16)	0.18107(18)	0.0418(22)
C(132)	0.52362(21)	0.20102(16)	0.24976(18)	0.0465(24)
C(133)	0.64708(21)	0.19530(16)	0.28464(18)	0.063(3)
C(134)	0.70731(21)	0.12075(16)	0.25083(18)	0.071(3)
C(135)	0.64408(21)	0.05192(16)	0.18214(18)	0.078(4)
C(136)	0.52062(21)	0.05764(16)	0.14726(18)	0.063(3)
C(211)	0.2403(3)	0.3649(3)	0.5002(3)	0.059(3)
C(212)	0.1718(3)	0.4332(3)	0.5350(3)	0.099(5)
C(213)	0.2302(3)	0.5094(3)	0.5976(3)	0.119(6)
C(214)	0.3572(3)	0.5173(3)	0.6255(3)	0.112(6)
C(215)	0.4258(3)	0.4489(3)	0.5908(3)	0.164(8)
C(216)	0.3673(3)	0.3727(3)	0.5281(3)	0.122(6)
C(221)	0.07303(24)	0.19513(23)	0.49196(20)	0.0481(25)
C(222)	0.13362(24)	0.14617(23)	0.56493(20)	0.065(3)
C(223)	0.06624(24)	0.08359(23)	0.61681(20)	0.088(4)
C(224)	-0.06172(24)	0.06996(23)	0.59572(20)	0.093(5)
C(225)	-0.12230(24)	0.11892(23)	0.52275(20)	0.095(5)
C(226)	-0.05493(24)	0.18150(23)	0.47087(20)	0.068(3)
C(311)	0.13525(23)	0.51989(20)	0.19601(19)	0.0420(22)
C(312)	0.01384(23)	0.53575(20)	0.16467(19)	0.059(3)
C(313)	-0.04260(23)	0.60171(20)	0.21507(19)	0.080(4)
C(314)	0.02238(23)	0.65180(20)	0.29681(19)	0.078(4)
C(315)	0.14378(23)	0.63593(20)	0.32815(19)	0.085(4)
C(316)	0.20022(23)	0.56997(20)	0.27775(19)	0.069(3)
C(321)	0.2627(3)	0.49940(17)	0.03714(22)	0.0440(23)
C(322)	0.2402(3)	0.59485(17)	0.02088(22)	0.072(3)
C(323)	0.2829(3)	0.64086(17)	-0.05464(22)	0.089(4)
C(324)	0.3480(3)	0.59143(17)	-0.11390(22)	0.080(4)
C(325)	0.3705(3)	0.49598(17)	-0.09764(22)	0.086(4)
C(326)	0.3278(3)	0.44997(17)	-0.02212(22)	0.073(3)

Table 2.10: Atomic co-ordinates for H atoms in $[Ru(S_2PPh_2)_2(PPh_3)(CO)]$.

	x	y	z	Ueq
H(112)	0.1950	-0.0028	-0.0330	0.0800
H(113)	0.1078	-0.1746	-0.0350	0.0800
H(114)	0.1055	-0.2562	0.1154	0.0800
H(115)	0.1905	-0.1660	0.2678	0.0800
H(116)	0.2778	0.0058	0.2698	0.0800
H(122)	0.1175	0.1453	-0.0347	0.0800
H(123)	0.1256	0.1908	-0.1992	0.0800
H(124)	0.3258	0.2424	-0.2493	0.0800
H(125)	0.5178	0.2486	-0.1348	0.0800
H(126)	0.5097	0.2031	0.0298	0.0800
H(132)	0.4770	0.2587	0.2759	0.0800
H(133)	0.6960	0.2486	0.3378	0.0800
H(134)	0.8029	0.1163	0.2778	0.0800
H(135)	0.6907	-0.0058	0.1560	0.0800
H(136)	0.4717	0.0043	0.0941	0.0800
H(212)	0.0734	0.4272	0.5134	0.0800
H(213)	0.1771	0.5624	0.6245	0.0800
H(214)	0.4025	0.5763	0.6740	0.0800
H(215)	0.5241	0.4550	0.6123	0.0800
H(216)	0.4204	0.3198	0.5012	0.0800
H(222)	0.2327	0.1567	0.5813	0.0800
H(223)	0.1131	0.0457	0.6733	0.0800
H(224)	-0.1139	0.0215	0.6359	0.0800
H(225)	-0.2214	0.1084	0.5064	0.0800
H(226)	-0.1018	0.2194	0.4144	0.0800
H(312)	-0.0365	0.4970	0.1014	0.0800
H(313)	-0.1366	0.6140	0.1908	0.0800
H(314)	-0.0213	0.7029	0.3358	0.0800
H(315)	0.1941	0.6747	0.3914	0.0800
H(316)	0.2942	0.5577	0.3020	0.0800
H(322)	0.1898	0.6331	0.0668	0.0800
H(323)	0.2655	0.7148	-0.0672	0.0800
H(324)	0.3811	0.6271	-0.1724	0.0800
H(325)	0.4209	0.4577	-0.1435	0.0800
H(326)	0.3452	0.3761	-0.0095	0.0800

Table 2.11: Anisotropic thermal parameters in $Å^2$.

	U_{11}	U_{22}	U_{33}	U_{23}	U_{13}	U_{12}
Ru	0.0355(2)	0.0285(2)	0.0302(2)	-0.0033(1)	0.0046(1)	0.0025(1)
P(1)	0.0400(6)	0.0286(5)	0.0330(5)	-0.0052(4)	0.0059(4)	0.0005(4)
S(1)	0.0555(7)	0.0580(7)	0.0377(6)	0.0030(5)	0.0083(5)	0.0180(5)
S(4)	0.0416(6)	0.0349(5)	0.0548(7)	-0.0024(4)	-0.0046(5)	0.0015(4)
S(3)	0.0449(5)	0.0291(5)	0.0375(5)	-0.0045(4)	-0.0023(4)	0.0004(4)
P(3)	0.0419(6)	0.0268(5)	0.0405(6)	-0.0049(4)	0.0030(4)	0.0021(4)
P(2)	0.0478(6)	0.0446(6)	0.0323(5)	-0.0051(4)	0.0062(4)	0.0020(5)
S(2)	0.0567(7)	0.0581(7)	0.0397(6)	0.0000(5)	0.0111(5)	0.0210(5)
O(1)	0.0515(18)	0.0558(20)	0.0874(25)	0.0030(17)	0.0144(17)	-0.0118(16)
C(1)	0.0430(23)	0.0410(23)	0.0433(22)	0.0014(18)	0.0064(17)	0.0020(20)
C(111)	0.0498(23)	0.0273(20)	0.0492(24)	-0.0092(17)	0.0127(18)	0.0052(16)
C(112)	0.0667(28)	0.0384(24)	0.0594(28)	-0.0103(21)	-0.0016(22)	-0.0030(20)
C(113)	0.0931(37)	0.0417(27)	0.0762(35)	-0.0190(25)	-0.0011(29)	-0.0128(24)
C(114)	0.0907(38)	0.0389(26)	0.0940(40)	-0.0087(27)	0.0251(31)	-0.0032(24)
C(115)	0.1359(51)	0.0346(26)	0.0812(37)	0.0004(25)	0.0372(35)	-0.0044(28)
C(116)	0.1133(42)	0.0320(24)	0.0577(29)	-0.0018(21)	0.0232(27)	-0.0019(24)
C(121)	0.0617(26)	0.0354(21)	0.0344(21)	-0.0084(16)	0.0086(19)	0.0045(18)
C(122)	0.0733(30)	0.0385(23)	0.0446(25)	-0.0086(18)	0.0045(22)	0.0162(20)
C(123)	0.1139(44)	0.0656(32)	0.0399(27)	-0.0074(23)	0.0002(27)	0.0360(30)
C(124)	0.1432(57)	0.0789(38)	0.0394(28)	-0.0006(25)	0.0192(34)	0.0256(37)
C(125)	0.1080(46)	0.0870(39)	0.0648(35)	0.0045(29)	0.0413(33)	-0.0038(33)
C(126)	0.0755(32)	0.0571(28)	0.0486(26)	0.0021(21)	0.0249(23)	-0.0033(23)
C(131)	0.0426(22)	0.0372(21)	0.0444(22)	0.0021(18)	0.0093(17)	0.0045(17)
C(132)	0.0428(23)	0.0424(23)	0.0515(25)	0.0001(19)	0.0013(19)	0.0030(18)
C(133)	0.0469(26)	0.0642(30)	0.0734(32)	-0.0051(24)	-0.0055(22)	0.0098(22)
C(134)	0.0476(27)	0.0827(36)	0.0806(36)	-0.0024(29)	0.0041(24)	0.0206(25)
C(135)	0.0611(31)	0.0864(38)	0.0855(37)	-0.0061(30)	0.0148(27)	0.0349(28)
C(136)	0.0563(28)	0.0650(30)	0.0659(30)	-0.0116(24)	0.0113(22)	0.0162(23)
C(211)	0.0701(30)	0.0549(28)	0.0458(25)	-0.0073(21)	0.0122(22)	-0.0164(23)
C(212)	0.0810(39)	0.0832(41)	0.1245(52)	-0.0553(39)	0.0118(36)	-0.0038(32)
C(213)	0.1529(69)	0.0756(43)	0.1183(55)	-0.0579(40)	0.0310(49)	-0.0198(42)
C(214)	0.1196(59)	0.1002(52)	0.1020(51)	-0.0386(41)	0.0030(44)	-0.0313(45)
C(215)	0.0879(53)	0.1750(86)	0.2044(96)	-0.0844(79)	-0.0503(57)	-0.0272(54)
C(216)	0.0740(42)	0.1183(55)	0.1579(70)	-0.0669(52)	-0.0252(42)	0.0038(38)
C(221)	0.0588(26)	0.0441(23)	0.0382(22)	-0.0154(18)	0.0110(19)	-0.0033(19)
C(222)	0.0793(33)	0.0625(30)	0.0505(27)	0.0041(23)	0.0109(24)	0.0025(25)
C(223)	0.1607(60)	0.0510(30)	0.0507(29)	0.0095(23)	0.0380(34)	0.0102(33)
C(224)	0.1270(55)	0.0641(35)	0.0873(44)	-0.0159(31)	0.0630(42)	-0.0249(36)
C(225)	0.0779(38)	0.1034(46)	0.0993(46)	-0.0109(38)	0.0420(35)	-0.0310(34)
C(226)	0.0628(31)	0.0740(32)	0.0625(30)	-0.0057(25)	0.0147(24)	-0.0096(25)
C(311)	0.0565(25)	0.0246(19)	0.0434(22)	-0.0018(16)	0.0087(18)	0.0074(17)
C(312)	0.0525(26)	0.0443(25)	0.0771(32)	-0.0110(22)	0.0061(23)	0.0080(20)
C(313)	0.0685(32)	0.0542(30)	0.1172(47)	-0.0074(30)	0.0235(32)	0.0190(25)
C(314)	0.1162(46)	0.0483(29)	0.0710(34)	-0.0092(25)	0.0387(32)	0.0200(29)
C(315)	0.1254(51)	0.0670(35)	0.0574(32)	-0.0256(27)	-0.0043(32)	0.0223(33)
C(316)	0.0821(34)	0.0520(28)	0.0651(31)	-0.0290(24)	-0.0123(25)	0.0149(25)
C(321)	0.0446(22)	0.0375(22)	0.0472(23)	0.0012(18)	0.0053(18)	-0.0021(17)
C(322)	0.0792(34)	0.0424(26)	0.0946(37)	0.0167(26)	0.0380(29)	0.0062(23)
C(323)	0.1090(45)	0.0510(30)	0.1075(45)	0.0306(31)	0.0434(37)	0.0087(29)
C(324)	0.0887(38)	0.0705(35)	0.0768(36)	0.0178(29)	0.0212(30)	-0.0172(29)
C(325)	0.1019(43)	0.0865(42)	0.0708(36)	0.0079(31)	0.0388(31)	0.0032(33)
C(326)	0.1039(39)	0.0483(28)	0.0671(31)	0.0080(23)	0.0375(29)	0.0095(26)

Table 2.12:Selected torsion angles (°) for $[Ru(S_2P\{OEt\}_2)_3]$.

S(1')	- Ru	- S(1)	- P(1)	0.07(10)	S(1)	- P(1) - O(1) -C(11)	51.6(8)
S(2)	- Ru	- S(3)	- P(2)	-1.90(11)	S(1')	- P(1) - O(1) -C(11)	-68.3(7)
S(3')	- Ru	- S(1)	- P(1)	-98.02(10)	O(1')	- P(1) - O(1) -C(11)	172.0(7)
S(2)	- Ru	- S(1)	- P(1)	170.77(10)	P(1)	- O(1) -C(11) -C(12)	173.0(8)
S(3)	- Ru	- S(1)	- P(1)	89.20(11)	Ru	- S(2) - P(2) - O(2)	-127.8(3)
S(2)	- Ru	-S(1')	- P(1)	-56.6(5)	Ru	- S(2) - P(2) - O(3)	122.8(3)
S(1)	- Ru	- S(2)	- P(2)	-95.95(12)	Ru	- S(3) - P(2) - O(2)	127.9(3)
S(2')	- Ru	- S(2)	- P(2)	92.22(12)	Ru	- S(3) - P(2) - O(3)	-123.3(3)
S(3')	- Ru	- S(2)	- P(2)	173.73(12)	S(2)	- P(2) - O(2) -C(21)	63.9(8)
S(1')	- Ru	- S(2)	- P(2)	-40.1(5)	S(3)	- P(2) - O(2) -C(21)	-56.2(8)
S(1)	- Ru	- S(3)	- P(2)	88.49(12)	O(3)	- P(2) - O(2) -C(21)	-175.6(8)
S(2')	- Ru	- S(3)	- P(2)	-97.72(12)	S(2)	- P(2) - O(3) -C(31)	-66.3(10)
S(3')	- Ru	- S(3)	- P(2)	-50.2(5)	S(3)	- P(2) - O(3) -C(31)	53.7(10)
S(1')	- Ru	- S(3)	- P(2)	170.71(12)	O(2)	- P(2) - O(3) -C(31)	173.4(9)
Ru	- S(1)	- P(1)	- O(1)	-125.7(3)	P(2)	- O(3) -C(31) -C(32)	-153.5(12)
					P(2)	- O(2) -C(21) -C(22)	-175.7(7)

Table 2.13: Selected least squares planes and interplanar angles for $[Ru(S_2P\{OEt\}_2)_3]$.

Plane	Atoms in plane	σ
1	Ru S1 S1' P1	0.00
2	Ru S2 S3 P2	0.02
3	P1 O1 O1' C11 C11'	0.04
4	P2 02 03 C21 C31	0.05

Interplanar angles (°)

1-2 82.8, 1-3 86.0, 1-4 51.5, 2-3 50.4, 2-4 89.29, 3-4 46.4.

σ = R.M.S. deviation of atoms from plane (Å).

Table 2.14: Selected torsion angles (°) for $[Ru(S_2PPh_2)_2(PPh_3)(CO)]$.

S(1)	-Ru - S(2)	- P(2)	1.41(5)	S(4)	- P(3)	-C(311)-C(312)	-153.62(20)
C(1)	-Ru - S(2)	- P(2)	95.93(13)	S(4)	- P(3)	-C(311)-C(316)	26.0(3)
S(4)	-Ru - S(1)	- P(2)	90.73(5)	S(3)	- P(3)	-C(311)-C(312)	-36.62(25)
S(2)	-Ru - S(1)	- P(2)	-1.39(5)	S(3)	- P(3)	-C(311)-C(316)	143.05(20)
P(1)	-Ru - S(4)	- P(3)	113.37(5)	S(4)	- P(3)	-C(321)-C(326)	55.9(3)
S(2)	-Ru - S(4)	- P(3)	-71.86(5)	S(3)	- P(3)	-C(321)-C(326)	-61.2(3)
C(1)	-Ru - S(4)	- P(3)	6.8(12)	C(211)	- P(2)	- S(2) - Ru	121.61(14)
P(1)	-Ru - S(3)	- P(3)	-104.23(5)	S(1)	- P(2)	-C(211)-C(212)	172.4(3)
S(1)	-Ru - S(3)	- P(3)	38.98(15)	S(2)	- P(2)	-C(211)-C(212)	52.4(3)
S(4)	-Ru - S(3)	- P(3)	-14.81(4)	S(4)	- P(3)	-C(321)-C(322)	-125.59(24)
S(2)	-Ru - S(3)	- P(3)	78.12(5)	S(1)	- P(2)	-C(211)-C(216)	-7.7(4)
C(1)	-Ru - S(3)	- P(3)	164.33(13)	S(2)	- P(2)	-C(211)-C(216)	-127.7(3)
Ru	- S(3) -P(3)	-C(321)	141.22(11)	S(1)	- P(2)	-C(221)-C(222)	54.7(3)
S(4)	-Ru - S(2)	- P(2)	-90.01(5)	S(1)	- P(2)	-C(221)-C(226)	-120.29(23)
P(1)	-Ru - S(1)	- P(2)	-178.15(5)	S(2)	- P(2)	-C(221)-C(222)	173.86(21)
S(3)	-Ru - S(1)	- P(2)	38.26(16)	S(2)	- P(2)	-C(221)-C(226)	-1.2(3)
C(1)	-Ru - S(1)	- P(2)	-87.19(13)	Ru	- S(3)	- P(3) -C(311)	-101.12(11)
S(1)	-Ru - S(4)	- P(3)	-153.08(5)	S(3)	- P(3)	-C(321)-C(322)	117.28(25)
Ru	- S(1)	- P(2) - S(2)	1.82(6)	S(1)	- P(2)	- S(2) - Ru	-1.76(6)
Ru	- S(1)	- P(2) -C(211)	-120.37(14)	C(221)	- P(2)	- S(2) - Ru	-122.51(11)
Ru	- S(1)	- P(2) -C(221)	124.28(11)	Ru	- S(4)	- P(3) -C(311)	102.68(10)
Ru	- S(4)	- P(3) - S(3)	-18.58(5)	Ru	- S(4)	- P(3) -C(321)	-138.78(12)
				Ru	- S(3)	- P(3) - S(4)	19.33(5)

Table 2.15: ^{1}H n.m.r. data for some 1,1-dithiolate complexes. [a]

complex	δ dithiolate/ppm [b]	δ phosphine/ppm [c]	T/K
$[Ru(S_2P\{OEt\}_2)_2(PPh_3)_2]$	3.7 m[d,e] , 1.1[f] t (7.0)[h]	7.0-7.4	293
$[Os(S_2P\{OEt\}_2)_2(PPh_3)_2]$	3.3,[e] 4.2 [f]br	7.0-7.2	293
$[Ru(S_2P\{OEt\}_2)_2(PEtPh_2)_2]$	3.9[e] br, 1.2[f] t (1.6)	7.0-7.3; 2.5 br, 0.5 m	298
$[Ru(S_2P\{OEt\}_2)_2(PMe_2Ph)_2]$	4.2[e] br, 1.3[f] t (7.0)	7.0-7.2; 1.5 d (20.3)	294
$[Ru(S_2PPh_2)_2(dppm)]$	-	6.8-8.0;[g]4.9 t (9.2)	293
$[Ru(S_2P\{OEt\}_2)_2(dppm)]$	4.3, 2.9[e]; 0.9, 1.3[f] t (7.1)	7.0-8.0; 4.9 t (10.5)	298
$[Ru(S2P\{OEt\}_2)_2(PPh_3)(CO)]$	0.9, 0.5[e]m ; 3.1, 4.2 m[f]	7.2-7.5	293

(a) measured in $CDCl_3$ solution; (b) resonances assigned to the dithiolate ligand; (c) resonances assigned to the phosphine ligand; (d) s-singlet, d-doublet, t- triplet, br-broad; (e) methylene protons of the dithiolate ligand; (f) methyl protons of the dithiolate resonance (g) protons of both the dithiolate and phosphine ligands; (h) coupling constant in Hz.

Table 2.16: ^{31}P n.m.r. data for some 1,1-dithiolate complexes.[a]

complex	δ dithiolate/ppm [b]	δ phosphine/ppm [c]	T/K
$[Ru(S_2P\{OEt\}_2)_2(PPh_3)_2]$	91.6 t[d] (4.9)[e]	46.9 t (4.9)	293
$[Os(S_2P\{OEt\}_2)_2(PPh_3)_2]$ [f]	107.7	-14.6	298
$[Ru(S_2P\{OEt\}_2)_2(PEtPh_2)_2]$	100.4 t (3.9)	39.3 t (3.9)	293
$[Ru(S_2P\{OEt\}_2)_2(PMe_2Ph)_2]$ [f]	103.0	22.5	294
$[Ru(S_2PPh_2)_2(PPh_3)_2]$	89.8 t (3.5)	43.9 t (3.5)	293
$[Ru(S_2PPh_2)_2(PEtPh_2)_2]$	89.0 t (4.9)	42.0 t (4.9)	290
$[Ru(S_2PPh_2)_2(PMe_2Ph)_2]$[f]	89.4	22.8	293
$[Ru(S_2PPh_2)_2(dppm)]$	87.8 t (5.5)	3.7 t (5.5)	290
$[Ru(S_2PPh_2)_2(PPh_3)(CO)]$	89.3 d (8.2); 85.1 s.	49.8 d (8.2)	290
$[Ru(S_2P\{OEt\}_2)_2(PPh_3)(CO)]$	103.4 d (2.4); 98.9 s.	48.2 d (2.4)	288

(a) measured in $CDCl_3$ solution; (b) the resonance assigned to the dithiolate ligand;
(c) The resonance assigned to the phosphine ligand; (d) s-singlet, d-doublet, t, triplet;
(e) Jpp in Hz; (f) no coupling was resolved for this complex but the peaks are broadened.

References.

1. D. Coucouvanis, *Prog. Inorg. Chem.*, 1970, **11**, 233.

2. R. P. Burns, A. P. McCullough, and C. A. McAuliffe, *Adv. Inorg. Chem. Radiochem.*, 1979, **22**, 303.

3. C. K. Jorgensen, *Acta Chem. Scand.*, 1962, **16**, 1048.

4. M. G. B. Drew, W. A. Hopkins, P. C. Mitchell and T. Colclough, *J. Chem. Soc., Dalton Trans.*, 1986, 351.

5. L. Ruiz-Ramirez, T. A. Stephenson and E. S. Switkes, *J. Chem. Soc., Dalton Trans.*, 1973, 1770.

6. D. L. Kepert, *Inorg. Chem.*, 1972, **11**, 561.

7. D. L. Kepert, *Prog., Inorg. Chem.*, 1977, **23**, 1.

8. E. I. Stieffel and G. F. Brown, *Inorg. Chem.*, 1972, **11**, 434.

9. H. Vincents, F. Schousboe-Jensen and R. G. Hazell, *Acta Chem. Scand.*, 1972, **26**, 1375.

10. C. Furlani, A. A. G. Tomlinson, P. Porta and A. Sgamellotti, *J. Chem. Soc., A*, 1970, 2929.

11. J. F. McConnell and A. Schwartz, *Acta Crystallogr., Sect B*, 1972, **28**, 1546.

12. J. G. Leipoldt and P. Coppens, *Inorg. Chem.*, 1973, **12**, 2269.

13. L. H. Pignolet, *Inorg. Chem.*, 1974, **13**, 2051.

14. D. J. Duffy and L. H. Pignolet, *Inorg. Chem.*, 1974, **13**, 2051.

15. K. Mislow and M. Raban, *Top. Stereochem.*, 1967, **1**, 1.

16. A. R. Hendrickson, J.M. Hope and R. L. Martin, *J. Chem. Soc., Dalton. Trans.*, 1976, 2032.

17. G. H. Wheeler, B. M. Mattson, C. L. Miessler and L. H. Pignolet, *Inorg. Chem.*, 1978, **17**, 340.

18. R. Chant, A. R. Hendrickson, R. L. Martin, and N. M. Rhode, *Inorg. Chem.*, 1975, **14**, 1894.

19. K. W. Given, S. H. Wheeler, B. S. Jick, L. J. Maheu and L. H. Pignolet, *Inorg. Chem.*, 1979, **18**, 1261.

20. B. M. Mattson, J. R. Heiman, and L. H. Pignolet, *Inorg. Chem.*, 1976, **15**, 564.

21. R. Chant, A. R. Hendrickson, R. L. Marrtin and N. M. Rohde, *Aust. J. Chem.*, 1973, **26**, 2533.

22. D. M. Appel, A. S. F. Boyd, I. W. Robertson, D. M. Roundhill and T. A..Stephenson, *Inorg. Chem.*, 1982, **21**, 449.

23. D. J. Cole-Hamilton and T. A. Stephenson, *J. Chem. Soc., Dalton Trans.*, 1974, 739.

24. W. Rudzinski, O. T. Behnke and Q. Fernando, *Inorg. Chem.*, 1977, **16**, 1207.

25. C. L. Raston and A. H. White, *J. Chem. Soc., Dalton Trans.*, 1975, 2418.

26. C. L. Raston and A. H. White, *J. Chem. Soc., Dalton Trans.*, 1975, 2422.

27. C. L. Raston and A. H. White, *J. Chem. Soc., Dalton Trans.*, 1975, 2410.

28. J. A. S. Duncan, PhD Thesis, University of Edinburgh, 1983.

29. I. W. Robertson, PhD Thesis, University of Edinburgh, 1981.

30. S. Brownstein, G. A. Heath, A. Sengupta and D. W. A. Sharp, *J. Chem. Soc., Chem. Commun.*, 1983, 609.

31. G. M. Sheldrick, SHELX76, Program for crystal structure refinement, University of Cambridge, 1976.

32. R. O. Gould and P. Taylor, CALC, Interactive molecular geometry program, University of Edinburgh, 1985.

33. P. T. Beurskens W. P. Bosman H. M. Doesbury T. E. M. Van der Hark P. A. J. Prick, J. Noordik, G. Beurskens, and R. O. Gould, DIRDIF, Applications of direct methods to difference structure factors, University of Nijmegen, The Netherlands, 1983.

34. N. Walker and D. Stuart, *Acta Crystallogr., Sect. A*, 1983, **39**, 158.

35. D.T. Cromer and J. L. Mann, *Acta Crystallogr., Sect. A*, 1968, **24**, 321.

36. P. D. Mallinson, K. W. Muir, ORTEP, *J. Appl. Cryst.*, 1985, **18**, 51.

37. W. D. S. Motherwell, PLUTO, University of Cambridge, 1976.

Chapter 3

Preparation and characterisation of tetracyanoethylene complexes of ruthenium and osmium.

3.1 Tetracyanoethylene.

Tetracyanoethylene (tcne) was first prepared in 1957 by Cairns *et. al.* of the Central Research Department of the Du Pont Chemical Company.[1] Since then it has been shown to be a versatile molecule with a wide range of reactions in both organic and inorganic chemistry. The commercial applications of tcne are diverse; amongst it many uses tcne (i) forms conducting films and "organic conductors", (ii) is a selective catalyst poison, (iii) is an analytical reagent (in the quantitative and qualitative determination of aromatic hydrocarbons and phosphine sulphides) and (iv) acts as a light stabiliser in polymeric materials. In this introduction the physical properties, the more common reactions, and the known transition-metal complexes of tcne will be reviewed.

Tcne was the first percyanocarbon synthesised and is a colourless, crystalline solid which sublimes readily at temperatures above 393K (1 atmosphere pressure) and has a melting point of 471-473K in a sealed tube.[2] The compound has a high thermal stability and remains completely unchanged up to temperatures of 873K, although at 1200K, decomposition to form cyanogen occurs. The molecular structure of tcne (see Figure 3.1) has been determined crystallographically, in both monoclinic[3,4] and cubic[5] forms, and by electron diffraction studies.[6]

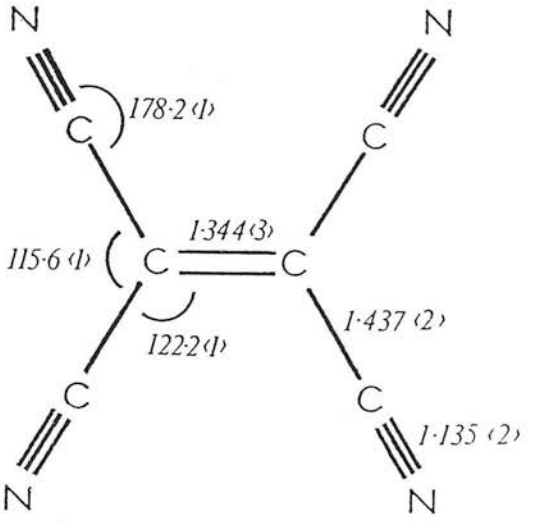

Figure 3.1: The molecular structure of tcne.[5]

Tcne is planar with the C=C bond length shorter (by 0.03Å) than predicted by molecular orbital (M.O.) calculations. This has been attributed to the electron withdrawing ability of the four cyano-groups.[5] Lipscomb and Penfold have used M.O. calculations to determine π-bond orders and π-electron populations for tcne, $tcne^{-}$, and $tcne^{2-}$.[7] In the neutral molecule the π-bond orders are C=C, 0.76; C≡N, 0.87; and C-C, 0.35.

The electron-withdrawing effect of the cyano-groups is responsible for the very high π-acidity of tcne[8]; the electron affinity of tcne has been calculated[9,10] at $3.17 eV mole^{-1}$ making it one of the strongest electron accepting organic molecules.[10] Consequently, tcne forms many highly-coloured charge-transfer complexes with aromatic π-donor molecules such as naphthalene and hexamethylbenzene.[11,12] The characteristic electronic absorption spectra of these charge-transfer adducts has

enabled the development of colorimetric methods for the qualitative and quantitative analysis of hydrocarbons using tcne.[13,14] Crystallographic studies of these charge-transfer complexes have been reported[11,12,15,16] and they have been reviewed by Vasudevan and Ramakrishnan.[17]

With sulphur donors such as tetrathiafulvene (ttf) [3.1], tcne and tetracyanoquinodimethane (tcnq) [3.2] produce a series of "organic conductors" ([ttf.tcnq] has a room temperature conductivity similar to that of graphite).[18]

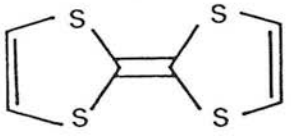

[3.1]

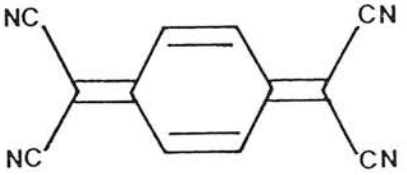

[3.2]

Complete electron transfer can occur readily to give the radical anion, $tcne^{\cdot-}$. Many salts of tcne are known.[19] The unpaired electron of $tcne^{\cdot-}$ has a characteristic e.s.r. spectrum (see Figure 3.2).

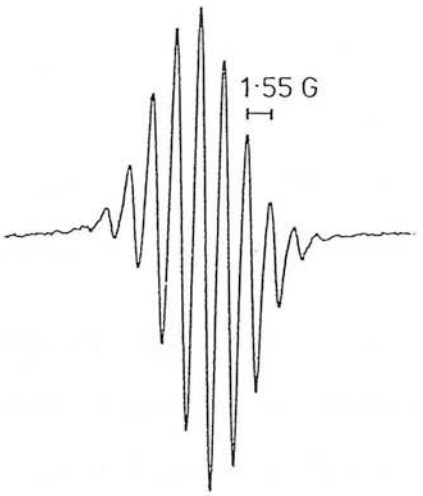

Figure 3.2 The e.s.r. spectrum of $tcne^{\cdot-}$.

As well as the nine lines observed due to coupling to four equivalent nitrogen atoms (I=1), two additional resonances are observed resulting from coupling to ^{13}C.[20]

Tcne undergoes many addition and substitution reactions.[21-23] The electron deficiency of the C=C double bond makes tcne one of the strongest dieneophiles known reacting vigourously with dienes at temperatures well below 273K.[21] With triphenylphosphine, tcne forms the addition products [3.3] and [3.4].[24,25]

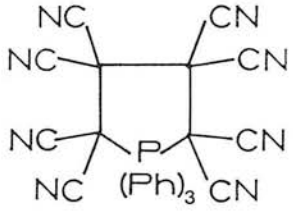

[3.3]

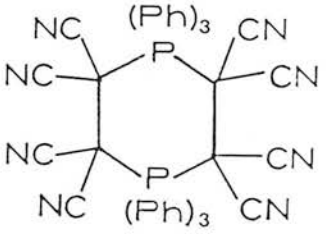

[3.4]

Tcne can be reduced to tetracyanoethane either by catalytic hydrogenation using platinum black or by reaction with thiols or potassium iodide.[21]

Substitution occurs when water reacts with tcne yielding tricyano-vinyl alcohol (and hydrogen cyanide as a bi-product). With primary and secondary amines, tcne affords tricyanovinylamines.[23] The urea-catalysed reaction of tcne with alcohols yields dicyanoketeneacetals.[22]

The versatility of tcne as a reagent is mirrored in its complexes with transition metal complexes. These adducts can be divided into (i) charge-transfer complexes in which partial or complete electron transfer from the

metal to tcne occurs, (ii) π-bound complexes in which the metal co-ordinates to the C=C double bond (or in theory the C≡N triple bond), (iii) σ-bonded complexes through the nitrogen atom, and (iv) complexes in which the tcne moiety is degraded or reacts with another ligand co-ordinated to the metal centre.

3.2 Charge-transfer complexes.

The earliest reactions of tcne with transition metals were concerned with the metallocenes.[26-30] This type of complex has been examined in an attempt to produce adducts with novel electrical and magnetic properties.

The solid state or solution reaction of ferrocene and tcne affords a product which was initially formulated[26] as the salt, $[(Cp)_2Fe]^+[tcne]^-$ ($Cp=\pi-C_5H_5$). Further research and a crystallographic study revealed that the complex, $[(Cp)_2Fe.tcne]$, is in fact formed.[27,28] With metallocenes which are more easily oxidised than ferrocene complete electron-transfer occurs on reaction with tcne. Thus, tcne and $[(Cp)_2Co]$ or bis(π-tetrahydroindenyl)iron afford the salts $[metallocene]^+[tcne]^-$.[29] Recently, workers at Du Pont characterised[30] $[(C_5Me_5)_2Fe]^+[tcne]^-$ by magnetic measurements and crystallography; the complex exhibits ferromagnetism above 60K. The crystal structure of the related species, [3.5], has also been reported.[31]

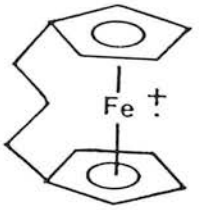

[3.5]

A blue 1:1 compound is prepared from $[(\pi\text{-}C_6H_6)_2Cr]$ and tcne; the e.s.r. spectrum of an acetonitrile solution confirms the presence of both $tcne^-$ and metal radicals.[32] Similarly, $[(C_5H_4R)_2WX_2]$ (X=Cl, Br, I; R=Me, Et, Pr^n) is oxidised by tcne.[33]

In solution, $[(Cp)_2Pb]$ affords a charge-transfer complex with tcne, but infrared analysis indicated that, in the solid state, a bridging cyano-alkene is present.[34] Similarly, electronic absorption spectroscopy implies the formation of a charge-transfer complex on the addition of tcne to $[PbR_4]$ ($R_4=Me_4$, Me_3Et, Me_2Et_2) before insertion of tcne into the Pb-R bond.[35]

Neither osmocene or ruthenocene form stable complexes with tcne. The relative ease of oxidation of ferrocene compared to osmocene and rutheneocene has been proposed to explain this observation.[36] However, if ruthenocene or osmocene solutions containing tcne are irradiated[37] then charge-transfer adducts are formed. Further photochemical excitation of these complexes at frequencies associated with *d-d*, or MLCT bands yields $[(Cp)_2M]^+[tcne]^-$ (M=Ru, Os).

Charge-transfer is observed[38] when tcne reacts with $[Pt_2S_2(PPh_3)_4]$, while oxidation of the metal adduct occurs with both $[CoR_2(bipy)_2]^+$ (R=Me, Et)[39] and $[Cr(CO)_2(dmpe)_2]$ (dmpe=dimethylphenylphosphinoethane).[40]

In summary, tcne (a strong π-acid) reacts with organometallic π-bases and other transition metal complexes to give charge-transfer complexes or salts of the anion radical. The extent of electron transfer depends on the oxidation potential of the basic substrate. The radical-anion complex can be characterised by e.s.r. and electronic absorption spectroscopy. In some cases charge-transfer may proceed co-ordination.

3.3 π-alkene bound complexes.

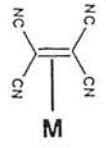

The binding of alkenes to transition-metal centres plays an important role in homogenous catalytic reactions such as alkene hydrogenation and dimerisation.[41] As model compounds for the intermediates in these reactions, cyano-alkenes have received considerable attention in both preparative and structural studies.[42]

The bonding model for transition-metal alkene complexes proposed by Chatt[43] and by Dewar and Duncanson[44] involves formation of a σ-bond by donation of π-electrons to the metal, and a π-bond by back donation from the

metal *d*-orbitals to the alkene π^*-orbital. The extent of backbonding will increase as the energy of the π^* level decreases. It is found that the energy of this level falls as the number of cyano-substituents increases. Thus, tcne and other strong π-acids form stable adducts of this type.[45]

3.3.1 Chromium, molybdenum, and tungsten complexes.

Tcne reacts with $[Cr(ArNC)_6]$ (Ar=Ph, p-MeOPh, p-tol) affording $[Cr(ArNC)_5(tcne)]$.[46] However, the related cyano-alkenes fumaronitrile (E-1,2-dicyanoethene, fmn) and acrylonitrile (1-cyanoethene, acn) only react photochemically. The carbonyl complexes, $[M(CO)_5(tcne)]$, have been prepared for all the members of the triad.[47]

Reaction of tcne with $[(Cp)Mo(CO)_2(\eta^2CH_3CNR)]$ (R=Me, Ph) yields $[(Cp)Mo(CO)_2(\eta^1CH_3CNR)(tcne)]$,[48] and with $[MoO(S_2CNR_2)_2]$ (R=Me, Et), affords $[MoO(S_2CNR_2)_2(tcne)]$ in which the tcne acts as an activated alkene.[49] The product of the latter reaction is a Mo(VI) species and is regarded as a model for the interaction of nitrogen with nitrogenase.[49] The mixed alkene-acetylene complex, $[W(CO)(RCCR')(S_2CNEt_2)_2(tcne)]$, (R=R'=Me, Ph; R=Ph, R'=H), has been prepared from $[W(CO)(RCCR')(S_2CNEt_2)_2]$ and tcne.[50]

3.3.2 Iron, ruthenium and osmium complexes.

Tcne acts as a "trap" for the molecular fragment produced on photolysis of $[Fe(CO)_3(P\{OAr\}_3)_2]$ (Ar=Ph, *o*-, and *p*-tolyl) in benzene, and the yellow complex, $[Fe(CO)_2(P\{OAr\}_3)_2(tcne)]$, can be isolated.[51] On addition of tcne to $[Fe(CO)(P\{OMe\}_3)_2(C_4Ph_4)]$, a green solution is formed from which green-black crystals of neutral $[Fe(CO)(P\{OMe\}_3)(\eta^2tcne)(C_4Ph_4)]$ are produced, although e.s.r. spectroscopy indicates that oxidation of the metal substrate by tcne is the first step of the reaction.[52]

The isonitrile complexes, $[Fe(CO)_{4-n}(CNR)_n(tcne)]$ (n=2, R=Bu^t, $PhCH_2$, 2,6-$Me_2C_6H_3$; n=3, R=Bu^t or 2,6-$Me_2C_6H_3$; n=4, R=2,6-$Me_2C_6H_3$), were characterised[53] by Albers *et. al.*, while Ashton and Manning prepared[54] the green complex *trans* -$[Fe(PPh_3)_2(CO)_2(tcne)]$ from $[Fe(PPh_3)_2(CO)_2(PhNSO)]$ and tcne in toluene.

Addition of tcne (and fmn) to $[Ru(NO)Cl(PPh_3)_2]$ produces $[Ru(NO)Cl(PPh_3)_2(L)]$ (L=tcne, fmn).[55] No osmium adducts of this type have been reported with tcne.

3.3.3 Cobalt, rhodium and iridium complexes.

As the e_{2g} level on the metal centre becomes filled the capacity of the metal for back-donation increases and the low lying π^* levels of tcne will readily accept this transfer of electron density. Therefore, the number of tcne complexes of this type for the cobalt and nickel

triads is extensive and particularly those complexes which are of overall low valence.

Reaction of $[(Cp)Co(CO)(PMe_3)]$ and tcne at room temperature results in displacement of the carbonyl ligand and substitution by an alkene bound tcne ligand.[57] Japanese workers reported[58] that tcne reacts with $[CoH(N_2)(PPh_3)_3]$ and $[Co(Me)(PPh_3)_3]$ to afford the complexes, $[CoH(tcne)_2(PPh_3)_2]$ and $[Co(tcne)_2(PPh_3)_2]$, respectively in which the tcne moiety is π-bound. However, the frequencies of ν_{CN} for these adducts suggest that the tcne ligand is N-bound (see Chapter 3.7.2).

With the adduct, *trans*-$[RhCl(CO)_2(PPh_3)_2]$, tcne affords $[Rh(CO)_2(PPh_3)_2(tcne)]$ which has *cis*-carbonyls; however, with $[RhCl(CO)_2(L)]$ (L=py, *p*-toluidine) the *trans*-adduct, $[RhCl(CO)_2(L)(tcne)]$, is formed.[59] On reaction of $[RhCl(CO)_2(L)(tcne)]$ with diphenylphosphinoethane (dppe), $[Rh(L)(tcne)(dppe)]$ is produced; with the analogous fmn adduct, the cyano-alkene is displaced to generate $[Rh(dppe)(CO)_2]^+$. Reaction of $[RhCl(CO)_2(L)(alkene)]$ (alkene=tcne, fmn) with sulphur or nitrogen chelates (e.g. bipy or $[PhSCH_2CH_2SPh]$) however, affords the adducts, $[Rh(chelate)(L)(alkene)]^+$.[60]

The complex, $[Rh(chel)(L)]^+$, (chel=bipy, phen; L=tcne, fmn, acn) is prepared from $[Rh(chel)(CO)_2]^+$ and the alkene.[61] The rate of reaction falls as the number of cyano-groups on the alkene decreases. Regeneration of

$[Rh(chel)(CO)_2]^+$ by reaction with carbon monoxide is possible for L=fmn or acn, but the tcne adduct is resistant to carbonylation. With another equivalent of chelate $[Rh(chel)_2(L)]^+$ can be generated.

Reaction of tcne with $[Rh(CO)Cl(PPh_2(CH_2)_nPPh_2)]_2$ gives the polymeric product, $[Rh(CO)Cl(dppe)(tcne)]_x$ (n=4), and complex [3.6] in which tcne adds to one rhodium centre (n=3).[62]

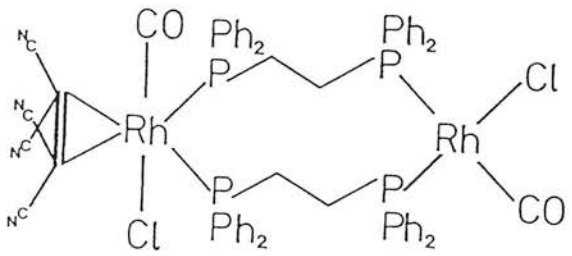

[3.6]

However, tcne cleaves $[(Cp)_2Rh_2(\mu CO)(CO)_2]$ affording the mononuclear species, [(Cp)Rh(CO)(tcne)].[63]

Tcne reacts with the adducts, $[Rh(PhNC)_2(PPh_3)_2]Cl$ and $[Rh(PhNC)_4]Cl$ to generate[64] $[Rh(PhNC)_2(PPh_3)(tcne)Cl]$ and $[Rh(PhNC)_3(tcne)Cl]$ respectively, but the perchlorate salt, $[Rh(p\text{-}RC_6H_4\text{-}NC)_4]^+[ClO_4]^-$ (R=CH_3, OCH_3, Cl) affords $[Rh(p\text{-}RC_6H_4\text{-}NC)_4(tcne)]^+$ with equimolar amounts of tcne.[65-67] The ^1H n.m.r. spectrum of this adduct is independent of temperature, however the fmn complex, $[Rh(p\text{-}MeC_6H_4\text{-}NC)_4(fmn)]^+$ exhibits fluctional behaviour consistent with rotation of the cyanoalkene.[66] The

analogous complex, $[Ir(p\text{-}MeC_6H_4\text{-}NC)_2(PPh_3)_2(tcne)]^+$, can be prepared from $[Ir(p\text{-}MeC_6H_4\text{-}CN)_2(PPh_3)_2]^+$ and tcne.[68]

The carbon monoxide ligand in $[RhCl(p\text{-}MeOC_6H_4NC)_2(CO)]$ is displaced by tcne, and addition of pyridine affords $[RhCl(p\text{-}MeOC_6H_4NC)_2(py)(tcne)]$.[64] The N-C stretching frequency in these complexes shifts to higher energy on co-ordination of tcne, and this is attributed to the depletion of *d*-electron density on the metal due to extensive back-bonding to tcne.[64]

The earliest iridium-tcne complexes were prepared by Baddley.[69,70] Reaction of tcne, fmn, and acn with $[IrX(CO)(EPh_3)_2]$ (ER_3=PPh_3, X=Cl, Br, I, NCO, NCS,[69] F[71]; ER_3=$AsPh_3$, X=Cl[69]; ER_3=PMe_2Ph, X=Cl[72]) affords the addition product, $[IrX(CO)(EPh_3)_2(alkene)]$, which is also prepared from $[IrCl_2(CO)(PPh_3)_2(AuPPh_3)]$ and tcne.[73] The order of increasing stability for these complexes is found to be tcne > fmn > acn and is attributed[69] to the relative energies of the alkene π^*-orbital.

Single-crystal X-ray diffraction studies of both the bromo-phosphine[74,75] and chloro-arsine[76] derivatives show that the C=C bond (1.506 and 1.507Å respectively) is longer than in the free ligand (1.344Å) implying that appreciable back-donation of electron density from the metal *d*π-orbitals into the π^*-orbital of the alkene occurs. Kinetic studies on some of the tcne complexes, $[MX(CO)(PR_3)_2(alkene)]$ (M=Rh, Ir), have been reported[77];

the rate of substitution is accelerated by electron-releasing substituents on the phosphine (which increase the nucleophilicity of the metal substrate) with the rate of reaction being (about nine times) faster for iridium than rhodium.

Tcne displaces N_2 from $[IrCl(N_2)(PPh_3)_2]$, but fmn affords $[IrCl(PPh_3)_2(fmn)]$ and $[IrCl(N_2)(PPh_3)_2(fmn)]$.[59] The authors concluded that for these complexes, and the $[Rh(chel)(alkene)]^+$ adducts, the donor capacity of fmn was more important than the π-acceptor capability, while for tcne the π-acceptor capacity was overwhelming.[59]

At room temperature, $[IrX_2(CO)_2]^-$ (X=Cl, Br, I) and tcne react immediately producing $[IrX_2(CO)_2(tcne)]^-$; simple alkenes are unreactive even at 373K.[78] Similarly, $[IrCl(NO)(PPh_3)_2(tcne)]^+$ is prepared from tcne and $[IrCl(NO)(PPh_3)_2]^+$, but no reaction is observed with fmn.[79] The rhodium complex, $[Rh(NO)(PPh_3)_2(tcne)]^+$, is generated from tcne and $[Rh(NO)(PPh_3)_3]$.[80] The novel nitrato-species, $[Ir(CO)(PPh_3)_2(NO_3)]$, adds tcne affording $[Ir(CO)(PPh_3)_2(NO_3)(tcne)]$.[81]

The acetylide complexes $[M(CO)(C_2R)(PPh_3)_2]$ (M=Rh, R=Me, Et,[82] Ph[83]; M=Ir, R=Me, Bu^t,[82] Ph[84]) add tcne to produce the corresponding $[M(CO)(C_2R)(PPh_3)_2(tcne)]$. Refluxing the rhodium-phenyl acetylide complex in acetonitrile affords $[Rh(NCMe)(C_2Ph)(PPh_3)_2(tcne)]$ which has been characterised by X-ray crystallography.[83] The

addition products found for rhodium and iridium contrast with the [2+2] cyclo-addition products observed for $[(Cp)Fe(CO)_2(CCPh)]$ and $[(Cp)W(CO)_3(CCPh)]$.[85,86]

Tcne adds to one end of the thiolato bridged iridium dimers, $[Ir(\mu\text{-}SBu^t)(CO)(PR_3)]_2$ (R=Me, Ph, OMe), and the crystal structure of the phosphite derivative has been reported.[87]

3.3.4 Nickel, palladium, and platinum complexes.

The diphosphine species, [Ni(dppb)(tcne)], is the product formed from both $[Ni(dppb)_2]$ and $[Ni(dppb)_2(CO)]$ and tcne.[88,89] The reaction of the latter with fmn however, affords a mixture of [Ni(dppb)(fmn)] and $[Ni(dppb)(CO)_2]$.[89]

The platinum complex $[Pt(tcne)(PR_3)_2]$ is prepared[90-92] from $[PtHX(PR_3)]$ (X=Br, Cl; R=Ph, Et),[90,91] $[Pt(PR_3)_3]$ (PR_3=P{=NR(NRR')}, R=Bu^t, R'=$SiMe_3$),[92] or $[Pt(PhCCH)(PR_3)_2]$ (R=Et, Ph)[90] with tcne. Similarly, the hydrido-complex, $[PtHCl(PPh_3)_2]$, loses HCl on reaction with tcne to afford $[Pt(PPh_3)_2(tcne)]$.[93] However, $[PtClMe(PMe_2Ph)_2]$ produces $[PtClMe(tcne)(PMe_2Ph)_2]$ with tcne.[94] This is believed to be the result of a strong H-Cl bond, and not, the ease of rupture of the Pt-R bond (R=H, Me).

The novel complex, $[PtH(CN)(tcne)(PEt_3)_2]$, is prepared from $[PtH(CN)(PEt_3)_2]$ and tcne.[93] This complex contains both a π-bound alkene and a hydride and is thus a model

for the hydrido species believed to be present in the homogenous catalytic reactions of alkenes. Similarly, the cationic species, $[PtH(PBu^t_3)_3]^+$, reacts with tcne to afford the hydrido-complex, $[PtH(tcne)(PBu^t_3)_2]$, but is unreactive to ethylene or tetrafluoroethylene.[95]

$[Pd(tcne)(PPh_3)_2]$ is prepared from the tetra-phosphine complex and tcne.[96]

3.4 Metal-N σ-bonded complexes.

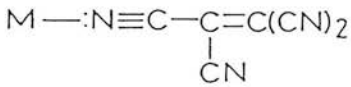

Although many organonitrile complexes of transition metals are known, this form of binding is rarely found for tcne. When $[(Cp)_2VX]$ (X=Cl, Br, I) and equimolar amounts of tcne are added together in tetrahydrofuran, $[(Cp)_2VX(tcne)]$ is formed as a microcrystalline product which decomposes rapidly on exposure to air.[97] A crystallographic study of $[(Cp)_2VBr(tcne)]$ revealed the molecular structure, but refinement of the data was insufficient to allow determination of bond lengths or angles.

Infrared data (see Chapter 3.7) suggests that this complex is formally a V^{IV} core bound to $tcne^{\cdot-}$ produced by complete electron transfer from the V^{III} centre to the co-ordinated tcne. The diamagnetism of the complex is believed to result from "a strong interaction of the

single vanadium electron with the π-electron density on $tcne^{\cdot-}$.

Photolysis of $[Mn(CO)_2(C_5Me_5)]$.THF in the presence of tcne (or tcnq) results in electron transfer to the cyanoalkene and σ-co-ordination through a single nitrogen to yield complex [3.7]. Addition of an excess of the manganese complex generates [3.8]. For both complexes the tcne is formally uninegative although a delocalised electronic structure is proposed for [3.8].[98]

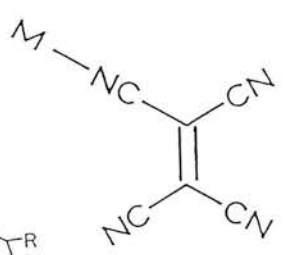

[3.7]

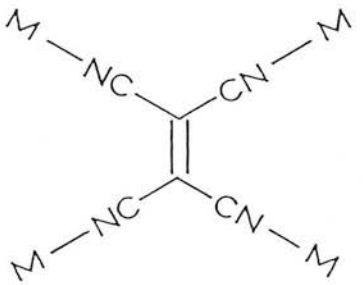

[3.8]

M =

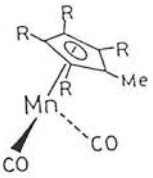

Tcne exhibits co-ordination through nitrogen with all three metals of the iron triad. E.s.r. studies show that equimolar amounts tcne and $[Fe(dppm)_2(C_2H_4)]$ react at 197K to form $[Fe(dppm)_2(C_2H_4)]^+[tcne]^-$.[99] On warming, ethylene is displaced affording the five-co-ordinate species [3.9]. Addition of another equivalent of tcne generates $[Fe(dppm)_2(tcne)]^+[tcne]^-$.

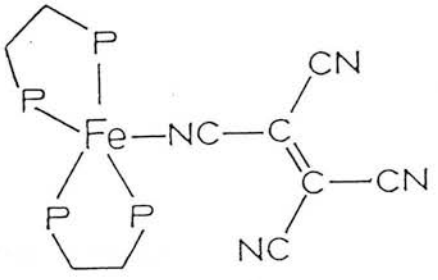

[3.9]

Moers and Langhout reported[100] that the reaction of $[RuCl_2(CO)(PCy_3)_2]$ and $[OsHCl(CO)(PCy_3)_2]$ with equimolar amounts of tcne (and fmn) produces $[RuCl_2(CO)(PCy_3)_2(L)]$ and $[OsHCl(PCy_3)_2(L)]$ (L=tcne, fmn) respectively. A two-fold excess of metal complex yields the adducts, $[\{RuCl(CO)(PCy_3)_2\}_2tcne]$ and $[\{OsHCl(CO)(PCy_3)_2\}_2tcne]$. Similarly, Amer *et. al.* have prepared the tcne-bridged poly-nuclear adducts, $[\{(H_3N)_5Ru\}_nL]^{2n+1}$ (L=fmn, n=2; L=tcne, n=4), and the complexes, $[Ru(NH_3)_5(L)]^{2+}$ (L=tcne, fmn) by reaction of tcne with excess and equimolar amounts of $[Ru(NH_3)_6]^{2+}$ respectively.[101]

In benzene, [Co(acacen)] ‡ [3.10] and tcne afford an intractable polymer which contains the reactants in a 1:1 ratio.[102]

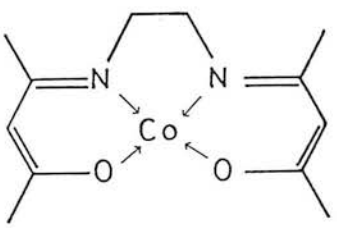

[3.10]

In the presence of pyridine, two isomeric forms (one green and one purple) of a complex analysing for $[\{Co(acacen)(py)\}_2tcne]$ are isolated. Infrared spectral data were used to propose structures [3.11], [3.12], and [3.13].

---

‡(acacen=N,N' ethylenebis[acetylacetoniminato])

M = Co(py)(acacen)

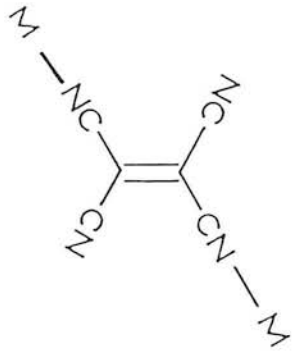

[3.11]

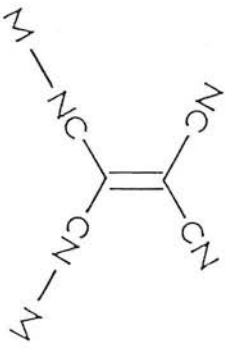

[3.12]

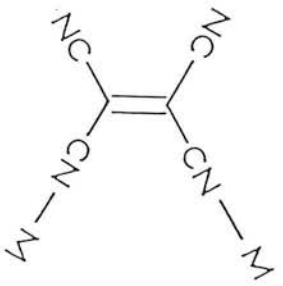

[3.13]

Structures [3.11] and [3.12] were favoured on steric grounds as calculation of approximate nearest-neighbour N-N distances indicate that the co-ordinated nitrogen atoms of the acacen ligand are 0.5Å further apart in [3.12] than in [3.13]. The diamagnetic behaviour of the complexes was assumed to be the result of tcne acting as a "bridge" providing a suitable molecular orbital for the unpaired electron on each Co^{II} ion to become paired.

In 1973, Beck reacted $[MCl(CO)(PPh_3)_2]$ (M=Rh, Ir) with $tcne^{-}$.[103] In addition to rearrangement products, the binuclear species, $[\{Ir(CO)(PPh_3)_2\}_2tcne]$, was prepared.

Mono- and bi-nuclear adducts were isolated when M^{c}Auliffe *et. al.* examined the reaction of Ni^{II} complexes with both tcne and tcnq.[104] With excess amounts of tcne, $[Ni_2(bdpa)_3(H_2O)]^{4+}$ affords the diamagnetic complex [3.14] and with the five co-ordinate $[Ni(dmpae)_2(NCS)]^{+}$, [3.15] and [3.16] are obtained. Infrared spectroscopy and

elemental analysis were used to assign complex [3.14] as containing a *cis*-bridging $tcne^{2-}$ di-anion. Complexes [3.15] and [3.16] however, contain neutral tcne ligands.

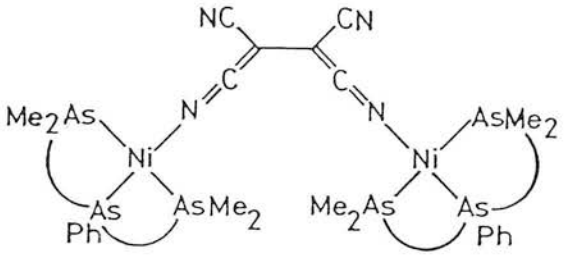

[3.14]

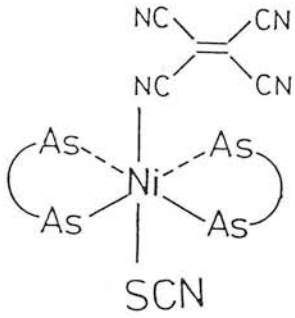

[3.15]

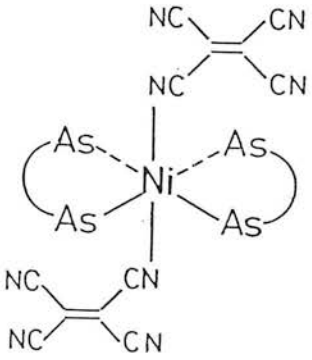

[3.16]

In general σ-N-bound co-ordination is less common for tcne. Reaction with excess ligand generally affords mono-nuclear products, while with 1:1 ratios, bi- or poly-nuclear adducts may be isolated. Electron transfer proceeds co-ordination for many complexes of this type. The characterisation of these adducts has been based mainly on interpretation of infrared spectral data. No examples have been reported where tcne acts as a chelate (through two nitrogen atoms), presumably because of steric constraints.

3.5 Other co-ordination modes.

The transition-metal complexes reviewed above deal exclusively with co-ordination modes in which the integrity of the tcne moiety is maintained. A number of reactions involving (i) insertion of tcne into a M-C, M-N, or M-H bond, (ii) Cyclo-addition, with an unsaturated ligand co-ordinated to the metal centre, and (iii) rearrangement of tcne, leading to fragmentation of the cyano-alkene, have been reported.

3.5.1 Insertion reactions.

Tcne has been shown to insert into metal-hydrogen, metal-carbon, and metal-nitrogen bonds. 1,2- and 1,4-insertions have been found furnishing both the tetracyanoalkyl [3.17], and keteneiminato [3.18] species, respectively.

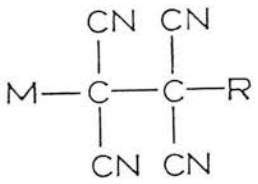

[3.17]

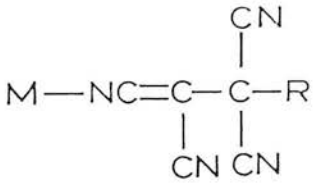

[3.18]

Treatment of $[IrH(CO)(PPh_3)_3]$ with excess tcne in benzene affords the novel insertion product $[Ir(CO)(PPh_3)_2(tcne)(N{=}C{=}C(CN)C(CN)_2H)]$.[105] This complex has both an olefin-bound tcne, and a dicyanomethylketene-iminato moiety formed by insertion of tcne into the Ir-H bond. The metal-keteneiminate bond can be thought of in

two extreme forms:-

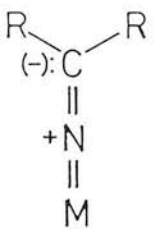

[3.19]

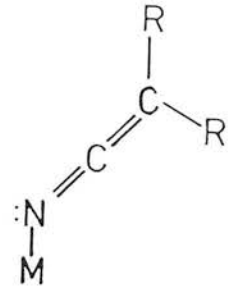

[3.20]

The adduct, $[Ir(CO)(PPh_3)_2(tcne)(N{=}C{=}C(CN)C(CN)_2H)]$, has an Ir-N-C bond angle of 169.9(7)° suggesting that the zwitterion structure plays a dominant role.[106]

Insertion of tcne into the metal-carbon bond of the complexes, $[(Cp)Fe(CO)_2R]$ (R=Me, Et, Pr^i, CH_2Ph, $(CH_3)Ph$), affords both cyanoalkyl and keteneiminate complexes.[107-109] ^1H n.m.r. and infrared spectroscopy confirm that no interconversion between isomeric forms occurs. The analogous $[(Cp)Mo(CO)_3R]$ complexes do not react in this way, but $[(Cp)Mo(CO)_2(L)R]$ ($L=PPh_3$, $P\{OPh\}_3$, R=Me, Et) furnishes both 1,2- and 1,4-insertion products which isomerise between cyanoalkyl and keteneiminate forms in solution.[110] The crystal structure of the cyanoalkyl adduct $[(Cp)Mo(CO)(PPh_3)(-C(CN)_2C(CN)_2CH_3)]$ has been determined.[111]

With the complex, $[(Cp)Fe(CO)(L)R]$ ($L=PPh_3$, $P\{OPh\}_3$; $R=CH_2Ph$), tcne affords the keteneiminate complex. However, if the alkyl group is changed to a methyl, ethyl, or n-propyl, then "carbonyl insertion" takes place and [3.21] is afforded.[110]

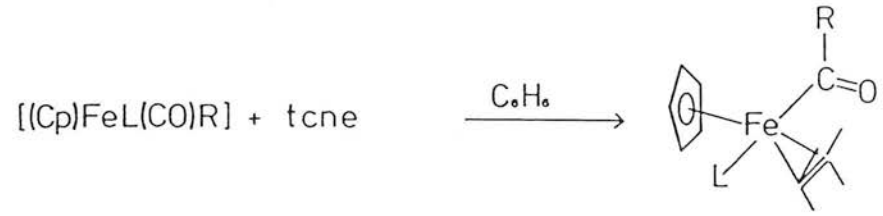

[3.21]

Thermal treatment or long term storage of [3.21] affords the keteneiminate and/or the parent complex.

Tcne reacts with $[(Cp)Cr(NO)_2R]$ ($R=CH_3$, CH_2Ph) to give both 1,2- and 1,4-insertion products, which interconvert in solution[112]. However, $[MR_2(bipy)]$ (M=Ni, R=Me, Et; M=Pt, R=Me) generate only keteneiminates on reaction with tcne.[113]

Tcne inserts into the Pt-N bond of the η^2-bonded nitroso-ligand in $[Pt(PPh_3)_2(PhNO)]$ to give the cyanoalkyl derivative [3.22].[114]

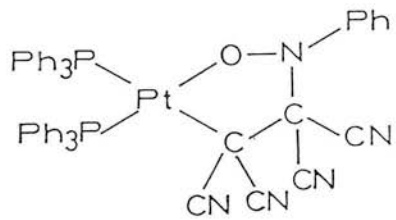

[3.22]

3.5.2 Cyclo-addition reactions.

Tcne is one of the strongest dieneophiles known.[22] Hence, the addition of tcne to $[(Cp)M(CO)_xCH_2C(R')=CR_2]$ (M=Fe, x=2; M=Mo, x=3; R'=H, R=Me; R'=Me, R=H) generates the 1,3 cyclo-addition complex [3.23].[115]

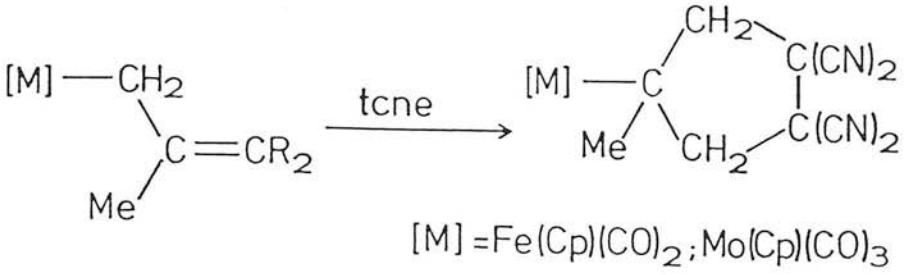

[3.23]

[M] = Fe(Cp)(CO)$_2$; Mo(Cp)(CO)$_3$

The crystal structure of the [3+2] cyclo-addition product formed from [(Cp)Fe(CO)$_2$(CH$_2$-C(CH$_3$)=CH$_2$)] and tcne has been reported.[116] Replacing a carbonyl ligand by P{OPh}$_3$ affords the keteneiminate complex and this is attributed to the steric bulk of the phosphite. In the same way (η^5cyclopentadienyl)(η^1cyclopropylmethyl)iron reacts with tcne to give the cyclo-addition product [3.24].[117]

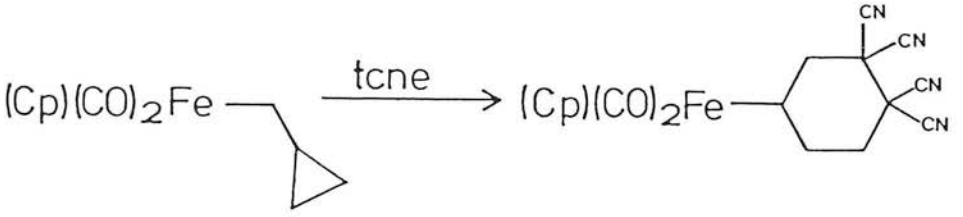

[3.24]

Tcne also undergoes Diels-Alder type addition when the product of the reaction between [Fe(CO)$_3$(η^4-cot)] (cot=cyclo-octatetraene) and [C$_7$H$_7$]$^+$ is allowed to react to tcne to give the addition product [3.25].[118]

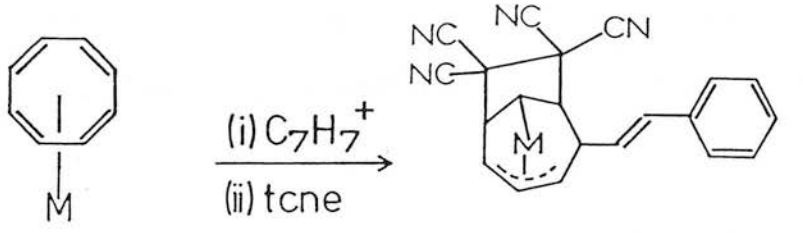

[3.25]

M=Fe(CO)3

3.5.3 Rearrangement reactions.

The complexes, $[(C_5Me_5)Rh(S\text{-}S)(MeOH)]BPh_4$, have been synthesised in this laboratory.[119] The co-ordinated methanol is easily displaced by Lewis bases generating the cationic species, $[(C_5Me_5)Rh(S\text{-}S)L]^+$ (L=PPh_3, PPh_2Me, $AsPh_3$, py, CO). However, attempts to displace the ligated methanol by addition of excess tcne and $Na[BPh_4]$ in methanol afforded the neutral triphenylcyanoborate complex [3.26].

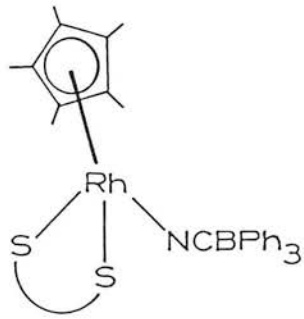

[3.26]

The BPh_3CN^- anion can be generated from the reaction of hydrogen cyanide with BPh_4^-. Earlier studies have shown[22] that hydrogen cyanide is formed when alkoxides react with tcne in the presence of certain catalysts and this probably explains the degradation of tcne in this reaction.

Similarly, Kemmit *et. al.* observed the formation of $[Pt(CN)_2(PPh_3)_2]$ from the reaction of tcne with the acetate complex, $[Pt(OCOCX_3)_2(PPh_3)_2]$ (X=F, H), in refluxing methanol.[120]

Bruce and co-workers have isolated the rearrangement

product [3.27] from the reaction of $[Ru(C_2Ph)(PPh_3)_2]$ and tcne.[121] These contrast with the [2+2] cyclo-addition products formed between tcne and $[(Cp)Fe(CO)_2(CCPh)]$.[85]

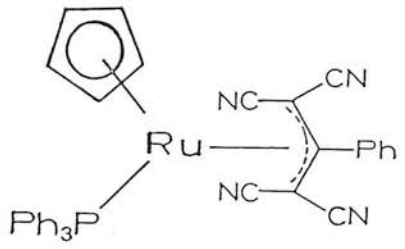

[3.27]

3.6 Results and discussion.

In light of the versatility of tcne as a ligand, and in order to extend the chemistry of the $[M(S_2PR_2)_2(PR_3)_2]$ compounds, the reaction of tcne with $[M(S_2PR_2)_2(PPh_3)_2]$ (M=Ru, Os; R=Me, Ph, OEt) has been examined. With equimolar, and excess, quantities of tcne the major products isolated analysed for $[\{Ru(S_2PR_2)_2(PPh_3)\}_2tcne]$ (R=Me, Ph, OEt) and $[M(S_2PR_2)_2(PPh_3)(tcne)]$ (M=Ru, Os; R=Me, Ph, OEt) respectively. The former complexes were found to exist as a mixture of isomers.

The mono-nuclear products, $[M(S_2PR_2)_2(PPh_3)(tcne)]$ (M=Ru, Os; R=Me, Ph, OEt), were prepared by dropwise addition of the orange-red complex $[M(S_2PR_2)_2(PPh_3)_2]$ (in methylene chloride) to excess tcne in the same solvent. After stirring for several hours, the volume of solvent was reduced and excess tcne was removed by filtration.

Addition of the filtrate to n-hexane gave a bright-green precipitate of the adduct, $[M(S_2PR_2)_2(PPh_3)(tcne)]$. Quantitative yields of $[Ru(S_2PR_2)_2(PPh_3)(tcne)]$ (R=Me, Ph, OEt), can also be prepared from $[\{Ru(S_2PR_2)_2(PPh_3)\}_2tcne]$ and an equimolar amount of tcne.

The bimetallic adducts, $[\{Ru(S_2PR_2)_2(PPh_3)\}_2tcne]$ (R=Me, Ph, OEt), were prepared from equimolar amounts of $[Ru(S_2PR_2)_2(PPh_3)_2]$ and tcne in methylene chloride. The complex was precipitated from solution by addition of n-hexane, affording the yellow-green binuclear species, $[\{Ru(S_2PR_2)_2(PPh_3)\}_2tcne]$. The binuclear adducts can also be prepared quantitatively from equimolar amounts of $[Ru(S_2PR_2)_2(PPh_3)_2]$ and $[Ru(S_2PR_2)_2(PPh_3)(tcne)]$ (R=Me, Ph, OEt). Attempts to prepare $[\{Os(S_2PR_2)_2(PPh_3)\}_2tcne]$ were unsuccessful. Although different experimental conditions were tried, the only isolable osmium species were the adducts, $[Os(S_2PR_2)_2(PPh_3)(tcne)]$ and/or unreacted $[Os(S_2PR_2)_2(PPh_3)_2]$.

Gentle reflux shortens the preparation times of both binuclear and mono-nuclear complexes, but excessive heating causes decomposition of the product. The $^{31}P-\{^1H\}$ n.m.r. spectra of these samples showed that $OPPh_3$ and the known adduct, $[tcne.PPh_3]$,[25] are also present in the precipitated solid of both mono- and bi-nuclear adducts.

In an attempt to obtain spectroscopically pure samples of $[Ru(S_2PR_2)_2(PPh_3)(tcne)]$, dry-column

chromatography[122] with a neutral alumina adsorbent and chloroform eluent was used. Interestingly, the green product isolated after chromatography was not found to be $[Ru(S_2PPh_2)_2(PPh_3)(tcne)]$, but the binuclear species, $[\{Ru(S_2PPh_2)_2(PPh_3)\}_2tcne]$. The activity of the column was found to affect the extent of this chemical change; as the activity of the alumina is decreased (see Chapter 3.14) a mixture of $[Ru(S_2PR_2)_2(PPh_3)(tcne)]$ and $[\{Ru(S_2PR_2)_2(PPh_3)\}_2tcne]$ is obtained. However, pure samples of $[Ru(S_2PR_2)_2(PPh_3)(tcne)]$ cannot be isolated as invariably, some conversion of $[Ru(S_2PR_2)_2(PPh_3)(tcne)]$ to $[\{Ru(S_2PR_2)_2(PPh_3)\}_2tcne]$ occurs during chromatography. These complexes have similar R_f values on this medium and are observed in one band.

This rearrangement may result from the known interaction of alumina (and other adsorbents) with tcne.[123-125] This property of tcne has led to its use as a specific catalyst poison.[126,127] Flockhart *et. al.* have shown[124] that an e.s.r. signal is observed when benzene solutions of tcne are added to alumina and suggests that the tcne ligand is reduced by the alumina. In addition, tcne can be chemisorbed and/or undergo chemical rearrangement (forming tricyanovinyl alcohol) on alumina.[128,129] Electrochemical studies (see Chapter 4) suggest that the conversion of the adducts, $[Ru(S_2PR_2)_2(PPh_3)(tcne)]$, to $[\{Ru(S_2PR_2)_2(PPh_3)\}_2tcne]$ during chromatography is consistent with electron transfer from the alumina to

$[Ru(S_2PR_2)_2(PPh_3)(tcne)]$.

Purification of the adducts, $[M(S_2PR_2)_2(PPh_3)(tcne)]$ and $[\{Ru(S_2PR_2)_2(PPh_3)\}_2tcne]$, can be achieved by preparative thin-layer chromatography (see experimental section). Some rearrangement of $[Ru(S_2PR_2)_2(PPh_3)(tcne)]$ occurs, but to a lesser extent than by the dry column method. Additionally, $[Ru(S_2PR_2)_2(PPh_3)(tcne)]$ and $[\{Ru(S_2PR_2)_2(PPh_3)\}_2tcne]$, have different R_f values on this medium and can be separated.

Figure 3.3 shows the inter-relation between the various complexes. The mono- and bi-nuclear products were fully characterised using the spectroscopic techniques described below. In addition, the adducts, $[Os(S_2PMe_2)_2(PPh_3)(tcne)]$ and $[Os(S_2PPh_2)_2(PPh_3)(tcne)]$, have been studied by single-crystal X-ray diffraction.

3.7 Infrared spectroscopy.

3.7.1 Tetracyanoethylene and its anions.

Devlin and co-workers have studied the vibrational spectra of neutral tcne and its ions.[130-137] Tcne has D_{2h} symmetry and has 24 fundamental vibrations. Four fundamental CN stretches are observed at 2262(IR), 2248(R), 2237(R), and 2228(IR)cm^{-1}.[131] The Raman active C=C stretching vibration occurs at 1569cm^{-1} in the neutral molecule. The strong fundamental bands at 600-1300cm^{-1} in the infrared spectrum are associated with the C-C bonds.

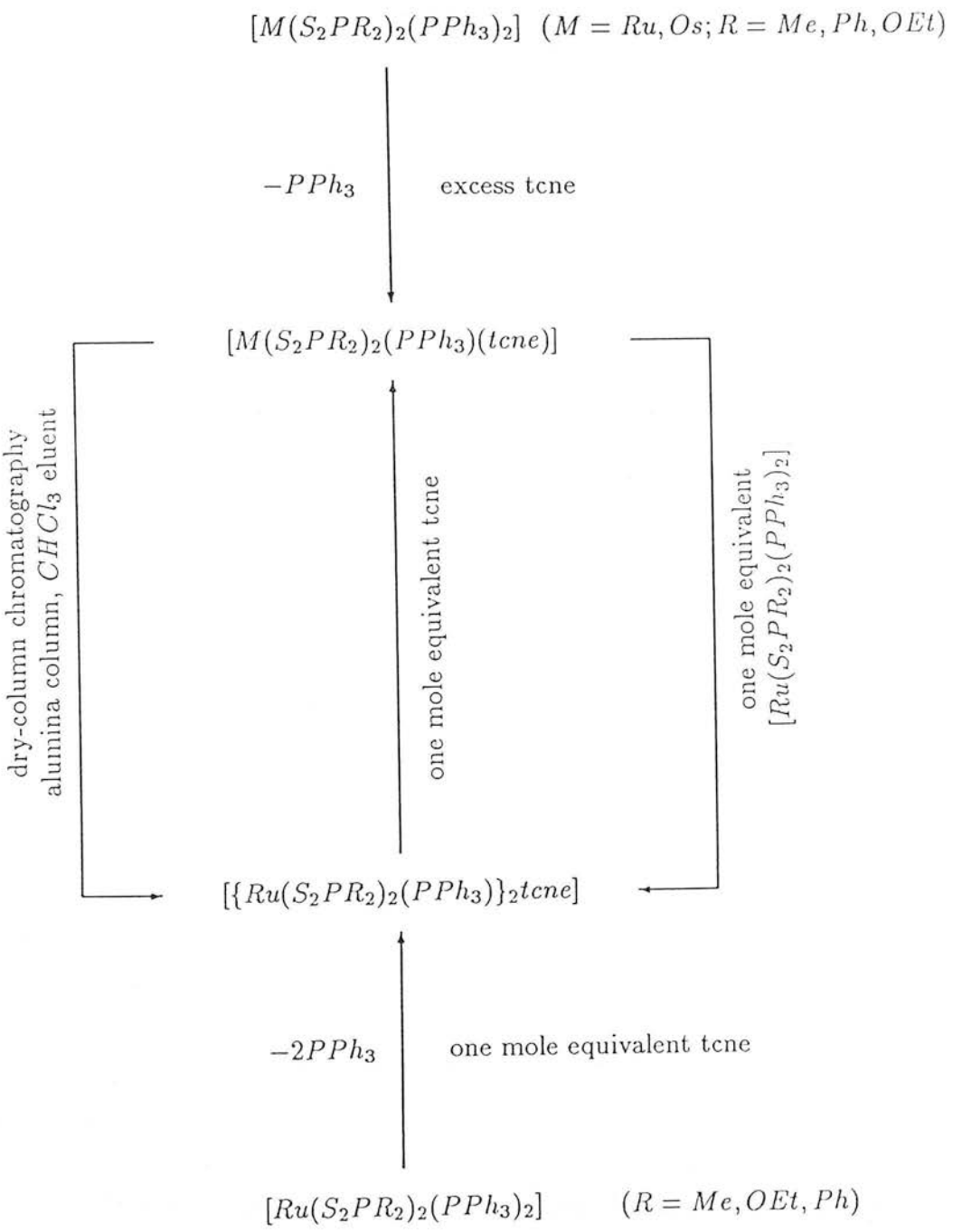

Figure 3.3: The inter-relationship between $[Ru(S_2PR_2)_2(PPh_3)tcne]$ and $[\{Ru(S_2PR_2)_2(PPh_3)\}_2tcne]$.

SCFMO and Huckel type calculations have shown[134] that the additional electron in the anion enters a molecular orbital of B_1 symmetry such that the C≡N and C=C bonds are weakened while the C-C bond order is increased.

The infrared spectrum of M^+tcne^- (M=Na, K, Li) is radically different from the neutral molecule in that there is an intense band at 1371cm^{-1} and a marked absence of absorptions in the 600-1300cm^{-1} region.[134] The intense band is assigned to the infrared-forbidden C=C stretch which has been activated by an "electron vibration" phenomenom (as observed for tcnq[133]), in accordance with the Ferguson-Matsen principle.[138,139] The frequency of this absorption is dependent on the electron affinity of the cation.[135] Thus, the frequency of $\nu_{C=C}$ moves noticeably towards that of neutral tcne as the electron affinity of (and hence the degree of back donation to) the cation increases. As a consequence of this vibronic activation an intense doublet at 2180-2201cm^{-1} is observed for the C≡N vibration. The splitting on this band vanishes in the glassy phase.[135]

The infrared spectrum of Na_2[tcne] is similar to that of Na[tcne].[136] The intense C≡N stretching bands are observed at lower frequency (89cm^{-1}) than for the radical anion. The C=C stretching absorption is also shifted to lower energy, and is observed at 1256cm^{-1}. The activation of this band is believed to be the result of charge-transfer to the polarizing Na^+ cation, or due to

geometrical change.[136] The shift to lower energy of both the C≡N and C=C stretching vibrations is predicted by molecuar orbital calculations which indicate that the additional electron enters an anti-bonding orbital with respect to these bonds.[136]

The addition of a third electron weakens the C≡N bonds further and bands at 1980 and 2032cm^{-1} are observed. Extended Huckel calculations show[136] that this electron enters the seventh M.O. of the π - system which is antibonding with respect to the nitriles and nonbonding otherwise. However, the assignment of the $\nu_{C=C}$ stretching vibration at 1346cm^{-1} for Na_3[tcne] suggests that this bond is in fact strengthened.

3.7.2 Transition metal complexes of tcne.

As discussed above tcne can co-ordinate in several different ways to a transition metal centre. The frequency, and multiplicity, of the ν_{CN} band has been found to be diagnostic of the binding mode of tcne in these complexes.

Charge-transfer complexes such as [$(Cp)_2$Fe][tcne],[27] and [$Pt_2S_2(PPh_3)_4$][tcne],[38] exhibit a small decrease in the cyano stretching frequency consistent with transfer of some electron density to the ligand.[134] If electron transfer is complete and a radical anion salt is formed e.g. [$(Cp)_2$Os]$^+$[tcne]$^-$,[37] then the ν_{CN} band is observed at around 2200cm^{-1}.

Complexes with an alkene-bound tcne moiety e.g. $[Pt(PEt_3)_2(tcne)]$,[90] $[IrBr(CO)(PPh_3)_2(tcne)]$,[69] and [Ni(dppb)(tcne)],[88] exhibit a single ν_{CN} band, at lower frequency (20-30cm^{-1}) than the free ligand.

Co-ordination through the C≡N bond has not been claimed for tcne. By analogy to acetylenes bound to a metal centre through the CC triple bond,[140] a large decrease in the C≡N vibrational frequency is expected for this co-ordination mode. Organic isocyanate and dialkylcyanamide complexes of transition metals, in which the metal is π-bound to the C≡N bond, typically exhibit C≡N absorptions 150 and 200cm^{-1} lower (respectively) than the free ligands.[141,142] Infrared spectral data assign this type of bonding in $[Mo(CO)_3X(NCCH_2CH_2CN)]$ (X=Cl,Br,I).[143]

Many N-bonded organonitrile complexes of transition metals are known[144] and these show a characteristic increase (30-100cm^{-1}) in ν_{CN} from the free nitrile. This shift results from an increase in the C≡N force constant upon co-ordination.[145] All such N-bonded complexes of tcne, however, show a decrease in frequency for the C≡N (and C=C) stretching vibrations.[97-104] This suggests that for tcne significant back-donation occurs, and that the acceptor orbital of tcne in this co-ordination mode is anti-bonding for the C≡N (and C=C) bond. Thus, Rettig and Wing assign bands at 2211,2152,2152 and 2128cm^{-1} in the infrared spectrum of $[(Cp)_2VCl(tcne)]$ to C≡N vibrations of N-co-ordinated tcne.[97] Additionally, a new

band observed at 1400cm^{-1} is identified as the C=C stretch of the co-ordinated tcne.

3.7.3 [M(S_2PR_2)$_2$(PPh_3)(tcne)] complexes.

The infrared spectrum of [M(S_2PR_2)$_2$(PPh_3)(tcne)] (M=Ru, Os; R=Me, Ph, OEt) is (within the limits of the solvent window) identical for KBr discs and methylene chloride solutions of the complex. Table 3.1 lists some spectral data for these complexes. The infrared spectrum of [Ru(S_2PPh_2)$_2$(PPh_3)(tcne)] (see Figure 3.4) exhibits intense absorptions in the 2100-2235cm^{-1} region, and a strong band around 1430cm^{-1}, which are not present in the vibrational spectra of the starting materials.

The low frequency of the nitrile absorption is consistent with C-N:——M σ-bonding, or π-bonding to the C-N bond. The N-bonding mode is preferred by comparison with other known transition-metal complexes of tcne (*vide supra*). Single-crystal X-ray diffraction studies of [Os(S_2PMe_2)$_2$(PPh_3)(tcne)], and [Os(S_2PPh_2)$_2$(PPh_3)(tcne)] (see Chapter 3.11) confirm that tcne is N-bonded to the metal centre. The new band at 1430cm^{-1} is assigned to the C=C stretch of co-ordinated tcne. The shift to lower energy of the C-N and C=C vibrational frequencies is consistent with back donation from the metal *d*π-orbitals into the LUMO of tcne (which is antibonding with respect to these bonds).

127

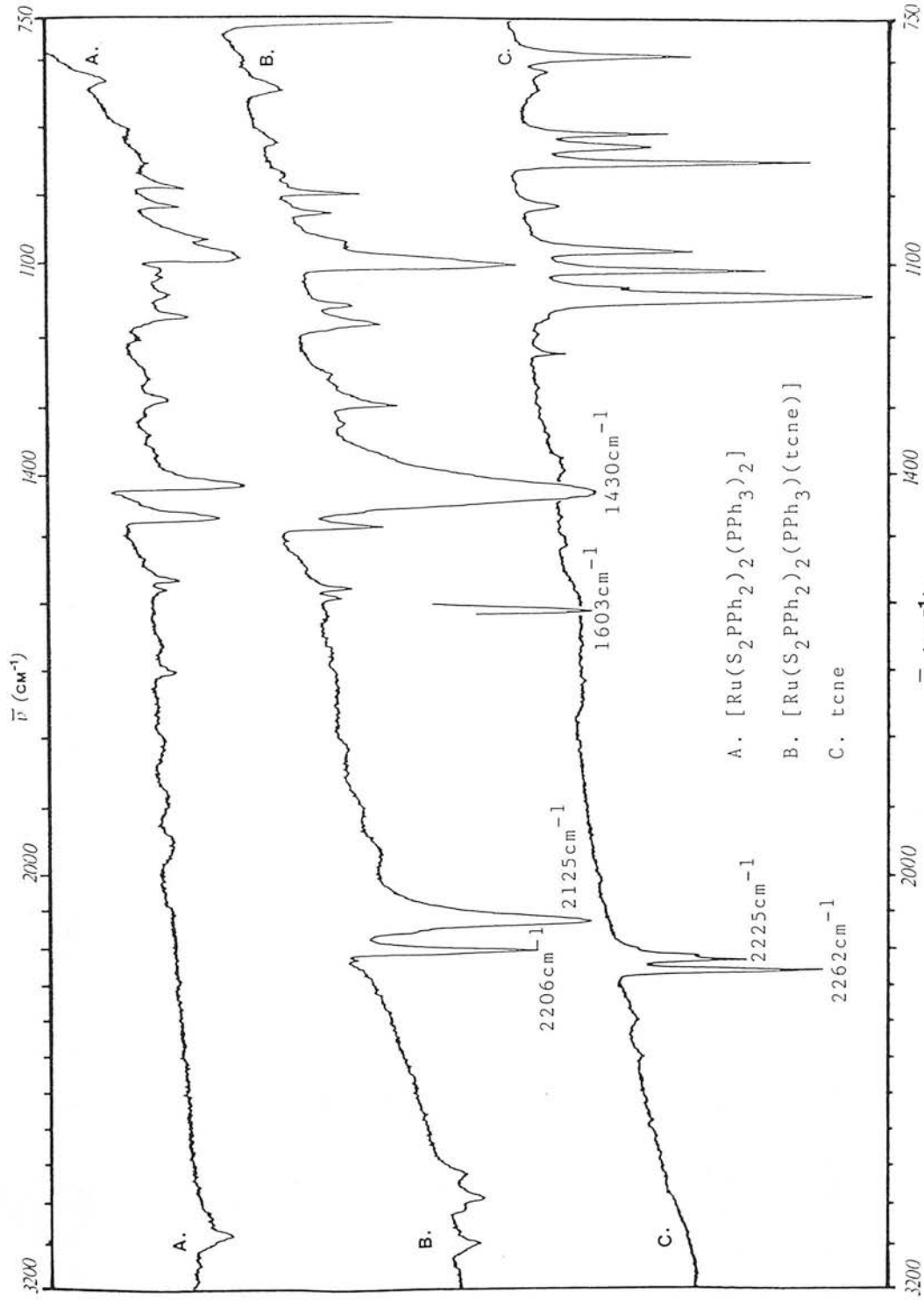

Figure 3.4: The infrared spectra of (a) $[Ru(S_2PPh_2)_2(PPh_3)_2]$, (b) $[Ru(S_2PPh_2)_2(PPh_3)(tcne)]$, and (c) tcne. All spectra recorded as KBr pellets.

Table 3.1: Selected infrared data for $[M(S_2PR_2)_2(PPh_3)(tcne)]$.[a]

M	R	$\bar{\upsilon}_{CN}/cm^{-1}$	$\bar{\upsilon}_{C=C}/cm^{-1}$
Ru	Me	2232 w; 2202, 2130 s, br[b]	1421 vs, br
Os	Me	2220 w; 2195 vs; 2100 s, br	1409 vs, br
Ru	Ph	2206 s; 2125 vs, br	1430 vs, br
Os	Ph	2195 s; 2100 s, br	1412 vs, br
Ru	OEt	2210 s; 2120 vs, br	1460 vs, br
Os	OEt	2200 s; 2100 s, br	1433 vs, br
tcne[c]		2262, 2225 s	1569 (R)
$[(Cp)_2VBr(tcne)]$[d]		2221, 2192, 2152, 2128	1437

(a) The samples were all recorded as KBr pellets from 4000-250cm^{-1}.

(b) w - weak, s - strong, vs - very strong, br - broad.

(c) Taken from reference 132. (d) Taken from reference 97.

Complete electron-transfer to the bound tcne moiety is assigned for $[(Cp)_2V^{IV}Br(tcne^-)]$ on the observation of $\nu_{C=C}$ at $1400cm^{-1}$ in the infrared spectrum.[97] It therefore seems likely that appreciable charge-transfer (from the metal to the tcne ligand) is prevalent in the adducts, $[M(S_2PR_2)_2(PPh_3)(tcne)]$. The extent and nature of this transfer will be examined in Chapter 4.

The frequency of the C=C stretching vibration in the complexes, $[M(S_2PR_2)_2(PPh_3)(tcne)]$ (M=Ru, Os; R=Me, Ph, OEt), varies with (a) the metal type and (b) the substituent on the dithiolate ligand. The C=C stretching frequencies are lower in energy for M=Os than for M=Ru suggesting that back-donation from the metal $d\pi$-orbitals to the tcne LUMO is greater for osmium. This is supported by the electrochemical and spectroelectrochemical studies of these complexes (see Chapter 4). For a particular metal, the $\nu_{C=C}$ absorption is observed at higher wavenumber (*ca.* $30cm^{-1}$) for the dithiophosphate complex compared with the analogous dithiophosphinate species.

3.7.4 $[\{Ru(S_2PR_2)_2(PPh_3)\}_2tcne]$ complexes.

The infrared spectrum of $[\{Ru(S_2P\{OEt\}_2)_2(PPh_3)\}_2tcne]$ is shown in Figure 3.5 and is typical of the complexes, $[\{Ru(S_2PR_2)_2(PPh_3)\}_2tcne]$ (R=Me, Ph, OEt). For all $[\{Ru(S_2PR_2)_2(PPh_3)\}_2tcne]$, a strong broad band at *ca.* $2100cm^{-1}$ and two weaker absorptions at *ca.* $2200cm^{-1}$ are observed, and are assigned to ν_{CN} of ligated tcne.

130

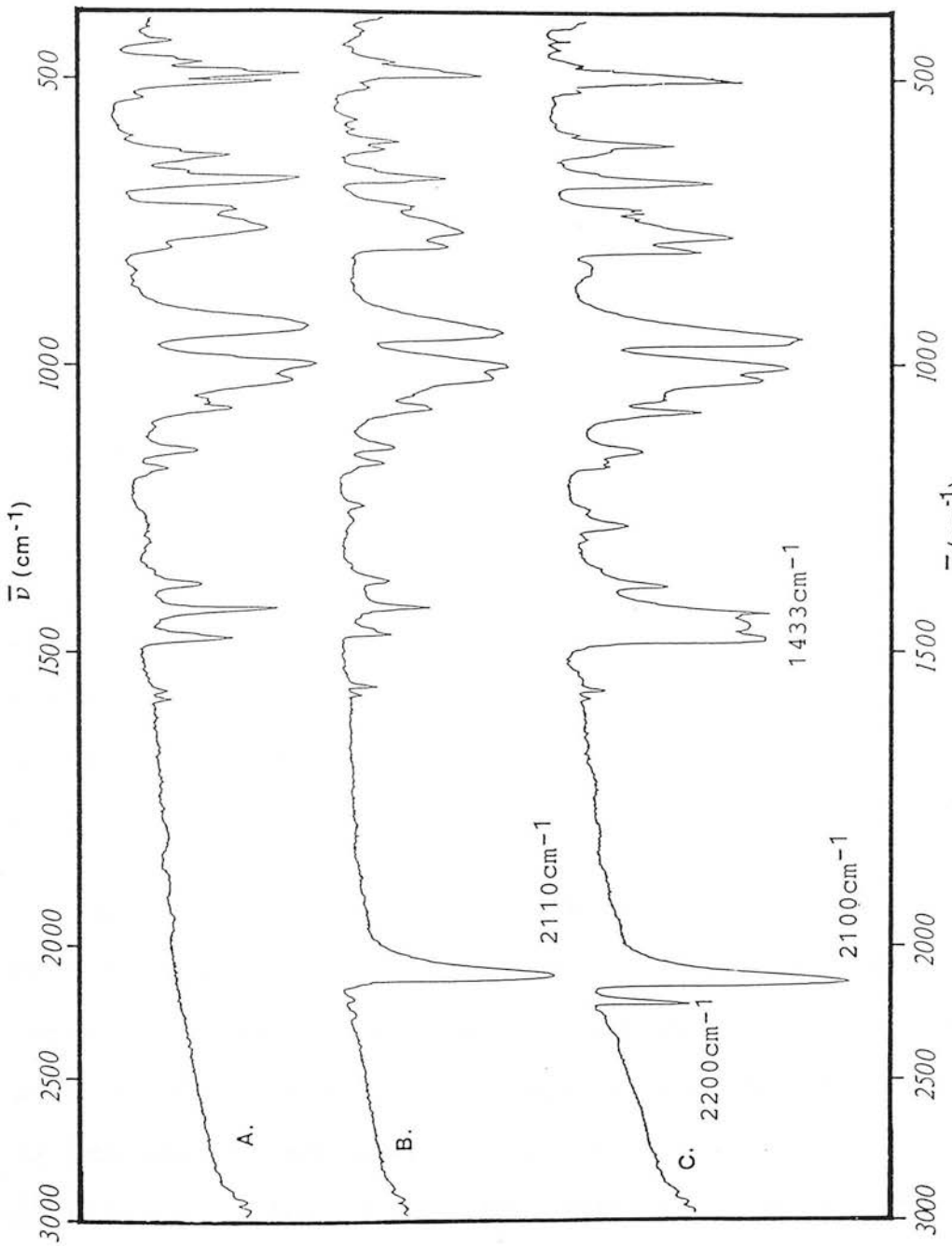

Figure 3.5: The infrared spectra of (a) $[Ru(S_2P\{OEt\}_2)_2(PPh_3)_2]$, (b) $[Ru(S_2P\{OEt\}_2)_2(PPh_3)]_2$tcne and (c) $[Ru(S_2P\{OEt\}_2)_2(PPh_3)(tcne)]$ (spectra recorded as KBr pellets).

Unlike the adducts, $[Ru(S_2PR_2)_2(PPh_3)(tcne)]$ (R=Me, Ph, OEt), the strong absorption assigned to the $\nu_{C=C}$ stretching vibration of co-ordinated tcne is absent in the vibrational spectra of the $[\{Ru(S_2PR_2)_2(PPh_3)\}_2tcne]$ complexes. Solution (methylene chloride) and solid (KBr discs) samples of $[\{Ru(S_2PR_2)_2(PPh_3)\}_2tcne]$ give identical infrared spectra (within the limits of the solvent window).

3.8 $^{31}P-\{^1H\}$ n.m.r. spectroscopy.

3.8.1 $[M(S_2PR_2)_2(PPh_3)(tcne)]$ complexes.

The adducts, $[M(S_2PR_2)_2(PPh_3)(tcne)]$ (M=Ru, Os; R=Me, Ph, OEt), show similar spectral patterns. $^{31}P-\{^1H\}$ n.m.r. spectral data for $[M(S_2PR_2)_2(PPh_3)(tcne)]$ is listed in Table 3.2 and the $^{31}P-\{^1H\}$ n.m.r. spectrum of $[Ru(S_2PPh_2)_2(PPh_3)(tcne)]$ is shown in Figure 3.6. The assignment of ligand type to each resonance is based on analogy with the parent complex, $[M(S_2PR_2)_2(PPh_3)_2]$.

In all the adducts, $[M(S_2PR_2)_2(PPh_3)(tcne)]$, the phosphine resonance is observed at lower chemical shift (*ca.* 60ppm lower) than the dithiophosphinate, and appears as a doublet (J_{PP}-12Hz). In some cases (see Table 3.2) a second smaller coupling (J_{PP}-1.5Hz) has been resolved. The dithiolate region of the spectrum (*ca.* δ100ppm) shows two distinct environments for these ligands, and a large doublet (J_{PP}=12Hz) and a singlet (or small doublet J_{PP}=1.5Hz) is observed. This pattern is similar to that

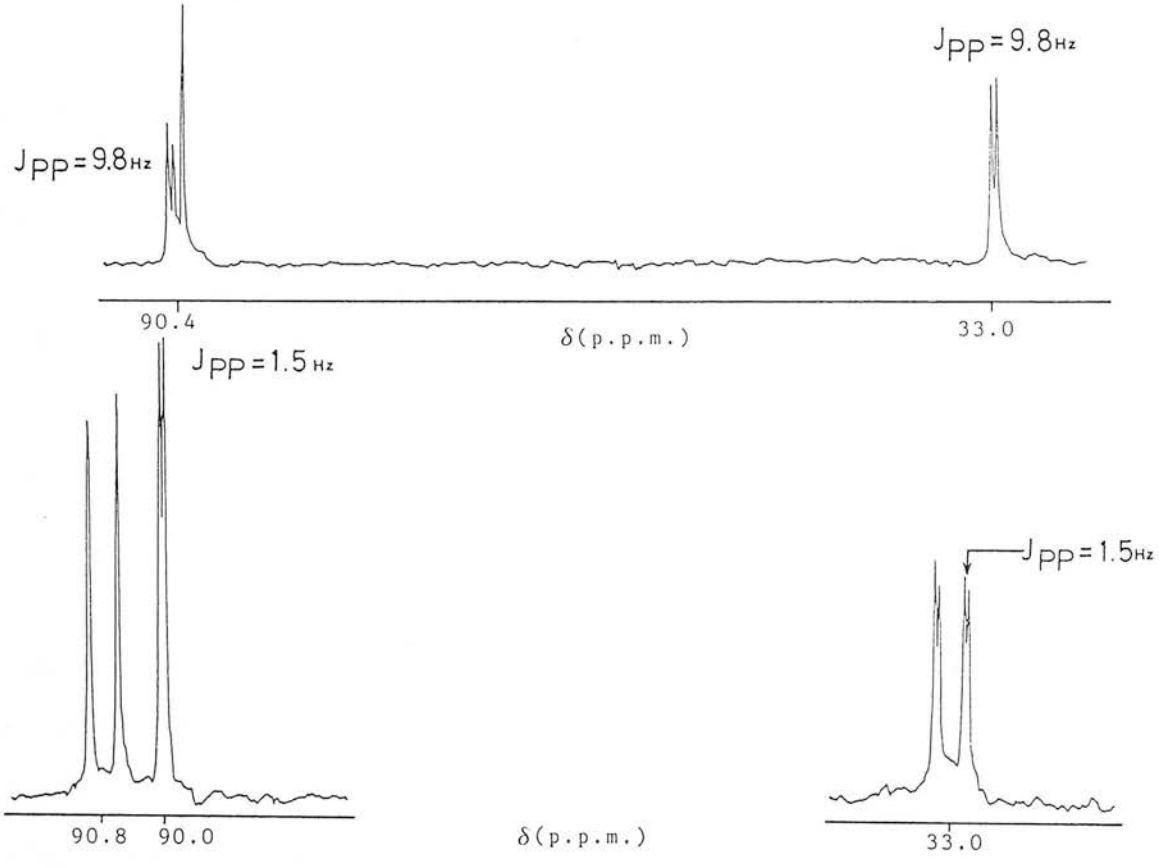

Figure 3.6: The $^{31}P-\{^{1}H\}$ n.m.r. spectrum of $[Ru(S_2PPh_2)_2(PPh_3)(tcne)]$ ($CDCl_3$ solution at 303K).

Table 3.2: $^{31}P-\{^{1}H\}$ n.m.r. spectral data for $[M(S_2PR_2)_2(PPh_3)(tcne)]$.[a]

M	R	δS_2PR_2/p.p.m.	δPPh_3/p.p.m.
Ru	Me	96.4 d[b] (12.4)[c]; 96.2 s	32.4 d (12.4)
Ru	Ph	90.8 d (9.8); 90.0 d (1.5)	33.0 d,d (9.8, 1.5)
Ru	OEt	104.5 d (4.4); 99.9 d (1.0) d	34.3 d,d (4.4, 1.0)
Os	Me[d]	128.0 d (13.2); 115.5 s	-40.3 d (13.2)
Os	Ph	120.9 d,d (12.2, 1.4); 105.8 t[e] (1.2)	-40.2 d,d (12.2, 1.0)
Os	OEt	136.4 d (7.4); 126.0 s	-35.3 d (7.4)

(a) Spectra recorded in $CDCl_3$ solution at 293K.

(b) s-singlet, d-doublet, d,d-doublet of doublets, t-triplet.

(c) Figures in brackets correspond to J_{PP} in Hz.

(d) Further coupling was observed on all resonances, but was not fully resolved.

(e) This is believed to be a "pseudo" triplet formed by two overlapping doublets.

recorded for $[Ru(S_2PR_2)_2(PPh_3)(CO)]$ (R=Me, Ph, OEt) (see Chapter 2.3.4) and is consistent with a *cis*-arrangement of ligands around the metal centre.

The $^{31}P-\{^1H\}$ n.m.r. spectrum of the crude reaction mixture also exhibits resonances at δ29.0, -5.0, and 23.1 ppm which are assigned to $OPPh_3$, PPh_3, and $[PPh_3.tcne]$ respectively, and confirms that PPh_3 is displaced from $[M(S_2PR_2)_2(PPh_3)_2]$ on reaction with tcne.

3.8.2 $[\{Ru(S_2PR_2)_2(PPh_3)\}_2tcne]$ complexes

Figure 3.7 shows the $^{31}P-\{^1H\}$ n.m.r. spectrum of $[\{Ru(S_2PPh_2)_2(PPh_3)\}_2tcne]$ which is typical of other $[\{Ru(S_2PR_2)_2(PPh_3)\}_2tcne]$ (R=Me, OEt). The multitude of resonances in the spectrum confirms that (in solution) the complex analysing for $[\{Ru(S_2PPh_2)_2(PPh_3)\}_2tcne]$ contains more than one species. However, the chemical shifts and relative intensities of the resonances are constant no matter how the complex is prepared, either by (i) direct reaction of equimolar amounts of tcne and $[Ru(S_2PPh_2)_2(PPh_3)_2]$, (ii) dry column chromatography of $[Ru(S_2PPh_2)_2(PPh_3)(tcne)]$, or (iii) from equimolar amounts of $[Ru(S_2PPh_2)_2(PPh_3)(tcne)]$ and $[Ru(S_2PPh_2)_2(PPh_3)_2]$.

By examining the relative intensities of the observed signals, four sets of phosphorus resonances are identified for the minor products in Figure 3.7. Each set consists of a singlet (a-d) between δ90.8 and 94.2 ppm, a doublet (a_1-d_1) at *ca.* δ90ppm (both assigned to the

135

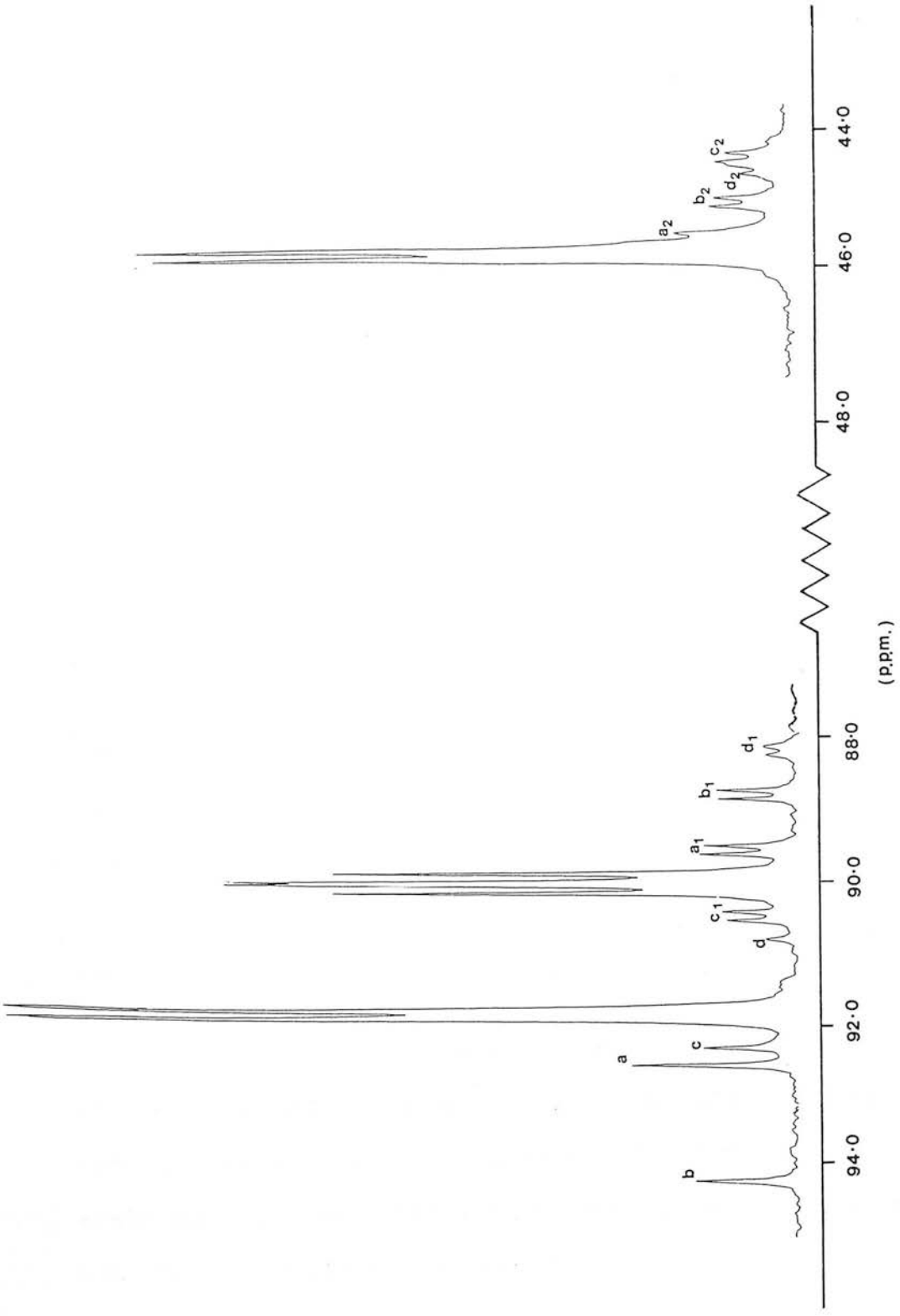

Figure 3.7: The $^{31}P-\{^{1}H\}$ n.m.r. spectrum of $[\{Ru(S_2PPh_2)_2(PPh_3)\}_2(tcne)]$ ($CDCl_3$ solution at 303K).

phosphorus atoms of the dithiolate ligands) and a doublet (a_2-d_2) at *ca.* δ45ppm (assigned to the co-ordinated triphenylphosphine).

The major product(s) of the reaction are observed as (i) two singlets at δ91.9 and 91.7ppm of equal intensity, (ii) an overlapping pair of doublets centred at δ90.0ppm, and (iii) a broadened doublet at δ45.6ppm. Resonances (i) and (ii) above are assigned to the phosphorus atoms of the dithiolate ligand and (iii) to co-ordinated triphenylphoshine. The ratio of the areas under the peaks for (i), (ii) and (iii) is 1.1:1.0:1.2 respectively.

As observed for the complexes, $[M(S_2PR_2)_2(PPh_3)(tcne)]$, two dithiolates and one triphenylphosphine are co-ordinated to the metal centre. One difference between the $^{31}P-\{^1H\}$ n.m.r. spectra of $[Ru(S_2PR_2)_2(PPh_3)(tcne)]$ and $[\{Ru(S_2PR_2)_2(PPh_3)\}_2tcne]$, lies in the chemical shift of the phosphine resonance. This is observed at higher chemical shift (10-12ppm) for $[\{Ru(S_2PR_2)_2(PPh_3)\}_2tcne]$ than for the analogous $[Ru(S_2PR_2)_2(PPh_3)(tcne)]$.

If these adducts are prepared from equimolar amounts of $[Ru(S_2PR_2)_2(PPh_3)_2]$ and tcne, then the $^{31}P-\{^1H\}$ n.m.r. spectrum of the reaction mixture also exhibits resonances assigned to PPh_3, $OPPh_3$ and $[PPh_3.tcne]$. These results will be discussed in Chapter 3.12.

3.9 ^{1}H n.m.r. Spectroscopy.

3.9.1 [M(S_2PR_2)$_2$(PPh_3)(tcne)] complexes.

The ^{1}H n.m.r. spectrum of [Ru(S_2PMe_2)$_2$(PPh_3)(tcne)] (Figure 3.8) exhibits the same spectral pattern as [Ru(S_2PMe_2)$_2$(PPh_3)(CO)]. The methyl protons appear as doublets with a one bond phosphorus-hydrogen coupling constant of *ca.* 13Hz. Four different methyl environments are observed; three doublets lie in the δ1.99-2.11ppm range with a fourth at δ0.95ppm. The superimposed doublets can be seen more clearly at smaller spectral widths and Figure 3.9 shows the expanded spectrum for [Os(S_2PMe_2)$_2$(PPh_3)(tcne)].

The ^{1}H n.m.r. spectrum of [Ru($S_2P\{OEt\}_2$)$_2$(PPh_3)(tcne)] recorded as a CD_2Cl_2 solution at 303K is shown in Figure 3.10. The methylene protons of the ethoxy groups are observed as two multiplets at δ4.2 and 3.1ppm; the ratio of the areas under these multiplets is 3:1 respectively. Similarly, the methyl protons are recorded as a multiplet (formed from three overlapping triplets) centred at δ1.4 ppm and a triplet at 0.9ppm; the ratio of areas under the methyl resonances is also 3:1. A similar pattern is observed for *cis*-[Ru($S_2P\{OEt\}_2$)$_2$(PPh_3)(CO)] (see Chapter 2.3.5).

The resonances at lower chemical shift are assigned to the protons nearest the ring currents of the phenyl rings (see Chapter 2.3.2). The existence of four distinct

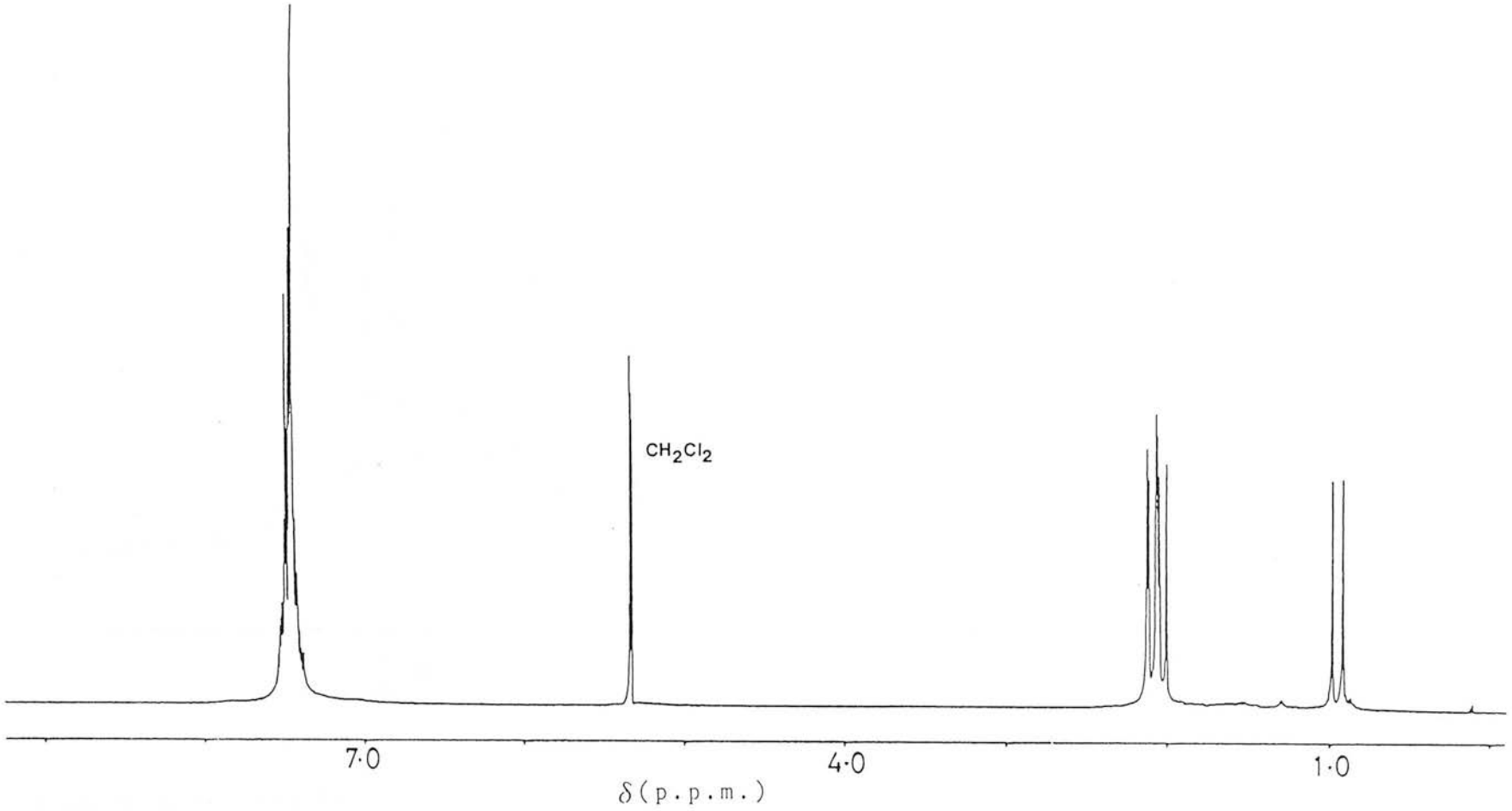

Figure 3.8: The ^{1}H n.m.r. spectrum of [Ru(S_2PMe_2)$_2$(PPh_3)(tcne)] (CD_2Cl_2 solution at 303K).

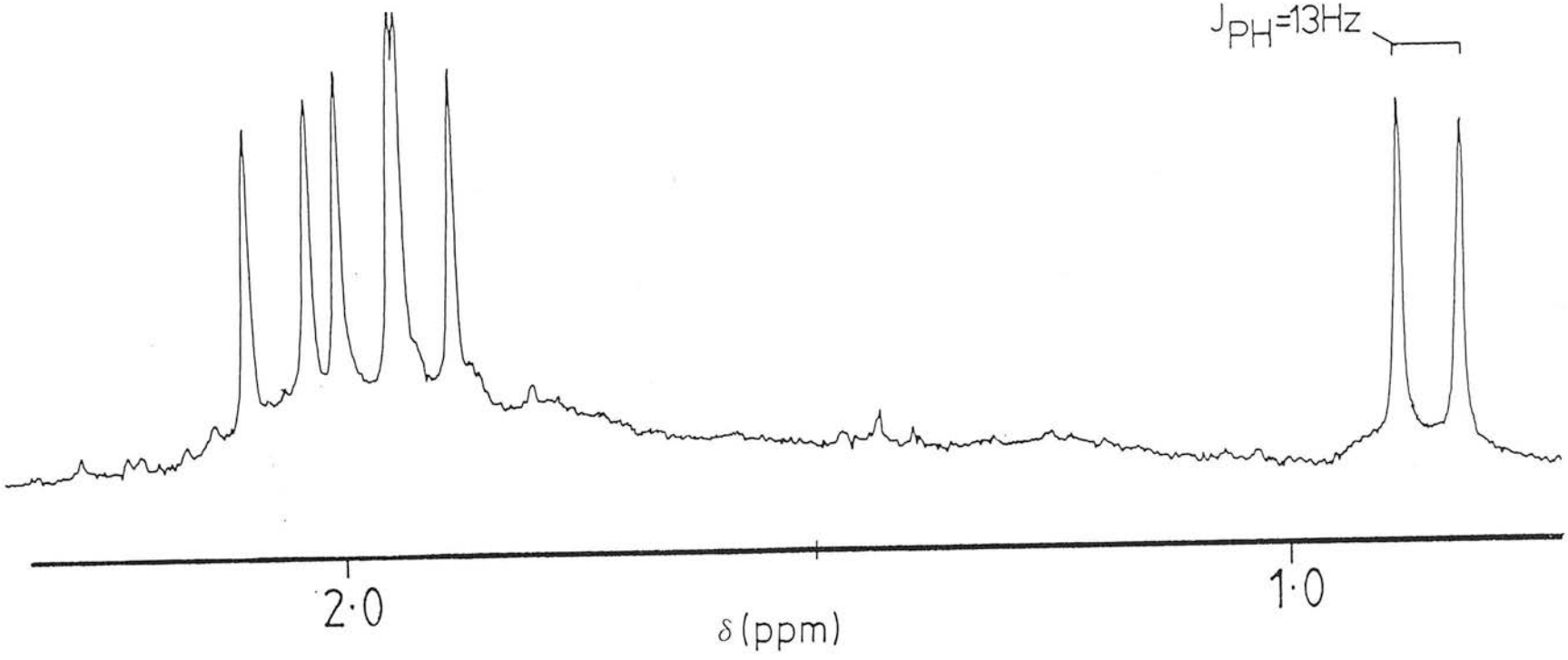

Figure 3.9: The ^1H n.m.r. spectrum of $[Os(S_2PMe_2)_2(PPh_3)(tcne)]$ (CD_2Cl_2 solution at 303K) between 2.5 and 0.5 p.p.m.

140

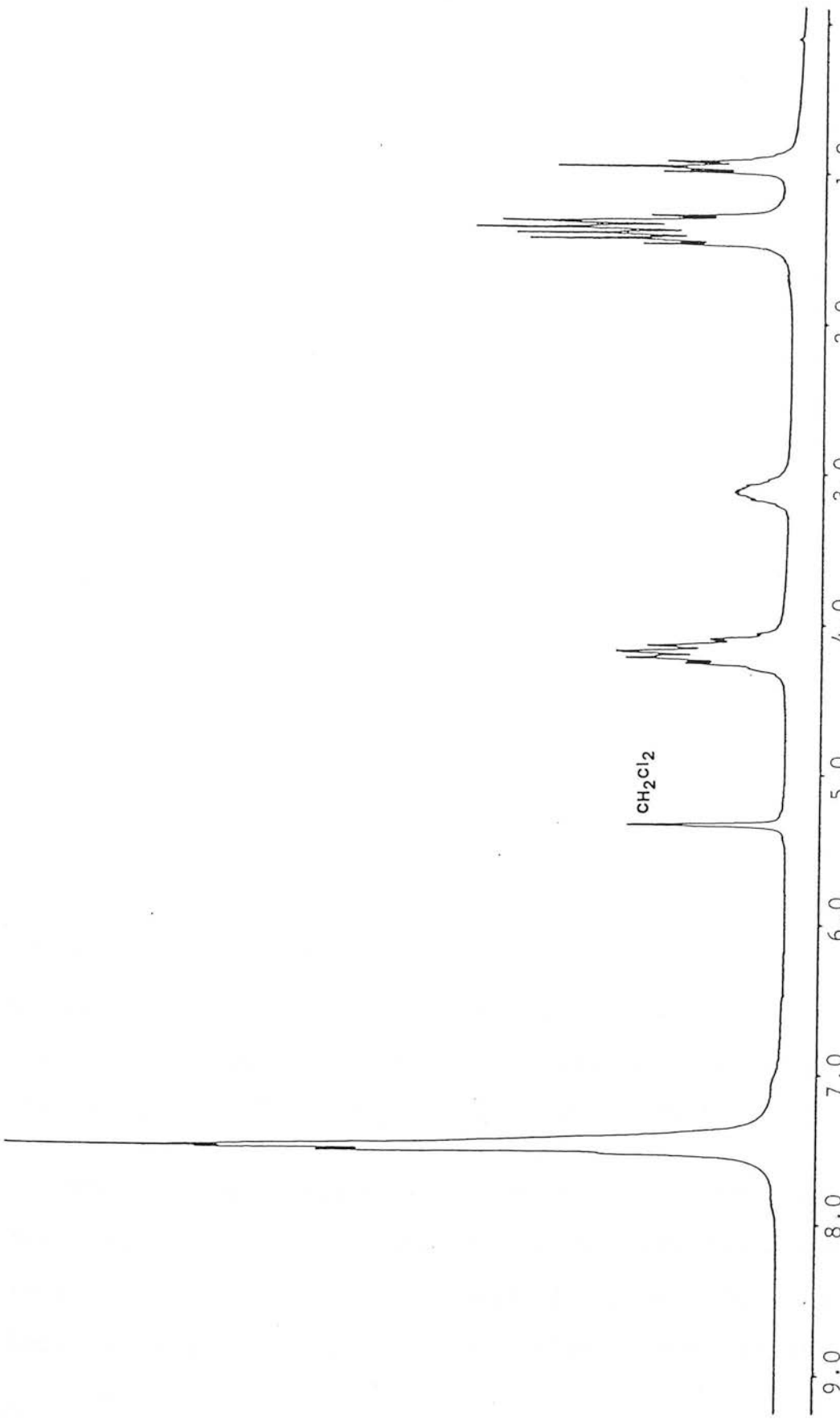

Figure 3.10: The ^1H n.m.r. spectrum of $[Ru(S_2P\{OEt\}_2)_2(PPh_3)(tcne)]$ (CD_2Cl_2 solution at 303K).

environments is consistent with a *cis*-configuration of ligands around the metal centre (only two environments are expected for a *trans* arrangement of ligands). The ratio of the areas under the peaks confirms the stochiometry of the adducts.

3.9.2 [{$Ru(S_2PR_2)_2(PPh_3)$}$_2$tcne] complexes.

The presence of several different isomers in solution makes detailed interpretation of these spectra difficult. The ^1H n.m.r. spectrum of [{$Ru(S_2PMe_2)_2(PPh_3)$}$_2$tcne] contains a large number of overlapping doublets in the δ0-2.5ppm region (the methyl protons of the dithiolate ligands) and a multiplet at δ6.0ppm (phenyl protons). A similarly complicated pattern is observed for the complex, [{$Ru(S_2P\{OEt\}_2)_2(PPh_3)$}$_2$tcne].

3.10 Mass spectroscopy.

The FAB mass-spectra of the $[M(S_2PR_2)_2(PPh_3)(tcne)]$ complexes (M=Ru, Os; R=Me, Ph, OEt) all exhibit parent ion peaks. However, for M=^{102}Ru the spectra are dominated by the fragment, $[^{102}Ru(S_2PR_2)_2(PPh_3)]^+$, formed by loss of tcne from the parent molecule. At lower m/z ratios (<500) the fragment, $[^{102}Ru(S_2PR_2)_2]^+$, is of greatest intensity.

The osmium analogues exhibit the same general features as the $[Ru(S_2PR_2)_2(PPh_3)(tcne)]$ complexes except that (from relative intensities) the parent ion appears less susceptible to fragmentation. The fragments,

$[^{192}Os(S_2PR_2)_2(PPh_3)]^+$ and $[^{192}Os(S_2PR_2)_2]^+$, are again readily identified. Interestingly, the higher m/z (>1500) region of the spectrum for $[Os(S_2PPh_2)_2(PPh_3)(tcne)]$ shows a peak at m/z=2031 corresponding to $[\{^{192}Os(S_2PPh_2)_2(PPh_3)\}_2tcne]^+$ which is not observed for other $[M(S_2PR_2)_2(PPh_3)(tcne)]$.

The FAB mass-spectra of $[\{Ru(S_2PR_2)_2(PPh_3)\}_2tcne]$ (R=Me, Ph, OEt) show peaks which correspond to $[\{^{102}Ru(S_2PR_2)_2(PPh_3)\}_2tcne]^+$ and thus, confirm the binuclear nature of these complexes. Other signals observed at lower m/z ratios correspond to the fragments, $[^{102}Ru_2(S_2PR_2)_4(PPh_3)_2(tcne)]^+$, $[^{102}Ru(S_2PR_2)_2(PPh_3)]^+$ and $[^{102}Ru(S_2PR_2)_2]^+$.

3.11 Crystal structures of $[Os(S_2PR_2)_2(PPh_3)(tcne)]$.

Recrystallisation of $[Os(S_2PR_2)_2(PPh_3)(tcne)]$ (R=Me, Ph) from a diethyl ether/60-80°pet.-ether mixture afforded small green-black crystals which were of suitable quality for diffraction purposes. To confirm the solid-state structure of these adducts, and in order to compare packing arrangements, single-crystal X-ray diffraction studies of both the methyl and phenyl derivatives were undertaken.

Figures 3.11 and 3.12 show the co-ordination sphere around the metal centre for $[Os(S_2PMe_2)_2(PPh_3)(tcne)]$ and $[Os(S_2PPh_2)_2(PPh_3)(tcne)]$ respectively, and Tables 3.3 and 3.4 list selected bond lengths for both complexes. In each structure the osmium centre is co-ordinated to two

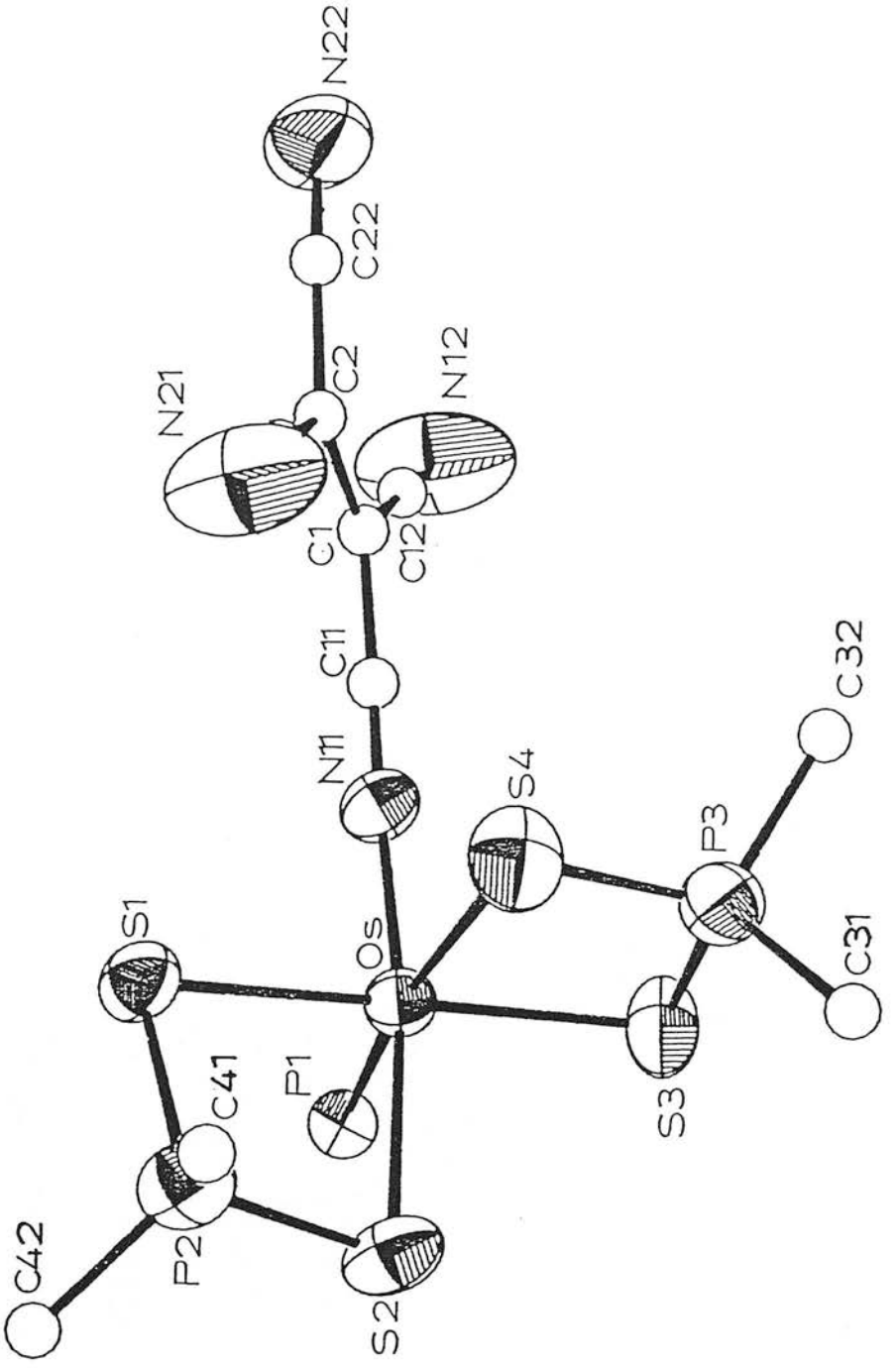

Figure 3.11: The molecular structure of $[Os(S_2PMe_2)_2(PPh_3)(tcne)]$. For clarity, the phenyl rings and the methyl protons are omitted.

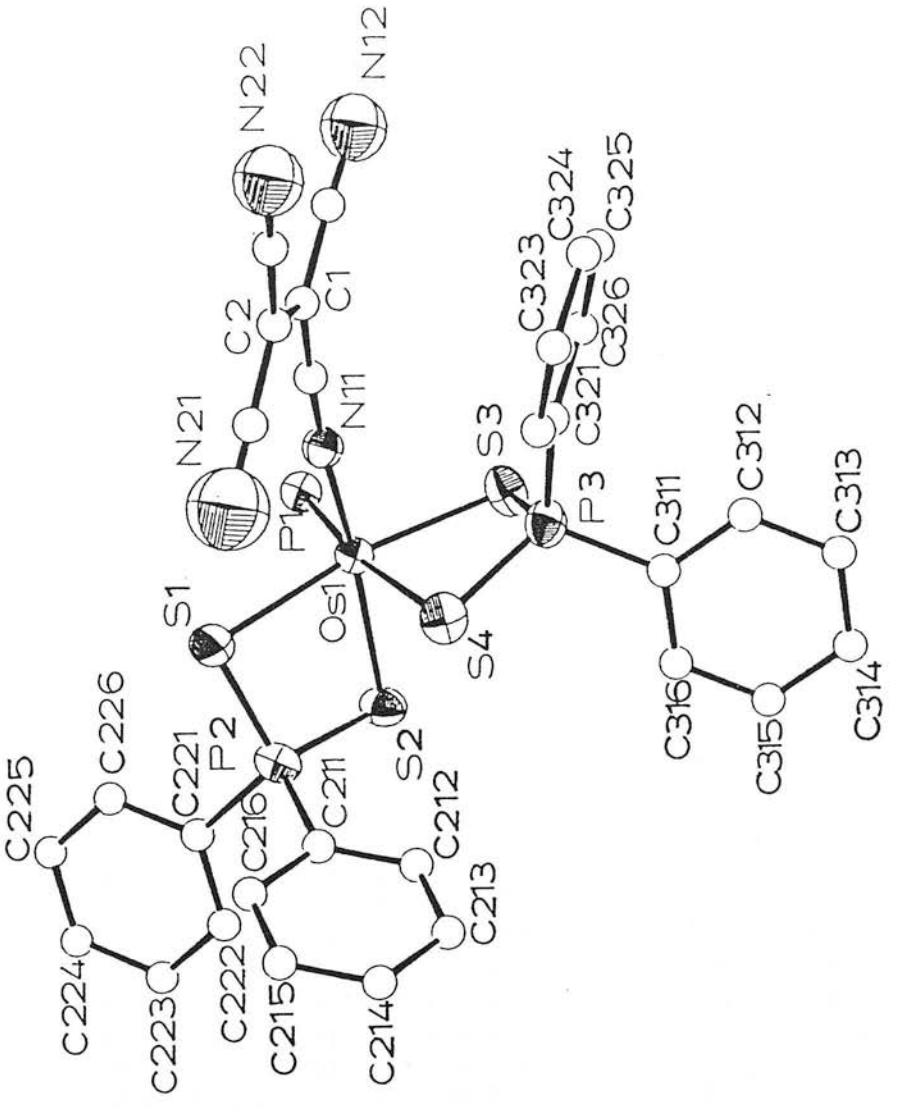

Figure 3.12: The molecular structure of $[Os(S_2PPh_2)_2(PPh_3)(tcne)]$. For clarity, the phenyl rings of the phosphine are omitted.

Table 3.3: Selected bond lengths (Å) and angles (°) for $[Os(S_2PMe_2)_2(PPh_3)(tcne)]$.

Bond Lengths(A) with standard deviations

Os -N(11)	1.899(7)	C(2) -C(21)	1.412(16)
Os - P(1)	2.3249(22)	C(2) -C(22)	1.445(15)
Os - S(1)	2.4590(23)	P(1) -C(111)	1.836(6)
Os - S(2)	2.456(3)	P(1) -C(121)	1.830(6)
Os - S(3)	2.384(3)	P(1) -C(131)	1.859(6)
Os - S(4)	2.522(3)	S(1) - P(2)	2.021(4)
C(1) - C(2)	1.360(13)	S(2) - P(2)	2.022(4)
N(11) -C(11)	1.143(11)	P(2) -C(41)	1.762(12)
N(12) -C(12)	1.142(18)	P(2) -C(42)	1.774(12)
N(21) -C(21)	1.142(17)	S(3) - P(3)	2.027(4)
N(22) -C(22)	1.131(16)	S(4) - P(3)	2.007(4)
C(1) -C(11)	1.410(13)	P(3) -C(31)	1.766(13)
C(1) -C(12)	1.436(15)	P(3) -C(32)	1.777(13)

Angles(degrees) with standard deviations

P(1) - Os -N(11)	94.25(21)	Os - S(2) - P(2)	87.74(12)
S(1) - Os -N(11)	90.94(21)	S(1) - P(2) - S(2)	103.16(15)
S(2) - Os -N(11)	170.54(21)	Os - S(3) - P(3)	88.80(12)
S(3) - Os -N(11)	95.53(21)	Os - S(4) - P(3)	85.47(13)
S(4) - Os -N(11)	85.21(21)	S(3) - P(3) - S(4)	104.57(16)
P(1) - Os - S(1)	101.84(8)	S(3) - P(3) -C(31)	110.9(5)
P(1) - Os - S(2)	90.94(8)	S(3) - P(3) -C(32)	110.6(4)
P(1) - Os - S(3)	89.40(8)	S(4) - P(3) -C(31)	111.8(5)
P(1) - Os - S(4)	170.37(8)	S(4) - P(3) -C(32)	114.1(4)
S(1) - Os - S(2)	80.25(8)	C(31) - P(3) -C(32)	105.0(6)
S(1) - Os - S(3)	166.59(8)	S(1) - P(2) -C(41)	112.3(4)
S(1) - Os - S(4)	87.78(8)	S(1) - P(2) -C(42)	112.6(4)
S(2) - Os - S(3)	92.42(9)	S(2) - P(2) -C(41)	111.9(4)
S(2) - Os - S(4)	90.98(9)	S(2) - P(2) -C(42)	111.9(4)
S(3) - Os - S(4)	81.09(9)	C(41) - P(2) -C(42)	105.2(6)
Os -N(11) -C(11)	172.2(7)	Os - P(1) -C(111)	112.69(20)
C(1) -C(11) -N(11)	174.1(10)	Os - P(1) -C(121)	118.21(20)
C(1) -C(12) -N(12)	178.2(13)	Os - P(1) -C(131)	115.48(19)
C(2) -C(21) -N(21)	176.5(13)	C(111)- P(1) -C(121)	104.0(3)
C(2) -C(22) -N(22)	176.4(12)	C(111)- P(1) -C(131)	102.1(3)
C(11) - C(1) -C(12)	117.2(9)	C(121)- P(1) -C(131)	102.5(3)
C(21) - C(2) -C(22)	117.5(9)	P(1) -C(111)-C(112)	122.9(4)
C(11) - C(1) - C(2)	124.1(9)	P(1) -C(111)-C(116)	117.1(4)
C(12) - C(1) - C(2)	118.7(9)	P(1) -C(121)-C(122)	122.8(4)
C(1) - C(2) -C(21)	120.7(9)	P(1) -C(121)-C(126)	117.1(4)
C(1) - C(2) -C(22)	121.8(9)	P(1) -C(131)-C(132)	119.7(4)
Os - S(1) - P(2)	87.68(11)	P(1) -C(131)-C(136)	120.1(4)

Table 3.4: Selected bond lengths (Å) and angles (°) for $[Os(S_2PPh_2)_2(PPh_3)(tcne)]$.

Bond Lengths(A) with standard deviations

Os -N(11)	1.858(10)	C(2) -C(22)	1.419(21)
Os - P(1)	2.324(3)	C(2) -C(21)	1.407(23)
Os - S(1)	2.455(4)	P(1) -C(111)	1.837(9)
Os - S(2)	2.459(3)	P(1) -C(121)	1.824(9)
Os - S(3)	2.395(3)	P(1) -C(131)	1.840(8)
Os - S(4)	2.516(3)	S(1) - P(2)	2.019(5)
C(1) - C(2)	1.401(19)	S(2) - P(2)	2.024(5)
C(11) -N(11)	1.213(17)	P(2) -C(211)	1.802(9)
C(12) -N(12)	1.153(21)	P(2) -C(221)	1.809(13)
C(22) -N(22)	1.162(22)	S(3) - P(3)	2.033(5)
C(21) -N(21)	1.12(3)	S(4) - P(3)	2.012(5)
C(1) -C(11)	1.379(19)	P(3) -C(311)	1.771(11)
C(1) -C(12)	1.436(19)	P(3) -C(321)	1.776(10)

Angles(degrees) with standard deviations

N(11) - Os - P(1)	94.6(3)	S(3) - P(3) - S(4)	103.76(20)
N(11) - Os - S(1)	92.8(3)	S(1) - P(2) -C(211)	112.7(3)
N(11) - Os - S(2)	171.7(3)	S(1) - P(2) -C(221)	111.7(4)
N(11) - Os - S(3)	91.0(3)	S(2) - P(2) -C(211)	112.8(3)
N(11) - Os - S(4)	87.1(3)	S(2) - P(2) -C(221)	114.1(4)
P(1) - Os - S(1)	100.60(12)	S(3) - P(3) -C(311)	109.6(4)
P(1) - Os - S(2)	90.96(11)	S(3) - P(3) -C(321)	113.6(4)
P(1) - Os - S(3)	89.67(12)	S(4) - P(3) -C(311)	114.8(4)
P(1) - Os - S(4)	170.28(11)	S(4) - P(3) -C(321)	110.5(4)
S(1) - Os - S(2)	80.16(11)	Os - P(1) -C(111)	114.0(3)
S(1) - Os - S(3)	168.70(12)	Os - P(1) -C(121)	116.2(3)
S(1) - Os - S(4)	88.85(11)	Os - P(1) -C(131)	115.8(3)
S(2) - Os - S(3)	95.08(11)	C(111)- P(1) -C(121)	104.7(4)
S(2) - Os - S(4)	88.40(11)	C(111)- P(1) -C(131)	101.3(4)
S(3) - Os - S(4)	80.74(11)	C(121)- P(1) -C(131)	103.1(4)
Os -N(11) -C(11)	173.2(10)	P(1) -C(111)-C(112)	122.7(7)
N(11) -C(11) - C(1)	172.0(14)	P(1) -C(111)-C(116)	117.3(7)
C(11) - C(1) - C(2)	120.8(12)	P(1) -C(121)-C(122)	120.3(7)
C(11) - C(1) -C(12)	117.5(12)	P(1) -C(121)-C(126)	119.8(7)
C(2) - C(1) -C(12)	121.6(12)	P(1) -C(131)-C(132)	120.2(6)
C(1) - C(2) -C(22)	120.5(13)	P(1) -C(131)-C(136)	119.8(6)
C(1) - C(2) -C(21)	118.9(14)	C(211)- P(2) -C(221)	102.9(5)
C(22) - C(2) -C(21)	120.6(14)	P(2) -C(211)-C(212)	121.8(7)
C(1) -C(12) -N(12)	177.5(16)	P(2) -C(211)-C(216)	118.2(7)
C(2) -C(22) -N(22)	179.2(17)	P(2) -C(221)-C(222)	120.5(9)
C(2) -C(21) -N(21)	174.4(20)	P(2) -C(221)-C(226)	119.5(9)
Os - S(1) - P(2)	87.09(16)	C(311)- P(3) -C(321)	104.8(5)
Os - S(2) - P(2)	86.87(15)	P(3) -C(311)-C(312)	121.7(8)
Os - S(3) - P(3)	87.36(16)	P(3) -C(311)-C(316)	118.2(8)
Os - S(4) - P(3)	84.56(15)	P(3) -C(321)-C(322)	119.0(7)
S(1) - P(2) - S(2)	102.97(20)	P(3) -C(321)-C(326)	120.7(7)

bidentate dithiolate ligands, one triphenylphosphine, and a monodentate, N-bound, tcne ligand. The co-ordination about the metal centre is distorted from ocathedral for both $[Os(S_2PMe_2)_2(PPh_3)(tcne)]$ and $[Os(S_2PPh_2)_2(PPh_3)(tcne)]$ The *trans*-angles range from 168 to 171° and the ligand "bite angles" are *ca.* 80°. This distortion results from the steric restraints imposed by the chelates and is observed for other transition metal complexes of the 1,1-dithiolates (see Chapter 2.2.1).

The Os-S4 bond, *trans* to the triphenylphosphine ligand, is the longest Os-S bond (2.522[3] and 2.516[3]Å for R=Me, Ph respectively) while the other sulphur (S3) of this chelate has the shortest bond to osmium (2.384[3] and 2.395[3]Å). The lengthening of the metal-sulphur bond *trans* to a phosphine ligand is also observed in the complexes, $[Ru(S_2PPh_2)_2(PPh_3)(CO)]$ (Chapter 2.3.6) and $[Ru(S_2PMe_2)_2(PMe_2Ph)_2]$.[146] Presumably this is the result of the strong *trans*-influence of the phosphine. The Os-S bonds for the chelate *trans* to the ligated tcne (S1,S2) are similar in length (2.455[4]-2.459[3]Å) Thus, the *trans* -influence of N-bound tcne appears to be smaller than that of triphenylphosphine.

The Os-N bond lengths are 1.899(7)Å (R=Me) and 1.858(10)Å (R=Ph) and the difference is just greater than 3σ. The nitrile bond is approximately linear with angles of 172.2(7) and 173.2(10)° (R=Me, Ph respectively) for Os-N11-C11 and angles of 174.1(10) and 172.0(14)° for

N11-C11-C1. The ligated tcne molecule maintains planarity (within the limits of experimental error) as indicated by internal torsion angles of *ca.* 0 and 180° (see Tables 3.3 and 3.4). Apart from N11, which is bound to osmium, the tcne moiety exhibits appreciable thermal disorder (as witnessed by the high anisotropic thermal parameters of the nitrogen atoms). The large uncertainties in the atomic positions within the tcne moiety prevent any detailed discussion of the internal geometry of the ligand. It is possible that repeating the experiment at low temperatures would result in more accurate determination of the tcne ligand.

The diffraction studies of $[Os(S_2PMe_2)_2(PPh_3)(tcne)]$ and $[Os(S_2PPh_2)_2(PPh_3)(tcne)]$ represent the first fully-refined crystallographic characterisation of tcne N-bound to a transition metal. A literature search, including examination of the Cambridge Crystallographic Database, has revealed few structural characterisations of complexes containing an osmium-nitrile bond. The only crystal structures of osmium-nitrile species reported to date are the cluster compounds, $[Os_4H_3(CO)_{12}(NCMe)_2]^+$, $[Os_3(CO)_{10}(\mu\text{-}H)(NCMe)_2]^+$ and $[Os_3(CO)_{10}(CON_3Ph)(NCMe)_2]$, which have osmium-nitrile bond lengths of between 2.071(17) and 2.130(13)Å.[147-149] Although these are longer than the Os-N bond in $[Os(S_2PR_2)_2(PPh_3)(tcne)]$ (R=Me, Ph), the value of any comparison between these structures is limited due to differences in formal oxidation state and

the different nature of the other ligands co-ordinated to the osmium centre.

Much interest has been shown in the electronically conducting properties of the "organic conductors" formed between tcne and tcnq, and sulphur donors such as ttf. Crystallographic studies have shown that the structure of these complexes consist of molecular stacks of the respective components and that the type of stacking plays an important role in the electronic properties of the complex.[150]

The unit cell of $[Os(S_2PMe_2)_2(PPh_3)(tcne)]$ (viewed along the C=C bond of the tcne moiety) is shown in Figure 3.13. The complex exists in the solid state as a structure containing staggered, parallel tcne ligands whose centres, related by the inversion centre at (0.5,0.5,0.5), are 4.66Å apart with a perpendicular separation of 3.12Å between the planes of the tcne moieties. A packing diagram viewed perpendicular to the plane of the cyano-alkene is shown in Figure 3.14.

No inter-molecular interaction is observed between the tcne ligands in $[Os(S_2PPh_2)_2(PPh_3)(tcne)]$, presumably as a result of steric constraints imposed by the phenyl rings. However, an intra-molecular interaction between the π-systems of the ligated tcne and one phenyl ring (C321-C326) of the dithiophosphinate is suggested by the orientation of these substituents (see Figure 3.12).

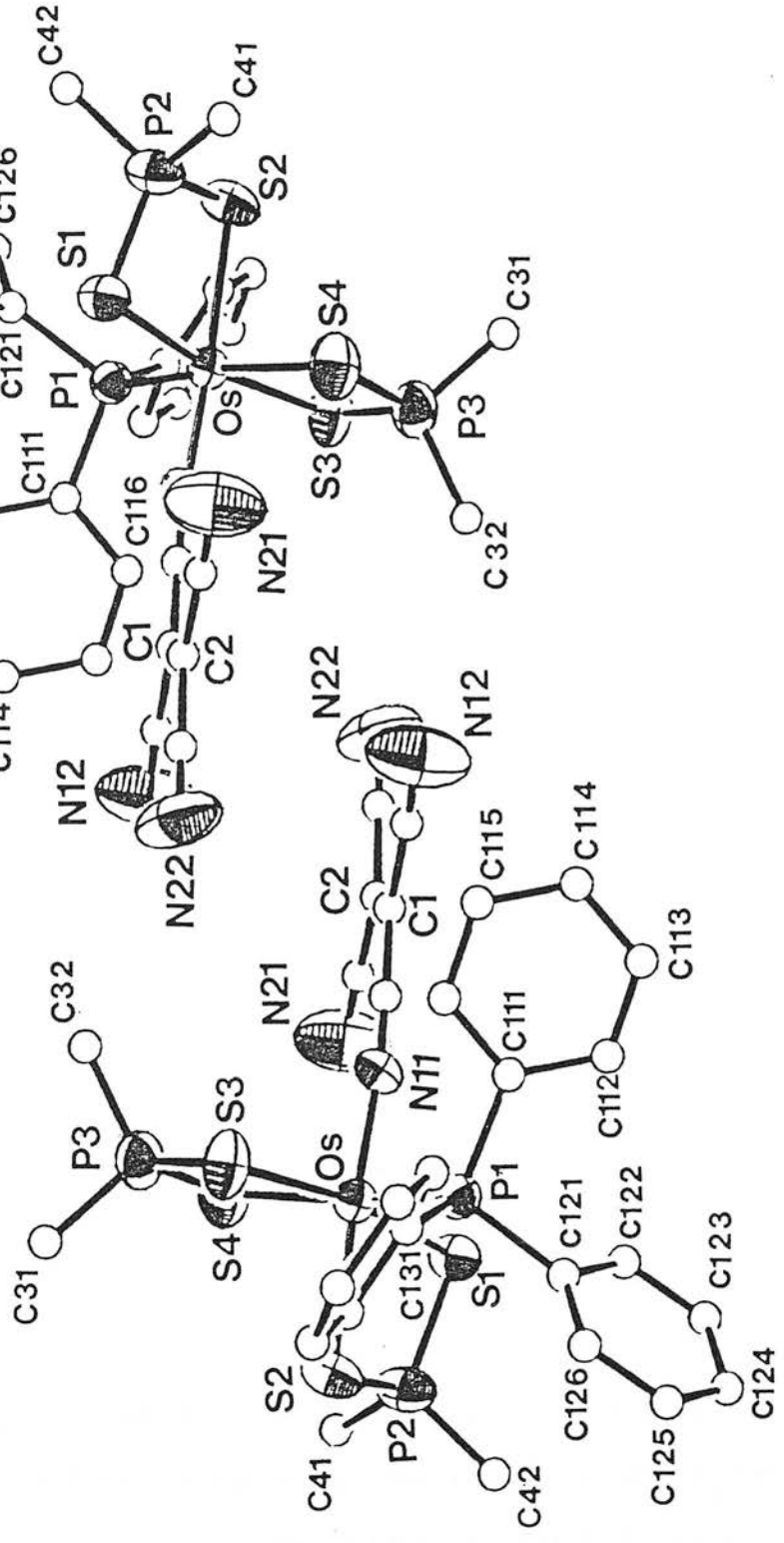

Figure 3.13: The unit cell of $[Os(S_2PMe_2)_2(PPh_3)(tcne)]$ viewed along the C1-C2 bond.

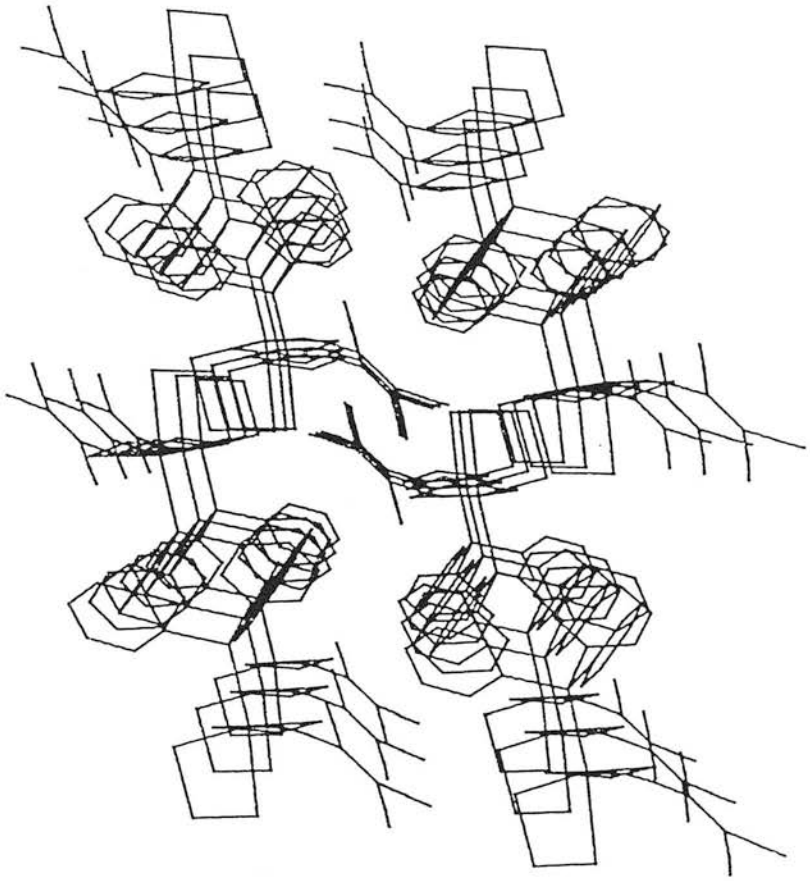

Figure 3.14: A schematic packing diagram showing the staggering of the tcne moieties in $[Os(S_2PMe_2)_2(PPh_3)(tcne)]$. The view is perpendicuar to the plane of the tcne ligand and the methyl groups of the dithiolate ligand are omitted for clarity.

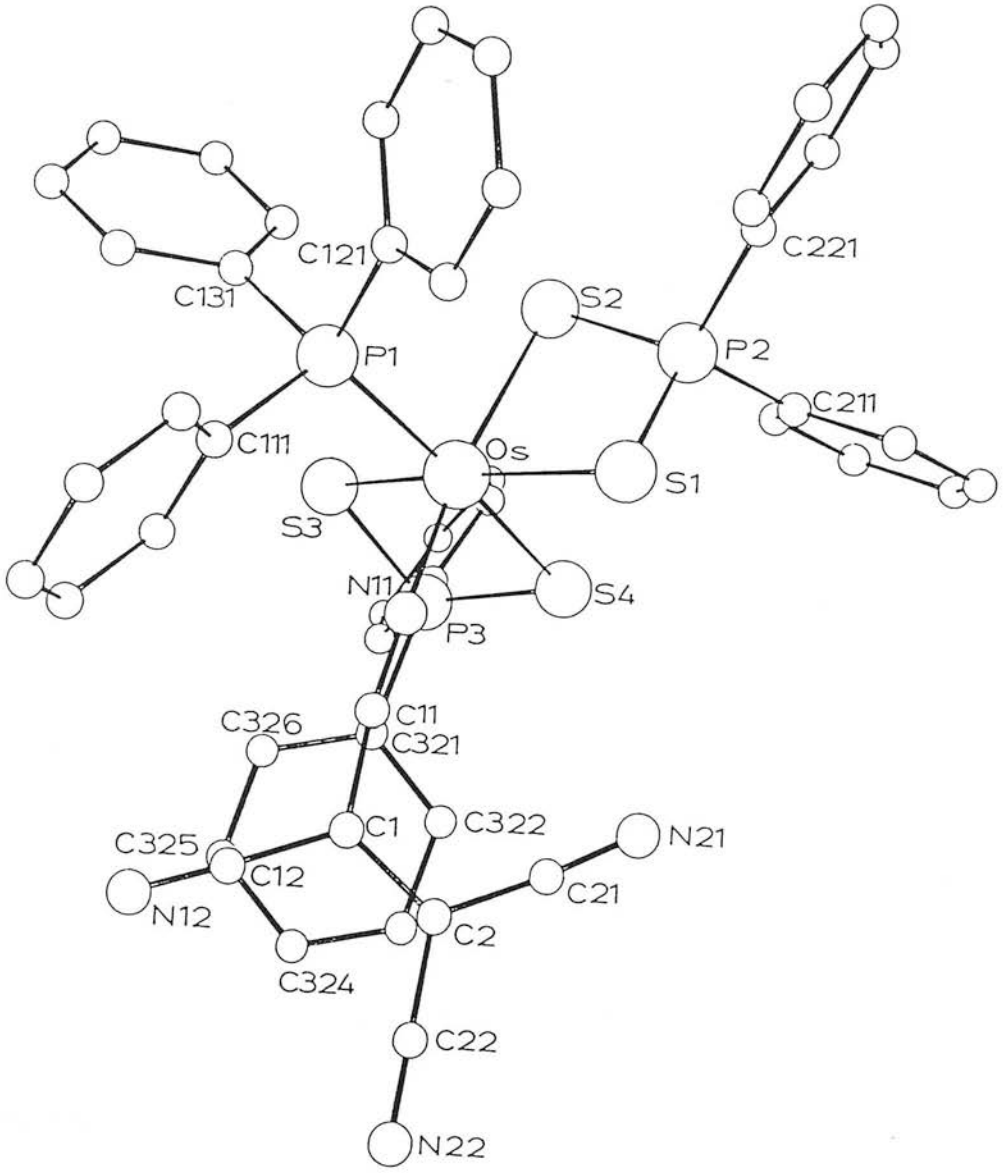

Figure 3.15: The molecular structure of $[Os(S_2PPh_2)_2(PPh_3)(tcne)]$ viewed perpendicular to the plane of the phenyl ring (C321-C326).

Calculations show that the least-squares mean planes of these moieties make a dihedral angle of 7.72° and are 3.615Å apart. The centres of gravity of the C_6N_4 moiety and the phenyl ring are displaced by 0.965Å (see Figure 3.15). Further evidence of an interaction is suggested by the bond angles around the phosphorus atom of the dithiolate; the S-P-C angles of the dithiolate differ significantly from the mean value of 112.1° for the chelate involved in the interaction, while the S-P-C angles of the second dithiolate ligand do not exhibit the same degree of deviation. The intra-molecular interaction is also favoured by the distortion of the Os-S1-S2-P2 ring from planarity which brings the phenyl ring closer to the tcne ligand.

Rettig and Wing proposed a similar intra-molecular interaction between the tcne moiety and the halide in $[(Cp)_2VX(tcne)]$ (X=Cl, Br, I) on the basis of the orientation of the tcne in the crystal structure of this complex, and from infrared spectral data.

3.12 Summary.

Treatment of $[M(S_2PR_2)_2(PPh_3)_2]$ (M=Ru, Os; R=Me, Ph, OEt) with excess tcne affords $[M(S_2PR_2)_2(PPh_3)(tcne)]$. The complexes have been shown to have a *cis*-configuration in solution and in the solid state. Crystallographic studies of $[Os(S_2PMe_2)_2(PPh_3)(tcne)]$ and $[Os(S_2PPh_2)_2(PPh_3)(tcne)]$ confirm that the tcne is co-ordinated through a single

nitrogen atom.

The reaction of $[Ru(S_2PR_2)_2(PPh_3)_2]$ (R=Me, Ph, OEt) with equimolar amounts of tcne yields a complex which is formulated as $[\{Ru(S_2PR_2)_2(PPh_3)\}_2tcne]$ (from elemental analysis). This formulation is supported by (i) the quantitative yield of $[\{Ru(S_2PR_2)_2(PPh_3)\}_2tcne]$ from equimolar amounts of $[Ru(S_2PR_2)_2(PPh_3)(tcne)]$ and $[Ru(S_2PR_2)_2(PPh_3)_2]$ and (ii) the quantitative conversion of $[\{Ru(S_2PR_2)_2(PPh_3)\}_2tcne]$ into $[Ru(S_2PR_2)_2(PPh_3)(tcne)]$ by reaction with an equimolar amount of tcne.

Infrared spectroscopy suggests that the tcne ligand is, as for $[Ru(S_2PR_2)_2(PPh_3)(tcne)]$, co-ordinated via the N-atom and that the complex is the same in both solid and solution states. The multitude of resonances in the $^{31}P-\{^1H\}$ n.m.r. spectrum of $[\{Ru(S_2PR_2)_2(PPh_3)\}_2tcne]$ reveals that more than one species is present in solution and imply that these adducts exist as isomeric mixtures.

Assuming the binuclear formulation to be correct geometric isomerism has previously been recorded for complexes involving a bridging tcne ligand.[102] Basolo noted that tcne can act as a bridging ligand in three co-ordination modes (see [3.11], [3.12], and [3.13]). Molecular models of $[\{Ru(S_2PPh_2)_2(PPh_3)\}_2tcne]$ (based on the dimensions found for $[Os(S_2PPh_2)_2(PPh_3)(tcne)]$) show that the *trans*-isomer [3.11] would have the least degree of steric interaction between ligands. The absence of a

strong C=C stretching vibration (as observed in the infrared spectra of $[M(S_2PR_2)_2(PPh_3)(tcne)]$) lends further credence to this arrangement; this vibration would be Raman active for the *trans* isomer, but infrared-active for the *cis*-form.

Geometric isomerism of this kind would result in, at most, three distinct sets of resonances in the $^{31}P-\{^1H\}$ n.m.r. spectra of $[\{Ru(S_2PR_2)_2(PPh_3)\}_2tcne]$. The additional resonances observed may result from mono- or poly-nuclear complexes or from configurational isomerism.

The molecular models of $[\{Ru(S_2PPh_2)_2(PPh_3)\}_2tcne]$ show that steric interactions exist between the co-ordinated ligands of each "end" of the complex. Thus, three extreme configurations can be envisaged (Figure 3.16) in which the phosphine ligands are *cis*, *trans* or staggered with respect to each other. These arrangements are extreme possibilities and the actual configuration may well lie between these.

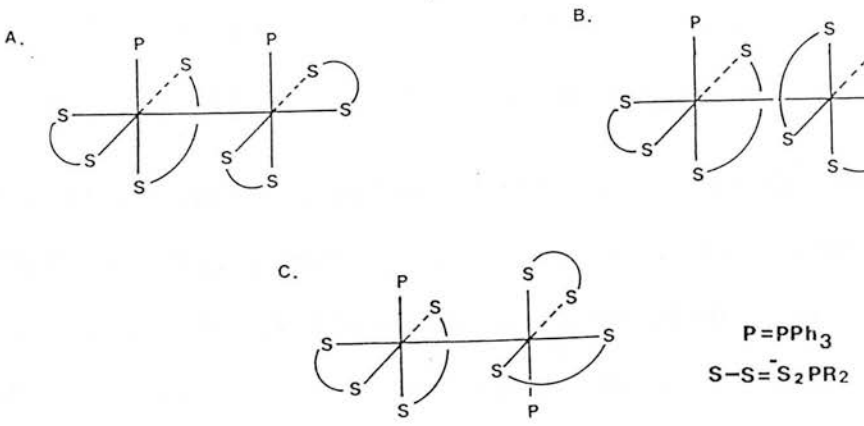

Figure 3.16: A schematic representation of the (a) cis, (b) staggered and (c) trans configurations of $[\{Ru(S_2PR_2)_2(PPh_3)\}_2tcne]$.

One result of such hindered rotation is to produce a binuclear species which has magnetically inequivalent "ends". The major dithiolate resonances in the $^{31}P-\{^{1}H\}$ n.m.r. spectra of the $[\{Ru(S_2PR_2)_2(PPh_3)\}_2tcne]$ adducts appear to be duplicated (see Figure 3.7). This pattern may arise from an isomeric mixture in which two major products are formed in equal amounts, or from a binuclear species which has magnetically inequivalent ends. The $^{31}P-\{^{1}H\}$ n.m.r. spectrum of $[\{Ru(S_2PPh_2)_2(PPh_3)\}_2tcne]$ does not show any significant changes between 233 and 303K. Decomposition of these complexes at higher temperatures has thwarted attempts to further elucidate their solution structure.

Earlier workers have used infrared spectroscopy to suggest that electron transfer occurs, from the metal to the ligated tcne, in transition metal complexes of N-bound tcne.[97,102-104] The position of ν_{CN} and $\nu_{C=C}$ in the infrared spectra of $[M(S_2PR_2)_2(PPh_3)(tcne)]$, and ν_{CN} for $[\{Ru(S_2PR_2)_2(PPh_3)\}_2tcne]$, is consistent with such an effect. The diamagnetism of these complexes has been explained by proposing extensive spin-pairing.

Chromatographed samples of $[M(S_2PR_2)_2(PPh_3)(tcne)]$ and $[\{Ru(S_2PR_2)_2(PPh_3)\}_2tcne]$ are e.s.r silent. However, an e.s.r. resonance <u>is</u> observed to grow when tcne is added to $[M(S_2PR_2)_2(PPh_3)_2]$ in methylene chloride and this is accompanied by a darkening of the solution. This effect is normally short lived, but for $[Os(S_2P\{OEt\}_2)_2(PPh_3)_2]$

the brown colouration persists long enough to be studied. On addition of tcne to $[Os(S_2P\{OEt\}_2)_2(PPh_3)_2]$ in methylene chloride, a broad band at $2180cm^{-1}$ is found in the infrared spectrum and an e.s.r. signal is observed to grow (with equimolar amounts of reactants this resonance consists of nine distinct lines). The electronic absorption spectrum of this solution exhibits a broad band at $24,000cm^{-1}$ which has the vibrational maxima associated with $tcne^{-}$ (see Chapter 4.3). These results point strongly to the presence of $tcne^{-}$ in solution.

Therefore, the first step in the reaction appears to be oxidation by tcne of the metal substrate forming $[M(S_2PR_2)_2(PPh_3)(tcne)]^+[tcne]^-$. The M^{III} complex is unstable although the reversibility of the $M^{II/III}$ couple is dependent on both the metal and ligand type (see Chapter 2.3.9). The species, $[M(S_2PR_2)_2(PPh_3)(tcne)]^+[tcne]^-$, must then decompose presumably leading to the loss of a phosphine ligand. If the complex, $[Ru(S_2PPh_2)_2(PMe_2Ph)_2]$, is added to tcne, then the resultant brown solution is stable indefinitely (if kept under an inert atmosphere). This agrees with electrochemical studies which show that electrogenerated samples of $[Ru(S_2PPh_2)_2(PMe_2Ph)_2]^+$ do not form daughter products.

In situ $^{31}P-\{^1H\}$ n.m.r. studies show that the first (observeable) species in the reaction of tcne with $[Ru(S_2PR_2)_2(PPh_3)_2]$ is $[Ru(S_2PR_2)_2(PPh_3)(tcne)]$. In the presence of excess $[Ru(S_2PR_2)_2(PPh_3)_2]$, rapid conversion of

$[Ru(S_2PR_2)_2(PPh_3)(tcne)]$ to $[\{Ru(S_2PR_2)_2(PPh_3)\}_2tcne]$ occurs. Addition to this solution of more tcne leads to the generation of $[Ru(S_2PR_2)_2(PPh_3)(tcne)]$. The above observations are consistent with the reaction pathway:-

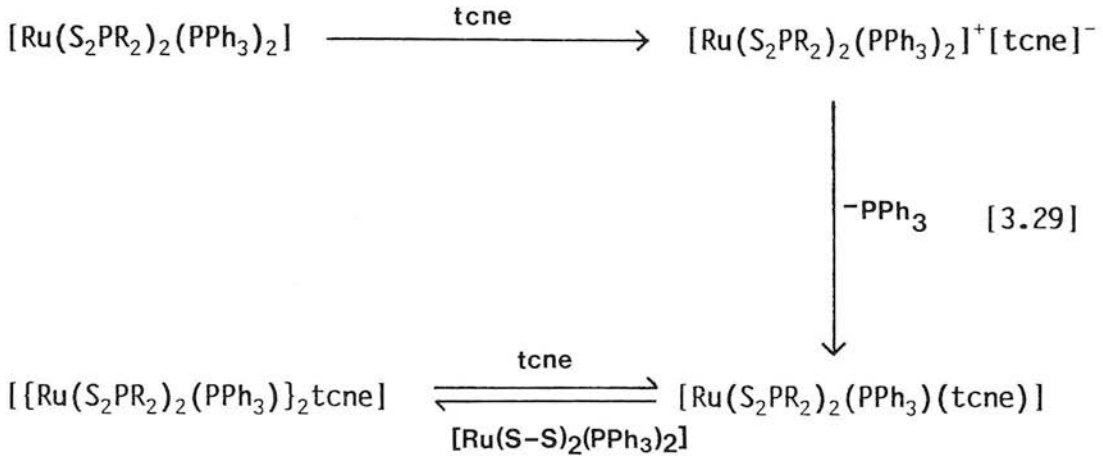

The formal oxidation state of the metal centre and the co-ordinated tcne ligand is not obvious. To investigate this problem we have studied the electrochemical and spectroelectrochemical properties of $[M(S_2PR_2)_2(PPh_3)(tcne)]$ and $[\{Ru(S_2PR_2)_2(PPh_3)\}_2tcne]$ in the next chapter.

3.13 Experimental methods.

Experimental and crystallographic methods were as described for Chapter 2.

3.14 Materials.

The metal complexes were prepared as outlined in Chapter 2. Tcne (Aldrich) was used as provided. The alumina used for dry-column chromatography was Woelm

Neutral Alumina Activity Grade 1 and was deactivated to the required activity by addition of glass distilled water. Homogenous distribution of water within the alumina was achieved by stirring or shaking the sample overnight.

Preparation of $[\{Ru(S_2PPh_2)_2(PPh_3)\}_2tcne]$.

(a) 0.12g (0.11mmole) of $[Ru(S_2PPh_2)_2(PPh_3)_2]$ was dissolved in degassed chloroform (20ml) in a flask fitted with a nitrogen inlet, condenser, and pressure-equalised dropping flask. Tcne, 0.014g (0.11mmole), in chloroform (10ml), was added dropwise over half an hour. After stirring the solution for several hours, concentrating the solvent on a Schlenk line, and addition of degassed 60-80° pet.-ether, afforded a yellow green precipitate which analysed for $[\{Ru(S_2PPh_2)_2(PPh_3)\}_2tcne]$. The complex was separated from any unreacted tcne, and the adduct, $[PPh_3.tcne]$, by thin layer chromatography (silica plate with methylene chloride eluent). The yield of product is essentially quantitative, but is reduced on purification by chromatography.

(b) If equimolar amounts of $[Ru(S_2PPh_2)_2(PPh_3)(tcne)]$ and $[Ru(S_2PR_2)_2(PPh_3)_2]$ are stirred overnight in degassed methylene chloride, then $[\{Ru(S_2PPh_2)_2(PPh_3)\}_2tcne]$ is generated in quantitative yields.

(c) Attempts to purify the $[Ru(S_2PPh_2)_2(PPh_3)(tcne)]$ adduct by dry - column chromatography[122] afforded

[{$Ru(S_2PPh_2)_2(PPh_3)$}$_2$tcne]. The alumina column was deactivated by addition of deionised water (7% by weight) and the product was eluted with chloroform. On isolation, the first green band was found to contain only [{$Ru(S_2PPh_2)_2(PPh_3)$}$_2$tcne]. If the alumina is progressively deactivated, then a mixture of [{$Ru(S_2PPh_2)_2(PPh_3)$}$_2$tcne] and [$Ru(S_2PPh_2)_2(PPh_3)$(tcne)] is obtained.

The complex is soluble in CH_2Cl_2 and $CHCl_3$ and is air sensitive in solution. The infrared spectrum shows bands at 2110 (s, br), 2200 and 2260cm^{-1} (w) assigned to ν_{CN}. Found: C 58.1; H 3.8; N 3.0;. Calculated for $C_{90}H_{70}N_4P_6Ru_2S_8$: C, 58.3; H, 3.8; N, 3.0.

Preparation of [{$Ru(S_2P\{OEt\}_2)_2(PPh_3)$}$_2$tcne].

The complex is prepared by the same techniques as [{$Ru(S_2PPh_2)_2(PPh_3)$}$_2$tcne]. The grass-green solid isolated is (from $^{31}P-\{^1H\}$ n.m.r. spectroscopy) a mixture of complexes in solution in which one particular species predominates. The complex is soluble in CH_2Cl_2, $CHCl_3$ and acetone and insoluble in n-hexane. Bands due to ν_{CN} are observed at 2110 (s, br) 2210 and 2260cm^{-1} (w) in the inrfrared spectrum. Found: C 43.6, H 4.4, N 3.6; calculated for $C_{58}H_{70}N_4P_6Ru_2S_8$: C 43.7, H 4.4, N 3.6.

Preparation of [{$Ru(S_2PMe_2)_2(PPh_3)$}$_2$tcne].

The complex was prepared and purified as for the phenyl derivative. The adduct is olive-green in colour

and decomposes in both the solid and solution states. The infrared spectrum shows bands at 2110 (s, br), 2210 and 2255cm^{-1} assigned to ν_{CN}. Found: C, 44.0; H, 3.8; N, 3.8. Calculated for $C_{50}H_{54}N_4P_6Ru_2S_8$: C, 44.3; H, 4.0; N, 4.1.

Preparation of $[Ru(S_2PPh_2)_2(PPh_3)(tcne)]$.

(a) 0.10g (0.09mmole) of $[Ru(S_2PPh_2)_2(PPh_3)_2]$ was dissolved in freshly stilled degassed methylene chloride (25ml) and added dropwise to 0.034g (0.27mmole) of tcne in methylene chloride (15ml). After stirring for 6 hours, the solvent volume was reduced to about 5ml and filtered to remove some excess tcne. Dropwise addition of the filtrate to degassed n-hexane (*ca.* 30mls) affords a dark green precipitate which was collected by filtration. The complex was separated from any unreacted starting materials and by-products by preparative TLC (silica adsorbent, chloroform eluent). The first green band (R_f=0.6) is extracted with methylene chloride, and then acetone. The solvent is removed (Schlenk line) and after dissolving the green solid in the minimum volume of methylene chloride affords, on precipitation with n-hexane, a suspension of $[Ru(S_2PPh_2)_2(PPh_3)(tcne)]$. Although the yield initially is almost quanitative, chromatography reduces this to around 50 % (depending on activity of the chromatographic materials etc.) of the pure complex. The second green band contains $[\{Ru(S_2PPh_2)_2(PPh_3)\}_2tcne]$.

(b) The same adduct is prepared quantitatively from equimolar amounts of tcne and [{$Ru(S_2PPh_2)_2(PPh_3)\}_2$tcne] in degassed chloroform and isolated as for (a).

The complex is soluble in CH_2Cl_2, $CHCl_3$ and acetone, and insoluble in n-hexane and pet-ether. In non-co-ordinating solvents, solutions of the complex are relatively air stable. In co-ordinating solvents slow decompostion occurs. Found: C, 58.0; H, 3.4; N, 5.8. Calculated for $C_{48}H_{35}N_4P_3RuS_4$: C, 58.2, H, 3.5; N, 5.7.

Preparation of $[Ru(S_2PMe_2)_2(PPh_3)(tcne)]$.

The methyl derivative is prepared in the same way as $[Ru(S_2PPh_2)_2(PPh_3)(tcne)]$. The complex obtained is dark-green in colour. Decomposition occurs rapidly in solution and slowly in the solid state. The product was purified in the same way as the $[Ru(S_2PPh_2)_2(PPh_3)(tcne)]$ adduct. Yields of this product were low (*ca.* 30%). Found: C, 45.0; H, 3.5; N, 7.4. Calculated for $C_{28}H_{27}N_4P_3RuS_4$: C, 45.3; H, 3.6; N, 7.6.

Preparation of $[Ru(S_2P\{OEt\}_2)_2(PPh_3)(tcne)]$.

Prepared as for $[Ru(S_2PPh_2)_2(PPh_3)(tcne)]$. The complex is bright green in colour and is the most air-stable of the ruthenium adducts prepared of this type. Calculated for $C_{32}H_{35}N_4O_4P_3RuS_4$: C, 44.6; H, 4.1; N, 6.5. Found C, 44.4; H, 4.0; N, 6.4.

Preparation of $[Os(S_2PMe_2)_2(PPh_3)(tcne)]$.

The osmium complexes were prepared as for $[Ru(S_2PR_2)_2(PPh_3)(tcne)]$. The isolated solids are bright-green in colour and have similar solubilities to the ruthenium complexes, but also dissolve in diethyl ether. Solutions of the osmium species undergo slow decompositon (several days) on exposure to air. Recrystallisation of $[Os(S_2PMe_2)_2(PPh_3)(tcne)]$ from diethyl ether/60-80°pet-ether mixtures affords rectangular, green-black, plates which are suitable for X-ray diffraction studies. Found: C 40.7, H 3.2, N 6.7. Calculated for $C_{28}H_{27}N_4P_3OsS_4$: C 40.5, H 3.2, N 6.7.

Crystal data for $[Os(S_2PMe_2)_2(PPh_3)(tcne)]$

$C_{28}H_{27}N_4OsP_3S_4$, M=830.9, triclinic, a=9.675(3), b=10.698(4), c=16.711(2)Å, α=89.72(3), β=73.39(3), γ=85.64(3)°, U=1689Å^3, (from θ values of 12 reflections measured at $\pm\omega$ with θ=13-14°, λ=0.71073Å), space group $P\bar{1}$, Z=2, D_x=1.633gcm^{-3}. Green-black plates, crystal dimensions 0.15 x 0.10 x 0.05mm, μ(Mo-Kα)=41.81cm^{-1}, F(000)=816.

Data collection and processing

The crystal was mounted on a Stoe-Siemens AED-2 four-circle diffractometer and data were collected in the ω-2θ mode with an ω scan width of (1.05+0.347tanθ)° using graphite-monochromated Mo-Kα radiation. Of 3700

reflections measured ($2.5<\theta<22.5°$; h,-10 to 10; k,-12 to 12; l,0 to 18), 3044 with $F>6\sigma(F)$ were used in all calculations. An initial absorption correction was made using 72 ψ scans (maximum and minimum transmission factors were 0.129 and 0.097 respectively). No crystal decay was apparent.

Structure analysis

The Patterson function was used to locate the osmium atom. All other non-hydrogen atoms were located by iterative cycles of least-squares refinement and difference Fourier synthesis. The Os, N, P and S atoms were refined anisotropically. At isotropic convergence, final absorption correction was made using DIFABS. All hydrogen atoms and the carbon atoms of the phenyl rings were refined in fixed, calculated positions (AFIX). The weighting scheme $w^{-1}=\sigma^2(F)+0.000313F^2$ gave satisfactory agreement analyses. At convergence, $(\Delta/\sigma)_{max}$ in the final cycle was 0.183 and the final values of R and R_w were 0.032 and 0.038 respectively for 185 parameters, S=1.122. The final Fourier synthesis showed no important features and the maximum and minimum residues were 0.65 and -0.79eÅ^3 respectively. Structure solution and refinement were carried out using SHELX76.

Preparation of $[Os(S_2PPh_2)_2(PPh_3)(tcne)]$.

Prepared in the same way as the methyl derivative. Recrystallisation from a diethyl ether/60-80° Petroleum

ether mixture again yielded green black plates of the desired product. X-Ray diffraction studies were carried out to determine any effect of changing from a sterically small, electron - donating, methyl substituent, to a larger, electron - withdrawing substituent, on the dithiolate ligand. Found: C, 53.2; H, 3.2; N, 5.1. Calc. for $C_{48}H_{35}N_4OsP_3S_4$: C, 53.4; H, 3.2; N, 5.2.

Crystal data for $[Os(S_2PPh_2)_2(PPh_3)(tcne)]$

$C_{48}H_{35}N_4OsP_3S_4$, M=1079.2, monoclinic, a=20.5384(25), b=9.5578(16), c=23.730(3)Å, β=100.13(4)°, U=4585.6Å^3, (from θ values of 40 reflections measured at ±ω with θ=15-17°, λ=0.71073Å), space group $P\,2_1/c$, Z=4, D_x=1.563gcm^{-3}. Green-black plates, crystal dimensions 0.15 x 0.15 x 0.05mm, μ(Mo-Kα)=30.99cm^{-1}, F(000)=2144.

Data collection and processing

The crystal was mounted on a Stoe-Siemens AED-2 four-circle diffractometer and data were collected in the ω-2θ mode using graphite-monochromated Mo-Kα radiation. Of 5220 reflections measured ($2.5<\theta<22.5°$, h -22 to 21, k 0 to 10, l 0 to 25), 3905 with $F>6\sigma(F)$ were used in all calculations. An initial absorption correction was made using 72 ψ scans (maximum and minimum transmission factors were 0.861 and 0.513 respectively). No crystal decay was apparent.

Structure analysis

The Patterson function was used to locate the osmium atom. All other non-hydrogen atoms were located by iterative cycles of least-squares refinement and difference Fourier synthesis. The Os, N, P and S atoms, and the carbon atoms of tcne were refined anisotropically. At isotropic convergence, final absorption correction was made using DIFABS. All hydrogen atoms and the carbon atoms of the phenyl rings were refined in fixed, calculated positions (AFIX). The weighting scheme of $w^{-1}=\sigma^2(F)+0.00061F^2$ gave satisfactory agreement analyses. At convergence, $(\Delta/\sigma)_{max}$ in the final cycle was 0.022 and the final values of R and R_w were 0.048 and 0.059 respectively for 247 parameters, S=1.135. The final difference Fourier synthesis showed no important features. with maximum and minimum residues of 1.06 and -1.00eÅ^{-3} respectively. Structure solution and refinement were carried out using SHELX76.

Preparation of $[Os(S_2P\{OEt\}_2)_2(PPh_3)(tcne)]$.

Prepared as for $[Os(S_2PMe_2)_2(PPh_3)(tcne)]$. However, on addition of tcne a dark-brown colouration was observed which persisted for several hours. On stirring overnight, a bright-green solution of $[Os(S_2P\{OEt\}_2)_2(PPh_3)(tcne)]$ was afforded. The complex was recrystallised from n-hexane. Found C, 40.7; H, 3.7; N, 5.9. Calculated for $C_{32}H_{35}N_4O_4OsP_3S_4$ C, 40.5; H, 3.7; N, 5.9.

Table 3.5: Atomic co-ordinates with esds for $[Os(S_2PMe_2)_2(PPh_3)(tcne)]$.

	x	y	z	U_{iso}
OS	0.16791(4)	0.33070(3)	0.211120(20	0.03989(21)
S(1)	0.37984(22)	0.30548(23)	0.10140(14)	0.0529(15)
S(2)	0.05733(25)	0.36055(25)	0.09166(15)	0.0622(17)
S(3)	-0.0449(3)	0.40163(23)	0.30320(17)	0.0643(17)
S(4)	0.2067(3)	0.56095(24)	0.21450(18)	0.0701(18)
P(1)	0.10006(22)	0.12663(21)	0.22590(13)	0.0420(13)
P(2)	0.2544(3)	0.3584(3)	0.02211(15)	0.0623(17)
P(3)	0.0216(3)	0.57724(24)	0.29485(17)	0.0628(17)
N(11)	0.2811(7)	0.3148(6)	0.2918(4)	0.048(5)
N(12)	0.4004(14)	0.2175(13)	0.5287(7)	0.146(11)
N(21)	0.5943(12)	0.5361(12)	0.2447(7)	0.131(10)
N(22)	0.7064(11)	0.4387(13)	0.4844(6)	0.125(10)
C(1)	0.4450(9)	0.3354(8)	0.3921(5)	0.0552(23)
C(2)	0.5528(10)	0.4123(9)	0.3773(6)	0.0600(25)
C(11)	0.3519(9)	0.3193(8)	0.3387(5)	0.0507(22)
C(12)	0.4209(12)	0.2681(11)	0.4676(8)	0.084(3)
C(21)	0.5787(12)	0.4823(11)	0.3046(8)	0.083(3)
C(22)	0.6415(12)	0.4290(10)	0.4358(7)	0.075(3)
C(31)	-0.1029(14)	0.6836(12)	0.2613(8)	0.105(4)
C(32)	0.0339(14)	0.6345(12)	0.3927(7)	0.104(4)
C(41)	0.2907(12)	0.5062(10)	-0.0206(7)	0.087(3)
C(42)	0.2769(13)	0.2541(11)	-0.0625(7)	0.095(4)
C(111)	0.1617(6)	0.0445(5)	0.3105(3)	0.0482(21)
C(112)	0.2429(6)	-0.0699(5)	0.3003(3)	0.0604(25)
C(113)	0.2887(6)	-0.1261(5)	0.3668(3)	0.084(3)
C(114)	0.2533(6)	-0.0679(5)	0.4435(3)	0.085(3)
C(115)	0.1722(6)	0.0465(5)	0.4537(3)	0.074(3)
C(116)	0.1263(6)	0.1027(5)	0.3872(3)	0.0575(24)
C(121)	0.1571(4)	0.0182(6)	0.1391(4)	0.0445(20)
C(122)	0.0623(4)	-0.0437(6)	0.1036(4)	0.063(3)
C(123)	0.1127(4)	-0.1263(6)	0.0381(4)	0.081(3)
C(124)	0.2580(4)	-0.1470(6)	0.0081(4)	0.073(3)
C(125)	0.3528(4)	-0.0851(6)	0.0436(4)	0.075(3)
C(126)	0.3023(4)	-0.0025(6)	0.1091(4)	0.062(3)
C(131)	-0.0939(5)	0.1114(5)	0.2524(3)	0.0438(20)
C(132)	-0.1829(5)	0.1791(5)	0.2089(3)	0.0565(24)
C(133)	-0.3269(5)	0.1602(5)	0.2236(3)	0.062(3)
C(134)	-0.3819(5)	0.0736(5)	0.2818(3)	0.066(3)
C(135)	-0.2929(5)	0.0059(5)	0.3253(3)	0.072(3)
C(136)	-0.1489(5)	0.0248(5)	0.3106(3)	0.0572(24)

Table 3.6: Atomic coordinates for H atoms in $[Os(S_2PMe_2)_2(PPh_3)(tcne)]$.

	x	y	z	U_{iso}
H(112)	0.2702	-0.1149	0.2409	0.0800
H(113)	0.3515	-0.2147	0.3590	0.0800
H(114)	0.2888	-0.1115	0.4951	0.0800
H(115)	0.1448	0.0915	0.5131	0.0800
H(116)	0.0635	0.1913	0.3950	0.0800
H(122)	-0.0502	-0.0276	0.1269	0.0800
H(123)	0.0394	-0.1741	0.0106	0.0800
H(124)	0.2971	-0.2109	-0.0426	0.0800
H(125)	0.4653	-0.1011	0.0204	0.0800
H(126)	0.3757	0.0454	0.1366	0.0800
H(132)	-0.1404	0.2462	0.1638	0.0800
H(133)	-0.3958	0.2126	0.1899	0.0800
H(134)	-0.4933	0.0590	0.2933	0.0800
H(135)	-0.3354	-0.0611	0.3704	0.0800
H(136)	-0.0800	-0.0276	0.3443	0.0800
H(31A)	-0.1160	0.6550	0.2016	0.0800
H(31B)	-0.0655	0.7764	0.2581	0.0800
H(31C)	-0.2033	0.6845	0.3037	0.0800
H(32A)	0.1086	0.5736	0.4176	0.0800
H(32B)	-0.0688	0.6362	0.4328	0.0800
H(32C)	0.0691	0.7281	0.3871	0.0800
H(41A)	0.2792	0.5751	0.0278	0.0800
H(41B)	0.2173	0.5323	-0.0598	0.0800
H(41C)	0.3976	0.5019	-0.0559	0.0800
H(42A)	0.2565	0.1607	-0.0408	0.0800
H(42B)	0.3840	0.2538	-0.0971	0.0800
H(42C)	0.2038	0.2842	-0.1010	0.0800

Table 3.7 Anisotropic thermal parameters in $Å^2$.

	U_{11}	U_{22}	U_{33}	U_{23}	U_{13}	U_{12}
OS	0.03920(19)	0.03905(21)	0.03983(22)	0.00122(14)	-0.00877(13)	-0.00479(13)
S(1)	0.0416(12)	0.0694(16)	0.0451(14)	0.0056(12)	-0.0070(10)	-0.0055(11)
S(2)	0.0513(14)	0.0751(18)	0.0603(17)	0.0188(14)	-0.0229(12)	-0.0118(12)
S(3)	0.0540(14)	0.0494(15)	0.0817(19)	-0.0091(13)	0.0083(13)	-0.0039(12)
S(4)	0.0703(17)	0.0460(15)	0.0882(20)	-0.0006(14)	-0.0027(15)	-0.0128(13)
P(1)	0.0421(12)	0.0412(13)	0.0408(13)	-0.0005(10)	-0.0090(10)	-0.0035(10)
P(2)	0.0578(15)	0.0805(19)	0.0467(15)	0.0157(13)	-0.0127(12)	-0.0102(13)
P(3)	0.0601(15)	0.0482(15)	0.0782(19)	-0.0100(13)	-0.0206(14)	-0.0019(12)
N(11)	0.044(4)	0.049(4)	0.050(5)	0.007(4)	-0.018(4)	0.000(3)
N(12)	0.163(11)	0.174(12)	0.107(9)	0.064(9)	-0.066(8)	-0.081(10)
N(21)	0.114(9)	0.177(12)	0.105(9)	0.049(8)	-0.041(7)	-0.065(8)
N(22)	0.081(7)	0.222(14)	0.071(7)	-0.037(8)	-0.028(6)	-0.008(8)

Table 3.8: Atomic co-ordinates with esds for $[Os(S_2P\,Ph_2)_2(PPh_3)(tcne)]$.

	x	y	z	U_{iso}
OS	-0.724950(20)	-0.21693(5)	-0.146540(20)	0.0307(3)
S(1)	-0.64304(17)	-0.3876(4)	-0.16736(15)	0.0464(23)
S(2)	-0.62920(16)	-0.0617(4)	-0.14508(14)	0.0428(21)
S(3)	-0.79084(17)	-0.0467(4)	-0.10828(13)	0.0459(22)
S(4)	-0.68601(17)	-0.2605(4)	-0.04144(13)	0.0445(21)
P(1)	-0.76995(16)	-0.1438(4)	-0.23857(13)	0.0364(19)
P(2)	-0.57416(16)	-0.2373(4)	-0.14542(14)	0.0424(22)
P(3)	-0.76434(17)	-0.1428(4)	-0.03125(13)	0.0427(21)
N(11)	-0.7884(5)	-0.3540(11)	-0.1436(4)	0.034(6)
N(12)	-0.9959(7)	-0.4955(17)	-0.1434(6)	0.093(12)
N(21)	-0.7193(7)	-0.6753(18)	-0.0646(9)	0.132(16)
N(22)	-0.9203(7)	-0.8352(15)	-0.0490(7)	0.093(12)
C(1)	-0.8698(6)	-0.5414(14)	-0.1190(5)	0.044(9)
C(2)	-0.8436(7)	-0.6568(15)	-0.0863(6)	0.054(9)
C(11)	-0.8288(7)	-0.4410(14)	-0.1357(5)	0.042(9)
C(12)	-0.9399(8)	-0.5182(15)	-0.1333(6)	0.052(10)
C(21)	-0.7745(9)	-0.6724(18)	-0.0728(8)	0.088(14)
C(22)	-0.8861(7)	-0.7543(15)	-0.0658(7)	0.062(11)
C(111)	-0.8480(4)	-0.2309(10)	-0.2688(3)	0.044(3)
C(112)	-0.8594(4)	-0.2909(10)	-0.3232(3)	0.060(4)
C(113)	-0.9200(4)	-0.3542(10)	-0.3441(3)	0.084(5)
C(114)	-0.9693(4)	-0.3576(10)	-0.3105(3)	0.083(5)
C(115)	-0.9580(4)	-0.2976(10)	-0.2560(3)	0.078(5)
C(116)	-0.8973(4)	-0.2343(10)	-0.2352(3)	0.055(4)
C(121)	-0.7178(5)	-0.1659(7)	-0.2927(4)	0.037(3)
C(122)	-0.6927(5)	-0.0492(7)	-0.3170(4)	0.064(4)
C(123)	-0.6530(5)	-0.0667(7)	-0.3585(4)	0.089(6)
C(124)	-0.6384(5)	-0.2009(7)	-0.3757(4)	0.084(5)
C(125)	-0.6634(5)	-0.3176(7)	-0.3514(4)	0.070(5)
C(126)	-0.7031(5)	-0.3001(7)	-0.3099(4)	0.058(4)
C(131)	-0.7941(3)	0.0415(9)	-0.2460(3)	0.037(3)
C(132)	-0.7552(3)	0.1436(9)	-0.2143(3)	0.055(4)
C(133)	-0.7733(3)	0.2842(9)	-0.2206(3)	0.061(4)
C(134)	-0.8303(3)	0.3227(9)	-0.2585(3)	0.060(4)
C(135)	-0.8693(3)	0.2205(9)	-0.2902(3)	0.073(4)
C(136)	-0.8512(3)	0.0799(9)	-0.2839(3)	0.059(4)
C(211)	-0.5218(4)	-0.2704(8)	-0.0775(4)	0.041(3)
C(212)	-0.5207(4)	-0.1812(8)	-0.0308(4)	0.063(4)
C(213)	-0.4786(4)	-0.2093(8)	0.0208(4)	0.071(4)
C(214)	-0.4376(4)	-0.3267(8)	0.0257(4)	0.075(5)
C(215)	-0.4387(4)	-0.4159(8)	-0.0210(4)	0.074(5)
C(216)	-0.4808(4)	-0.3878(8)	-0.0726(4)	0.056(4)
C(221)	-0.5160(6)	-0.2311(13)	-0.1944(5)	0.048(3)
C(222)	-0.4579(6)	-0.1532(13)	-0.1811(5)	0.136(8)
C(223)	-0.4136(6)	-0.1482(13)	-0.2194(5)	0.162(10)
C(224)	-0.4275(6)	-0.2211(13)	-0.2711(5)	0.091(6)
C(225)	-0.4856(6)	-0.2990(13)	-0.2844(5)	0.204(14)
C(226)	-0.5298(6)	-0.3040(13)	-0.2461(5)	0.185(12)
C(311)	-0.7479(4)	-0.0153(11)	0.0235(4)	0.053(4)
C(312)	-0.7932(4)	0.0144(11)	0.0593(4)	0.072(5)
C(313)	-0.7802(4)	0.1215(11)	0.0997(4)	0.104(6)
C(314)	-0.7219(4)	0.1989(11)	0.1042(4)	0.139(9)
C(315)	-0.6766(4)	0.1692(11)	0.0684(4)	0.139(9)
C(316)	-0.6896(4)	0.0621(11)	0.0281(4)	0.082(5)
C(321)	-0.8278(4)	-0.2490(11)	-0.0117(4)	0.055(4)
C(322)	-0.8102(4)	-0.3632(11)	0.0244(4)	0.077(5)
C(323)	-0.8590(4)	-0.4396(11)	0.0449(4)	0.091(6)
C(324)	-0.9253(4)	-0.4019(11)	0.0293(4)	0.102(6)
C(325)	-0.9429(4)	-0.2877(11)	-0.0067(4)	0.101(6)
C(326)	-0.8941(4)	-0.2113(11)	-0.0273(4)	0.082(5)

Table 3.9: Atomic coordinates for H atoms in $[Os(S_2PPh_2)_2(PPh_3)(tcne)]$.

	x	y	z	U_{iso}
H(112)	−0.8212	−0.2884	−0.3493	0.0800
H(113)	−0.9288	−0.4007	−0.3862	0.0800
H(114)	−1.0163	−0.4066	−0.3266	0.0800
H(115)	−0.9961	−0.3001	−0.2300	0.0800
H(116)	−0.8885	−0.1878	−0.1931	0.0800
H(122)	−0.7041	0.0547	−0.3037	0.0800
H(123)	−0.6336	0.0236	−0.3773	0.0800
H(124)	−0.6076	−0.2145	−0.4078	0.0800
H(125)	−0.6520	−0.4215	−0.3647	0.0800
H(126)	−0.7225	−0.3905	−0.2911	0.0800
H(132)	−0.7110	0.1138	−0.1850	0.0800
H(133)	−0.7431	0.3633	−0.1961	0.0800
H(134)	−0.8443	0.4315	−0.2634	0.0800
H(135)	−0.9134	0.2503	−0.3195	0.0800
H(136)	−0.8813	0.0009	−0.3084	0.0800
H(212)	−0.5525	−0.0904	−0.0346	0.0800
H(213)	−0.4778	−0.1403	0.0569	0.0800
H(214)	−0.4050	−0.3484	0.0657	0.0800
H(215)	−0.4069	−0.5067	−0.0171	0.0800
H(216)	−0.4816	−0.4568	−0.1087	0.0800
H(222)	−0.4471	−0.0967	−0.1411	0.0800
H(223)	−0.3686	−0.0879	−0.2091	0.0800
H(224)	−0.3932	−0.2173	−0.3007	0.0800
H(225)	−0.4963	−0.3555	−0.3244	0.0800
H(226)	−0.5748	−0.3643	−0.2564	0.0800
H(312)	−0.8383	−0.0455	0.0558	0.0800
H(313)	−0.8153	0.1444	0.1274	0.0800
H(314)	−0.7119	0.2818	0.1355	0.0800
H(315)	−0.6315	0.2291	0.0720	0.0800
H(316)	−0.6545	0.0391	0.0004	0.0800
H(322)	−0.7588	−0.3924	0.0364	0.0800
H(323)	−0.8454	−0.5280	0.0729	0.0800
H(324)	−0.9631	−0.4611	0.0452	0.0800
H(325)	−0.9942	−0.2585	−0.0188	0.0800
H(326)	−0.9077	−0.1229	−0.0552	0.0800

Table 3.10: Anisotropic thermal parameters in $Å^2$.

	U_{11}	U_{22}	U_{33}	U_{23}	U_{13}	U_{12}
OS	0.0297(3)	0.0315(3)	0.0300(3)	0.0029(3)	0.00518(18)	0.0007(3)
S(1)	0.0374(20)	0.0400(23)	0.0604(23)	−0.0081(17)	0.0099(17)	−0.0001(16)
S(2)	0.0358(20)	0.0375(22)	0.0539(21)	0.0037(17)	0.0090(16)	−0.0025(16)
S(3)	0.0502(22)	0.0498(24)	0.0371(19)	0.0053(16)	0.0115(16)	0.0132(18)
S(4)	0.0503(20)	0.0463(24)	0.0347(17)	0.0085(16)	0.0033(15)	0.0102(17)
P(1)	0.0361(19)	0.0347(20)	0.0372(18)	0.0032(16)	0.0071(14)	0.0007(16)
P(2)	0.0325(18)	0.046(3)	0.0473(20)	0.0027(16)	0.0084(15)	0.0033(16)
P(3)	0.0508(22)	0.0441(22)	0.0325(18)	−0.0019(16)	0.0108(16)	−0.0024(18)
N(11)	0.048(7)	0.023(6)	0.030(6)	0.006(5)	0.005(5)	0.008(6)
N(12)	0.056(10)	0.115(14)	0.105(12)	0.027(10)	0.015(9)	−0.014(10)
N(21)	0.035(9)	0.105(15)	0.247(22)	0.070(14)	−0.005(11)	0.004(9)
N(22)	0.081(11)	0.049(9)	0.149(15)	0.034(9)	0.033(10)	−0.004(8)
C(1)	0.040(8)	0.045(9)	0.045(8)	−0.008(7)	0.009(6)	−0.014(7)
C(2)	0.045(9)	0.041(9)	0.071(10)	0.011(8)	−0.002(7)	−0.009(8)
C(11)	0.051(9)	0.036(9)	0.036(7)	0.001(6)	0.004(7)	0.006(8)
C(12)	0.054(10)	0.044(10)	0.055(9)	0.015(7)	0.004(8)	−0.019(8)
C(21)	0.056(12)	0.063(14)	0.138(17)	0.023(11)	−0.006(11)	−0.012(10)
C(22)	0.047(9)	0.042(12)	0.092(12)	0.014(8)	−0.004(8)	0.009(8)

Table 3.11: Selected torsion angles (°) for $[Os(S_2PMe_2)_2(PPh_3)(tcne)]$.

C(2)	- C(1)	-C(11)	-N(11)	-10.9(99)	S(2)	- Os	- S(1) - P(2)	7.38(11)
C(11)	- C(1)	- C(2)	-C(21)	-0.4(15)	S(2)	- Os	- S(3) - P(3)	-92.29(12)
C(11)	- C(1)	- C(2)	-C(22)	177.4(9)	S(2)	- Os	- S(4) - P(3)	94.00(12)
C(12)	- C(1)	- C(2)	-C(21)	-178.7(10)	S(2)	- Os	- P(1) -C(111)	178.05(22)
C(12)	- C(1)	- C(2)	-C(22)	-0.8(15)	S(2)	- Os	- P(1) -C(121)	56.66(23)
C(12)	- C(1)	-C(11)	-N(11)	167.4(90)	S(2)	- Os	- P(1) -C(131)	-65.13(22)
Os	- P(1)	-C(111)	-C(112)	-124.6(5)	S(3)	- Os	-N(11) -C(11)	-87.5(52)
Os	- P(1)	-C(111)	-C(116)	54.1(5)	S(3)	- Os	- S(1) - P(2)	-50.2(4)
Os	- P(1)	-C(121)	-C(122)	-122.6(4)	S(3)	- Os	- S(2) - P(2)	161.33(12)
Os	- P(1)	-C(121)	-C(126)	58.1(5)	S(3)	- Os	- S(4) - P(3)	1.71(12)
Os	- P(1)	-C(131)	-C(132)	47.5(5)	S(3)	- Os	- P(1) -C(111)	-89.54(22)
Os	- P(1)	-C(131)	-C(136)	-137.9(4)	S(3)	- Os	- P(1) -C(121)	149.08(23)
Os	- S(1)	- P(2)	- S(2)	-9.08(14)	S(3)	- Os	- P(1) -C(131)	27.28(22)
Os	- S(1)	- P(2)	-C(41)	111.5(4)	S(4)	- Os	-N(11) -C(11)	-7.0(52)
Os	- S(1)	- P(2)	-C(42)	-129.9(4)	S(4)	- Os	- S(1) - P(2)	-84.00(12)
Os	- S(2)	- P(2)	- S(1)	9.09(14)	S(4)	- Os	- S(2) - P(2)	80.21(12)
Os	- S(2)	- P(2)	-C(41)	-111.8(4)	S(4)	- Os	- S(3) - P(3)	-1.69(12)
Os	- S(2)	- P(2)	-C(42)	130.4(4)	S(4)	- Os	- P(1) -C(111)	-80.5(6)
Os	- S(3)	- P(3)	- S(4)	2.16(15)	S(4)	- Os	- P(1) -C(121)	158.2(5)
Os	- S(3)	- P(3)	-C(31)	122.9(5)	S(4)	- Os	- P(1) -C(131)	36.4(6)
Os	- S(3)	- P(3)	-C(32)	-121.1(5)	N(11)	- Os	- S(1) - P(2)	-169.17(23)
Os	- S(4)	- P(3)	- S(3)	-2.05(14)	N(11)	- Os	- S(2) - P(2)	14.1(13)
Os	- S(4)	- P(3)	-C(31)	-122.2(5)	N(11)	- Os	- S(3) - P(3)	82.57(23)
Os	- S(4)	- P(3)	-C(32)	118.9(5)	N(11)	- Os	- S(4) - P(3)	-94.67(23)
S(1)	- Os	-N(11)	-C(11)	80.7(52)	N(11)	- Os	- P(1) -C(111)	6.0(3)
S(1)	- Os	- S(2)	- P(2)	-7.37(11)	N(11)	- Os	- P(1) -C(121)	-115.4(3)
S(1)	- Os	- S(3)	- P(3)	-35.9(4)	N(11)	- Os	- P(1) -C(131)	122.8(3)
S(1)	- Os	- S(4)	- P(3)	174.21(12)	P(1)	- Os	- S(1) - P(2)	96.29(11)
S(1)	- Os	- P(1)	-C(111)	97.82(22)	P(1)	- Os	- S(2) - P(2)	-109.23(12)
S(1)	- Os	- P(1)	-C(121)	-23.57(24)	P(1)	- Os	- S(3) - P(3)	176.78(12)
S(1)	- Os	- P(1)	-C(131)	-145.36(21)	P(1)	- Os	- S(4) - P(3)	-7.5(6)
S(2)	- Os	-N(11)	-C(11)	59.6(58)	P(1)	- Os	-N(11) -C(11)	-177.3(52)

Table 3.12 Selected least squares planes and interplanar angles for $[Os(S_2PMe_2)_2(PPh_3)(tcne)]$.

Plane	Atoms in plane	σ
1	Os S1 S2 P2	0.08
2	Os S3 S4 P3	0.02
3	C1 C2 C11 C12 C22 C21 N11 N12 N22 N21	0.02
4	C1' C2' C11' C12' C22' C21' N11' N12' N22' N21'	0.02

Interplanar angles (°)

1-2 88.73, 1-3 45.7, 2-3 84.3, 3-4 0.1.

σ = R.M.S. deviation of atoms from plane (Å).

Table 3.13: Selected torsion angles (°) for $[Os(S_2PPh_2)_2(PPh_3)(tcne)]$.

C(11) - C(1) - C(2) -C(21)	-2.9(21)	S(2) - Os - P(1) -C(121)	56.5(4)
C(11) - C(1) - C(2) -C(22)	175.4(13)	S(2) - Os - P(1) -C(131)	-64.7(3)
C(12) - C(1) - C(2) -C(21)	-178.8(14)	S(3) - Os - P(1) -C(111)	-86.6(3)
C(12) - C(1) - C(2) -C(22)	-0.5(21)	S(3) - Os - P(1) -C(121)	151.6(4)
Os - S(1) - P(2) - S(2)	-14.28(18)	S(3) - Os - P(1) -C(131)	30.4(3)
Os - S(3) - P(3) - S(4)	16.26(19)	S(4) - Os - P(1) -C(111)	-95.6(7)
S(2) - Os - S(1) - P(2)	11.59(15)	S(4) - Os - P(1) -C(121)	142.6(7)
S(3) - Os - S(4) - P(3)	12.90(15)	S(4) - Os - P(1) -C(131)	21.4(8)
S(1) - Os - S(3) - P(3)	-35.8(7)	S(1) - P(2) -C(211)-C(212)	-116.4(7)
S(1) - Os - S(4) - P(3)	-171.49(16)	S(1) - P(2) -C(211)-C(216)	64.6(8)
S(2) - Os - S(3) - P(3)	-100.26(15)	S(1) - P(2) -C(221)-C(222)	-168.0(9)
S(2) - Os - S(4) - P(3)	108.32(15)	S(1) - P(2) -C(221)-C(226)	12.5(11)
S(3) - Os - S(1) - P(2)	-54.3(6)	S(2) - P(2) -C(211)-C(212)	-0.2(9)
S(3) - Os - S(2) - P(2)	158.10(15)	S(2) - P(2) -C(211)-C(216)	-179.2(6)
S(4) - Os - S(1) - P(2)	-76.99(16)	S(2) - P(2) -C(221)-C(222)	75.7(11)
S(4) - Os - S(2) - P(2)	77.55(15)	S(2) - P(2) -C(221)-C(226)	-103.8(10)
N(11) - Os - P(1) -C(111)	4.4(5)	S(3) - P(3) -C(311)-C(312)	102.8(9)
N(11) - Os - P(1) -C(121)	-117.4(5)	S(3) - P(3) -C(311)-C(316)	-73.3(9)
N(11) - Os - P(1) -C(131)	121.4(4)	S(3) - P(3) -C(321)-C(322)	152.5(7)
N(11) - Os - S(1) - P(2)	-164.0(3)	S(3) - P(3) -C(321)-C(326)	-33.9(9)
N(11) - Os - S(2) - P(2)	20.5(22)	S(4) - P(3) -C(311)-C(312)	-140.9(8)
N(11) - Os - S(3) - P(3)	74.2(3)	S(4) - P(3) -C(311)-C(316)	42.9(9)
N(11) - Os - S(4) - P(3)	-78.6(3)	S(4) - P(3) -C(321)-C(322)	36.4(9)
P(1) - Os - S(1) - P(2)	100.71(16)	S(4) - P(3) -C(321)-C(326)	-150.1(7)
P(1) - Os - S(2) - P(2)	-112.15(15)	Os - S(2) - P(2) -C(211)	-107.6(3)
P(1) - Os - S(3) - P(3)	168.81(16)	Os - S(1) - P(2) -C(221)	-137.1(4)
P(1) - Os - S(4) - P(3)	22.0(7)	Os - S(2) - P(2) -C(221)	135.5(5)
S(1) - Os - P(1) -C(111)	98.2(3)	Os - S(3) - P(3) -C(311)	139.3(4)
S(1) - Os - P(1) -C(121)	-23.7(4)	Os - S(3) - P(3) -C(321)	-103.8(4)
S(1) - Os - P(1) -C(131)	-144.8(3)	Os - S(4) - P(3) -C(311)	-135.1(4)
S(2) - Os - P(1) -C(111)	178.3(3)	Os - S(4) - P(3) -C(321)	106.6(4)

Table 3.14 Selected least squares planes and interplanar angles for $[Os(S_2PPh_2)_2(PPh_3)(tcne)]$.

Plane	Atoms in plane	σ
1	Os S1 S2 P2	0.12
2	Os S3 S4 P3	0.14
3	C321-C326	0.00
4	C1 C2 C11 C12 C22 C21 N11 N12 N22 N21	0.05

Interplanar angles (°)

1-2 89.7, 1-3 41.0, 1-4 46.7, 2-3 68.0, 2-4 60.6, 3-4 7.7.

σ = R.M.S. deviation of atoms from plane (Å).

Table 3.15: ^{1}H n.m.r data for $[M(S_2PR_2)_2(PPh_3)(tcne)]$ complexes.[a]

M	R	δPPh_3/ppm[b]	δ R/ppm[c]
Ru	Me	7.25-7.75 m.	2.05 m, 0.88 d(12.9).[d]
Ru	OEt	7.25-7.75 m.	4.20 m, 3.11 m;[e] 1.38 m, 0.98 t[f](7.0).[g]
Os	Me	7.25-7.50 m.	2.00 m, 0.88 d (12.9).[d]
Os	OEt	7.25-7.50 m.	4.15 m, 3.05 m;[e] 1.30 m, 0.94 t[f](7.0).[g]
Os	Ph	7.00-8.00 m.[h]	

(a) recorded as CD_2Cl_2 solutions at 293K; (b) the protons of the phenyl rings; (c) the protons of the dithiolate ligand; (d) J_{PH} in Hz; (e) the methylene protons of the ethoxy substituent; (f) the methyl protons of the ethoxy substituent; (g) J_{HH} in Hz; (h) this multiplet includes the protons of the dithiolate substituent.

References

1. T. L. Cairns, R. A. Cairns, D. D. Coffman, V. A. Engelhardt, R. E. Heckert, E. L. Little, E. G. McGeer, B. McKusick, and W. J. Middleton, *J. Am. Chem. Soc.*, 1957, **79**, 2340.

2. T. L. Cairns, R. A. Cairns, D. D. Coffman, V. A. Engelhardt, R. E. Heckert, E. L. Little, E. G. McGeer, B. C. McKusick, W. J. Middleton, R. M. Scribner, C. Theobald, and H. Winberg, *J. Am. Chem. Soc.*, 1958, **80**, 2775.

3. D. A. Bekoe and K. N. Trueblood, *Z. Kristallogr.*, 1960, **1**, 113.

4. U. Druck and H. Guth, *Z. Kristallogr.*, 1982, **103**, 161.

5. R. G. Little, D. Pautler and P. Coppens, *Acta Crystallogr.*, 1971, **27**, 1493.

6. H. Hope, *Acta Chem. Scand.*, 1968, **22** ,1057.

7. B. R. Penfold and W. N. Lipscomb, *Acta Crystallogr.*, 1961, **14**, 589.

8. R. E. Merrifield and W. D. Phillips, *J. Am. Chem. Soc.*, 1958, **80**, 2778.

9. S. Chowdhury and P. Kerbale, *J. Am. Chem. Soc.*, 1986, **108**, 5453.

10. L. E. Lyons and L. D. Palmer, *Aust. J. Chem.*, 1976, **29**, 1919.

11. R. M. Williams and S. C. Wallwork, *Acta Crystallogr.*, 1967, **22**, 899.

12. E. Maverick, K. N. Trueblood, D. A. Bekoe, *Acta Crystallogr., Sect. B*, 1978, **34**, 2777.

13. D. S. Tarbell and T. Huang, *J. Org. Chem.*, 1959, **24**, 887.

14. G. Shenk and M. Ozolins, *Anal. Chem.*, 1962, **33**, 1562.

15. I. Ikemoto, H. Kuroda, *Acta Crystallogr., Sect. B*, 1968, **24**, 383.

16. H. Irngartinger and A. Goldmann, *Z. Kristallogr.*, 1979, **97**, 149.

17. K. Vasudevan and V. Ramakrishnan, *Rev. Pure Appl. Chem.*, 1967, **17**, 95.

18. R. C. Wheland and J. l. Gillson, *J. Am. Chem. Soc.*, 1958, **80**, 2806.

19. O. W. Webster, W. Mahler and R. E. Benson, *J. Org. Chem.*, 1960, **25**, 1470.

20. W. D. Phillips, J. C. Rowell, S. I. Weissman, *J. Chem. Phys.*, 1960, **33**, 626.

21. W. J. Middleton, R. E. Herbert, E. L. Little and C. G. Krespan, *J. Am. Chem. Soc.*, 1958, **80**, 2783.

22. W. J. Middleton and V. A. Engelhardt, *J. Am. Chem. Soc.*, 1958, **80**, 2789.

23. B. C. M^{c}Kusick, R. E. Heckert, T. L. Cairns, D. D. Coffman, and H. F. Mower, *J. Am. Chem. Soc.*, 1958, **80**, 2806.

24. G. S. Reddy and C. D. Weiss, *J. Org. Chem.*, 1963, **28**, 1822.

25. J. E. Douglas, *Inorg. Chem.*, 1972, 11, 654.

26. O. W. Webster, W. Mahler and R. E. Benson, *J. Am. Chem. Soc.*, 1962, **84**, 3678.

27. M. Rosenblum, R. W. Fish and C. Bennett, *J. Am. Chem. Soc.*, 1964, **86**, 5166.

28. E. Adman, M. Rosenblum, S. Sullivan and T. N. Margulis, *J. Am. Chem. Soc.*, 1967, **89**, 4540.

29. R. L. Brandon, J. H. Osiek and A. Ottenberg, *J. Org. Chem.*, 1966, **31**, 1214.

30. J. S. Miller, J. C. Calabrese, H. Rommelmann, S. R. Chittipeddi, J. H. Zhang, W. Reiff and A. J. Epstein, *J. Am. Chem. Soc.*, 1987, **109**, 769.

31. D. A. Lemenovski, R. A. Stukan, M. Y. Antipin, Y. L. Slovokhotov, A. E. Kalinin and Y. T. Struchkov, *Koord. Khim.*, 1981, **7**, 240.

32. J. W. Fitch and J. J. Lagowski, *Inorg. Chem.*, 1965, **4**, 864.

33. A. Tumanov, L. N. Zakharov, P. G. Sennikov, A. N. Egorochkin, G. Razuvaev, A. S. Smirniv and V. A. Dodonov, *J. Organomet. Chem.*, 1984, **263**, 213.

34. A. K. Holliday, P. H. Makin, R. J. Puddephat and J. D. Wilkins, *J. Organomet. Chem.*, 1973, **57**, C45.

35. H. C. Gardner and J. K. Kochi, *J. Am. Chem. Soc.*, 1976, **98**, 2460.

36. T. Kuwana, D. E. Bublitz and G. Hoh, *J. Am. Chem. Soc.*, 1960, **82**, 5811.

37. S. Sostero, A. Duatti, P. Zanella and O. Traverso, *J. Organomet. Chem.*, 1978, **157**, 437.

38. C. E. Briant, C. J. Gardner, T. S. A. Hor, N. D. Howells, and D. M. P. Mingos, *J. Chem. Soc., Dalton Trans.*, 1984, 2645.

39. S. Fukuzumi, K. Ishikawa and T. Tanaka, *J. Chem. Soc., Dalton Trans.*, 1985, 899.

40. J. A. Connor and P. I. Riley, *J. Organomet. Chem.*, 1979, **174**, 173.

41. S. Carra and R. Ugo, *Inorg. Chim. Acta Rev.*, 1967, 1, 49.

42. W. H. Baddley, *Inorg. Chim. Acta Rev.*, 1968, 2, 5.

43. M. J. S. Dewar, *Bull. Soc. Chim. Fr.*, 1951, **18**, C 71.

44. J. Chatt and L. A. Duncanson, *J. Chem. Soc.*, 1953, 2939.

45. H. W. Quinn and J. H. Tsai *Adv. Inorg. Chem. and Radiochem.*, 1969, **12**, 217.

46. K. Iuchi, S. Asada, T. Kinugasa, K. Kanamori and A. Sugimori, *Bull Chem. Soc. Jpn.*, 1976, **49**, 577.

47. M. Herberhold, *Angew. Chem., Int. Ed. (Engl.)*, 1968, **7**, 305.

48. R. D. Adams, D. F. Chodosh, *J. Am. Chem. Soc.*, 1977 **99**, 6544.

49. P. W. Schneider, D. C. Bravard, J. W. M^{c}Donald and W. E. Newton, *J. Am. Chem. Soc.*, 1972, **94**, 8640.

50. J. R. Morrow, T. Tonker and J. L. Templeton, *J. Am. Chem. Soc.*, 1985, **107**, 6957.

51. S. M. Grant and A. R. Manning, *J. Chem. Soc., Dalton Trans.*, 1979, 1789.

52. N. G. Connelly, R. L. Kelly and M. Whiteley, *J. Chem. Soc., Dalton Trans.*, 1981, 34.

53. M. O. Albers, N. J. Colville and E. Singleton, *J. Chem. Soc., Dalton Trans.*, 1982, 1069.

54. H. C. Ashton and A. R. Manning, *Inorg. Chem.*, 1983, **22**, 1440.

55. O. Gandolfi, B. Giovannitti, M. Ghedini and G. Dolcetti, *J. Organomet. Chem.*, 1976, **104**, C41.

56. O. Gandolfi, B. Giovannitti, M. Ghedini and G. Dolcetti, *J. Organomet. Chem.*, 1976, **129**, 207.

57. H. Werner and B. Juthani, *J. Organomet. Chem.*, 1981, **209**, 211.

58. Y. Kubo, A. Yamamoto, S. Ikeda, *J. Organomet. Chem.*, 1973, **59**, 353.

59. P. Uguagliati, G. Deganello, L. Busetto and U. Belluco, *Inorg. Chem.*, 1969, **8**, 1625.

60. L. Busetto, G. Carturan, A. Palazzi and U. Belluco, *J. Chem. Soc., A*, 1970, 474

61. G. Mestroni, A. Camus and G. Zassinovich, *J. Organomet. Chem.*, 1974, **65**, 119.

62. A. L. Balch and B. Tulyathan, *Inorg. Chem.*, 1977, **16**, 2840.

63. F. Faraone, S. Schiavo, G. Bruno, P. Piraino and G. Bombieri, *J. Chem. Soc., Dalton Trans.*, 1983, 1813.

64. T. Boschi, P. Uguagliati and B.Crociani, *J. Organomet. Chem.*, 1971, **30**, 283.

65. K. Kawakami, T. Kaneshima and T. Tanaka, *J. Organomet. Chem.*, 1972, **34**, C21.

66. T. Kaneshima, K. Kawakami and T. Tanaka, *Inorg. Chem.*, 1974, **13**, 1974.

67. K. Kawakami, K. Take-Uchi and T. Tanaka, *Inorg. Chem.*, 1975, **14**, 877.

68. K. Kawakami, M-A Haga and T. Tanaka, *J. Organomet. Chem.*, 1973, **60**, 363.

69. W. H. Baddley, *J. Am. Chem. Soc.*, 1968, **90**, 3705.

70. W. H. Baddley, *J. Am. Chem. Soc.*, 1966, **88**, 4545.

71. C. T. Mortimer, J. L. McNaughton, J. Burgess, M. J. Hacker, R. D. W. Kemmit, M. I. Bruce, G. Shaw and F. G. A. Stone, *J. Organomet. Chem.*, 1973, **47**, 439.

72. A. J. Deeming and B. L. Shaw, *J. Chem. Soc.*, **A**, 1969, 1128.

73. G. Dolcetti, M. Nicolini, M. Giustiniani and U. Belluco, *J. Chem. Soc., A*, 1969, 1387.

74. J. A. McGinnety and J. A. Ibers, *J. Chem. Soc. Chem. Commun.*, 1968, 235.

75. L. Manojlovi-Muir and J. A. Ibers, *Diss. Farad. Soc.*, 1969, **47**, 84.

76. J. B. R. Dunn, R. Jacobs and C. J. Fritchie Jun., *J. Chem. Soc., Dalton Trans.*, 1972, 2007.

77. M-A Haga, K Kawakami and T. Tanaka, *Inorg. Chem.*, 1976, **8**, 1946.

78. D. Forster, *Inorg. Chem.*, 1972, **11**, 2270.

79. R. J. Fitzgerald and H-M. W. Lin, *Inorg. Chem.*, 1972, **31**, 2270.

80. G. La Monica, G. Navazio and P. Sandrini, *J. Organomet. Chem.*, 1971, **31**, 89.

81. D. N. Cash and R. O. Harris, *Can. J.. Chem.*, 1971, **49**, 3821.

82. C. K. Brown, D. Georgiou and G. Wilkinson, *J. Chem. Soc., A*, 1971, 3120.

83. M. I. Bruce, T. W. Hambley, M. R. Snow and A. G. Swincer, *J. Organomet. Chem.*, 1982, **235**, 105.

84. R. H. Walter and B. F. G. Johnson, *J. Chem. Soc., Dalton Trans.*, 1978, 381.

85. A. Davison and J. P. Solar, *J. Organomet. Chem.*, 1979, **166**, C13.

86. M. I. Bruce, T. W. Hambley, J. R. Rodgers, M. Snow and A. G. Swincer, *ibid.*, 1982, **226**, C1.

87. A. Maisonnat, J-J. Bunnet and R. Poilblanc, *Inorg. Chem.*, 1980, **19**, 3168.

88. B. Corain, M. Bressan and P. Rigo, *J. Organomet. Chem.*, 1971, **28**, 133.

89. B. Corain, L. De Nardo and G. Favero, *ibid.*, 1977, **125**, 105.

90. W. H. Baddley and L. M. Venazi, *Inorg. Chem.*, 1966, **5**, 33.

91. G. Bombieri, E. Forsellini, C. Panattoni, R. Gratziani, and G. Bandoli, *J. Chem. Soc., A*, 1970, 1313.

92. O. J. Scherer, R. Konrad, E. Guggolz and M. L. Ziegler, *Chem. Ber.*, 1983, **116**, 2676.

93. P. Uguagliati and W. H. Baddley, *J. Am. Chem. Soc.*, 1968, **90**, 5446.

94. C. T. Mortimer, M. Wilkinson and R. J. Puddephat, *J. Organomet. Chem.*, 1979, **165**, 269.

95. R. G. Goel and R. C. Srivastava, *Can. J. Chem.*, 1982, **61**, 1352.

96. W. H. Baddley, *Inorg. Chim. Acta Rev.*, 1968, **2**, 7.

97. M. F. Rettig and R. M. Wing, *Inorg. Chem.*, 1969, **8**, 2685.

98. R. Gross and W. Kaim, *Angew. Chem.*, 1987, **99**, 257.

99. S. D. Ittel, C. A. Tolman, P. J. Krusic, A. D. English, and J. P. Jesson, *Inorg. Chem.*, 1978, **17**, 3432.

100. F. G. Moers and J. P. Langhout, *Inorg. Nucl. Chem.*, 1977, **39**, 591.

101. S. I. Amer, T. P. Dasgupta, P. M. Henry, *Inorg. Chem.*, 1983, **22**, 1970.

102. A. L. Crumbliss and F. Basolo, *Inorg. Chem.*, 1971, **10**, 1676.

103. W. Beck, R. Schlodder and W. H. Lechler, *J. Organomet. Chem.*, 1973, **54**, 303.

104. B. L. Booth, C. A. M^{c}Auliffe, G. L. Stanley, *J. Chem. Soc., Dalton Trans.*, 1982, 535.

105. J. S. Ricci, J. A. Ibers, M. S. Fraser and W.H. Baddley, *J. Am. Chem. Soc.*, 1970, **92**, 3489.

106. J. S Ricci and J. A. Ibers, *J. Am. Chem. Soc.*, 1971, **93**, 2391.

107. S. R. Su, J. A. Hanna and A. Wojcicki, *J. Organomet. Chem.*, 1970, **21**, P21.

108. S. R. Su and A. Wojcicki, *ibid.*, 1971, **31**, C34.

109. S. R. Su and A. Wojcicki, *Inorg. Chim. Acta*, 1974, **8**, 55.

110. S. R. Su and A. Wojcicki, *Inorg. Chem.*, 1975, **14**, 89.

111. M. R. Churchill and S. W-Y. Chang, *Inorg. Chem.*, 1975, **14**, 98.

112. J. A. Hanna and A. Wojcicki, *Inorg. Chim. Acta*, 1974, **9**, 55.

113. N. Chaudhury, M. G. Kerke and R. J. Puddephat, *J. Organomet. Chem.*, 1974, **73**, C17.

114. S. Cenini, F. Porta, M. Pizzotti and G. La Monica, *J. Chem. Soc., Dalton Trans.*, 1984, 355.

115. S. R. Su and A. Wojcicki, *J. Organomet. Chem.*, 1971, **31**, C34.

116. M. R. Churchill and S. W-Y. Chang, *J. Am. Chem. Soc.*, 1973, **95**, 5931.

117. W. P. Giering and M. Rosenblum, *J. Am. Chem. Soc.*, 1971, **93**, 5299.

118. K. Broadley, N. G. Connelly, R. M. Mills, M. W. Whiteley and P. Woodward, *J. Chem. Soc., Dalton Trans.*, 1984, 683.

119. D. R. Robertson and T. A. Stephenson, *J. Organomet. Chem.*, 1976, **107**, C46.

120. D. M. Barlex and R. D. W. Kemmitt, *J. Chem. Soc., Dalton Trans.*, 1972, 1436.

121. M. I. Bruce, J. R. Rodgers, M. R. Snow and A. G. Swincer, *J. Chem. Soc., Chem. Commun.*, 1981, 271.

122. B. Loev and M. M. Goodman, *Chem. Ind.*, 1967, 2026.

123. B. D. Flockhart, C. Naccache, J. A. N. Scott, R. C. Pink, *J. Chem. Soc., Chem. Comm.*, 1965, 238.

124. B. D. Flockhart, I. R. Leith and R. C. Pink, *Trans. Faraday Soc.*, 1969, **65**, 542

125. F-M. Pan, J. C. Hemminger and S. Ushioda, *J. Phys. Chem.*, 1985, **89**, 862.

126. F. Figueras Roca, L. De Mourgues and Y. Trambouze, *J. Catalysis*, 1969, **14**, 107.

127. F. Figueras, A. Nohl, L. De Mourgues and Y. Trambouze, *Trans. Faraday Soc.*, 1971, **67**, 1155.

128. U. Mazur and K. W. Hipps, *J. Phys. Chem.*, 1982, **86**, 5105.

129. U. Mazur and K. W. Hipps, *ibid.*, 1984, **88**, 1555.

130. C. E. Looney and J. R. Downing, *J. Am. Chem. Soc.*, 1958, **80**, 2840.

131. F. A. Miller, O. Sala, P. Devlin, J. Overend, E. Lippert, W. Luder, H. Moser, and J. Varchim, *Spectrochim. Acta*, 1964, **20**, 1233.

132. P. Devlin, J. Overend and B. Crawford Jr., *ibid.*, 1964, **20**, 23. and A. Rosenberg and J.P.Devlin, *ibid.*, 1965, **21**, 1613.

133. T. Takenaka and S. Hayashi, *Bull. Chem. Soc. Jpn.*, 1964, **37**, 1216.

134. J. Stanley, D. Smith, B. Latimer and J. P. Devlin, *J. Phys. Chem.*, 1966, **70**, 2011.

135. J. C. Moore, D. Smith, Y. Youhne and J. P. Devlin, *ibid.*, 1971, **75**, 325.

136. M. S. Khatkale and J. P. Devlin, *ibid.*, 1979, **83**, 1636.

137. J. J. Hinkel and J. P. Devlin, *J. Chem. Phys.*, 1973, **58**, 4750.

138. E. E. Ferguson and F. A. Matsen, *J. Chem. Phys.*, 1958, **29**, 105

139. E. E. Ferguson and F. A. Matsen, *J. Am. Chem. Soc.*, 1960, **82**, 3268.

140. G. E. Coates and F. Glockling, in *"Organometallic Chemistry"*, H. Zeiss Ed., Reinold Publishing Corp., New York, 1960, p461.

141. R.B King and M. B. Bisnette, *Inorg. Chem.*, 1966, **5**, 300.

142. H. Bock and H. Dieck, *Chem. Ber.*, 1966, **99**, 1966.

143. M.F. Farona and N.J. Bremner, *J. Am. Chem. Soc.*, 1966, **88**, 3735.

144. R. A. Walton, *Quart. Rev. (London)*, 1965, **19**, 126.

145. K.F. Purcell and R.S. Drago, *J. Am. Chem. Soc.*, 1966, **88**, 919.

146. J. D. Owen and D. J. Cole-Hamilton, *J. Chem. Soc., Dalton Trans.*, 1974, 1867.

147. C. E. Anson, E. J. Ditzel, M. Fajardo, H. D. Holden, B. F. G. Johnson, J. Lewis, J. Puga and P. R. Raithby, *J. Chem. Soc., Dalton Trans.*, 1984, 2723.

148. B. F. G. Johnson, J. Lewis, W. J. H. Nelson, J. Puga, P. R. Raithby and K. H. Whitmire, *J. Chem. Soc., Dalton Trans.*, 1983, 1339.

149. K. Burgess, B. F. G. Johnson, J. Lewis and P. R. Raithby, *J. Chem. Soc., Dalton Trans.*, 1982, 2119.

150. Z. G. Soos, *Ann. Rev. Phys. Chem.*, 1974, **25**, 121.

Chapter 4

Electrochemical and spectroelectrochemical studies on $[M(S_2PR_2)_2(PPh_3)(tcne)]$ and $[\{Ru(S_2PR_2)_2(PPh_3)\}_2tcne]$.

4.1 Introduction.

Free tcne undergoes two, one-electron reductions at +0.20 and -1.18V vs SCE. The first reduction has been characterised as fully reversible.[1-6] *In situ* e.s.r. spectroscopic measurements have assigned this redox-step to be the one-electron reduction of tcne to form the radical anion, $tcne^{\cdot-}$. The second reduction has been found to be electrochemically quasi-reversible, although no detailed study of this process has been reported.[3]

Tcne has been studied spectroelectrochemically (as a function of electrochemical potential) by resonance Raman,[4] infrared,[3,5] and electronic spectroscopy.[3] The electrogenerated, or chemically synthesised, mono-anion was found to decompose in the presence of atmospheric oxygen.[3]

4.1.1 Redox studies of ligated tcne complexes.

The reported electrochemical studies of complexes containing σ-N co-ordinated tcne concern $[Ru(NH_3)_5(L)]^{2+}$ (L=tcne, fmn), $[\{Ru(NH_3)_5\}_nL]^{2n+}$ (L=tcne, n=4; fmn, n=2),[7] $[(Cp)Mn(CO)_2(L)]$ and $[\{(Cp)Mn(CO)_2\}_4(L)]$ (L=tcne, tcnq).[8]

The mononuclear tcne species, $[Ru(NH_3)_5(tcne)]^{2+}$, exhibits one oxidation (0.40V vs SCE) and one reduction (-0.10V vs SCE) in acetonitrile.[7] The reduction is assigned as tcne-based, and is shifted (by 0.3V) more negative of the first reduction of the free ligand.

No other reduction is reported. Acetonitrile solutions of $[Ru(NH_3)_5(tcne)]^{2+}$ are deep blue-green in colour with a $d\pi-\pi^*$ MLCT band (assigned as Ru^{II} to tcne) at 13,700cm^{-1} ($\varepsilon=7.6x10^3 cm^{-1}mole^{-1}dm^3$) with a shoulder at higher energy. The oxidised complex exhibits a band at 14,350cm^{-1} ($\varepsilon=3.6x10^3 cm^{-1}mole^{-1}dm^3$). The fmn adduct, $[Ru(NH_3)_5(fmn)]^{2+}$, exhibits no reductive behaviour and a MLCT band is observed at 21,450cm^{-1} ($\varepsilon=7.6x10^3 cm^{-1}mole^{-1}dm^3$).[7]

The tetranuclear complex, $[\{Ru(NH_3)_5\}_4tcne]^{8+}$, shows four metal-based oxidations and a single, tcne-based, reduction (-0.30V vs SCE). $[\{Ru(NH_3)_5\}_4tcne]^{8+}$ exhibits a MLCT band at 12,900cm^{-1} ($\varepsilon=2.0x10^4 cm^{-1}mole^{-1}dm^3$). No obvious inter-valence charge-transfer (IVCT) band is observed in the electronic absorption spectrum of the first oxidised product. This contrasts with the first oxidation product of $[\{Ru(NH_3)_5\}_2fmn]^{4+}$, which exhibits such a band at 10,250cm^{-1} ($\varepsilon=150 cm^{-1}mole^{-1}dm^3$). The authors suggest[7] that $[\{Ru(NH_3)_5\}_2fmn]^{5+}$ belongs to a class II weakly coupled system,[9] whereas, the analogous tcne mixed-valence system is strongly delocalised.

Recently, the manganese complexes $[(C_5R_5)Mn(CO)_2(L)]$ and $[\{(C_5R_5)Mn(CO)_2\}_4(L)]$ (L=tcne, tcnq; R=Me, H) have been reported.[8] These adducts are formed by electron transfer reactions, in which the cyanoalkene is formally reduced, and the manganese centre oxidised i.e. the product can be formulated as $[(Cp)Mn(II)(CO)_2(tcne^-)]$. The mono- and tetra-nuclear tcne complexes exhibit one

reduction which is shifted (0.2-0.4V depending on the substituents on the cyclopentadiene ring and the number of manganese centres to which tcne is co-ordinated) to more negative potential than free tcne. Charge-transfer bands at 12,000cm^{-1} are assigned as LMCT from $tcne^{-}$ to Mn(II). All of the manganese complexes are, however, e.s.r. silent, and solutions of both $[(Cp)Mn(CO)_2(tcne)]$ and $[\{(Cp)Mn(CO)_2\}_4tcne]$ give sharp n.m.r. signals. This is believed the result of extensive coupling between the unpaired electrons of $tcne^{-}$ and Mn(II).[8]

All the electrochemical studies of free tcne, and its N-bound transition-metal complexes have, to date, been determined in strongly co-ordinating solvents. The complexes, $[M(S_2PR_2)_2(PPh_3)(tcne)]$ (M=Ru, Os; R=Me, Ph, OEt), however, decompose in co-ordinating solvents. Therefore, the electrochemistry of these complexes was examined in methylene chloride. Consequently, it was necessary to examine the redox behaviour of free tcne in this solvent.

4.2 Redox studies on tcne in methylene chloride.

The cyclic voltammogram of tcne, exhibits two reductions (as determined by stirred d.c. voltammetry) at +0.40V and -0.70V ‡ and is shown in Figure 4.1.

---

‡The second reduction of tcne is quasi-reversible and therefore, the reduction potential given is the value of E_{pf} at a scan rate of 100mVs^{-1} at 288K

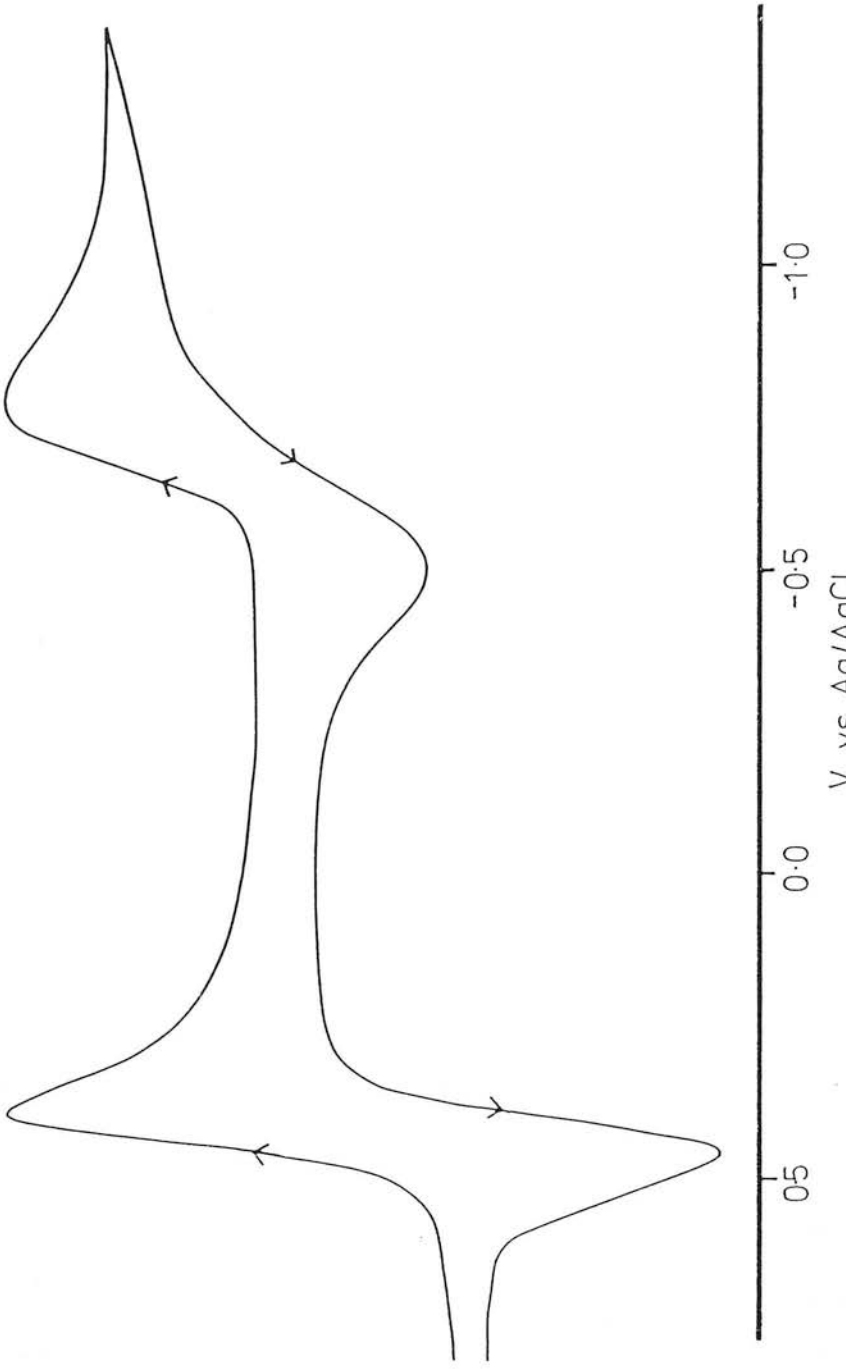

Figure 4.1: The cyclic voltamogram of tcne in methylene chloride solution at 288 K ($v=100\ mVs^{-1}$).

The first reduction is fully reversible, while the second, as reported earlier,[3] is electrochemically quasi-reversible, that is, the separation (ΔE_p) of the forward peak potential (E_{pf}) and the return peak potential (E_{pr}) is greater than 59mV at 298K (and dependent on scan rate). However, the ratio of the forward wave current maximum (i_{pf}), to the return wave current maximum (i_{pr}), is equal to 1.00 (see Table 4.1). An earlier study of the second reduction of tcne in acetonitrile observed the large peak-peak separation, but the current ratio was much greater than 1.00.[3]

$v/\ mVsec^{-1}$	$\Delta E(E_{pf}-E_{pr})/mV$	$i_{pf}/i_{pr}-$
16	170	0.98
25	185	1.00
36	205	1.13
49	220	0.98
64	240	0.99
81	255	1.00
100	270	0.97
121	280	0.96
144	310	0.97
400	420	0.95

Table 4.1: ΔE_p and i_{pf}/i_{pr} as a function of v for $tcne^{1-/2-}$.

The reduction processes in methylene chloride were characterised electrochemicaly by altering the scan rate (v) and recording i (the current at E_p) and ΔE_p (E_{pf}-E_{pr}) as a function of v (see Figure 4.2) Close examination of the second reduction shows that the peak separation (as expected for a quasi-reversible process) varies greatly with scan rate (see Table 4.1), whereas the peak separation for the first reduction shows only a small variation with scan speed which can be related to residual uncompensated iR drop.

In Figure 4.3 the limiting current (i_l) is plotted versus $[v]^{1/2}$. It is immediately obvious that whereas the graph is non-linear for the second reduction, the first reduction shows a linear relationship. This result, taken in conjunction with the above mentioned current ratio observation, implies that on the time scale examined, the quasi-reversibility of the $tcne^{1-/2-}$ couple is indicative of sluggish electrode electron-transfer which suggests that the doubly reduced tcne molecule undergoes a geometrical change[‡].

The long term stability of the first reduction product, $tcne^{-}$, in methylene chloride, was evaluated using controlled potential reversal coulometry in bulk solution. The radical anion is produced in a 100% quantum

---

[‡] A distortion from planarity has been suggested for $tcne^{2-}$ on the basis of infrared spectroscopy.[3]

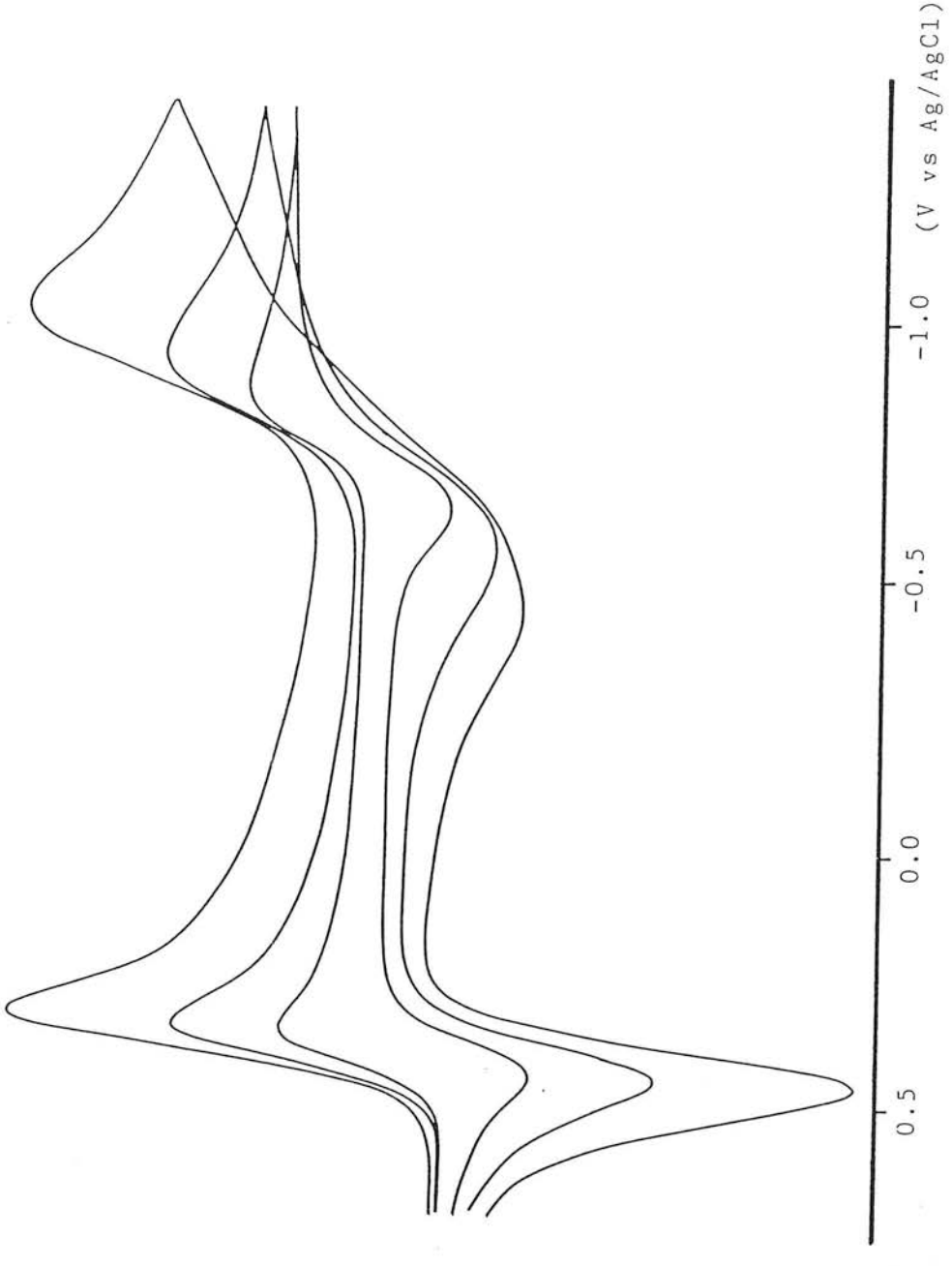

Figure 4.2: The cyclic voltammogram of tcne in methylene chloride solution at varying scan rate; (a)v=16 mVs^{-1},(b)v=100 $mVs^{1}$and (c)v=225 mVs^{1}(T=288 K).

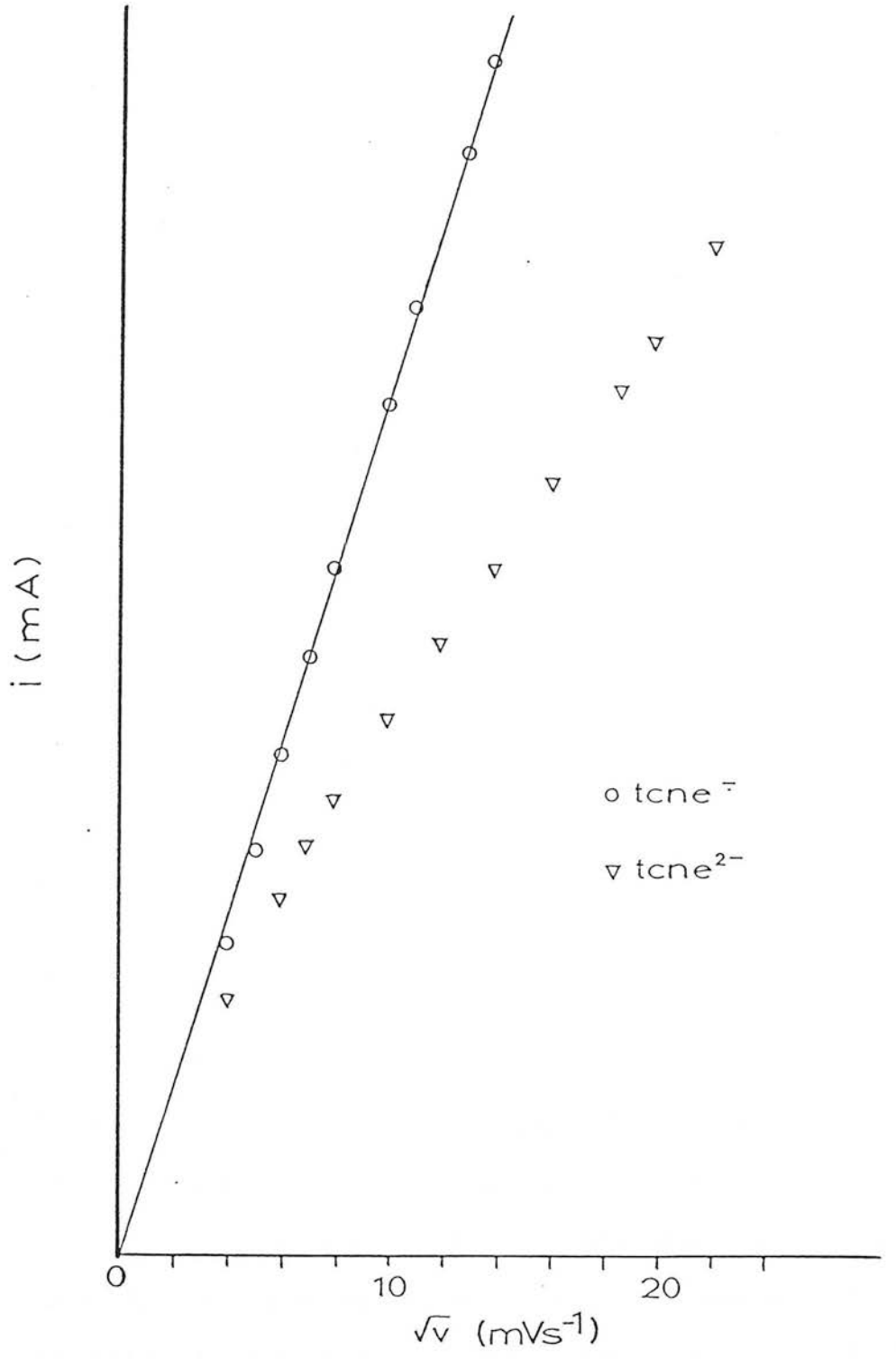

Figure 4.3: Graph of v vs i_p for the $tcne^{0/-}$ and $tcne^{-/2-}$ couples at 288K in methylene chloride.

yield but is, however, susceptible to atmospheric oxygen. Attempts to electrogenerate the second reduction product have proved unsuccessful. Examination of the oxidative range, showed no sign of any oxidation product of tcne within the potential range of 0.0 to +2.5V (in methylene chloride).

4.3 Spectroelectrochemical studies of tcne.

As spectroelectrochemical studies of the complexes, $[M(S_2PR_2)_2(PPh_3)(tcne)]$, were undertaken, it was useful to examine the electronic spectrum of the various oxidation states of tcne in methylene chloride. Free tcne shows a $\pi \longrightarrow \pi^*$ transition in the ultraviolet region at 36,100cm^{-1}. The spectrum of the first reduction product, $tcne^-$, is shown in Figure 4.4. Attempts to generate the di-anion of tcne were unsuccessful, even at 223K.

4.4 Redox studies of $[M(S_2PR_2)_2(PPh_3)(tcne)]$.

Infrared spectral data for $[M(S_2PR_2)_2(PPh_3)(tcne)]$ (M=Ru, Os; R=Me, OEt, Ph) suggest that electron transfer to the co-ordinated tcne moiety is appreciable (see Chapter 3.7.3). For free tcne and its anions, Devlin and co-workers have proposed that the degree of electron transfer to the tcne ligand is related to the position of the $\nu_{C=C}$ stretching vibration.[10] Similarly, Aihara has proposed[11] that the frequency of this vibration is related to the π-bond order of the C=C bond. On this basis, the tcne moiety in $[M(S_2PR_2)_2(PPh_3)(tcne)]$ has a π-bond order

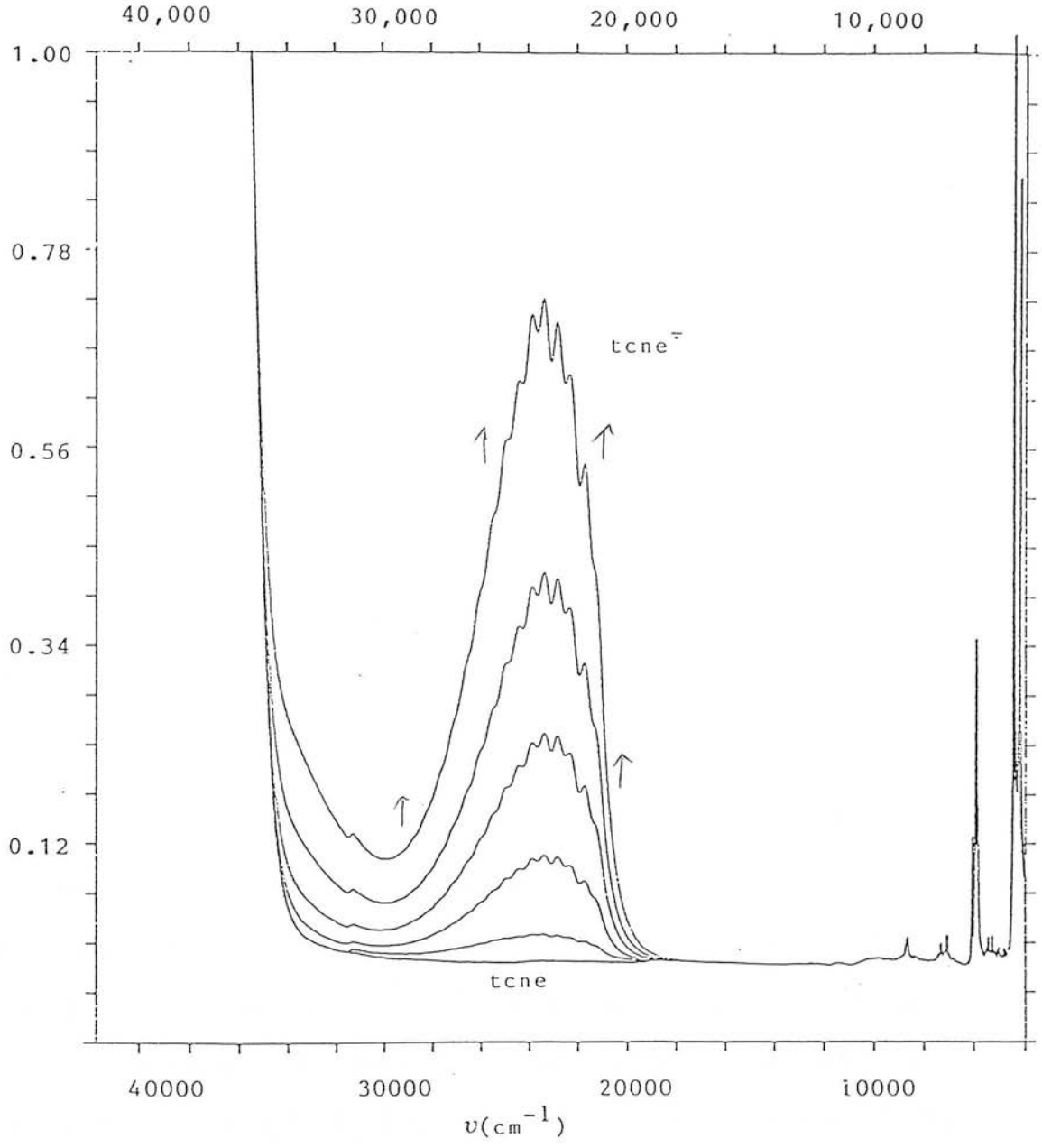

Figure 4.4: The electronic absorption spectrum of tcne and $tcne^{\bullet-}$ in methylene chloride solution. The radical anion was electrogenerated *in situ* at 288 K.

of approximately 0.6. Earlier reports on complexes of N-bound tcne, however, have interpreted the large decrease in $\nu_{C=C}$ as being evidence of complete electron transfer from the metal centre to the ligated tcne.[8,12-14] Thus, these complexes can be regarded formally as $tcne^-$ co-ordinated to an oxidised metal centre.

As discussed in Chapter 3.12, the transfer of an electron preceeding co-ordination is implied in the reaction of $[Os(II)(S_2P\{OEt\}_2)_2(PPh_3)_2]$ with tcne to yield the intermediate, $[Os^{III}(S_2P\{OEt\}_2)_2(PPh_3)]^+[tcne]^-$, before forming $[Os(S_2P\{OEt\}_2(PPh_3)(tcne)]$. In order to investigate the exact electronic nature of the adducts, $[M(S_2PR_2)_2(PPh_3)(tcne)]$, their electrochemical and spectroelectrochemical properties were examined.

4.4.1 Reductive behaviour.

Two reductions are observed for all complexes of type, $[M(S_2PR_2)_2(PPh_3)(tcne)]$, (M=Ru, Os; R=Me, OEt, Ph). A typical cyclic voltammogram of the reductive range of these species is shown in Figure 4.5 and the relevant potentials are shown in Table 4.2. A similarity between the electrochemical behaviour of free tcne and the complexes, $[M(S_2PR_2)_2(PPh_3)(tcne)]$, is immediately apparent; both exhibit two reductions the first being fully reversible and the second electrochemically quasi-reversible. The first reduction has been shown to be a one-electron process by coulometry (at temperatures

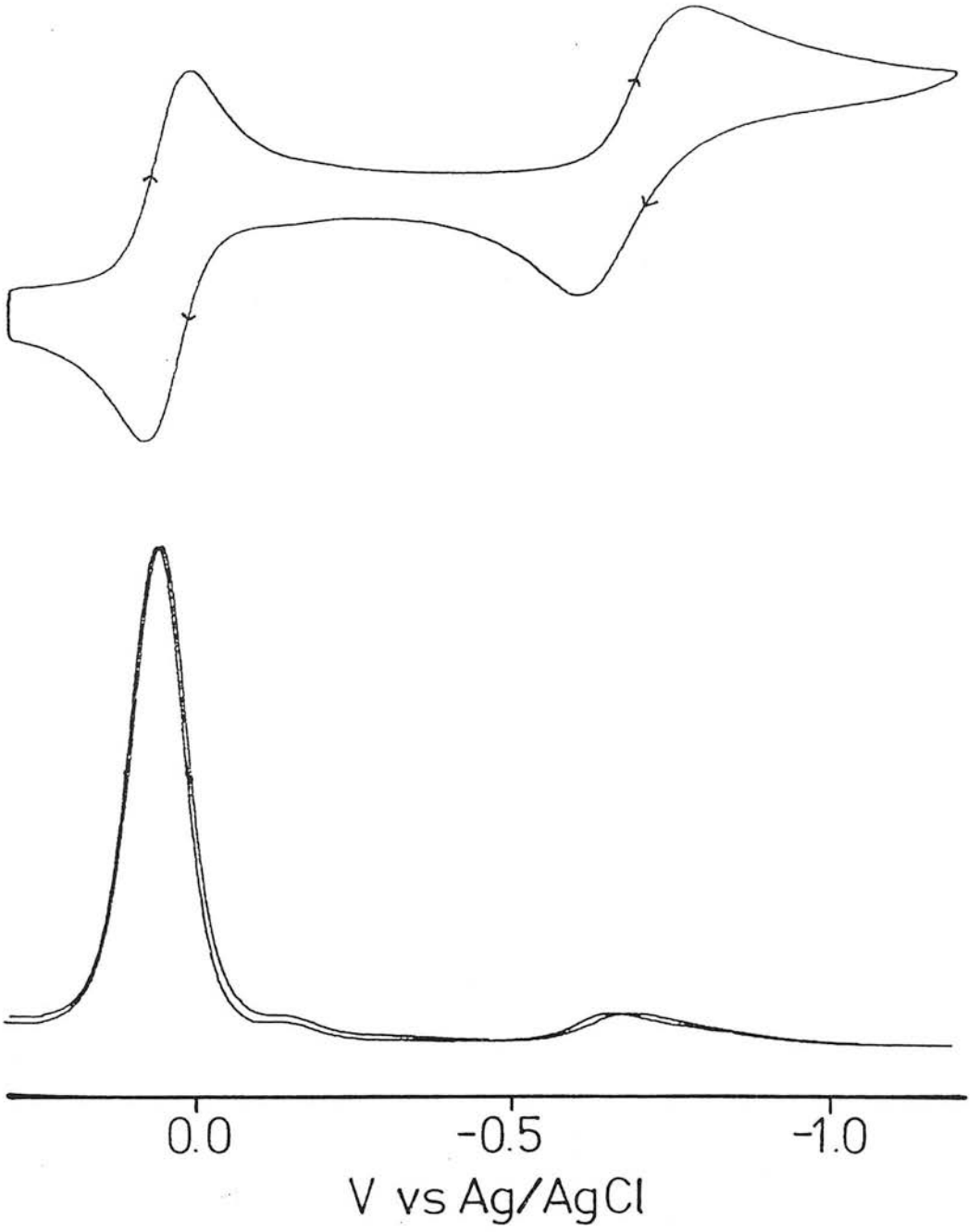

Figure 4.5: The cyclic voltammogram and A.C. voltammogram of $[Ru(S_2PMe_2)_2(PPh_2)(tcne)]$ in methylene chloride at 288 K. The two one-electron reductions are characteristic of this type of complex.

Table 4.2: Redox Potentials for $[M(S_2PR_2)_2(PPh_3)(tcne)]$[a]

M	R	$E_{\frac{1}{2}}(0/+1)$/ V[b]	$E_{\frac{1}{2}}(+1/+2)$/ V[c]	$E_{\frac{1}{2}}(0/-1)$/ V[d]	$E_{\frac{1}{2}}(-1/-2)$/ V[e]
Ru	Me	+0.95	+1.40	+0.06	-0.74
Ru	Ph	+1.00	+1.56	+0.08	-0.78
Ru	OEt	+1.05	+1.62	+0.15	-1.05
Os	Me	+0.90	+1.26	-0.18	-0.79
Os	Ph	+0.94	+1.36	-0.14	-0.74
Os	OEt	+1.01	+1.47	-0.04	-0.72

a- Measured at 288K in methylene chloride solvent, 0.5 M $TBA^+BF_4^-$. All potentials vs Ag/AgCl reference electrode at which the ferrocene|ferrocinium couple is observed at 0.56V

b- Potential determined by A.C. Voltammetry.

c- Irreversible oxidation. Potential given determined by measuring the difference between i_{pf} for both oxidations and adding this value to the potential of the first oxidation.

d- Determined by A.C. Voltammetry.

e- Quasi-reversible wave. Potential determined relative to the first reduction as in (c).

below 253K).‡ The potential at which this reduction occurs is dependent on both the organic substituents of the dithiolate ligand, and on the central metal. For all the adducts, $[M(S_2PR_2)_2(PPh_3)(tcne)]$, the first reduction is shifted (by *ca.* 0.4V) to more negative potential than that of free tcne (which is reduced at +0.4V).

The second reduction for $[M(S_2PR_2)_2(PPh_3)(tcne)]$ is quasi-reversible in nature. The separation (ΔE_p) between E_{pf} and E_{pr}, measured at the same temperature (288K) and scan rate ($100mVs^{-1}$), varies from one complex to another, being 80mv for $[Os(S_2PPh_2)_2(PPh_3)(tcne)]$ and 230mv for $[Ru(S_2PPh_2)_2(PPh_3)(tcne)]$ (see Table 4.3).

M	R	$\Delta E(E_{pf}-E_{pr})/mV$
Ru	Me	180
Ru	Ph	230
Ru	OEt	200
Os	Me	140
Os	Ph	80
Os	OEt	160

Table 4.3: ΔE_p for $[M(S_2PR_2)_2(PPh_3)(tcne)]^{-1/-2}$

‡At room temperature, reduction of $[Ru(S_2PR_2)_2(PPh_3)(tcne)]$ (R=Me, Ph, OEt) affords $[\{Ru(S_2PR_2)_2(PPh_3)\}_2tcne]$ and $tcne^-$.

Decreasing the temperature leads to an appreciable broadening of this wave. The product of the second reduction is unstable at room temperature for all $[M(S_2PR_2)_2(PPh_3)(tcne)]$. The di-anion can be reversibly generated at 238K only for $[Os(S_2PPh_2)_2(PPh_3)(tcne)]$; coulometric studies at 238K have shown the second reduction to be a one-electron process.

The reductions are all ligand-based affording co-ordinated $tcne^{-}$, as will be discussed below. The most striking feature is the shift of the tcne reductions to more negative potential upon ligation. This is also observed for $[Ru(NH_3)_5(tcne)]^{2+}$ and $[Mn(CO)_2(C_5R_5)(tcne)]$ (R=H, Me).[7,8] Previous studies in this laboratory on the complexes, $[M(chel)_3]^{n+}$ (chel=bipy, phen; M=Ru, n=2; M=Ir, n=3), have shown that ligand-based reductions are generally shifted to more positive potentials on co-ordination to a metal centre.[15] This positive shift has been reported as a general trend for ligand-based reductions when co-ordinated to a transition metal.[16] The negative shift in reduction potential of co-ordinated tcne may result from a geometrical change (the symmetry of the tcne moiety is altered from D_{2h} to a local symmetry of C_s on co-ordination) which may lead to a consequent rise in the energy of the LUMO of tcne. Alternatively, this negative shift may reflect a large degree of back donation from the metal centre to the ligated tcne moiety.

Back donation from the metal $d\pi$ orbitals into the LUMO of tcne will have the effect of increasing the electron density on the ligand. As a result addition of an electron to the co-ordinated tcne moiety will become more difficult, and this will manifest itself in a negative potential shift for this reduction. The extent of this shift will depend on the π-donor capacity of the metal. The reduction of the $[Os(S_2PR_2)_2(PPh_3)(tcne)]$ complexes is more negative than the analogous $[Ru(S_2PR_2)_2(PPh_3)(tcne)]$ species (see Table 4.2). This observation is consistent with Os^{II} being a better π-donor than Ru^{II}. A detailed discussion of the electronic nature of these complexes will be made in Chapter 4.5.

The reductive behaviour of these complexes is also dependent on the type of substituent on the dithio-acid co-ordinated to the metal. Changing this ligand from $^-S_2PMe_2$ to $^-S_2PPh_2$ results in a small change in the observed redox potentials (see Table 4.2). However, if $^-S_2P\{OEt\}_2$ is the chelating ligand, then larger shifts (*ca.* 100mV) to more positive potentials result.

4.4.2 Oxidative behaviour.

The complexes, $[M(S_2PR_2)_2(PPh_3)(tcne)]$ (M=Ru, Os; R=Me, Ph, OEt), exhibit two oxidations, the reversibility of these processes varying with the metal type. For the ruthenium species the first oxidation is irreversible at room temperature, with concomittant daughter product

formation observed electrochemically by new voltammetric waves 0.5V more negative than the parent oxidation waves (see Figure 4.6a). At this temperature a second irreversible oxidation is observed shifted by +0.2V more positive of the first oxidation (see Figure 4.6a). On cooling to temperature below 253K, the primary oxidation of $[Ru(S_2PR_2)_2(PPh_3)(tcne)]$ (R=Me, Ph, OEt) becomes quasi-reversible and a second irreversible oxidation is now observed at 0.5V more positive of the first oxidation; the second oxidation observed at room temperature disappears on cooling (see Figure 4.6b). This implies that the second oxidation observed at room temperature is also a daughter product of the initial oxidation process. The osmium analogues are more stable, the first oxidation being quasi-reversible at room temperature. Only one daughter product is observed at room temperature, or at temperatures down to 223K (see Figure 4.7). The return wave of this daughter species is observed 0.5V more negative than the first oxidation. A second irreversible oxidation is observed at potentials 0.5V more positive of the first oxidation. Attempts to bulk electrogenerate the initial oxidation products of $[M(S_2PR_2)_2(PPh_3)(tcne)]$, even at 223K, have proved unsuccessful.

The strong electron withdrawing effect of tcne is reflected in the large positive shift of the first oxidation (assuming it is metal-based) of the adducts,

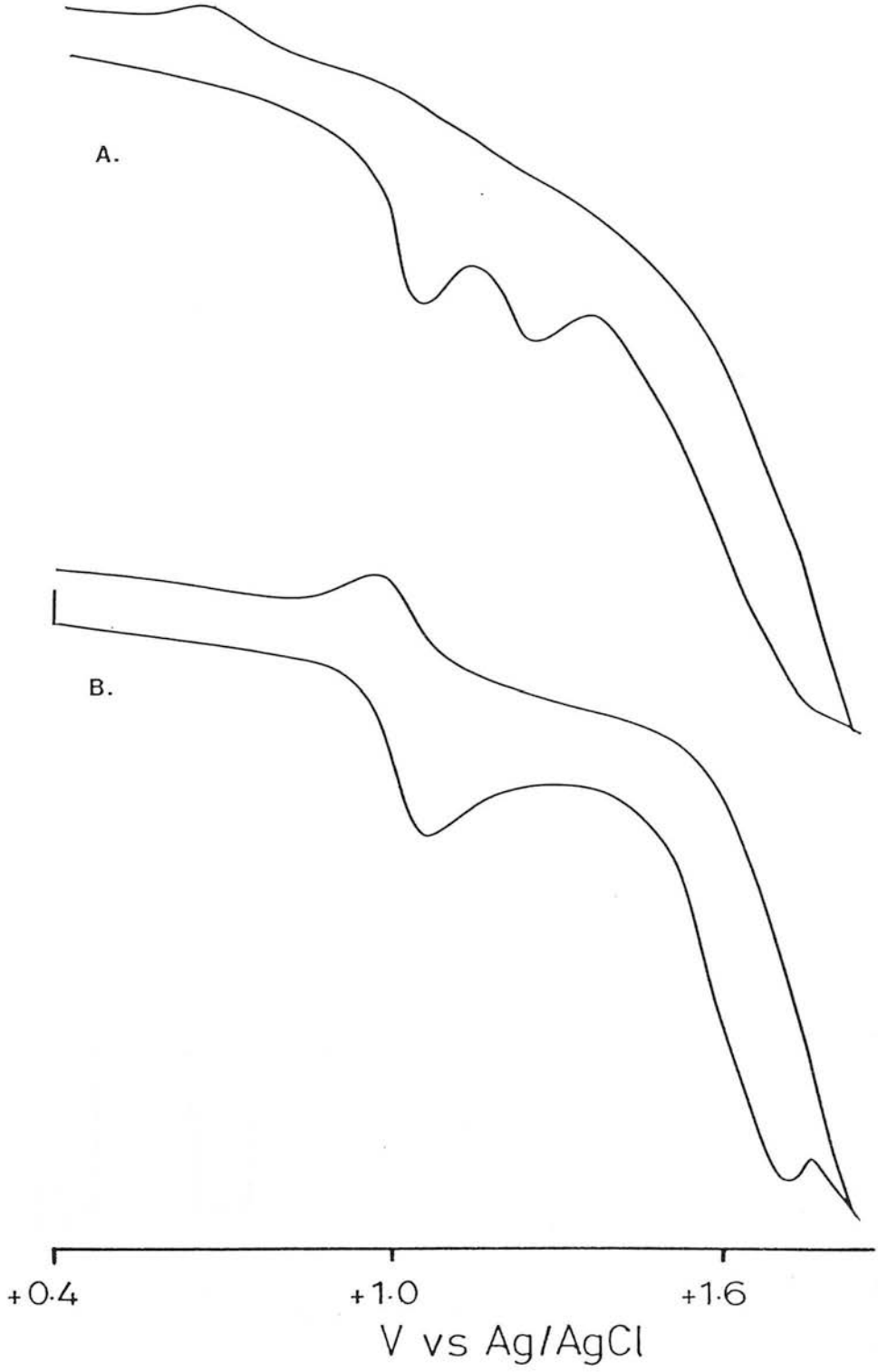

Figure 4.6: The cyclic voltammogram of $[Ru(S_2PPh_2)_2(PPh_3)(tcne)]$ in methylene chloride at (a) 288K and (b) 253K.

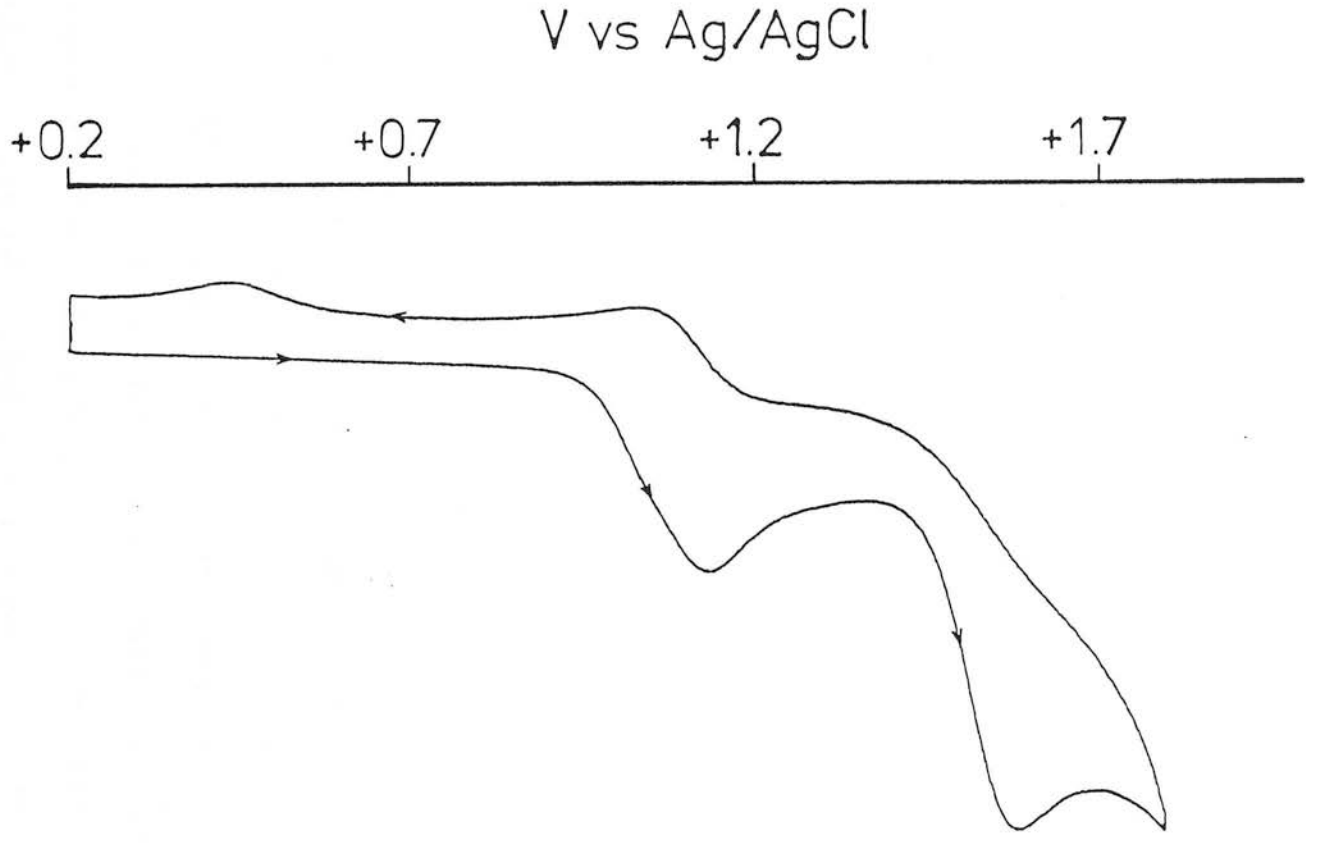

Figure 4.7: The cyclic voltammogram of $[Os(S_2PPh_2)_2(PPh_3)(tcne)]$ in methylene chloride at 288 K.

$[M(S_2PR_2)_2(PPh_3)(tcne)]$, relative to the parent $[M(S_2PR_2)_2(PPh_3)_2]$ species. Thus, replacing one phosphine ligand by tcne results in a 500-700mV positive shift in the first oxidation.

Interestingly, the potential of the first oxidation is independent of both ligand and metal. Thus, the $M^{II/III}$ couple for $[M(S_2PR_2)_2(PPh_3)_2]$ is 200mV more positive (harder to oxidise) for M=Ru than M=Os, whereas in the complexes, $[M(S_2PR_2)_2(PPh_3)(tcne)]$, the difference is only 5mV. Similarly, the first oxidation potentials of $[M(S_2PR_2)_2(PPh_3)(tcne)]$ exhibit a 10mV spread for all $^-S_2PR_2$ (R=Me, Ph, OEt) compared with a 120mV difference between $^-S_2P\{OEt\}_2$ and $^-S_2PR_2$ (R=Me, Ph) in the parent $[M(S_2PR_2)_2(PPh_3)_2]$ complex.

4.5 The electronic spectra of $[M(S_2PR_2)_2(PPh_3)(tcne)]$.

The complexes $[M(S_2PR_2)_2(PPh_3)(tcne)]$ (M=Ru, Os; R=Me, Ph, OEt) are strongly coloured. The electronic absorption spectrum of these species exhibits an intense CT band ($\varepsilon \approx 10^5 cm^{-1}mole^{-1}dm^3$) at low-energy between 13,000 and 11,000cm^{-1} (see Figure 4.8 and Table 4.4). This region of the electronic absorption spectrum is optically transparent for $[Ru(S_2PR_2)_3]^{n+}$ (R=Ph, OEt; n=0, +1, -1) and $[M(S_2PR_2)_2(PPh_3)_2]^{n+}$ (M=Ru, Os; R=Me, Ph, OEt; n=0, +1). Similar absorption bands are observed for the complexes, $[(Cp)Mn(CO)_2tcne]$ and $[Ru(NH_3)_5(tcne)]^{2+}$, and these have been assigned to charge-transfer processes between the

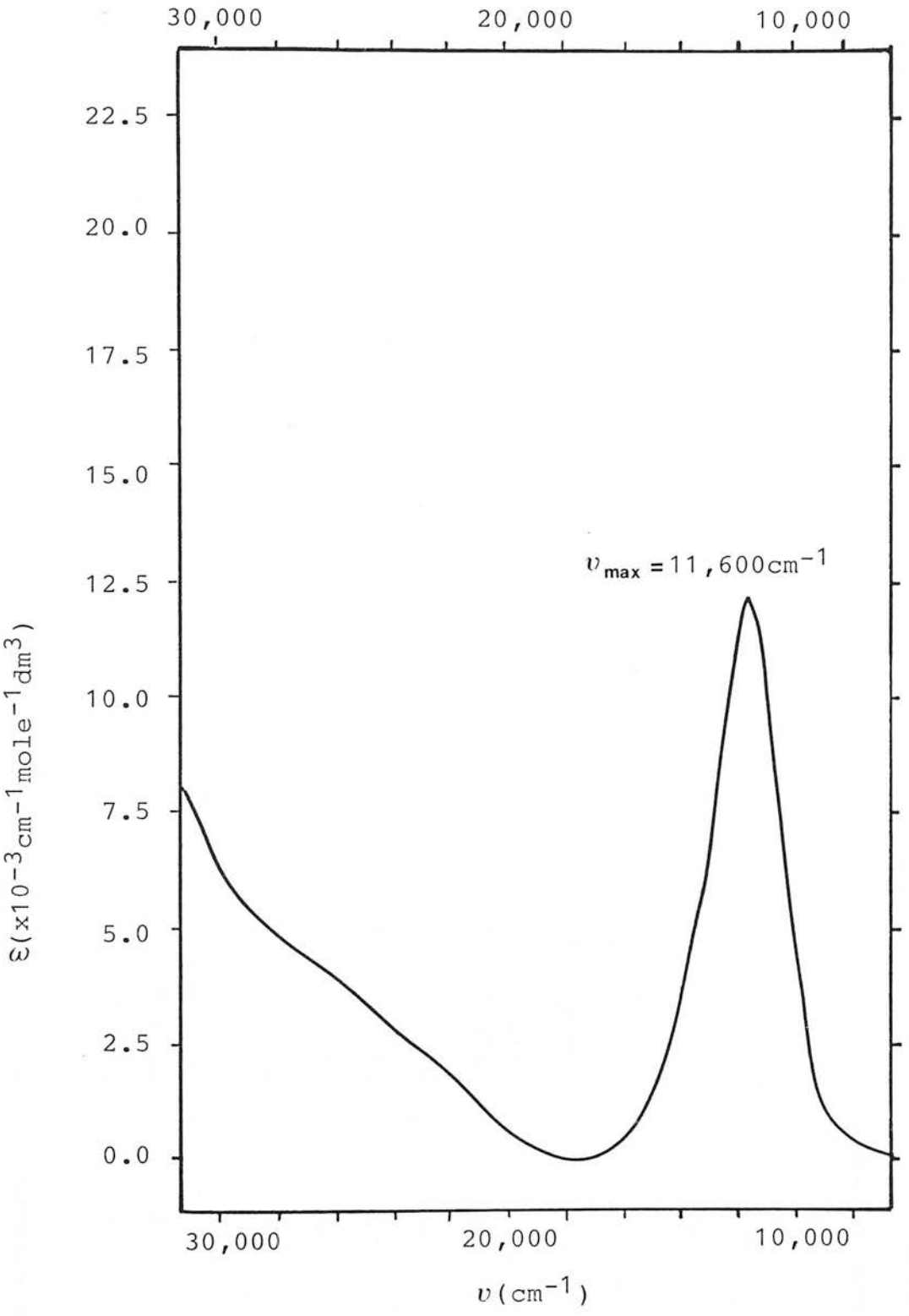

Figure 4.8: The electronic absorption spectrum of $[Ru(S_2PMe_2)_2(PPh_3)(tcne)]$ in methylene cloride at 288K.

Table 4.4: Electronic spectral data for $[M(S_2PR_2)_2(PPh_3)(tcne)]^n$

M	R	n	υ MLCT/cm^{-1} (a)	$\upsilon(\Pi^* \longrightarrow \Pi^{**})$/cm^{-1} (b)	υ(other)/cm^{-1}
Ru	Me	0	11,600 (12.5)(c)	-	-
Ru	Ph	0	11,400 (14.0)	-	-
Ru	Ph	-1	13,500 (4.0)	23,630 (4.1)	-
Ru	OEt	0	11,800 (11.4)	-	37,000 (14.8)
Ru	OEt	-1	14,200 (3.1)	23,900 (2.8)	38,250 (18.6)
Os	Me	0	13,700 (19.2)	-	-
Os	Me	-1	9,800 (4.2) 13,100 (5.1)	24,950 (3.6)	-
Os	Ph	0	13,600 (24.3)	-	-
Os	Ph	-1	10,150 (5.2) 13,350 (5.7)	24,800 (7.9)	-
Os	OEt	0	13,800 (17.2)	-	33,750 (7.0)
Os	OEt	-1	11,000 (3.9) 13,850 (5.4)	24,950 (4.3)	36,700 (9.4)

(a) Metal to tcne CT band; for M=Os, n=-1 two bands of equal intensity are observed.

(b) The transition assigned to the $\Pi^* \longrightarrow \Pi^{**}$ transition of co-ordinated tcne .

(c) Values in brackets represent $\epsilon \times 10^{-3}$ $cm^{-1}mole^{-1}dm^3$.

metal and co-ordinated tcne.[7,8] In line with this (and from the spectroelectrochemical studies of Chapter 4.6) the low-energy absorptions of $[M(S_2PR_2)_2(PPh_3)(tcne)]$, are also assigned as charge-transfer processes from the metal centre to tcne. For all $[Os(S_2PR_2)_2(PPh_3)(tcne)]$ a second band, of lesser intensity, is observed at lower energy and this is assigned to a triplet state.

The electronic transition between the metal and tcne can be modelled in two extreme forms. The first simple model (Figure 4.9a) shows a transition ($\nu 1$) between a donor level (the metal $d\pi$ orbital) and an acceptor orbital (the π^* LUMO of tcne) which are energetically separated (E1) so as to prevent a large degree of overlap between the two. The transition ($\nu 1$) can therefore be regarded, at least formally, as from a purely metal-based orbital to a purely tcne-based orbital.

In the second model the relative energies (and symmetry) of the HOMO and LUMO are such that the orbitals can effectively overlap and form molecular orbitals (see Figure 4.9b). This overlap would raise and lower the energy of the HOMO and LUMO respectively. The observed transition ($\nu 2$) would occur at an energy greater than the difference between the pure metal and pure ligand orbitals (E2).

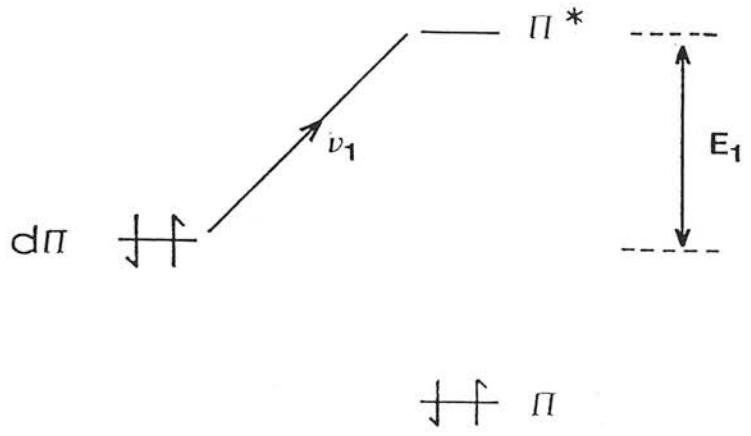

Metal HOMO tcne

Figure 4.9a:

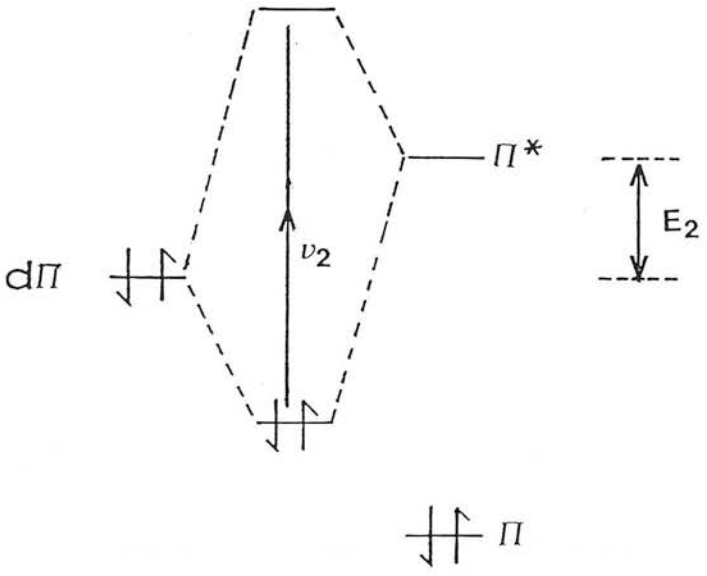

Metal HOMO tcne

Figure 4.9b:

$$E_1 > E_2 \; ; \; \nu_1 < \nu_2$$

Figure 4.9: Proposed electronic structure responsible for the low energy MLCT bands in $[M(S_2PR_2)(PPh_3)(tcne)]$.

From the simple model, assuming that the acceptor level of the cyanoalkene to be the same for analogous ruthenium and osmium $[M(S_2PR_2)_2(PPh_3)(tcne)]$ complexes, the energy of the MLCT band would lie at higher energies for the ruthenium complexes than for the osmium complexes, since the 5*d* orbitals of the osmium are at higher energy than the ruthenium 4*d* orbitals. The electronic spectral data for these complexes is shown in Table 4.4 . It is obvious from these results that the MLCT band invariably lies at higher energies for the osmium complexes. This observation implies that the second model provides a better interpretation for the osmium species i.e. the energies of the osmium $d\pi$ orbitals and the π^* LUMO of tcne permit appreciable mixing of the orbitals to occur. The corresponding orbitals in the ruthenium complexes will also mix, but the electronic spectral data suggest that the extent of this mixing is less than in the analogous osmium complexes.

4.6 Spectroelectrochemical studies.

The relevant data are summarised in Table 4.4 and Figures 4.10-4.14. Spectroelectrochemical studies on $[M(S_2PR_2)_2(PPh_3)(tcne)]$ (M=Ru, Os; R=Me, Ph, OEt) were carried out in methylene chloride.

The electronic absorption spectra of the adducts, $[Ru(S_2PPh_2)_2(PPh_3)(tcne)]$ and $[Ru(S_2PPh_2)_2(PPh_3)(tcne)]^-$,

are shown in Figures 4.10a and 4.10b respectively. On reducing the complex at an electrogeneration potential of -0.15V at 213K, the CT band, present in the neutral molecule at 11,500cm^{-1} (ε=14,000$cm^{-1}mole^{-1}dm^3$), collapses as a new band appears at 13,500cm^{-1} (ε=4,000$cm^{-1}mole^{-1}dm^3$). A further absorption is observed to grow at 23,630cm^{-1} (ε=4,100$cm^{-1}mole^{-1}dm^3$). The spectrum of the neutral complex can be regenerated in total upon reversing the applied potential to its initial value. Isosbestic points are observed at 13,800, 19,500, 22,200, and 24,900cm^{-1}, implying a simple one-to-one conversion of starting material to final complex.

Similar electronic spectra are obtained upon electrogeneration of $[Os(S_2PPh_2)_2(PPh_3)(tcne)]^-$ at -0.35V and 233K (see Figure 4.11). Once again the low-energy CT band (13,500cm^{-1}, ε=24,250$cm^{-1}mole^{-1}dm^3$), and the related triplet collapse. However, this time the new band appears at slightly lower energy. The electronic spectrum of the anion exhibits a double band with maxima at 10,150cm^{-1} (ε=5,200$cm^{-1}mole^{-1}dm^3$), and 13,350cm^{-1} (ε=5200$cm^{-1}mole^{-1}dm^3$). A further band is also observed to grow at 24,800cm^{-1} (ε=7,950$cm^{-1}mole^{-1}dm^3$). Isosbestic points are present at 8,600, 11,800, 19,000, 23,000, 24,000 29,300, 31,400 and 37,000cm^{-1}. The spectrum of the starting material can be fully regenerated by returning the potential to 0.0V.

Unlike all other complexes of this type, the second reduction product of $[Os(S_2PPh_2)_2(PPh_3)(tcne)]$ is stable

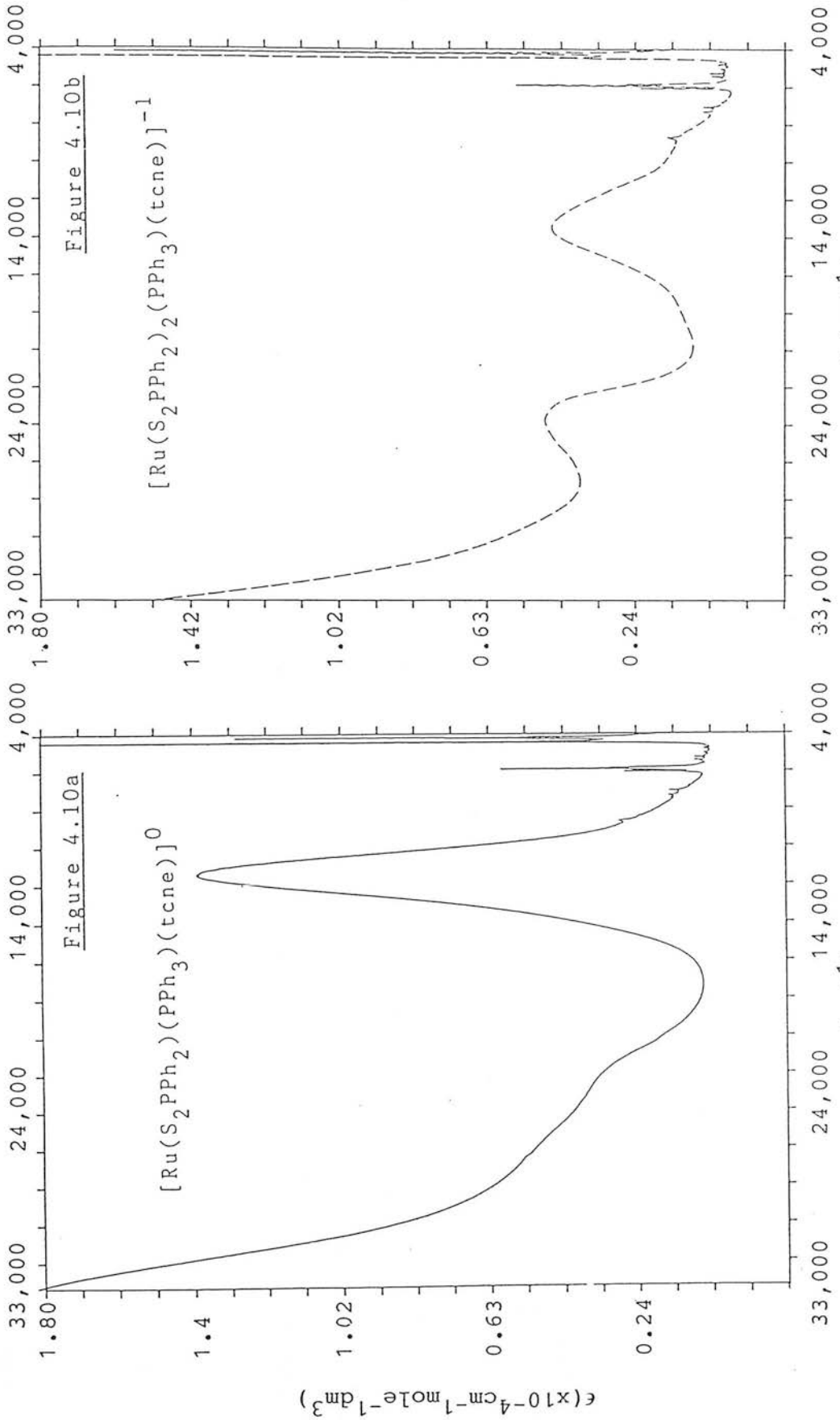

Figure 4.10: The electronic absorption spectrum of $[Ru(S_2PPh_2)_2(PPh_3)(tcne)]^{0/-1}$ in methylene chloride at 228 K.

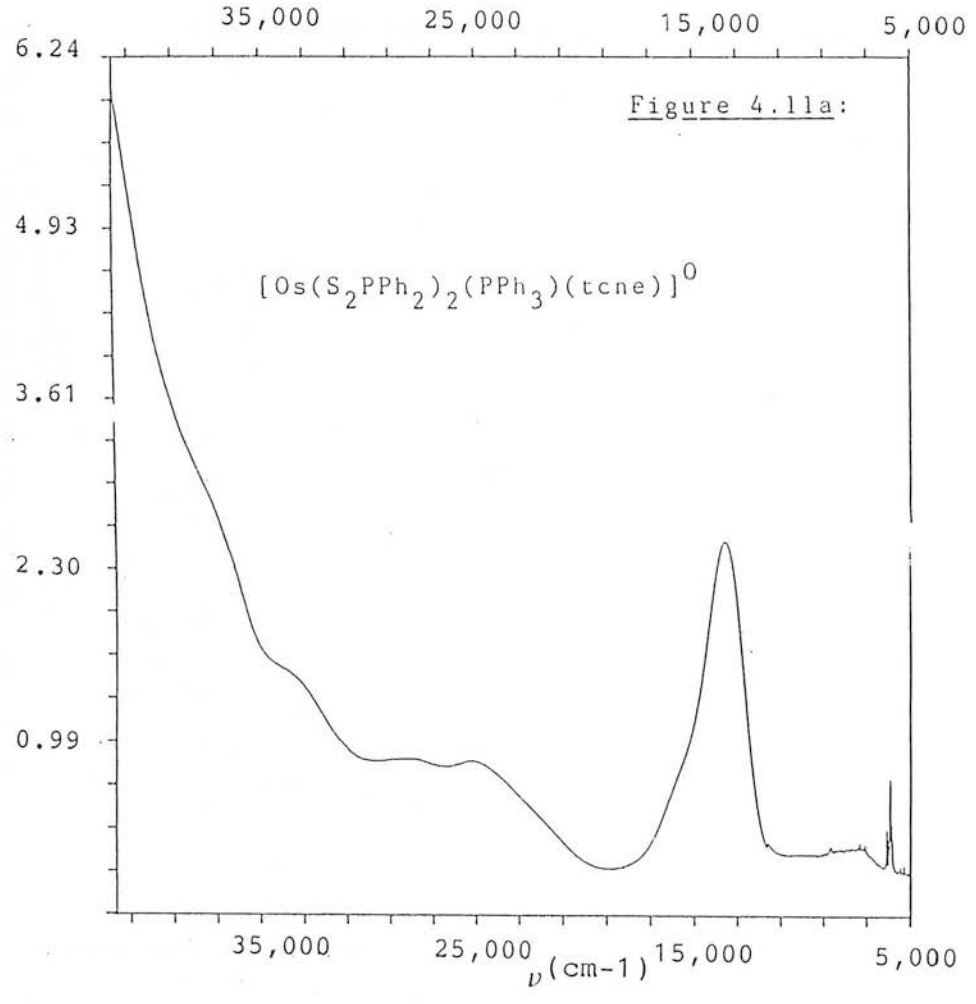

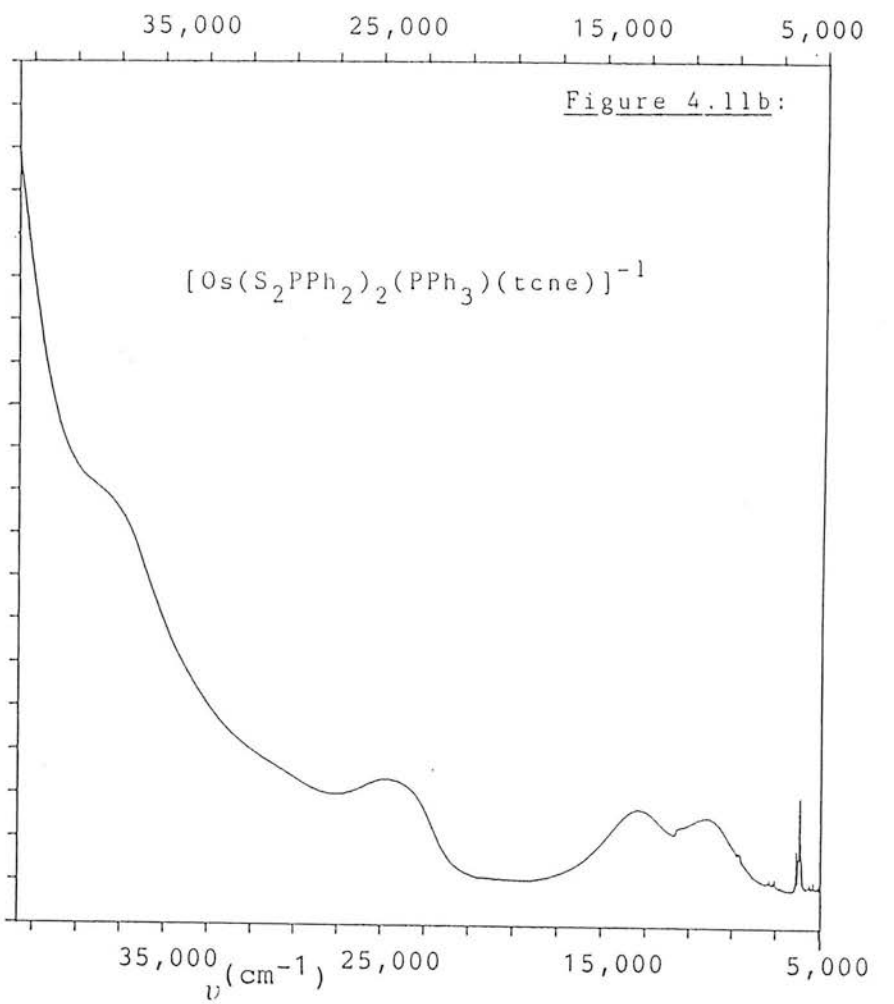

Figure 4.11: The electronic absorption spectrum of $[Os(S_2PPh_2)_2(PPh_3)(tcne)]^{0/-1}$ in methylene chloride at 218K.

at low temperatures. The resulting spectrum of $[Os(S_2PPh_2)_2(PPh_3)(tcne)]^{2-}$, generated at -1.0V and 238K is shown in Figure 4.12. The spectrum is almost featureless, with all the bands observed in the mono-reduced species collapsing completely. Two isosbestic points are present at 22,200 and 35,000cm^{-1}. If the di-anion is prepared in a single step from $[Os(S_2PPh_2)_2(PPh_3)(tcne)]$, then no isosbestic points are observed, although the final spectrum is the same, implying that the double reduction proceeds *via* two one-electron steps.

The electronic absorption spectra of the neutral and mono-reduced product of $[Ru(S_2P\{OEt\}_2)_2(PPh_3)(tcne)]$ and $[Os(S_2P\{OEt\}_2(PPh_3)(tcne)]$ (electrogenerated at -0.10 and -0.30V respectively) are shown in Figures 4.13 and 4.14. On reduction, the low-energy CT band collapses and new bands appear at higher energy for the ruthenium complex and lower energy for the osmium complex. Once more a band at around 24,000cm^{-1} is observed in the absorption spectrum of the mono-reduced complexes. It was not possible to generate reversibly the doubly-reduced complex in either case. Attempts to do so invariably led to (irreversible) bleaching of the solution.

Similar spectral characteristics are observed in the absorption spectrum of $[Os(S_2PMe_2)_2(PPh_3)(tcne)]$ and the reduced product, $[Os(S_2PMe_2)_2(PPh_3)(tcne)]^-$, which was electrogenerated at -0.35V and 248K (see Figure 4.15).

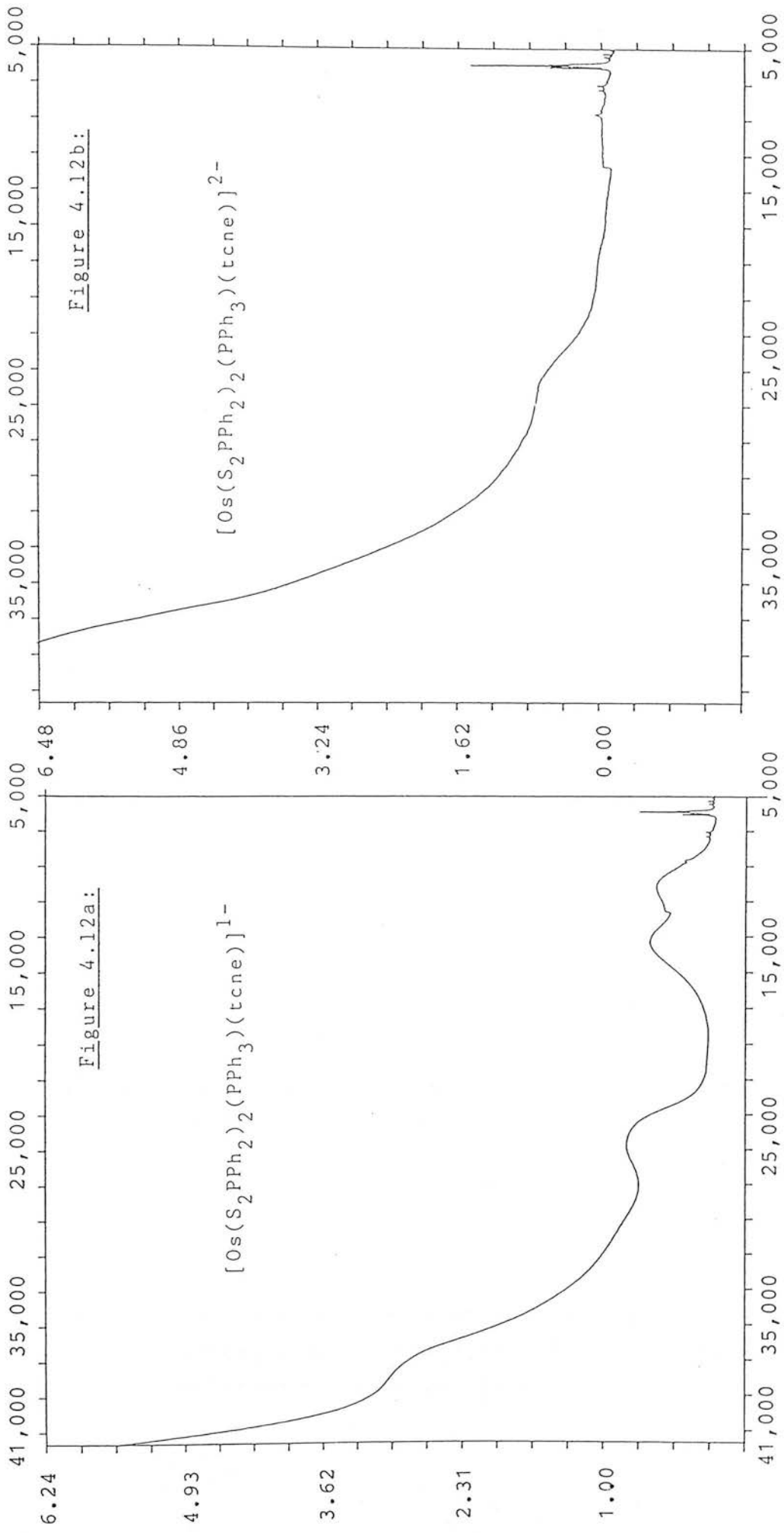

Figure 4.12: The electronic spectrum of $[Os(S_2PPh_2)_2(PPh_3)(tcne)]^{1-/2-}$ in methylene chloride solution at 218 K.

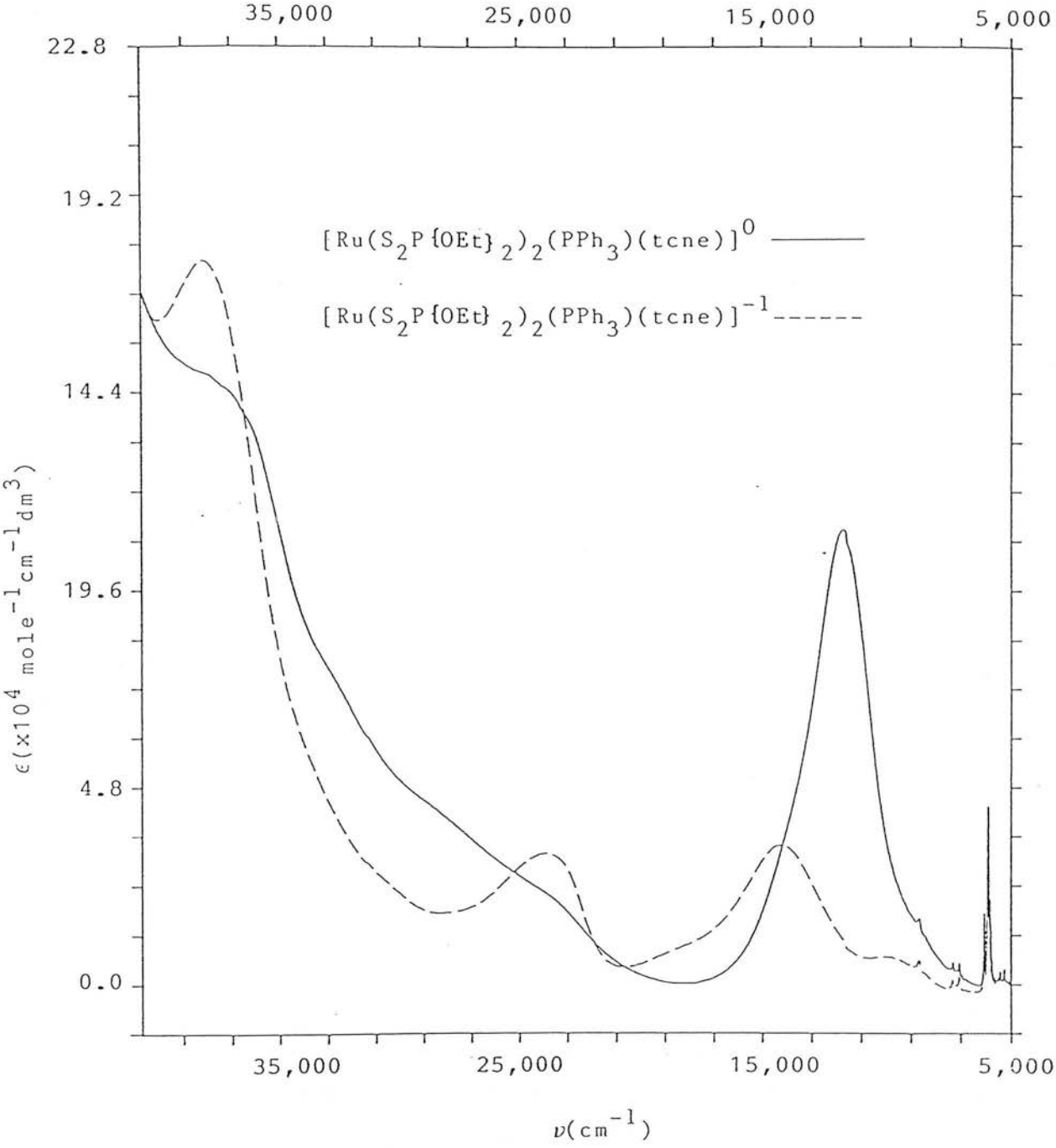

Figure 4.13: The electronic absorption spectrum of $[Ru(S_2P\{OEt\}_2)_2(PPh_3)(tcne)]^{0/-1}$ in methylene chloride solution at 231 K.

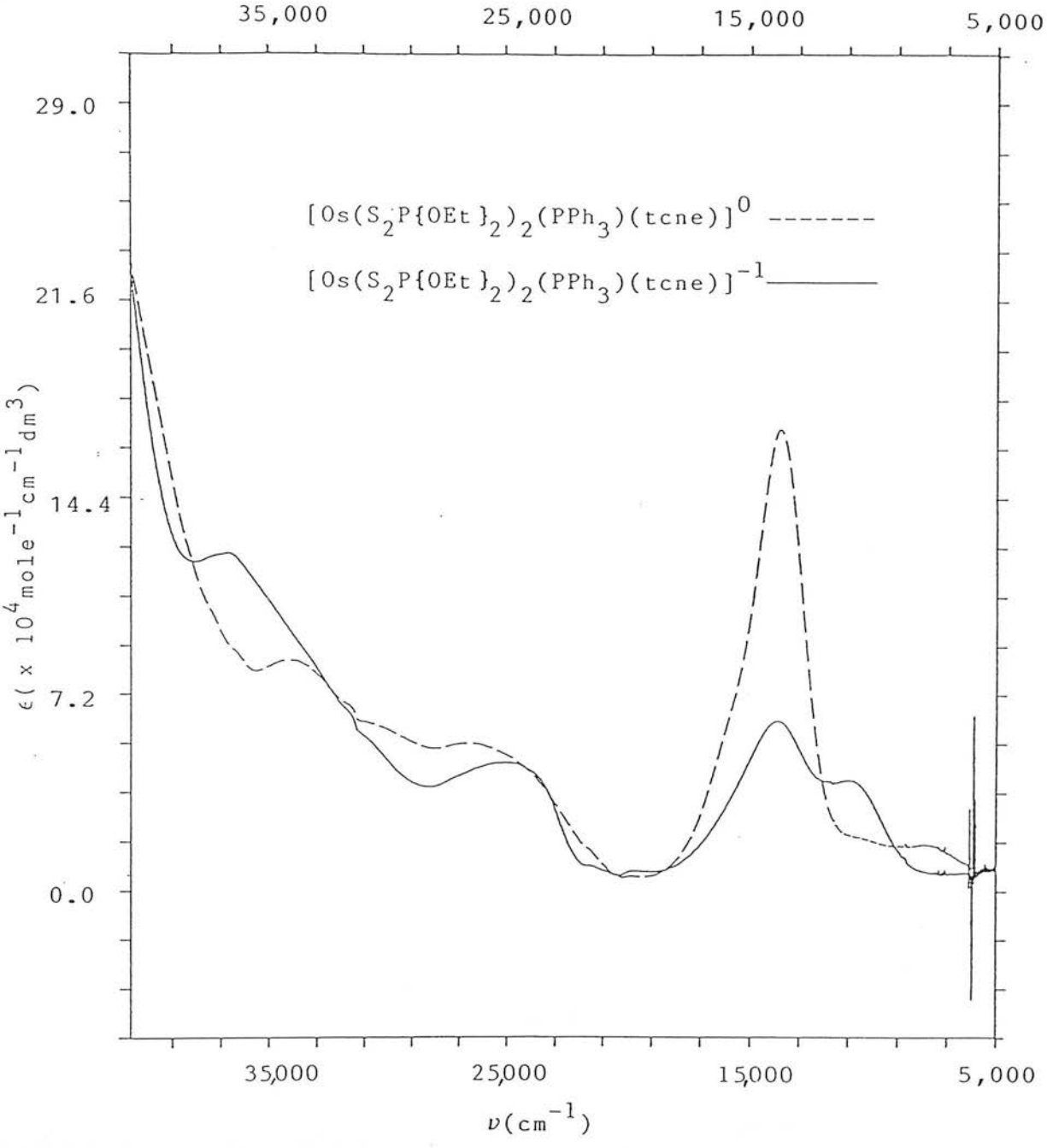

Figure 4.14: The electronic absorption spectrum of $[Os(S_2P\{OEt\}_2)_2(PPh_3)(tcne)]^{0/-1}$ in methylene chloride solution at 251 K.

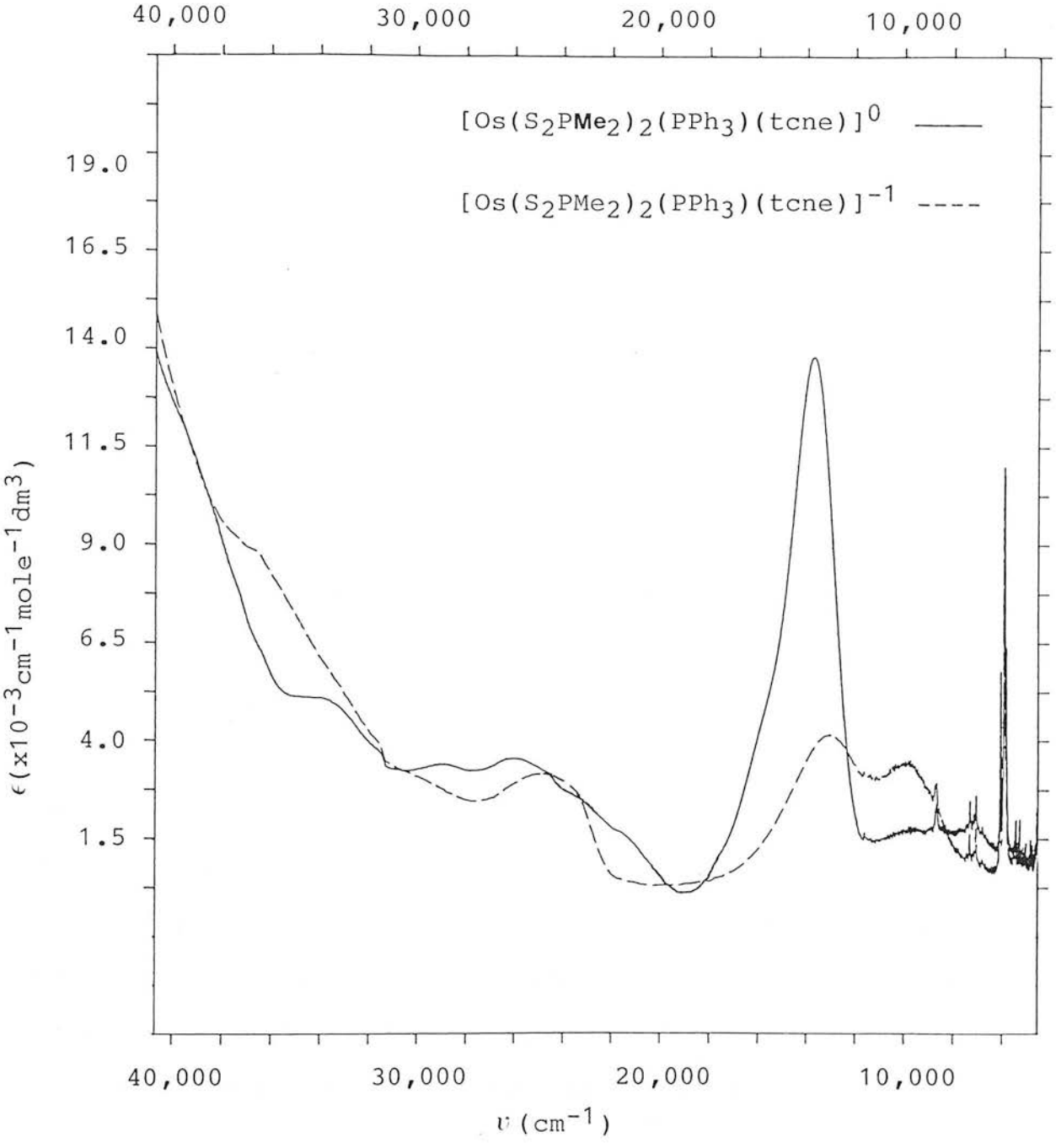

Figure 4.15 The electronic absorption spectrum of $[Os(S_2PMe_2)_2(PPh_3)(tcne)]^{0/-1}$ in methylene chloride at 235K.

4.7 Assignment of absorption bands.

The spectral changes associated with reducing the complexes, $[M(S_2PR_2)_2(PPh_3)(tcne)]$, to their corresponding mono-anion can be summarised as follows: (i) the collapse of the intense low-energy band, (ii) the growth of moderate intensity band or bands in the near-infrared and (iii) the growth of a new band at around 24,000cm^{-1}.

Associated spectroelectrochemical studies on free tcne and $tcne^-$ also show the progressive growth of a band at approximately 24,000cm^{-1} (ε=7,000$cm^{-1}mole^{-1}dm^3$) as tcne is reduced (see Figure 4.4). This has been assigned to a $\pi^* \longrightarrow \pi^{**}$ transition of $tcne^-$.[3] The same assignment is, therefore, given to the ligated tcne of the ruthenium and osmium mono-anions. The appearance of this absorption in $[M(S_2PR_2)_2(PPh_3)(tcne)]^-$ complexes suggests that the first reduction of $[M(S_2PR_2)_2(PPh_3)(tcne)]$ is tcne-based. As discussed above, the low-energy bands (11,000-13,000cm^{-1}) in the absorption spectra of $[M(S_2PR_2)_2(PPh_3)(tcne)]$ have been assigned to a MLCT band ($d\pi$ metal-based $\longrightarrow \pi^*$ tcne-based). The same assignment is given in the mono-anion complexes to the near-infrared band.

Generation of $[M(S_2PR_2)_2(PPh_3)(tcne)]^-$ effects a decrease in the intensity of the low-energy band. The reduction of the complex results in addition of an electron to the LUMO of tcne. This would be expected to reduce in intensity any charge-transfer, originating from

the metal to this orbital, as is observed experimentally.

Any electronic model must explain the different shifts found in the MLCT band for the mono-reduced $[M(S_2PR_2)_2(PPh_3)(tcne)]$ complexes. Both the electronic models (see Figure 4.9) have an anti-bonding LUMO. Addition of an electron to this orbital will cause the energy of this electronic level to fall. Consequently, a transition from the metal-based orbital to the ligand-based LUMO, will be of lower energy for the mono-reduced species, $[M(S_2PR_2)_2(PPh_3)(tcne)]^-$, than for the neutral species. This red-shift is observed for the $[Os(S_2PR_2)_2(PPh_3)(tcne)]$ products. However, in the analogous ruthenium complexes this absorption is actually blue-shifted in the reduced product. A possible explanation for this is as follows. The degree of overlap between the metal $d\pi$ and ligand π^* appears, from the spectral data, to be a function of the relative energies of these levels. Any change in the energy of one or both of these electronic levels will affect the degree of overlap, and hence the energy of the MLCT absorption. As mentioned above, the degree of overlap for the neutral $[Ru(S_2PR_2)_2(PPh_3)(tcne)]$ complexes is smaller than for the analogous osmium species, with the observed transition between more localised orbitals on the metal and ligand (Figure 4.9a). On addition of an electron to the ligand LUMO however the resulting drop in energy of this level allows greater mixing of the $d\pi$ and ligand π^* orbitals.

Thus, the molecular orbital picture of Figure 4.9b should be applied to the $[Ru(S_2PR_2)_2(PPh_3)(tcne)]^-$ complexes, thereby accounting for the blue-shifted MLCT band.

Upon the second reversible reduction of the complex, $[Os(S_2PPh_2)_2(PPh_3)(tcne)]$, complete collapse of the low-energy CT band and the disappearance of the band at 24,000cm^{-1} occurs. The di-anion of free tcne has been reported as colourless which suggests that the separation between the HOMO and LUMO of $tcne^{2-}$ is energetically large.[17] Assuming that the energy gap between the HOMO and LUMO in the co-ordinated di-anion is also large, it is, therefore, not surprising to find that all the tcne associated transitions at lower energies disappear on generation of $[Os(S_2PPh_2)_2(PPh_3)(tcne)]^{2-}$ to give a featureless absorption spectrum.

In conclusion, the electrochemical and spectroelectrochemical data can only be satisfactorily explained by assuming that both one-electron reductions of $[M(S_2PR_2)_2(PPh_3)(tcne)]$ are tcne-based, and furthermore that the low-energy charge-transfer band is from a metal-based orbital to a tcne-based orbital.

4.8 $[\{Ru(S_2PR_2)_2(PPh_3)\}_2tcne]$ complexes

The redox chemistry of $[\{Ru(S_2PR_2)_2(PPh_3)\}_2tcne]$ (R=Me, Ph, OEt) was examined in methylene chloride solution. The relevant electrochemical potentials for $[\{Ru(S_2PR_2)_2(PPh_3)\}_2tcne]$, are shown in Table 4.5.

Examination of the cyclic voltammetry of these complexes at greater current sensitivity shows the presence of other redox processes which is consistent with the presence of an isomeric mixture (see Chapter 3.5.2). The following discussion refers only to the electrochemistry of the major isomers.

4.8.1 Reductive behaviour.

The binuclear complexes, $[\{Ru(S_2PR_2)_2(PPh_3)\}_2tcne]$ (R=Me, Ph, OEt), exhibit two reductions (by stirred d.c. voltammetry) and Figure 4.16 shows the cyclic voltammogram of $[\{Ru(S_2PPh_2)_2(PPh_3)\}_2tcne]$ for the reductive range. As observed for the mononuclear $[Ru(S_2PR_2)_2(PPh_3)(tcne)]$, the first reduction is electrochemically reversible ($E_{pf}-E_{pr}=60mV$; $i_{pf}/i_{pr}=1.0$; $v=10-200mVs^{-1}$) while the second reduction is quasi-reversible ($E_{pf}-E_{pr}=400mV$). Coulometric studies show that the first reduction is a one-electron step for all $[\{Ru(S_2PR_2)_2(PPh_3)\}_2tcne]$.

4.8.2 Oxidative behaviour.

The cyclic voltamograms of the oxidative range of $[\{Ru(S_2PPh_2)_2(PPh_3)\}_2tcne]$ at 288 and 220K are shown in Figure 4.17 and the oxidation potentials are listed in Table 4.5. Electrochemical studies at room temperature and 220K show that the $[\{Ru(S_2PR_2)_2(PPh_3)\}_2tcne]$ species undergo two oxidations. At room temperature the first oxidation is quasi-reversible in nature affording a

Table 4.5: Redox potentials for $[\{Ru(S_2PR_2)_2(PPh_3)\}_2tcne]$.[a]

R	$E^{0/-1}$ /V [b]	$E^{-1/-2}$ V [c]	$E^{0/+1}$ /V [d]	$E^{+1/+2}$ /V [e]
Me	-0.13	-0.82	+0.66	+1.15
Ph	-0.13	-0.81	+0.68	+1.11
OEt	-0.14	-1.04	+0.82	+1.22

(a) recorded in methylene chloride at 288K;

(b) quasi-reversible, potential quoted=E_{pf}; (c) reversible;

(d) quasi-reversible at 288K, but reversible at T<233K.

(e)irreversible, potential quoted=E_{pf} .

Table 4.6: Spectral data for $[\{Ru(S_2PR_2)_2(PPh_3)\}_2tcne]^n$.[a]

M	R	n	ν_{max} /cm^{-1}
Ru	Me	0	9,400 (26.2),[b] 24,000 (5.2).
Ru	Ph	0	9,350 (23.7), 24,000 (5.4).
Ru	Ph	-1	11,650 (8.8), 23,800 (4.7).
Ru	OEt	0	9,850 (39.6), 24,200 (14.8). 32,200 (18.2), 37,300 (51.8)
Ru	OEt	-1	12,400 (15.5), 23,800 (4.1), 38,200 (59.2)

(a) measured in methylene chloride at 288K,

(b) figures in brackets represent $\varepsilon \times 10^{-3} cm^{-1} mole^{-1} dm^3$.

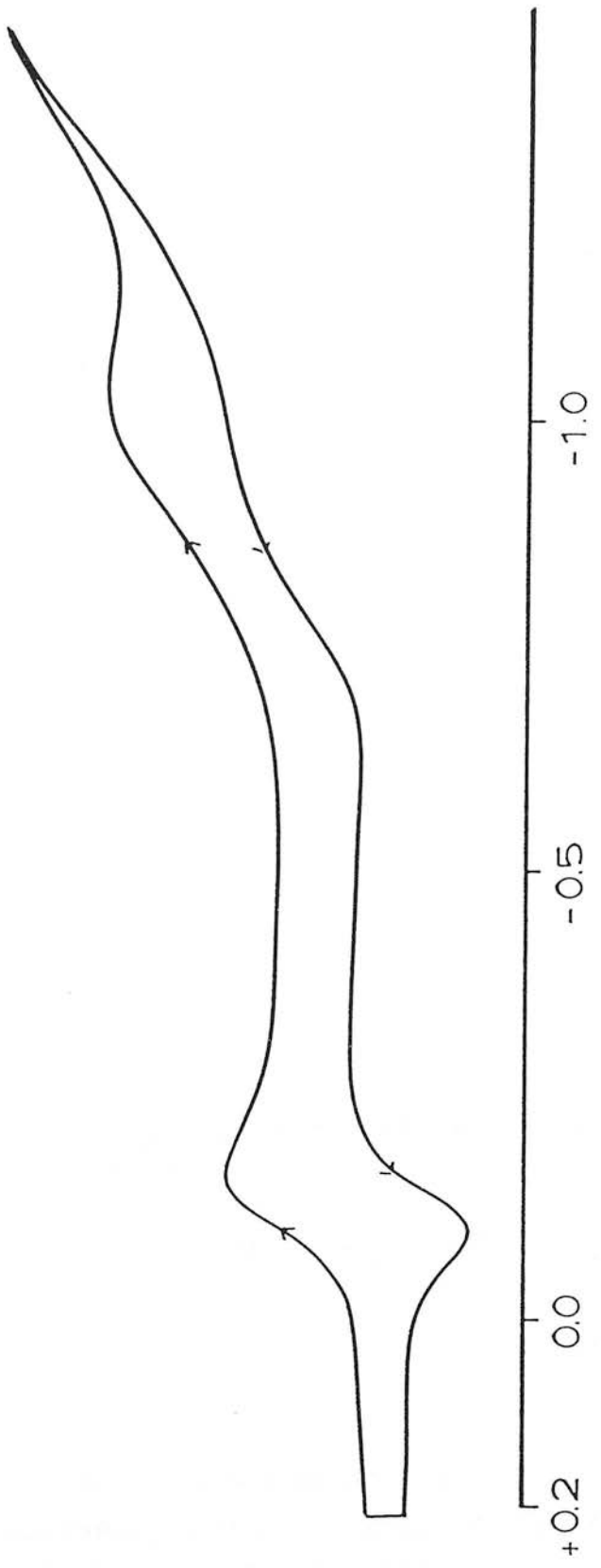

Figure 4.16: he cyclic voltammogram of [{Ru(S_2PPh_2)$_2$(PPh_3)}$_2$tcne] (+0.2 to 1.5V) in methylene chloride solution at 288K.

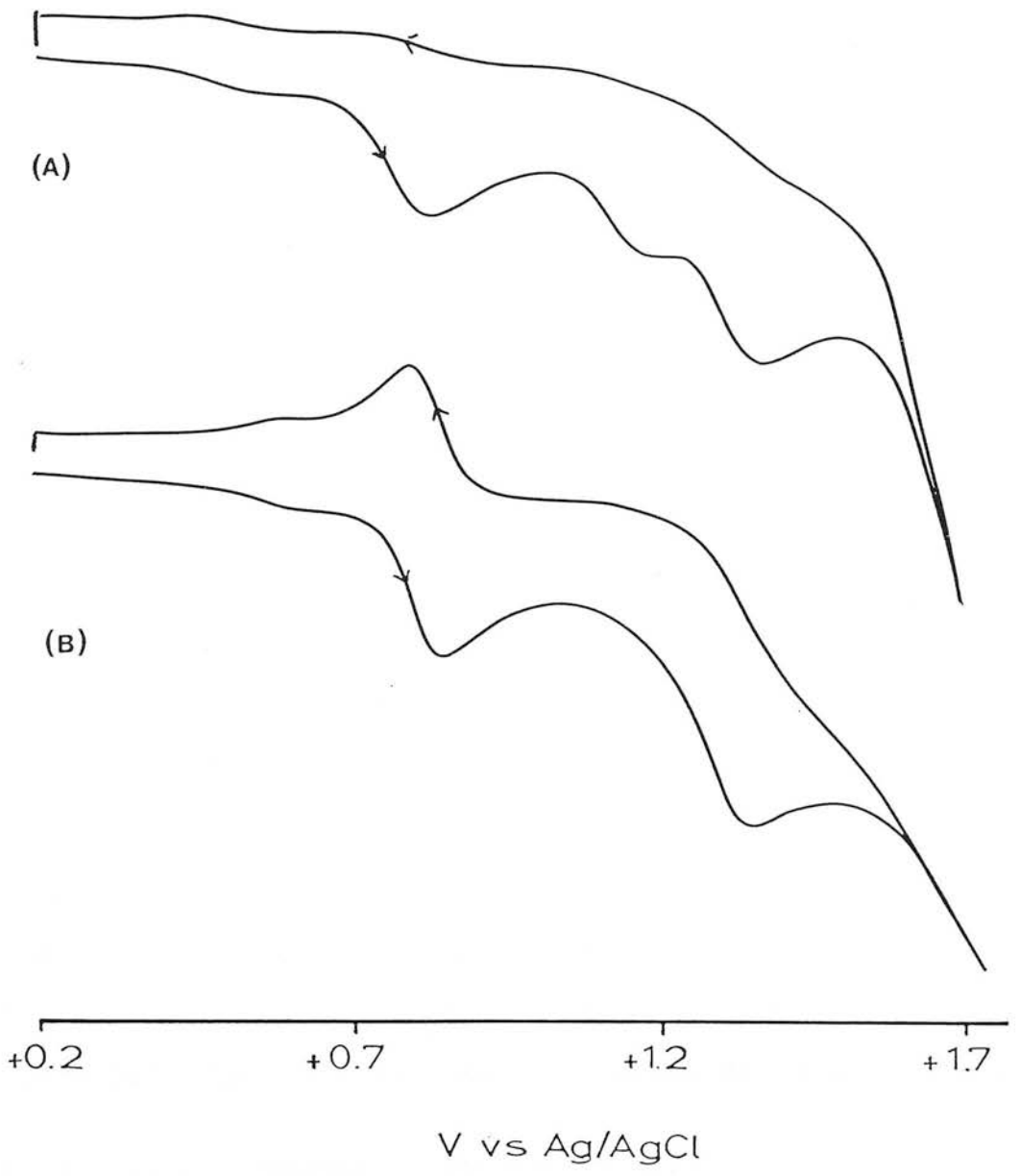

Figure 4.17: The cyclic voltammogram (+0.2 to +1.7V) of [{Ru(S_2PPh_2)$_2$(PPh_3)}$_2$tcne] at (a) 288K and (b) 233K in CH_2Cl_2 solution.

daughter product (observed as a redox wave at *ca.* 0.8V in the cyclic voltammogram). On cooling to 220K, the first oxidation becomes electrochemica lly reversible (with concomittant loss of daughter product formation), but is unstable on the time-scale required for bulk coulometry. A second quasi-reversible oxidation is observed 0.4V positive of the first (even at 288K). The instability of the oxidised species prevents accurate coulometric studies, but stirred d.c. voltammetry suggests that these are also one-electron processes.

Examination of Tables 4.2 and 4.5 shows that the first reduction is harder (*ca.* 300mV) for the binuclear species, $[\{Ru(S_2PR_2)_2(PPh_3)\}_2tcne]$ (R=Me, Ph, OEt), than for the corresponding $[Ru(S_2PR_2)_2(PPh_3)(tcne)]$; the reverse is true for the first oxidation which is 200-300V easier for the binuclear complex. However, it is interesting to note that the first reduction of $[\{Ru(S_2PR_2)_2(PPh_3)\}_2tcne]$ appears to be relatively independent of the dithiolate type, while the first oxidation potential varies with ligand type (*ca.* 160mV). An interpretation of this observation is discussed below.

4.9 Electronic absorption spectroscopy.

The binuclear complexes, $[\{Ru(S_2PR_2)_2(PPh_3)\}_2tcne]$ (R=Me, Ph, OEt), are green in colour. Spectroscopic data for these complexes are listed in Table 4.6.

Solutions of the binuclear species exhibit an intense

charge-transfer band at low energy (*ca.* 10,000cm^{-1}, $\varepsilon=10^4 cm^{-1}mole^{-1}dm^3$). A similar band is observed for the mononuclear complexes, $[Ru(S_2PR_2)_2(PPh_3)(tcne)]$, although at higher energies (*ca.* 11,000cm^{-1}). However, in addition to the low energy band, an absorption is also present at around 24,000cm^{-1} ($\varepsilon=5,000 cm^{-1}mole^{-1}dm^3$) for the binuclear species. This band is not present in the absorption spectra of $[M(S_2PR_2)_2(PPh_3)(tcne)]$ (M=Ru, Os; R=Me, Ph, OEt), but bands of this energy are exhibited by the mono-anion, $[M(S_2PR_2)_2(PPh_3)(tcne)]^-$, and we attributed these to the $\pi^* \longrightarrow \pi^{**}$ transition of co-ordinated tcne. Thus, the electronic nature of the binuclear species, $[\{Ru(S_2PR_2)_2(PPh_3)\}_2tcne]$, appears to be different to that of the mono-nuclear adducts. To investigate this further we have carried out spectroelectrochemical investigations of the $[\{Ru(S_2PR_2)_2(PPh_3)\}_2tcne]$ complexes.

4.10 Spectroelectrochemical studies.

Figures 4.18 and 4.19 show the electronic absorption spectra of $[\{Ru(S_2P\{OEt\}_2)_2(PPh_3)\}_2tcne]$ and $[\{Ru(S_2PPh_2)_2(PPh_3)\}_2tcne]^{0/-1}$ respectively; spectral data for these complexes is summarised in Table 4.6.

For both complexes the low energy band collapses with concomittant growth of another (less intense) absorption at higher energy. No growth of an absorption at 24,000cm^{-1} is recorded for $[\{Ru(S_2PR_2)_2(PPh_3)\}_2tcne]$ (in contrast to the species, $[Ru(S_2PR_2)_2(PPh_3)(tcne)]$, which exhibit a

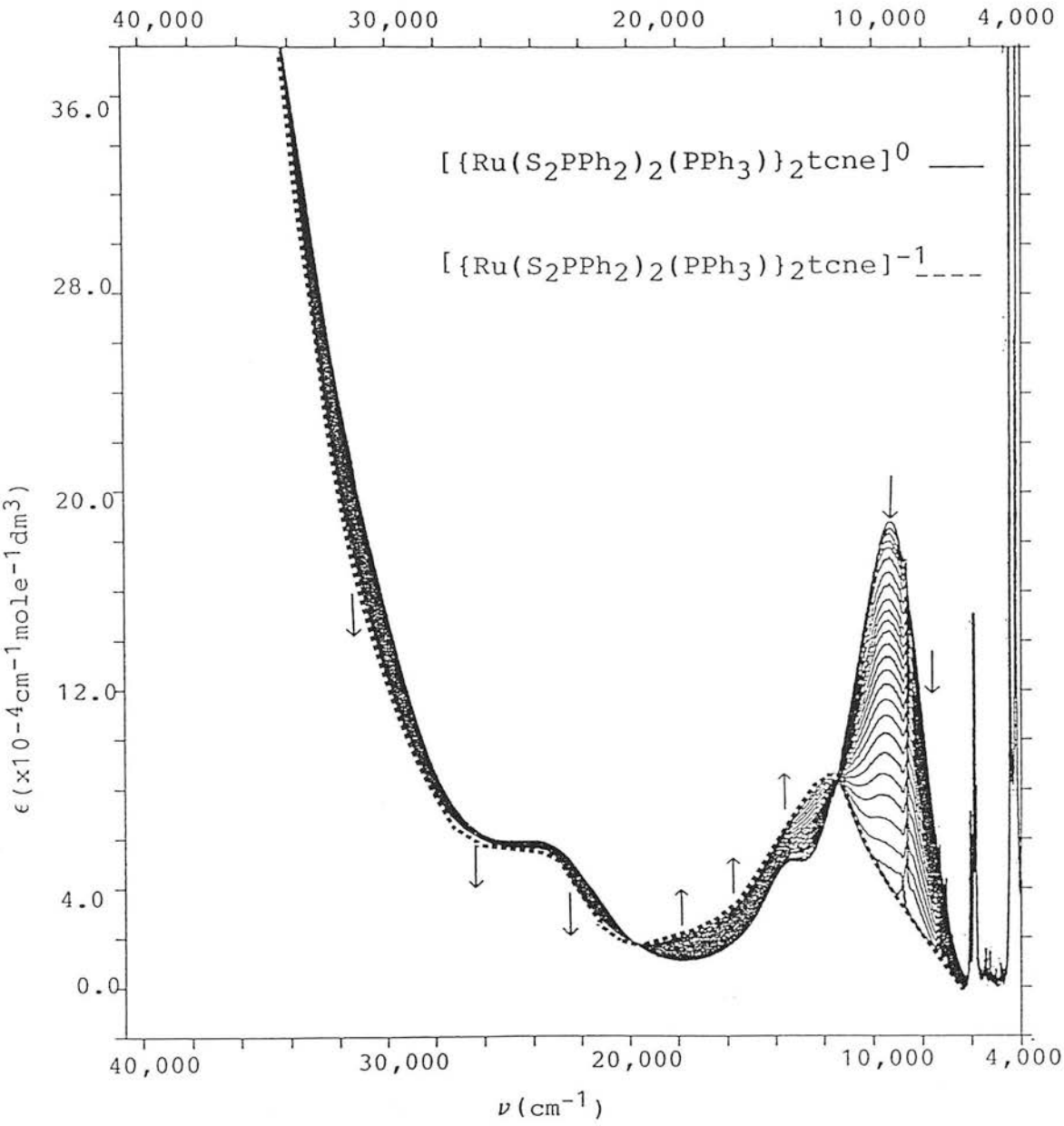

Figure 4.18: The electronic absorption spectrum of $[\{Ru(S_2PPh_2)_2(PPh_3)\}_2tcne]^{0/-1}$ in methylene chloride at 235K.

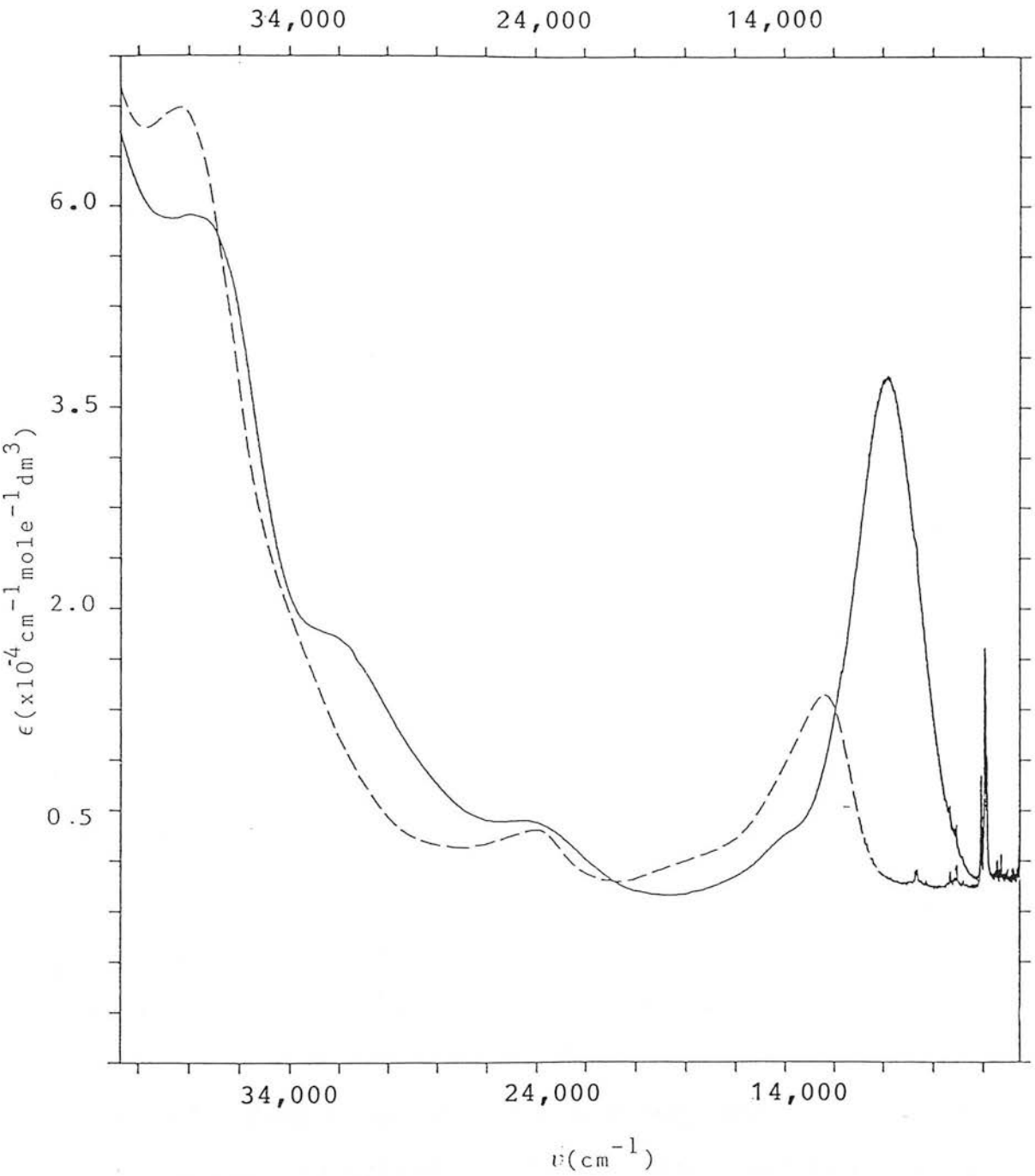

Figure 4.19: The electronic absorption spectrum of $[\{Ru(S_2P(OEt)_2)_2(PPh_3)\}_2tcne]^{0/-1}$ in methylene chloride solution at 233 K.

band at *ca.* 24,000cm^{-1} due to the $\pi^{*} \longrightarrow \pi^{**}$ transition of co-ordinated tcne^{-} on reduction. Isosbestic points are observed and imply a one-to-one conversion. Regeneration of the starting spectrum can be attained by switching the applied potential to 0.0V.

The observation of a band at 24,000cm^{-1} in the spectrum of [{Ru(S_2PR_2)$_2$(PPh_3)}$_2$tcne] in both the neutral and mono-anion states suggests that the binuclear complexes are formally Ru^{II}/Ru^{III} species in which the metal centre is bridged by tcne^{-}.‡ However, the electronic structure of these complexes is likely to be complicated by the possibility of conjugation between the metal centres. Earlier workers have indeed suggested that tcne is a strongly conjugating ligand.[8]

Further study is obviously required on the complexes, [{Ru(S_2PR_2)$_2$(PPh_3)}$_2$tcne], particularly with the aim of synthesising a derivative which can be reversibly oxidised in an O.T.T.L.E. cell. This would hopefully be of use in confirming that the oxidation is ligand-based (by the disappearance of the band assigned to the $\pi^{*} \longrightarrow \pi^{**}$ transition of tcne) and may shed some light on the conjugative properties of tcne in these complexes.

---

‡This type of electron transfer (from the metal centre to co-ordinated tcne) has been proposed for the complexes, [(Cp)Mn(CO)$_2$(tcne)], [(Cp)VBr_2(tcne)], and [Ni(dmpa)$_2$(tcne)].[12-14] Extensive interaction between the unpaired electrons of the metal and tcne has been invoked to explain the observed diamagnetism and n.m.r. spectra of these complexes.

4.11 Experimental methods.

The $[M(S_2PR_2)_2(PPh_3)(tcne)]$ (M=Ru, Os; R=Me, Ph, OEt) and $[\{Ru(S_2PR_2)_2(PPh_3)\}_2tcne]$ (R=Me, Ph, OEt) complexes were prepared as discussed in Chapter 3. All electrochemical studies were carried out in HPLC grade methylene chloride, which was stored over potassium hydroxide pellets for one week, and was stilled over P_2O_5 before use. The supporting electrolyte was $TBABF_4$ and the electrolyte concentration was 0.5 molar in methylene chloride. Prior to electrochemical measurements the cell and electolyte solution were purged with argon.

A conventional glass cell with a three electrode configuration was used. A Pt microelectrode and Pt electrode were used as the working and counter electrode respectively. The redox processes were referenced against a Ag/AgCl reference electrode which was separated from the bulk solution by a glass frit. The ferrocene/ferrocinium couple was measured at 0.56V and all redox potentials, except where otherwise stated, are quoted with reference to the Ag/AgCl reference used. A Princeton Applied Research Model 170 instrument was used for both cyclic voltammograms and electrogeneration experiments. Cyclic voltammograms were measured between 20-500mVs^{-1}, and routine measurement were made at 100mVs^{-1}. A.C. voltammograms were recorded at 20mVs^{-1}. Coulometric studies were carried out in an "H" cell. The working electrode was a Pt basket (surface area 15cm^2)

and this was separated from the auxilliary electrode by glass frits.

Spectroelectrochemical studies were made at a Pt O.T.T.L.E. supported in a teflon cell block. The Pt O.T.E. was mounted in the beam of a Perkin-Elmer Lambda 9 spectrophotometer. A Ag/AgCl reference electrode and Pt counter electrode were fitted out of the path of the beam, and were separated from the bulk solution. The solutions, and the spectrophotometer were purged with nitrogen before electrogeneration. The temperature was varied using cooled nitrogen gas and recorded using a Comark 5000 Digital Thermometer. A Metrohm E506 potentiosat provided a constant potential source. The extinction coefficients obtained at low temperature have been corrected for measurements taken on standard solutions at 293K. The sharp peaks observed in the electronic absorption spectra at low energy ($\nu<10,000cm^{-1}$) are due to the solvent and the supporting electrolyte.

References.

1. P. H. Rieger, I. Bernal, and G. K. Fraenkel, *J. Am. Chem. Soc.*, 1961, **83**, 3918.

2. D. S. Acker and W. R. Hertler, *J. Am. Chem. Soc.*, 1962, **84**, 3370.

3. D. L. Jeanmaire, M. R. Suchanski and R. P. Van Duyne, *J. Am. Chem. Soc.*, 1975, **97**, 1699.

4. J. E. Pemberton and R.P. Buck, *Appl. Spectroscop.*, 1981, **35**, 571.

5. J. Daschbach, D. Heisler, and S. Pons, *Appl. Spectroscop.*, 1986, **40**, 489.

6. S. Pon, T. Davidson, and A. Berwick, *Chem. Abstracts.* **98**, 62459, from *Gov. Rep. Announce. Index (U.S)*, 1982, **82**, 5396.

7. S. I. Amer, T. P. Dasgupta, and P. M. Henry, *Inorg. Chem.*, 1983, **22**, 1970.

8. R. Gross and W. Kaim, *Angew. Chem., Int. Ed. Engl.*, 1987, **26**, 251.

9. N. S. Hush, *Prog. Inorg. Chem.*, 1967, **8**, 391.

10. J. Stanley, D. Smith, B. Latimer and J. Devlin, *J. Phys. Chem.*, 1966, **70**, 2011.

11. J-H. Aihara, *Bull. Chem. Soc. Jpn.*, 1980, **53**, 3404.

12. M. F. Rettig and R. M. Wing, *Inorg. Chem.*, 1969, **8**, 1969.

13. B. L. Booth, C. A. M^{c}Auliffe and G. L. Stanley, *J. Chem. Soc., Dalton Trans.*, 1982, 535.

14. W. Beck, R. Schlodder and K. H. Lechler, *J. Organomet. Chem.*, 1973, **54**, 303.

15. L. J. Yellowlees, PhD. Thesis, University of Edinburgh, 1982.

16. W. Kaim, *Coord. Chem. Rev.*, 1987, **76**, 187.

17. M. S. Khatkale and J. P. Devlin, *J. Phys. Chem.*, 1979, **83**, 1636.

Chapter 5

Preparation and characterisation of fumaronitrile complexes of ruthenium and osmium.

5.1 Introduction

Fumaronitrile (fmn, E-2-butenedinitrile) is a white crystalline solid which has a melting point of 368K and sublimes readily at atmospheric pressure.[1] Figure 5.1 shows the molecular structure of fmn (by X-ray crystallography).[2] The molecule is planar with a central C=C bond of 1.25 Å.

Recent calculations on organo-cyano molecules show that fmn has a relatively large electron affinity (1.24eVmole^{-1}), but smaller than that of tcne (3.17eVmole^{-1}).[3]

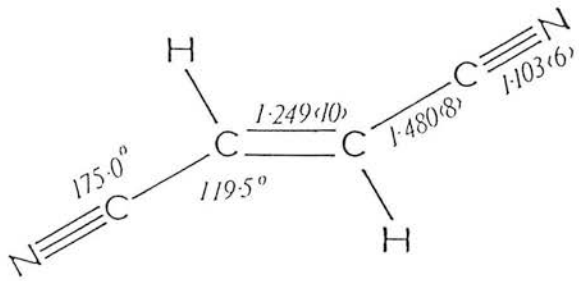

Figure 5.1 The molecular structure of fmn.[2]

Many transition metal complexes of fmn have been reported and in most of these the fmn ligand is π-bound to the metal centre *via* the C=C bond. Thus, complexes such as, $[IrClN_2(PPh_3)_2(fmn)]$, $[RhCl(CO)(py)(fmn)]$, and $[(Cp)Ru(PMe_3)(fmn)]^+$ all exhibit π-alkene co-ordination.[4,5] The adducts, [Ir(fmn)(MeO-coe)(phen)] (MeO-coe=8-methoxy-cyclo-oct-4enyl), and $[IrH(CO)(PPh_3)_2(fmn)]$ have been studied by X-ray crystallography.[6,7] The central C=C bond in these complexes (1.43-1.49Å) is longer than in the

free ligand (1.25Å), consistent with transfer of electron density from the metal into the π^*-orbital of fmn. As observed for analogous tcne complexes, the electronic properties of the cyano-groups result in an enhanced stability for π-alkene complexes of fmn over other "simple" alkenes.[8]

The species, $[Ru(NH_3)_5(fmn)]^{2+}$, $[\{Ru(NH_3)_5\}_2fmn]^{4+}$,[9] $[RuCl_2(CO)(PCy_3)_2(fmn)]$ and $[\{OsHCl(CO)(PCy_3)_2\}_2fmn]$ are among the few reported N-bound fmn adducts.[10] Russian workers have characterised polynuclear adducts with CuCl involving bridging, N-bound fmn ligands.[11] Thus, fmn (like tcne) can bind to a transition metal as both a monodentate and a bridging ligand.

5.2 Results and discussion.

The complexes, $[Ru(S_2PR_2)_2(PPh_3)_2]$ (R=Me, Ph, OEt), react with fmn (in chloroform) to afford a mixture of $[Ru(S_2PR_2)_2(PPh_3)(fmn)]$ and $[\{Ru(S_2PR_2)_2(PPh_3)\}_2fmn]$. With an excess of ligand, $[Ru(S_2PR_2)_2(PPh_3)(fmn)]$ predominates and a red-purple species is produced; if the metal complex is in two fold excess the isolated product contains mainly $[\{Ru(S_2PR_2)_2(PPh_3)\}_2fmn]$ which is blue in colour. These complexes are analogous to the tcne species discussed in Chapter 3.

As observed for the tcne species, the adducts, $[Ru(S_2PPh_2)_2(PPh_3)(fmn)]$ and $[\{Ru(S_2PPh_2)_2(PPh_3)\}_2fmn]$, can

be interconverted. Dry-column chromatography of a sample which contains (predominantly) $[Ru(S_2PPh_2)_2(PPh_3)(fmn)]$ affords good yields of $[\{Ru(S_2PPh_2)_2(PPh_3)\}_2fmn]$. The binuclear complex can also be obtained if solutions of $[Ru(S_2PR_2)_2(PPh_3)(fmn)]$ are heated under vacumn; this presumably results from loss of fmn which sublimes readily. Addition of $[Ru(S_2PR_2)_2(PPh_3)_2]$ to a solution of $[Ru(S_2PR_2)_2(PPh_3)(fmn)]$ results in the formation of $[\{Ru(S_2PR_2)_2(PPh_3)\}_2fmn]$. Addition of fmn to solutions of $[\{Ru(S_2PR_2)_2(PPh_3)\}_2fmn]$ produces $[Ru(S_2PR_2)_2(PPh_3)(fmn)]$. Separation of the two products is not easily achieved since they are readily interconverted and have similar solubilities and chromatographic characteristics.

The fmn ligand is easily displaced by tcne at 288K to give $[Ru(S_2PR_2)_2(PPh_3)(tcne)]$ and $[\{Ru(S_2PR_2)_2(PPh_3)\}_2tcne]$ (depending on the quantity of tcne added).

5.3 Infrared spectroscopy.

Free fmn exhibits a band at $2230cm^{-1}$ in the infrared spectrum assigned to the C-N stretching vibration[12,13]; a band at $1610cm^{-1}$ in the Raman spectrum is observed for $\nu_{C=C}$.[12]

If fmn is co-ordinated to a transition metal through the C=C bond, then ν_{CN} is shifted to lower wavenumber by $10-20cm^{-1}$.[5,6,14] For complexes in which fmn is N-bound to the metal centre, the C-N stretching vibrations are

recorded at lower frequencies (*ca.* 60-100cm^{-1}).[9,10]

Table 5.1 lists some infrared data for the complexes, [Ru(S_2PR_2)$_2$(PPh_3)(fmn)] and [{Ru(S_2PR_2)$_2$(PPh_3)}$_2$fmn]. For both adducts, the nitrile absorption is observed as a strong (broad) band at *ca.* 2180cm^{-1}, characteristic of N-bound fmn.[9,10] The decrease in frequency of ν_{CN} for the fmn complexes (60cm^{-1}) is much less than that of the tcne complexes discussed in Chapter 3. This may reflect the degree of backdonation from the metal *d*-π orbitals into the ligand π^* of the cyano-alkene.

5.4 ^{31}P-{^{1}H} n.m.r. spectroscopy

The ^{31}P-{^{1}H} n.m.r. spectra of [Ru(S_2PPh_2)$_2$(PPh_3)(fmn)] and [{Ru(S_2PPh_2)$_2$(PPh_3)}$_2$fmn] are shown in Figures 5.2 and 5.3 respectively and Table 5.2 lists spectral data for these adducts. In addition to signals for the mono- and bi-nuclear adducts, a resonance characteristic of free PPh_3 is present in the crude reaction mixture.

The spectrum of [Ru(S_2PPh_2)$_2$(PPh_3)(fmn)] (Figure 5.2) is similar to that of [Ru(S_2PR_2)$_2$(PPh_3)(tcne)] and [Ru(S_2PR_2)$_2$(PPh_3)(CO)] (R=Me, Ph, OEt) and therefore, assigns a *cis*-configuration to the ligands in both [{Ru(S_2PR_2)$_2$(PPh_3)}$_2$fmn] and [Ru(S_2PR_2)$_2$(PPh_3)(fmn)].

The relative intensities of the resonances observed for samples of [{Ru(S_2PR_2)$_2$(PPh_3)}$_2$fmn] (Figure 5.3) suggest that (as for [{Ru(S_2PR_2)$_2$(PPh_3)}$_2$tcne]) this

Table 5.1: Infrared spectral data for $[\{Ru(S_2PR_2)_2(PPh_3)\}_n fmn]$.[a]

R	n	υ_{CN}/cm-1
Me	1	2180 s, br.[b]
Me	2	2190 s, br.
Ph	1	2190 s, br.
Ph	2	2185 s, br.
OEt	1	2195 s, br.
OEt	2	2185 s, br.

(a) recorded as KBr pellets; (b) s-strong, br-broad.

Table 5.2: Electronic spectral data for $[\{Ru(S_2PR_2)_2(PPh_3)\}_n fmn]$.[a]

R	n	υ /cm-1
Me	1	19,300 (6.4)[b]
Me	2	17,300 (13.2)
Ph	1	19,300 (6.1)
Ph	2	17,350 (13.4)
OEt	1	19,700 (7.2)
OEt	2	17,600 (15.0)

(a) Measured in CH_2Cl_2 solution at 293K;

(b) $\epsilon \times 10^{-3}$ $cm^{-1}mole^{-1}dm^3$.

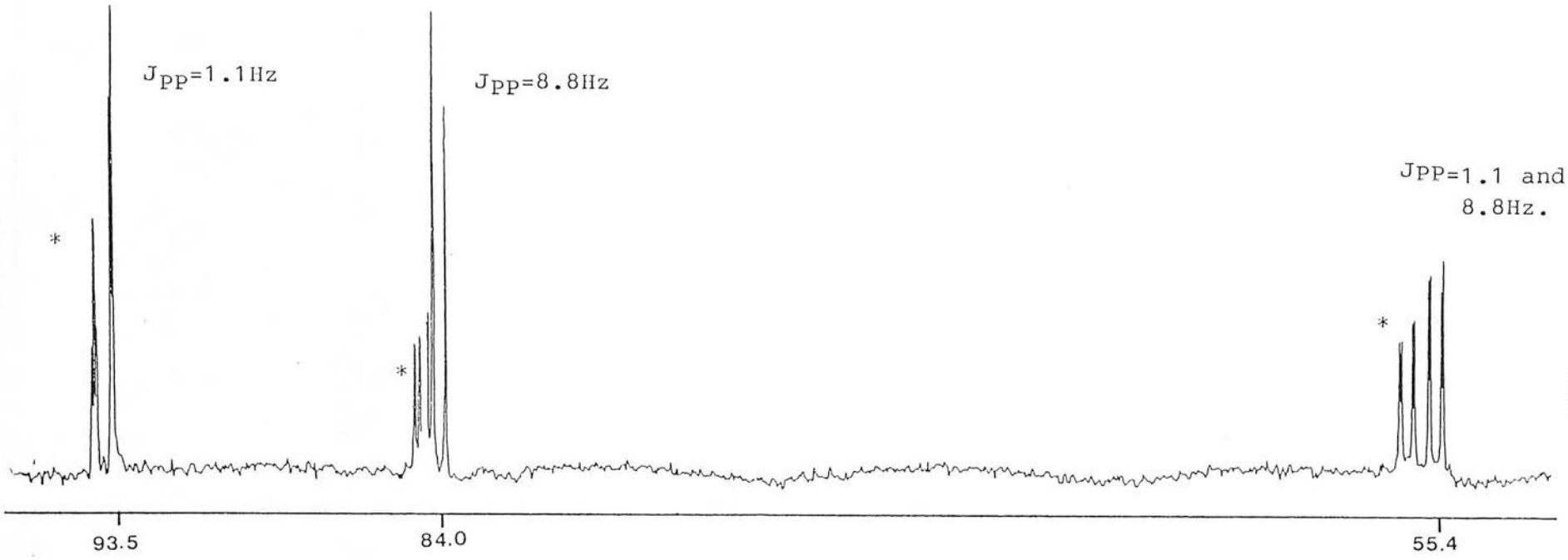

Figure 5.2: The $^{31}P-\{^{1}H\}$ n.m.r. spectrum of $[Ru(S_2PPh_2)_2(PPh_3)(fmn)]$ in $CDCl_3$ solution at 298K. The resonances marked "*" correspond to the binuclear species (see Figure 5.3).

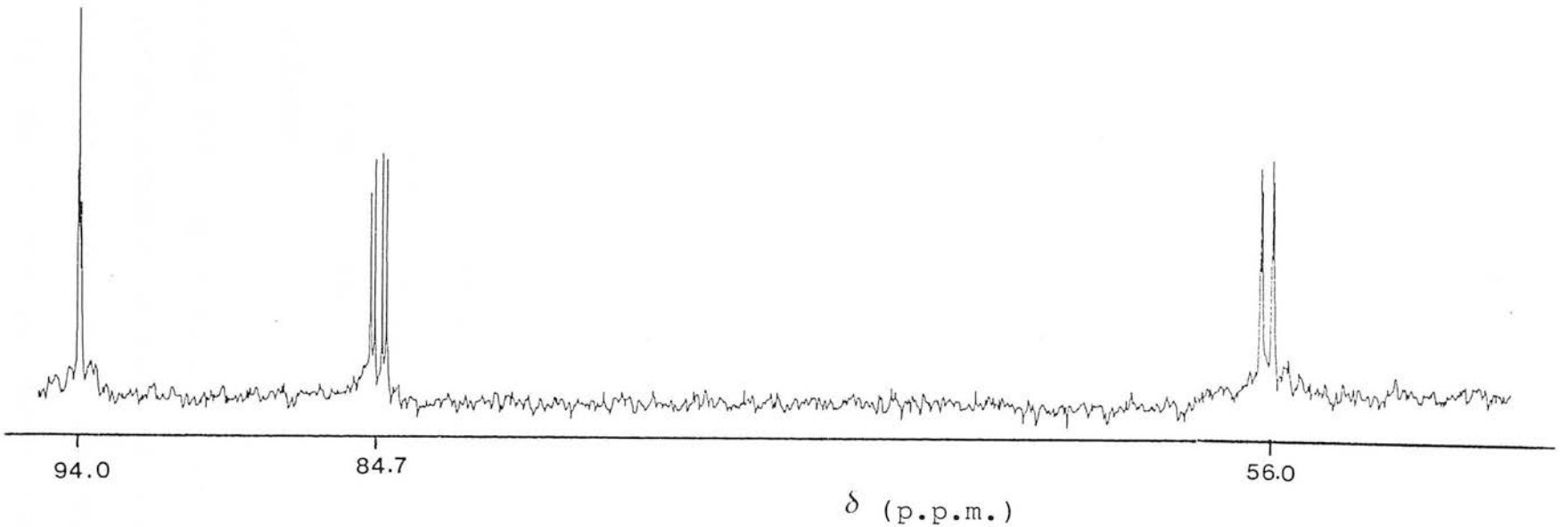

Figure 5.3: The $^{31}P-\{^{1}H\}$ n.m.r. spectrum of $[\{Ru(S_2PPh_2)_2(PPh_3)\}_2(fmn)]$ in $CDCl_3$ solution at 298K.

complex may be a mixture of two isomers formed in equal amounts, or one species with magnetically inequivalent ligands. However, it is interesting to note that the pattern of minor resonances observed for $[\{Ru(S_2PR_2)_2(PPh_3)\}_2tcne]$ is not repeated for the fmn complexes. This may reflect the reduced possibilities for geometric isomerism of the type discussed for $[\{Ru(S_2PR_2)_2(PPh_3)\}_2tcne]$ (R=Me, Ph, OEt) in Chapter 3.12.

If $^{31}P-\{^1H\}$ n.m.r. spectroscopy is used to record the progress of the reaction of $[Ru(S_2PR_2)_2(PPh_3)(fmn)]$ (M=Me, Ph, OEt) with tcne, then $[Ru(S_2PR_2)_2(PPh_3)(tcne)]$ is observed initially on adding tcne. On standing this species is converted to $[\{Ru(S_2PR_2)_2(PPh_3)\}_2tcne]$. On addition of an excess of tcne to the sample, complete conversion to $[Ru(S_2PR_2)_2(PPh_3)(tcne)]$ results.

5.5 Electronic spectroscopy

The electronic spectra of $[Ru(S_2PR_2)_2(PPh_3)(fmn)]$ and $[\{Ru(S_2PR_2)_2(PPh_3)\}_2fmn]$ (R=Me, Ph, OEt) (Figures 5.4 and 5.5) exhibit CT bands between 17,000 and 20,000cm^{-1} (ε=4-8x10^3$cm^{-1}mole^{-1}dm^3$). Table 5.3 lists spectral data for these complexes.

As observed for the analogous tcne complexes, the binuclear species exhibit a band at lower energy (and greater intensity) than the analogous mononuclear species, while the absorption bands for R=OEt lie at

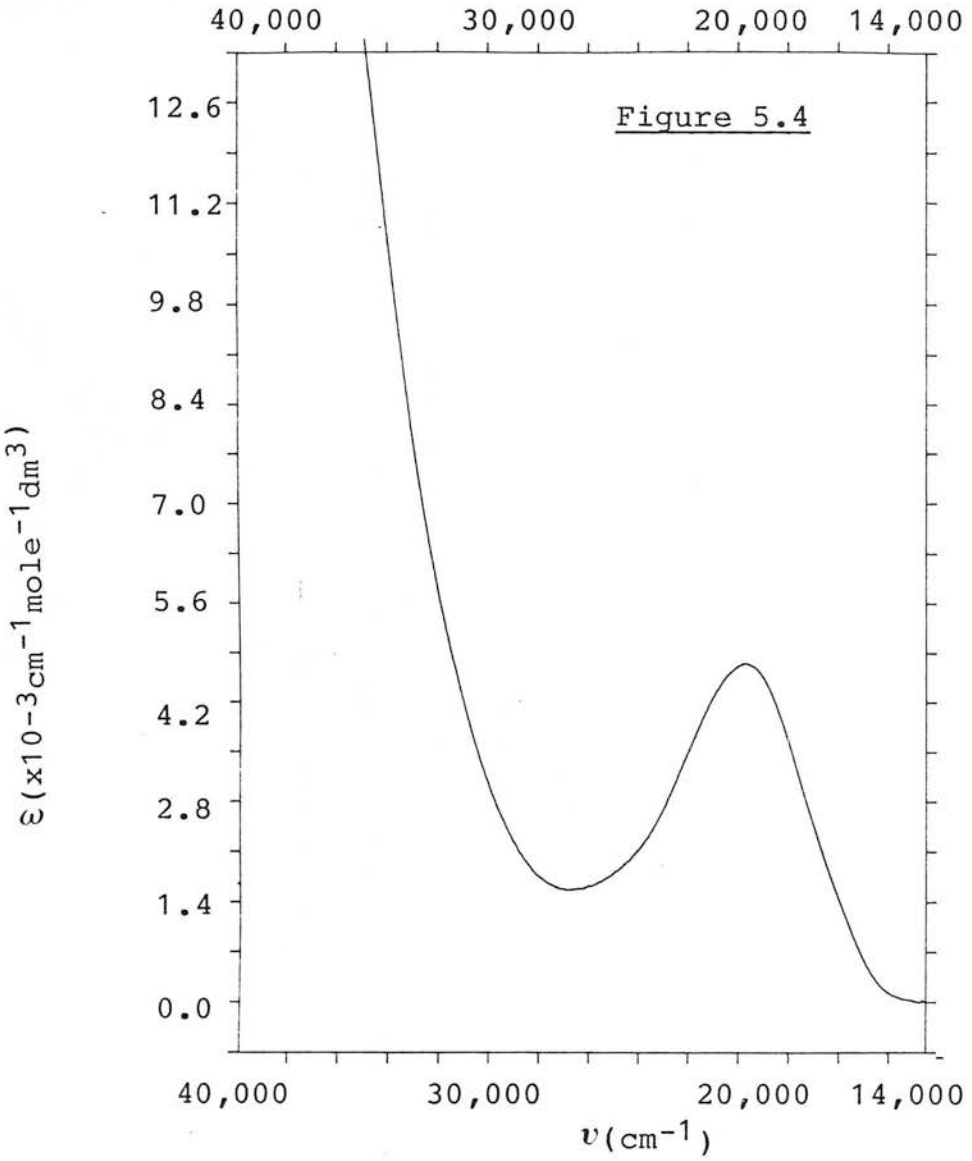

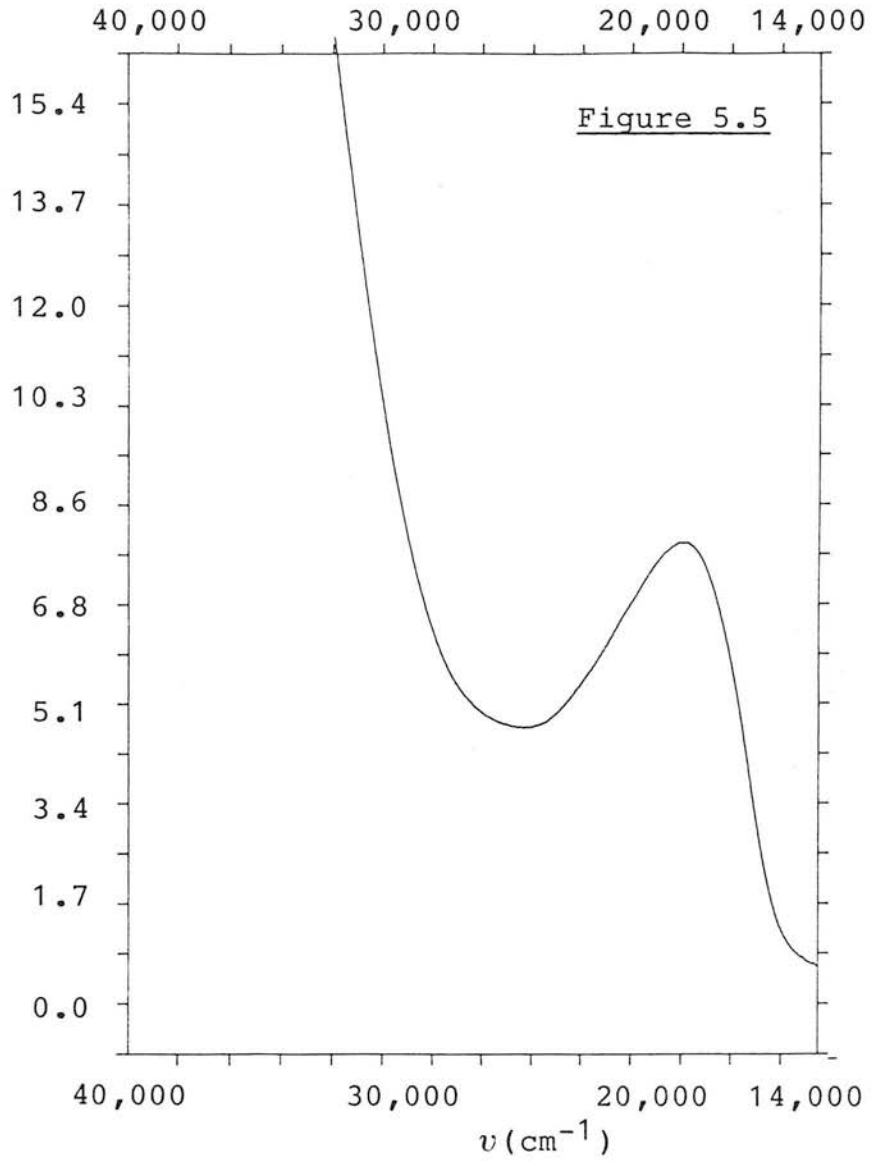

Figures 5.4 and 5.5: The electronic absorption spectra of $[Ru(S_2PPh_2)_2(PPh_3)(fmn)]$ and $[\{Ru(S_2PPh_2)_2(PPh_3)\}_2fmn]$ respectively (solutions in CH_2Cl_2 at 293K).

higher energy ($300cm^{-1}$) than for R=Me, Ph. Consequently, we assign these bands as charge-transfer between Ru^{II} and fmn.

The difference in energy between the π^* orbital of free tcne and fmn is *ca.* $15,500cm^{-1}$ (the LUMO of tcne lies at lower energy than fmn).[3] If the fmn and tcne species are strictly analogous, the MLCT bands for the fmn complex might be expected to lie $15,500cm^{-1}$ to higher energy of the corresponding tcne complex. Examination of Tables 4.4, 4.6 and 5.3 show that the MLCT bands of $[\{Ru(S_2PR_2)_2(PPh_3)\}_2fmn]$ and $[Ru(S_2PR_2)_2(PPh_3)(fmn)]$ are found at *ca.* $8,000cm^{-1}$ to higher energy than the tcne analogues. This discrepancy may relate to the degree of overlap between the ruthenium $d\pi$ orbitals and the LUMO of the cyano-alkene.

As discussed in Chapter 4.5, the extent to which the metal and ligand orbitals overlap is partly related to the relative energies of the orbitals involved. Thus, the results of Chapter 4 suggest that for the species, $[M(S_2PR_2)_2(PPh_3)(tcne)]$, the overlap is greater for M=Os than for M=Ru. However, in comparing the adducts, $[Ru(S_2PR_2)_2(PPh_3)(fmn)]$ and $[Ru(S_2PR_2)_2(PPh_3)(tcne)]$, the extent of any overlap will be mainly related to the energy of the LUMO of the cyano-alkene. Thus, the tcne complex will produce the greater overlap as the π^*-orbital of tcne would be expected to be found at lower

energy than the π^*-orbital of fmn. This increased overlap is also implied by the larger value of ε for the tcne complexes. Consequently, as outlined in Chapter 4.5, the energy gap between the HOMO and LUMO is effectively increased and the MLCT band for the tcne complexes is observed at energies greater than might be predicted.

5.6 Experimental methods and materials.

The methods and materials used were as for Chapter 2. Fumaronitrile (Aldrich) was supplied as technical grade and recrystallised from acetone-hexane mixtures prior to use.

Reaction of $[Ru(S_2PPh_2)_2(PPh_3)_2]$ with fmn.

When $[Ru(S_2PPh_2)_2(PPh_3)_2]$ (0.10g, 0.09mmole) and fmn (0.04g, 0.51mmole) are added to degassed CH_2Cl_2, the red colour of the solution darkens and gives a purple solution on stirring (2-3 hours). Precipitation (n-hexane) affords a maroon solid which contains both $[Ru(S_2PPh_2)_2(PPh_3)(fmn)]$ and $[\{Ru(S_2PPh_2)_2(PPh_3)\}_2fmn]$. Preparative T.L.C. (silica plate, $CHCl_3$ eluent) shows a single band, the leading edge is purple and the trailing edge is maroon in colour. If the material is isolated and again run down another plate, the purple colouration appears less intense. On a dry-column complete conversion to the navy-blue, $[\{Ru(S_2PPh_2)_2(PPh_3)\}_2fmn]$ can be achieved. However, solutions of these "pure" samples

"contaminated" with $[Ru(S_2PPh_2)_2(PPh_3)(fmn)]$ on standing. The difficulty in obtaining analytically pure samples is reflected in the analysis figures obtained for these complexes. Calculated for $C_{90}H_{72}N_2P_6Ru_2S_8$: C=58.7, H=3.89, N=1.58; Found: C=57.5, H=3.92, N=1.56. It is not possible to obtain pure samples of the mononuclear complex as they readily lose fmn.

Reaction with $[Ru(S_2PMe_2)_2(PPh_3)_2]$

The methyl analogues, $[Ru(S_2PMe_2)_2(PPh_3)(fmn)]$ and $[\{Ru(S_2PMe_2)_2(PPh_3)\}_2fmn]$, were prepared as above. Pure samples of the binuclear complex were prepared by repeated preparative T.L.C. runs of a single sample. The methyl derivatives decompose rapidly on exposure to air. Calculated for $C_{48}H_{56}N_2P_6Ru_2S_8$: C=44.2, H=4.29, N=2.14; found C=43.5, H=4.31, N=2.23.

Reaction with $[Ru(S_2P\{OEt\}_2)_2(PPh_3)_2]$

The complexes, $[Ru(S_2P\{OEt\}_2)_2(PPh_3)(fmn)]$ and $[\{Ru(S_2P\{OEt\}_2)_2(PPh_3)\}_2fmn]$, were prepared as above. Heating of the maroon solution with excess fmn under vacuum affords a solution of $[\{Ru(S_2P\{OEt\}_2)_2(PPh_3)\}_2fmn]$ (and a crystalline deposit of fmn on the side of the flask). Preparative T.L.C. of the blue solution yields relatively pure samples of $[\{Ru(S_2P\{OEt\}_2)_2(PPh_3)\}_2fmn]$. Both the mono- and bi-nuclear complexes are highly soluble in non-polar solvents.

References

1. Eyre and Spottiswood (Pub.), *The Dictionary of Organic Compounds*, 1965, **4**, 1474.

2. D. Britton and W. B. Gleason, *Cryst. Struct. Comm.*, 1982, **11**, 1155.

3. S. Chowdbury and P Kebarle, *J. Am. Chem. Soc.*, 1986, **108**, 5453.

4. P. Uguagliati, G. Deganello, L. Busetto and U. Belluco, *Inorg. Chem.*, 1969, **8**, 1625.

5. L. E. Manzer, *Inorg. Chem.*, 1976, **15**, 2354.

6. N. Bresciani-Pahor, M. Calligaris, G. Nardin and P. Delise, *J. Chem. Soc., Dalton Trans.*, 1976, 762.

7. L. Manojlovic-Muir, K. Muir and J. A. Ibers, *Diss. Faraday Soc.*, 1969, **47**, 84.

8. W. H. Baddley, *J. Am. Chem. Soc.*, 1968, **90**, 3705.

9. J. I. Amer, T. P. Dasgupta and P. M. Henry, *Inorg. Chem.*, 1983, **22**, 1970.

10. F. G. Moers and J. P. Langhout, *J. Inorg. Nucl. Chem.*, 1977, **39**, 591.

11. P. Zavalli, M. Myskiv and V. S. Fundamenskii, *Kristallografiya*, 1984, **29**, 60. From *Chem. Abstracts*, 1984, **100**, 165796k.

12. F. A. Miller, O. Sala, P. Devlin, J. Overend, E. Lippert, W. Luder, H. Moser and J. Varchim, *Spectrochim. Acta*, 1964, **20**, 1247.

13. P. Devlin, J. Overend and B. Crawford, *ibid.*, 1964, **20**, 23.

14. B. Giovannitti, O. Gandolfi, M. Ghedini and G. Dolcetti, *J. Organomet. Chem.*, 1977, **129**, 207.

APPENDIX

Electrochemical Techniques

The main voltammetric techniques used in this work were cyclic and a.c. voltammetry. Typical waveshapes for a reversible one-electron process are shown in Figure A-1.

Cyclic voltammetry

This technique involves the application of a triangular potential ramp to the cell. Stationary electrodes in quiescent solution and fast scan rates (v=10-500mVs^{-1}) are used to minimise diffusion and convection effects. Unless otherwise stated a scan rate of 100mVs^{-1} was employed to record cyclic voltammograms in this work. The potential midway between the cathodic and anodic peak potentials (E_{pc} and E_{pa} in Figure A-1) is equal to $E_{1/2}$.

A.c. voltammetry

In this technique a small sinusoidal alternating potential is superimposed on a linearly increasing d.c. potential. The alternating component of current is then monitored selectively as a function of the d.c. potential. For a fully reversible redox process E_p corresponds to $E_{1/2}$. The scan rate used to determine potentials quoted in this work is 20mVs^{-1} unless otherwise stated.

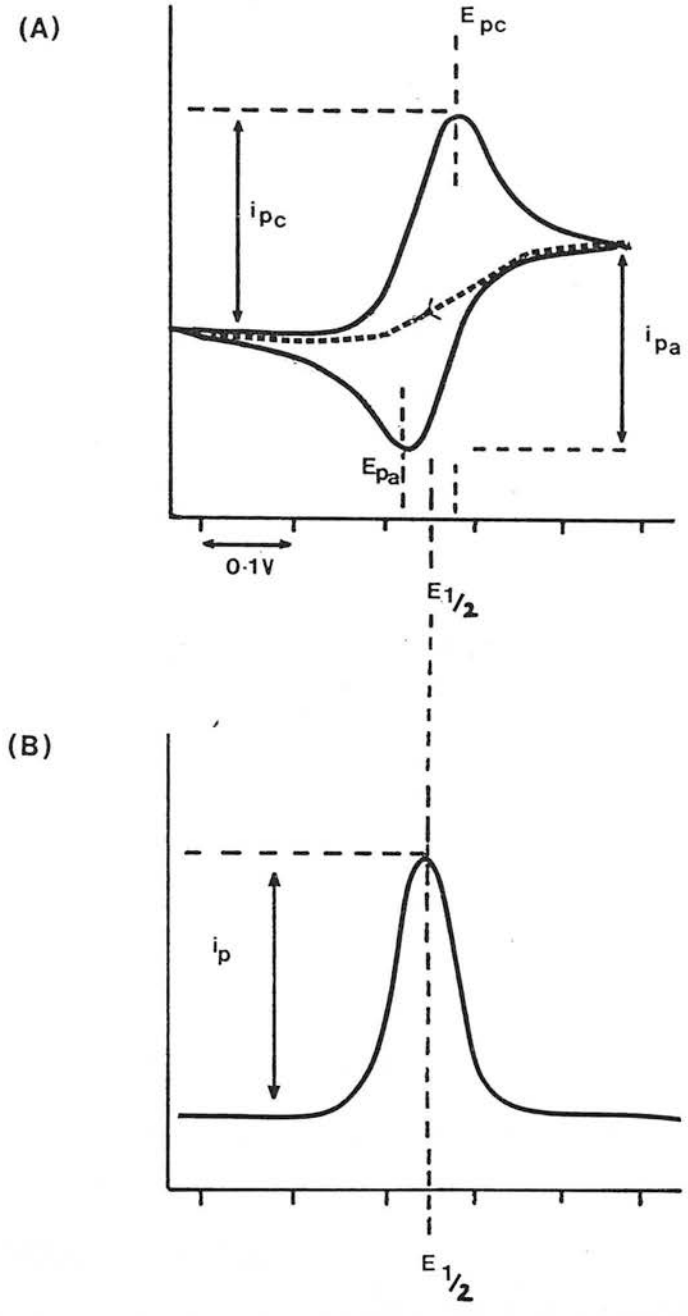

Figure A-1: Typical waveshapes for a reversible one-electron process for (a) cyclic voltammmetry and (b) a.c. voltammetry. The dotted line in Figure (a) represents the return current flow for an irreversible process.

Common reversibility criteria for these techniques are as follows

Cyclic voltammetry

reversible

$E_{1/2}$ is independent of scan rate (**v**);

$E_{pc}-E_{pa}=59/n$ mV independent of **v**;

$E_{pc}+E_{pa}/2=E_{1/2}$ (and is independent of concentration);

a plot of I_p vs. $\mathbf{v}^{1/2}$ is linear and passes through the origin;

$i_{pc}/i_{pa}=1$ independent of **v**.

quasi-reversible

E_p is dependent on **v**;

$E_{pc}-E_{pa}$ increases as **v** increases;

$I_p/\mathbf{v}^{1/2}$ is independent of **v**;

i_{pc}/i_{pa} (generally)=1.

irreversible

E_p changes with **v**;

$I_p/\mathbf{v}^{1/2}$ is independent of **v**

no current on reverse scan.

A.c. Voltammetry

$E_p=E_{1/2}$;

the half-height peak width=90/n mV;

the wave is symmetric;

a plot of I_p vs $\omega^{1/2}$ is linear and passes through the origin (ω=applied; a.c. frequency).

Coulometry

This technique was used to determine the number of electrons transferred in a redox step (**n**) by bulk electrogeneration of a known quantity of the redox-active species. Integration of the current passed w.r.t. time gives the number of coulombs of charge passed. From the relationship **n=C.M/m.F** (where **n**=no. of electrons transfered, **C**=charge passed, **M**=formula weight of compound, **m**=mass of sample added to cell and **F**=Faraday's constant) the value of **n** can be found. Certain checks are made to ensure that the redox process is reversible and that complete conversion to the oxidised or reduced species has occurred. These are that (i) the bulk electrogeneration process is only stopped once the current flow is <3% of the initial current, (ii) the oxidised or reduced product must undergo complete conversion to the starting complex on returning the potential to the initial value and (iii) stirred d.c. voltammetry should give the same magnitude for the diffusion limited current flow (i_d) after each electrogeneration step. The temperatures at which coulometric studies were undertaken are reported in the text (and are usually the same as that at which spectroelectrochemical experiments were performed on the complex in question). Details of the experimental set-up can be found in Chapter 4.11.

Spectroelectrochemical techniques

Spectroelectrochemistry in this work is interpreted as the monitoring of the electronic spectrum (from 5000-40,000cm^{-1}) of a complex in solution as a function of applied potential. Figure A-2 shows a cut-away diagram of the O.T.T.L.E. cell used. The experimental details are listed in Chapter 4.11. The temperatures at which these experiments were performed are listed in the text. The following procedure was observed in order to ensure the validity of the data. The experiment was carried out at temperatures at which electrochemical studies had shown the redox process to be fully reversible. The electrogeneration step is only considered finished when no further change in shape or intensity occured in the absorption spectrum. Finally, the potential was returned to the initial value to ensure that the original spectrum can be regenerated in full.

N.m.r. Spectroscopy

Unless otherwise stated the n.m.r. spectra of the complexes in this work are run in $CDCl_3$ solution and values given are uncorrected for solvent. All $^{31}P-\{^1H\}$ n.m.r. spectra were recorded on a JEOL FX-60MHz machine. All ^1H n.m.r. spectra were recorded on a Brucker 200MHz machine except for the spectra of the complexes $[Os(S_2PMe_2)_2(PPh_3)(tcne)]$ and $[Ru(S_2P\{OEt)_2)_2(PPh_3)_2]$ which were recorded on a Brucker 90MHz machine and the spectra of $[Ru(S_2P\{OEt\}_2)_2(PPh_3)(CO)]$ and $[Os(S_2P\{OEt\}_2)_2(PPh_3)_2]$

which were obtained using a Brucker 360MHz machine.

Mass spectroscopy

FAB mass-spectral data for some dithiolate complexes of ruthenium and osmium are listed in Table A-1. All samples were recorded using 3-nitro-benzyl alchohol as a matrix.

Table A-1: Selected mass-spectral data for some dithiolate complexes of ruthenium and osmium.

complex	Mass no. of $^{102}Ru/^{192}Os$ peak	probable ion
$[Ru(S_2P\{OEt\}_2)_3]$	657 (1.2)	$[Ru(S_2P\{OEt\}_2)_3]^+$
	472 (1.0)	$[Ru(S_2P\{OEt\}_2)_2]^+$
$[Ru(S_2PPh_2)_3]$	849 (1.0)	$[Ru(S_2PPh_2)_3]^+$
	600 (11.0)	$[Ru(S_2PPh_2)_2]^+$
$[Ru(S_2P\{OEt\}_2)_2(PPh_3)(CO)]$	762 (1.0)	$[Ru(S_2P\{OEt\}_2)_2(PPh_3)(CO)]^+$
	734 (3.8)	$[Ru(S_2P\{OEt\}_2)_2(PPh_3)]^+$
$[Ru(S_2P\{OEt\}_2)_2(PPh_3)_2]$	996 (1.0)	$[Ru(S_2P\{OEt\}_2)_2(PPh_3)_2]^+$
	811 (4.4)	$[Ru(S_2P\{OEt\}_2)(PPh_3)]^+$
	734 (6.7)	$[Ru(S_2P\{OEt\}_2)_2(PPh_3)]^+$
	472 (3.4)	$[Ru(S_2P\{OEt\}_2)_2]^+$
$[Os(S_2P\{OEt\}_2)_2(PPh_3)_2]$	1086 (1.0)	$[Os(S_2P\{OEt\}_2)_2(PPh_3)_2]^+$
	824 (11.8)	$[Os(S_2P\{OEt\}_2)_2(PPh_3)]^+$
$[Ru(S_2P\{OEt\}_2)_2(PEtPh_2)_2]$	900 (1.0)	$[Ru(S_2P\{OEt\}_2)_2(PPh_3)_2]^+$
	715 (2.4)	$[Ru(S_2P\{OEt\}_2)(PPh_3)_2]^+$
	686 (14.2)	$[Ru(S_2P\{OEt\}_2)_2(PPh_3)]^+$
$[Ru(S_2P\{OEt\}_2)_2(dppm)]$	983 (3.4)	$[Ru(S_2P\{OEt\}_2)_2(dppm)]^+$
	734 (1.0)	$[Ru(S_2P\{OEt\}_2)(dppm)]^+$
$[Os(S_2PPh_2)_2(PPh_3)(tcne)]$	2031 (1.0)	$[\{Os(S_2PPh_2)_2(PPh_3)\}_2tcne]^+$
	1081 (525.9)	$[Os(S_2PPh_2)_2(PPh_3)(tcne)]^+$
	953 (673.1)	$[Os(S_2PPh_2)_2(PPh_3)]^+$
	690 (292.3)	$[Os(S_2PPh_2)_2]^+$
$[Os(S_2PMe_2)_2(PPh_3)(tcne)]$	832 (1.0)	$[Os(S_2PMe_2)_2(PPh_3)(tcne)]^+$
	703 (23.5)	$[Os(S_2PMe_2)_2(PPh_3)]^+$
	442 (16.0)	$[Os(S_2PMe_2)_2]^+$
$[Ru(S_2P\{OEt\}_2)_2(PPh_3)(tcne)]$	733 (1.0)	$[Ru(S_2P\{OEt\}_2)_2(PPh_3)(tcne)]^+$
	472 (1.3)	$[Ru(S_2P\{OEt\}_2)_2]^+$
$[Ru(S_2PPh_2)_2(PPh_3)(tcne)]$	862 (1.0)	$[Ru(S_2PPh_2)_2(PPh_3)]^+$
	600 (1.7)	$[Ru(S_2PPh_2)_2]^+$
$[\{Ru(S_2P\{OEt\}_2)_2(PPh_3)\}_2tcne]$	1596 (1.0)	$[\{Ru(S_2P\{OEt\}_2)_2(PPh_3)\}_2tcne]^+$
	734 (180.5)	$[Ru(S_2P\{OEt\}_2)_2(PPh_3)]^+$
	472 (109.8)	$[Ru(S_2P\{OEt\}_2)_2]^+$

(a) Figures in brackets correspond to the relative intensities of the peaks.

Lecture courses attended.

"The Electronic Structures of Inorganic Molecules."
Drs. L. J. Yellowlees and A. J. Welch,
University of Edinburgh.

"Microcomputers."
Dr. A Rowley and Mr A. King, University of Edinburgh.

"Chemical Technology and Industrial Chemistry."
Drs. A. J. Nicol, L. H. Mustoe and R. S. Sinclair,
Paisley College of Technology.

"Recent Developments in Electrochemistry."
Drs G. A. Heath and H. Girault, University of Edinburgh.

"An Introduction to the Cambridge Structural Database.
Drs. O. Kennard, S. A Bellard, G. Watson and F.H. Allen,
University of Cambridge, and T. Brown University of Edinburgh.

"Current Inorganic Research at Edinburgh."
Drs. G. A. Heath, M. Schroder, A. J. Welch, T. A. Stephenson
and Prof. E. A. V. Ebsworth.

"Multipulse N.M.R."
Dr I. H. Sadler, University of Edinburgh.

"Molecular Electronics."
Profs. R. W. Munn and J. O. Williams, UMIST.

"Mass Spectrometry."
Prof. K. R. Jennings, University of Warwick.

Meetings attended.

"R.S.C. Scottish Electrochemistry Group, Butler Meeting (1987)."

"R.S.C. Scottish Dalton Group Meeting (1985,1986)."

"R.S.C. Platinum Metals Conference (1987)."

"British Crystallographic Assoc., Spring Meeting (1987)."

"Departmental Inorganic Colloquia and Friday Discussion group."

"University of Strathclyde Inorganic Club (1985,1986,1987)."